Department of Chemistry

Operando Characterisation of Oxide-Supported Bimetallic Pd-Pt Nanocatalysts for Methane Oxidation

Submitted in partial fulfilment of the requirements for the degree of Doctor of Philosophy

Alexander Ian Large

June 2021

Supervised by Professor Georg Held & Dr Roger Bennett

Declaration

I confirm that this is my own work and the use of all material from other sources has been properly referenced and fully acknowledged.

Signed

Alexander Large

Abstract

Near-ambient pressure x-ray photoelectron spectroscopy (NAP-XPS) was utilised to understand the relationship between the surface chemistry and reactivity of catalysts for the complete oxidation of methane. This reaction is of interest for removing unburnt methane in vehicle exhausts, due to the high global warming potential of methane.

A wide range of palladium, platinum, and palladium-platinum catalysts - both real powder catalysts and model systems - were studied for complete methane oxidation.

Powder catalyst studies showed that palladium was significantly better than platinum in all relevant tested conditions. Exchanging palladium for platinum showed some benefits, most importantly decreasing the deactivation suffered in wet conditions - a key negative of palladium catalysts.

NAP-XPS was utilised to investigate whether understanding the surface states could aid the development of catalysts. This showed some correlations between activity and palladium oxidation state for alumina-supported samples, with benefits seen to retaining significant amounts of Pd(0) on the surface. Pd-Pt catalysts consistently had a higher presence of reduced palladium, compared to Pd catalysts. An increased platinum presence ensures more Pd(0) is present on the catalyst, partially explaining the increased activity of bimetallic catalysts under select conditions.

Support effect studies compared silica, alumina and silica-alumina supported catalysts of equivalent loading. A mixed silica-alumina support ($90Al_2O_3$-$10SiO_2$) typically performed best, though the margins between this, silica and alumina were often very small for a given condition. NAP-XPS showed a less direct correlation between oxidation of palladium and catalytic activity, with other effects of support variation (grain size, particle size) having greater impacts.

Issues with charging and signal in NAP-XPS experiments prompted the development of thin film model catalysts, utilising thin layers of alumina with nanoparticles of palladium

deposited onto the surface using a cluster source. This method allowed for the production of samples with similar surface loadings, which were superior in regards to sample charging for XPS. Additionally, they were shown to behave in similar ways under methane oxidation conditions by NAP-XPS, with dynamic reduction and oxidation of palladium.

Temperature-programmed NAP-XPS work on palladium foils under reaction conditions showed that a lower oxygen concentration or higher water concentration in the gas feed caused the oxidation of palladium to be inhibited. Pd-Pt foils were studied, with even greater inhibition of Pd oxidation seen with higher Pt loading. Where palladium was oxidised, platinum was typically migrating into the bulk of the foil. Platinum migrating to the bulk of Pd-Pt systems was also seen in thin film studies. Combined with the powder results, this is a clear sign that platinum presence aids palladium retaining a reduced state.

Acknowledgements

To all of the people who have been my supervisors over the last few years: Georg Held, Roger Bennett, Federica Venturini, Rosa Arrigo and Tugce Eralp-Erden, for putting up with all my questions - intelligent and otherwise - listening to many presentations, and always offering useful advice and guidance.

To everyone who has spent time on beamtime with me, without whom this thesis would be not be nearly as dense: Georg Held, Dave Grinter, Roger Bennett, Kevin Lovelock, Panayiotis Tsaousis, Jake Seymour, Kanak Roy, and Wilson Quevedo Garzon.

To all the people at Johnson Matthey Technology Centre who provided me with their time, assistance, and their expertise in wide range of techniques: Tugce Eralp-Erden, Agnes Raj, Riho Green, Emily Brooke, Martha Briceno de Gutierrez, Hanita Gill, Dogan Ozkaya, Monik Panchal and Neel Makwana.

To everyone past and present at beamline B07 VerSoX at Diamond Light Source, for their continual assistance: Georg Held, Federica Venturini, Dave Grinter, Pilar Ferrer-Escorihuela, Rosa Arrigo, Kanak Roy, Wilson Quevedo Garzon, Andrew Watts and Matthijs Van Spronsen.

To Andrey Shavorskiy and Suyun Zhu at the HIPPIE beamline at MAX IV, for their assistance and patience with some samples which showed horrendous charging under their beam.

To Tomas Skala at the Materials Science beamline at Elettra, for his assistance with the thin film experiments.

To Paolo Lacovig at SuperESCA at Elettra, for not being too angry when we pushed a sample into a gate valve.

To Luca Artiglia at NanoXAS at Swiss Light Source, for helping with NAP-XPS measurements and continually providing new sample supports when we welded our model samples to them.

To Rongsheng Cai and Richard Palmer, for the use of their cluster source and their related expertise in nanoparticle preparation.

To Lizzie Jones, for preparing a huge amount of alumina thin films via anodization, saving me a lot of time in the process.

To the people who have allowed me to join them to explore a wide range of exotic locations: Tugce Eralp-Erden (Berlin), Rosa Arrigo (also Berlin, twice), and Panayiotis Tsaousis (Manchester).

To everyone at the University of Reading, who allowed me to sit in my basement office and just get on with everything in peace.

To all the undergraduate students I demonstrated to & briefly taught inorganic chemistry to at the University of Reading, for providing much unexpected entertainment and an often welcome distraction.

To Sophie, for always putting up with me, despite my continual tendency to go to foreign countries (such as Oxfordshire) for weeks at a time, often at short notice.

To my mum and dad, for their continual support, in spite of their lack of knowledge or interest in my research work.

Abbreviations

Abbreviation	**Full Term**
(N)AP-XPS	(Near) Ambient pressure x-ray photoelectron spectroscopy
BET	Brunauer, Emmett and Teller
COM	Complete oxidation of methane
DLS	Diamond Light Source
DRIFTS	Diffuse reflectance infra-red fourier transform spectroscopy
EDX	Energy dispersive x-ray spectroscopy
FT-IR	Fourier transform infra-red spectroscopy
FWHM	Full width (of) half maximum
ICP-MS	Inductively coupled plasma mass spectrometry
IMFP	Inelastic mean free path
LEED	Low energy electron diffraction
MACS	Matrix assisted cluster source
NGV	Natural gas vehicle
PGM	Platinum group metal(s)
POM	Partial oxidation of methane
RT	Room temperature (298 K)
SCAT	Synthetic catalytic activity test
SCLS	Surface core level shift
SEM	Scanning electron microscopy
SLS	Swiss Light Source
Syngas	Synthesis gas, carbon monoxide and hydrogen
TEM	Transmission electron microscopy
TOF	Turnover frequency
TPD	Temperature programmed desorption
TPR	Temperature programmed reduction
TP-XPS	Temperature programmed x-ray photoelectron spectroscopy
UHV	Ultra high vaccum
VerSoX	Versatile soft x-ray
XANES	X-ray absorption near-edge spectroscopy
XPS	X-ray photoelectron spectroscopy
(P)XRD	(Powder) X-ray diffraction

Contents

1 Introduction

For many years, a key area in chemical research has been clean energy, with the need to develop cleaner fuels ever increasing. Unfortunately, for a new fuel to viably replace fossils fuels, it would need to be readily available in vast quantities, easily distributable and usable on a mass scale, cause less problematic emissions than existing fuels, and not carry a significantly higher cost. One candidate fuel source which has been considered in recent years is methane, and when considering the key points mentioned previously, it is clear why. First of all, there are large global methane reserves, which were recently found to be larger still due to the discovery and developed understanding of methane hydrates (methane stored in frozen water). In addition, complete combustion of methane produces only water and carbon dioxide. Natural gas engines using this reaction have a much lower chance for release of nitrates and other problematic species, when compared to traditional fossil fuels. There are some key issues with using methane as a fuel however, primarily: the high operating temperatures required for effective combustion of methane (often 300 °C or higher); and the unburnt methane which is released from the exhaust. In addition to this, methane is emitted from traditional combustion engine exhausts, so catalysts for methane oxidation can be employed across a range of engine types. Exhaust catalyst technology is a key research area, with tightening regulation necessitating more effective catalysts. [1] It is likely that in future generations of the Euro emission regulations methane emissions will be further restricted from all categories, so exhaust methane conversion catalysts will become relevant on a wider scale. The next version of the emissions standards, which will be Euro 7, is proposed to come into effect from 2025. [2,3]

In this project, the aim was to synthesize a range of oxide supported platinum-palladium bimetallic nanocatalysts for methane oxidation. Platinum group metal (PGM) catalysts have formed a key component of many exhaust catalysts, and are expected to continue to be important in this area. [4] The core analytical technique for this project is near-ambient pressure x-ray photoelectron spectroscopy (NAP-XPS), which allows us to study the catalyst surfaces under reaction conditions. This will be complemented by catalytic activity tests and a range of additional characterization techniques, such as transmission electron microscopy (TEM), x-ray photoelectron spectroscopy (XPS) and carbon monoxide (CO) chemisorption. This will aid us in developing a greater understanding of the methane oxidation processes. In turn this will better guide future methane oxidation catalyst production.

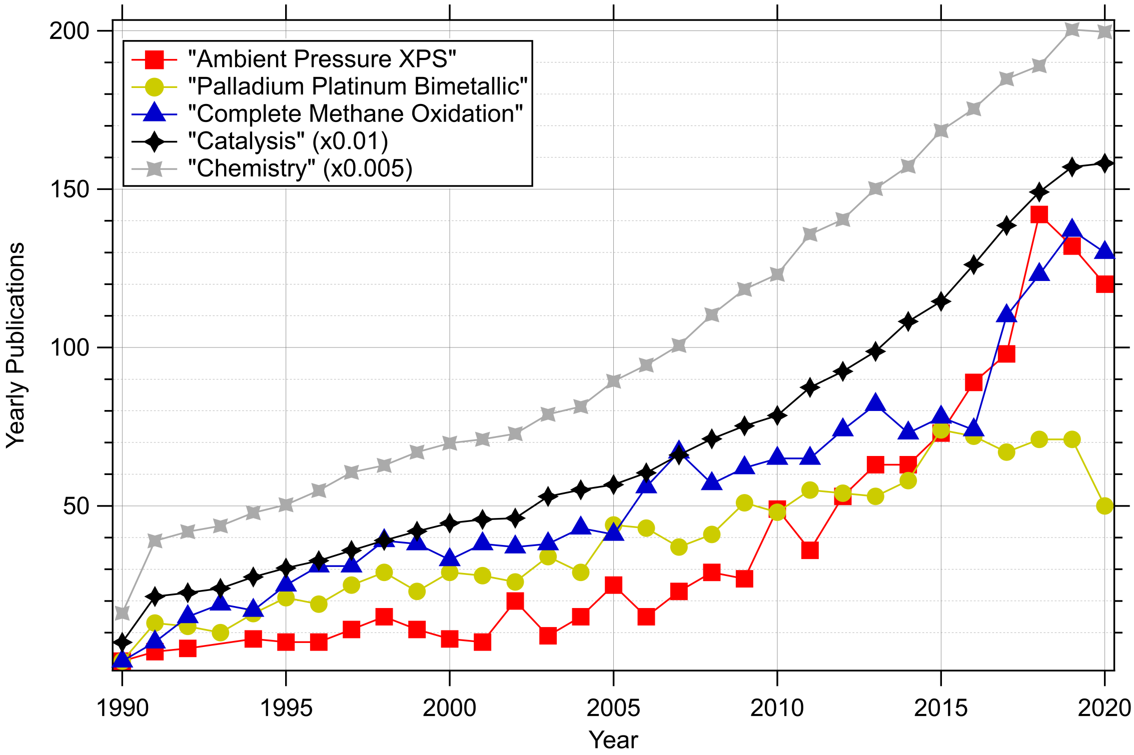

Figure 1.1: Yearly publication records for specific relevant topic terms, from Web of Science. Data for "catalysis" and "chemistry" are rescaled by 0.01 and 0.005 respectively, due to the higher research output for these two more general terms.

As shown in Fig. 1.1, there is a continual increase in publications of papers using the topics "ambient pressure XPS", "complete methane oxidation" and "palladium platinum bimetallic" over the last 30 years. [5–9] Whilst there is a drop in these three categories in 2020, searches for general terms such as "chemistry" and "catalysis" also show minimal change from 2019 to 2020, likely a result of the restriction on research due to Covid-19 and the resulting lockdowns.

1.1 Heterogeneous Catalysis

The field of heterogeneous catalysis has been one of the richest sources of chemical advancement, and continues to expand to this day. To generalise, it is a process whereby a catalyst lowers the activation barrier of a reaction, where the reactants are of a different state to the catalyst. Most often, this is presented as a solid catalyst (often a transition metal) operating with a gaseous reaction mixture, though this is not always the case. A wide range of industrially crucial processes rely on heterogeneous catalysts, and would be unviable (chemically or commercially) without them. One of the most widely known examples is the Haber-Bosch process, in which nitrogen and hydrogen gases are converted to ammonia over an iron catalyst. [10–12] This reaction is crucial in the agricultural industry, due to the use of ammonia (and related products) in fertilizers, of which the process creates over 400 million tonnes per year. Some of the other most relevant reactions in this field include: methanol synthesis from syngas (copper and zinc oxides); methanol oxidation in direct methanol fuel cells (platinum and ruthenium); and the oxidation of carbon monoxide (on platinum or palladium "three way catalysts"). [13–22] In heterogeneous catalyst design, a critical goal is always maximising active surface area for a given amount of catalyst. This is of particular relevance when using PGMs as catalysts, as cost can become prohibitive when using large amounts. It is common now for catalysts to comprise of nanomaterials, as they offer a high surface area to volume ratio, and can often be produced from facile syntheses.

Catalysts will typically be characterised by a number of core methods. These include testing the catalytic activity, such as with synthetic catalyst activity testing (SCAT, described in section 2.2.2), from which turnover frequency (TOF) and activation energy (EA) can be determined. Other commonly referenced terms include the T50, which is the temperature at which the reaction reaches 50% conversion (with T90 used for 90% conversion, etc). [23–26] In addition, catalysts which contain nanoparticles will typically undergo particle size analysis. This can be conducted via multiple methods, more usually with transmission electron microscopy (TEM). When discussing different catalysts it is important that the loading is clear. Typically this will be quoted as a weight percentage, relative to the support material, but with varying supports and metals, 5 wt.% can represent very different metal : support atomic ratios. For bimetallic alloyed systems, it is more common to refer to an atomic ratio, with the total loading quoted as a weight percentage.

1.1.1 Mechanisms

There are a number of mechanisms which can occur for the heterogeneous catalysis of a bimolecular reaction, the details of which are outlined below. [27–29] Three main mechanisms will be covered in Fig. 1.2.

The Langmuir-Hinshelwood mechanism involves the adsorption of two reactant molecules onto adjacent sites of the catalyst surface. The reactant molecules will react on the surface, and then desorb.

The Eley-Rideal mechanism involves first the adsorption of one reactant onto the catalyst surface, which then reacts with a gas phase molecule of the other reactant, before the new species desorbs.

The Mars-van Krevelen mechanism can occur where the catalyst is a metal oxide. The reactant can abstract an oxygen from the oxide surface, to form an oxidation product. The surface vacancy of the catalyst can be filled from the support (normally an oxide species with a high oxygen storage capacity and oxygen mobility, such as ceria), or from oxygen in the gas phase of the reaction.

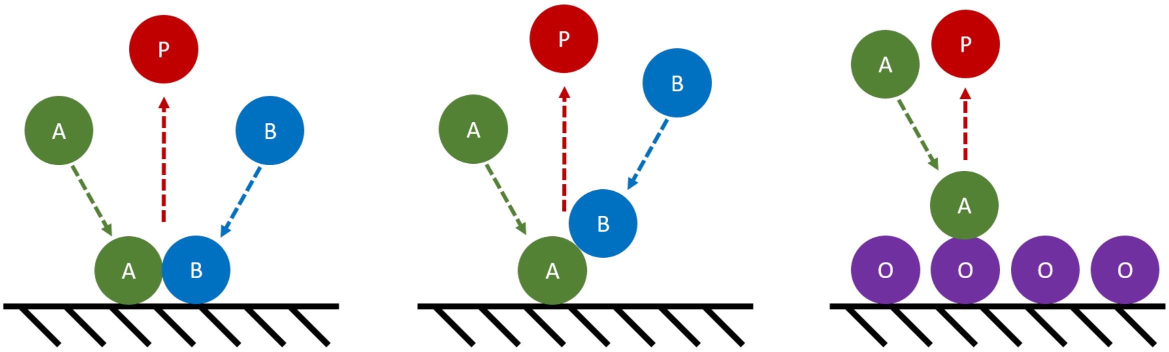

Figure 1.2: Diagrams of the three mechanisms (from left): Langmuir-Hinshelwood, Eley-Rideal, and Mars-van Krevelen. The A and B represent reactants, P represents products, O represents surface oxide, and the black line represents the catalyst surface.

1.2 Methane Oxidation

For many years, researchers have been designing catalysts for the oxidation of methane. In the early 19th century, Sir Humphry Davy invented a lamp to increase the safety of operations in coal mines. [30] Whilst not strictly described as such, this is likely one of the earliest cases of deliberate methane oxidation. One of the first research papers on the topic came in 1927 where Yant and Hawk presented their investigations on methane oxidation by a range of metals and metal oxides. From their studies they found the most efficient catalysts to be cobaltic oxide, manganese dioxide and nickel oxide. [31] In the years which have followed, significant progress has been made in developing more functional methane oxidation catalysts. Methane has proven much more difficult to oxidize as compared to propane, propene and carbon monoxide over typical Pd/alumina catalysts. [32] Methane was also shown to be harder to oxidise than other tested alkanes over Pd, Ni and Pt catalysts, due to the relatively higher bond strength. [33]

1.2.1 Complete Oxidation of Methane (COM)

The complete oxidation of methane (COM) is a reaction which converts methane and oxygen to carbon dioxide and water. The reaction scheme is shown in Fig. 1.3.

$$CH_4 + 2\,O_2 \longrightarrow CO_2 + 2\,H_2O$$

Figure 1.3: Reaction scheme for the complete oxidation of methane.

Methane has been considered as a fuel source for transportation, including in dual fuel systems with typical diesel combustion engines. A core benefit of this reaction as a fuel source is the low amount of carbon dioxide produced per unit of fuel, due to the low C:H ratio in methane compared to other carbon based fuel sources. Methane is a more energy rich fuel than gasoline or diesel, with a full combustion energy of 50.1 $MJkg^{-1}$ (compared to 42.9 $MJkg^{-1}$ or 42.5 $MJkg^{-1}$ respectively). [34] It has been estimated that global reserves for methane hydrates are roughly equivalent to the reserves of gas and coal, so there are no significant issues of scalability in terms of the accessible volume of gas. [35] Whilst the conversion of methane is relatively efficient in natural gas engines, there is still some unburnt methane which is released through the exhaust. As such, it is necessary to both develop catalysts for methane combustion which minimise the unburnt methane, and to develop catalysts which will convert remaining unburnt methane in the exhaust. This should ensure that methane emissions are minimised, and increase the viability of methane as an alternative cleaner fuel source. Exhaust catalytic converters are already ubiquitous for combustion engined vehicles, and typically comprise of multiple stages to handle different pollutant gases.

A range of research groups have studied the viability of natural gas engines in real vehicles, often for comparison to traditional diesel fuel. With these studies, cross-study comparisons can be difficult, due to the often vastly different vehicles, engines, usage cycles, and post-combustion catalysts which are employed. A study by Nylund et al. focusing on buses found that (state of the art in 2004) compressed natural gas (CNG) engines produced less problematic emissions than equivalent diesel engines by around 20%, under the same usage. [36] This was one of the first studies of its type which showed CNG engines could be viable in terms of energy and emissions, which in part can be attributed to their use of exhaust treatment of gases, which had not always been present in prior studies. The work of Lopez et al. in Madrid, testing various fuels on refuse collection lorries, showed that compressed natural gas gave lower total greenhouse gas emissions than the comparative diesel and bio-diesel fuels. [37] The issue of the "CO_2e" (carbon dioxide equivalent, a measure of the global warming potential of gases relative to CO_2) was discussed by Stettler et al., who found that whilst a CNG engine would reduce CO_2 emission by up to 9%, the CO_2e emission would be much higher (up to 127% higher in some cases) due to the methane emitted. [38] As commercial CNG vehicles become less of a novelty, there is the consideration that not only can they be beneficial in terms of emissions, but that the cost can also be reduced compared to similar diesel vehicles. In Reading, which now has the UK's largest fleet of CNG buses, it has been calculated that they will have a cheaper lifetime cost than conventional diesel buses, despite higher initial costs. [39] This is in addition to the primary benefits of releasing 30-50 % less NO_x and negligible amounts of particulate matter, though they acknowledge that CO_2 emissions are at best unchanged. In other recent work, Worth et al. explored the effectiveness of a range of palladium and palladium-platinum catalysts in dual fuel systems, with their key interest being in achieving full conversion at moderate temperatures with their ideal system having a Pd:Pt ratio of 6:1. [40]

A large amount of work on complete methane oxidation catalysis has however not focused on the real world implementation of the catalysts, instead focusing purely on lab studies. A review by Li and Hoflund was published in 2003 which covered a wide range of complete methane oxidation catalysts, with a range of metals, supports and reaction mixtures. [41] The review primarily covers alumina-supported catalysts, as these are the most common, but also references titania, silica and zirconia supported palladium catalysts. Significant differences were seen with loading, particle size, gas ratios, support and preparation methods. This shows the importance of consistency within reporting, as with so many variables, determining the optimal catalysts is impossible. Typically the catalysts will be metallic nanoparticles dispersed on support material, to achieve maximum surface area with minimal usage of (often expensive) PGMs.

Typical complete methane oxidation experiments are conducted in gas compositions with ratios between 1 : 2 and 1 : 100 of methane : oxygen, with oxygen partial pressures up to atmospheric levels (210 mbar). Total pressures, including flow gases of nitrogen (or other inerts) will typically be 1 bar. Experimental temperatures can vary significantly with the catalyst, but typically activity is observed from 200 °C upwards, and at higher temperatures in wet conditions. [41–43]

1.2.2 Partial Oxidation of Methane (POM)

The partial oxidation of methane, shown in Fig. 1.4, is a process which converts methane and oxygen to carbon monoxide and hydrogen, a mixture which is known as "syngas" (synthesis gas). Syngas is used as a starting mixture for a wide range of potential fuel products, and so production of syngas is a very useful reaction. Currently syngas is primarily industrially produced by steam reforming, which is a highly endothermic process reliant on high temperature, even when utilizing nickel catalysts.

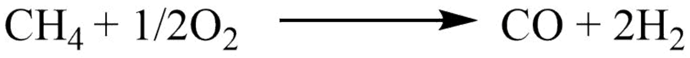

$$CH_4 + 1/2O_2 \longrightarrow CO + 2H_2$$

Figure 1.4: Reaction scheme for the partial oxidation of methane.

One of the first reports of the partial oxidation of methane was in 1929 by Liander, who was interested in the use of natural gas in the ammonia process. [44] A review from 2008 by Enger et al. considered examples of palladium, platinum, cobalt, and ruthenium catalysts, amongst a range of others. [45] The conversion of syngas to useful products is of relevance here, and a thorough review on this topic was performed by Subramani and Gangwal in 2008. [46] A wide variety of catalysts were referenced, using rhodium, palladium, cobalt, nickel and many others. Whilst rhodium allowed for direct syngas to ethanol conversion, they do highlight that this is a high cost metal, meaning it is not an ideal scalable option. Higher alcohol synthesis was viable using more cost-effective metals such as copper and zinc on oxide supports, though the output of these falls significantly short of that of the commercially used routes.

1.3 Platinum Group Metals (PGMs)

Platinum group metals (PGMs) are 6 metals spanning groups 8, 9 and 10 of the periodic table. The 6 metals are ruthenium, rhodium, palladium, osmium, iridium and platinum, which can be further divided into the iridium sub-group (ruthenium, osmium and iridium) and the palladium sub-group (rhodium, palladium and platinum). The relevant section of the periodic table is shown in Fig. 1.5. A 2010 Johnson Matthey report showed that PGMs were mostly used in autocatalysts (51% of use), followed by jewellery (16%), and investment and electrical (each 9%), and there is some use of PGMs across a broad range of industries [47]. A primary use of PGMs as catalysts is in vehicle exhaust systems, currently in the form of the "three way catalytic converter".

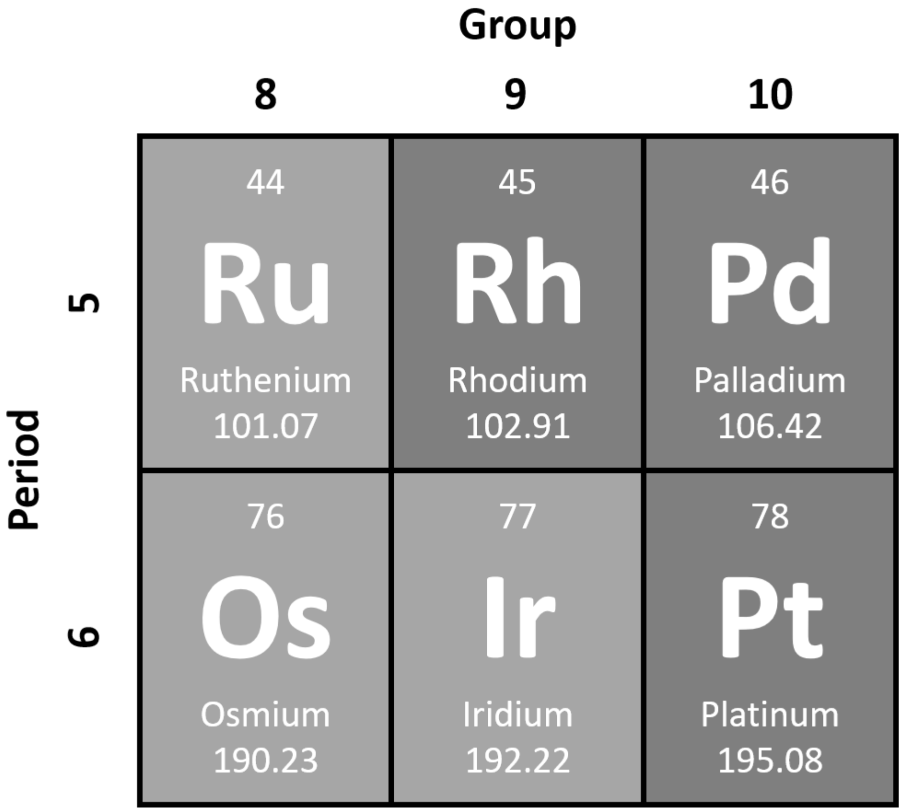

Period \ Group	8	9	10
5	44 Ru Ruthenium 101.07	45 Rh Rhodium 102.91	46 Pd Palladium 106.42
6	76 Os Osmium 190.23	77 Ir Iridium 192.22	78 Pt Platinum 195.08

Figure 1.5: Details of the 6 metals referred to as "PGMs".

1.3.1 Palladium Catalysts

Various common synthesis routes and supports for palladium catalysts were discussed by Toebes et al. [48] This included the method used in this experiment (known as either dry impregnation or incipient wetness impregnation), along with a range of other common catalyst preparation methods such as co-precipitation, photo deposition, and many more besides. Studying both literature and patents, it is clear that a vast range of reactions have been aided by palladium catalysts. [49] In 2010, the Nobel Prize in Chemistry was awarded to Heck, Negishi and Suzuki for "palladium-catalyzed cross couplings in organic synthesis".

Early Palladium Methane Oxidation Catalysts

One of the first uses of PGMs for methane oxidation catalysis was presented in 1961 by Anderson, who studied a wide range of metals and metal oxides, which included Pd/Al_2O_3 and Pt/Al_2O_3. [50] They showed that the activity (per gram of catalyst) was highest with the Pt catalyst, followed by Pd and a selection of less noble metals (Cr, Mn, Cu, etc). Further early work by Firth and Holland focused on a wider range of PGMs (Pt, Pd, Ir and Rh), studying activation energies and pressure effects [51]. They noted that Pd showed different activation energies at different temperatures, at 139 $kJmol^{-1}$ below 290 °C and 52 $kJmol^{-1}$ above 290 °C. The other metals studied showed no such change, but in the high temperature region (>290 °C) no activation energy was as low as that of palladium. They suggested that given the similarity in the activation energy over palladium and the heat of formation of palladium oxide, that the active palladium may be similar to palladium oxide. By comparison to prior studies of Pd-Au alloys, they suggest also that palladium oxide is reliant on the d-orbital hybridization. The alloying of palladium with gold, which has more d-electrons than palladium, is considered to be detrimental to the formation of palladium oxide.

Work published in 1981 by Chen and Ruckenstein studied nanoscale palladium particles dispersed on alumina thin films and their behaviour under oxygen [52]. They found that at low temperatures (350 °C) the smaller palladium crystallites spread across the surface, and this spreading was much more prevalent at 500 °C. This spreading behaviour was attributed to the wetting angle of palladium oxide being smaller than that of palladium metal. Above temperatures where PdO is stable (920 °C in this case), the crystallites sinter on the surface of the alumina. An example of some types of wetting behaviour is shown in Fig. 1.6.

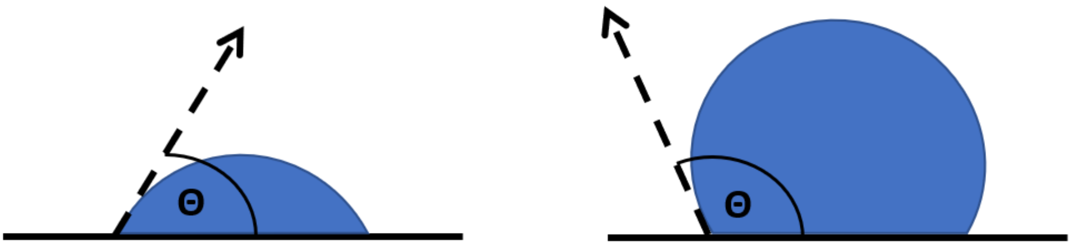

Figure 1.6: Diagram of wetting behaviour, showing an example of good wetting (left, $\theta < 90\,°$) and poor wetting (right, $\theta > 90\,°$), where θ is the "contact angle", defining the angle between solid-liquid and liquid-gas interface.

Kinetics and Active Sites

Research by McCarty in 1995 on Pd supported on γ-alumina and La_2O_3-$11Al_2O_3$ studied the kinetics of methane combustion catalysis over PdO. [53] He noted a hysteresis in activity for methane combustion caused by a layer of chemisorbed oxygen being formed on the palladium surface, and explained that the chemisorbed layer also prevents the growth of the (active) palladium oxide. Chemisorption is a process in which a reaction takes place between a surface and an adsorbate, whilst physisorption only has van der Waal's forces holding the two together. In addition, the ability for re-oxidation was shown to be support dependant, and additional free energy was required for the formation of high surface area PdO nanoparticles.

Garbowski et al. suggested that the reaction would proceed via a Mars van Krevelen mechanism (see Fig. 1.2), whereby the methane reacts with oxygen which had previously adsorbed onto the surface [54]. This is in contrast with the aforementioned work of McCarty, which noted the presence of chemisorbed oxygen was inhibiting the reaction. [53] They also suggest that complete oxidation of bulk palladium is not necessary for effective methane combustion.

At the same time, Burch studied the active state of palladium in alumina supported catalysts [55]. Like many catalysts of this style, it was produced using incipient wetness impregnation using a palladium nitrate precursor. They used a wide range of pre-treatment conditions, and a short pre-treatment in hydrogen was found to yield the smallest particles (4.5 nm diameter) with the highest metal surface area ($4.4\ m^2g^{-1}$). By comparison, a similar pre-treatment in air yielded particles of 6.1 nm diameter and surface area of 3.3 m^2g^{-1}. The dispersions, as measured by CO chemisorption, were also quite different, at 20% and 15% respectively. Samples treated in dry air or nitrogen show good initial activity, whilst the hydrogen treated sample shows poor initial activity. However, after one hour on stream it shows significantly greater activity than any other treatment. By comparison, when catalysts were aged for a longer period (16 hours compared to 1 hour) the sample aged in nitrogen showed the best initial and one-hour activity, whilst a catalyst treated in hydrogen never showed the activity increase it showed after only a 1 hour treatment. As a result of these findings, they concluded that there is no direct causal link between the metal dispersion and the initial activity of the catalysts. They show that for many conditions there is no significant change in dispersion with lengthened treatment, but there is a change in initial activity. In general, a wet pre-treatment atmosphere led to a poorer initial activity. They suggest this may be the result of the wet aging forming a different morphology of palladium particles which is less active, though the nature of this morphology was not specifically studied here.

Pan et al. performed a density functional theory (DFT) study of C-H bond cleavage over PdO clusters on H-BEA (protonated beta zeolite) [56]. They found that PdO strongly interacts with an acidic proton on the H-BEA support, and bonds to four oxygen atoms, including three within the H-BEA, with the overall structure said to closely resemble bulk PdO. They state that one proton from H-BEA and an oxygen atom from PdO are the sites that participate in the cleavage of the C-H bond in methane, demonstrating again that PdO is the active site whilst showing the benefit of also having acidic sites.

Operando x-ray absorption near-edge spectroscopy (XANES) characterisation from Matam et al. concluded that the active site of Pd for methane oxidation was variable with reaction temperature. [57] Below 950K, PdO was the primary active site, but above this both PdO and metallic Pd can act as the catalyst. They also showed that higher temperatures treatment leads to larger PdO particles, and that this was beneficial for low temperature catalysis. Hellman et al. used a combined DFT & in situ x-ray diffraction (XRD) approach to understanding the active sites for palladium. [58] Their conclusion was that either thick PdO(101) films or metallic palladium were necessary for effective methane oxidation. Methane rich (5.5:1 methane:oxygen) condition studies by Bychkov showed strong activity for metallic palladium, though this is reported to only be relevant for this methane rich condition, as the metal sites remain free for the key step C-H bond activation. [59]

Support Effects

Whilst much of the prior work has utilised alumina as a support, zeolites and other metal oxides have often been looked at as potential supports for Pd catalysts. One of the most common metal oxides has been zirconia (ZrO_2). Fujimoto prepared PdO_x/ZrO_2 catalysts, and studied the effects of pre-treatments and particle dispersion on the activity. Methane oxidation turnover rates were found to increase with increasing Pd crystallite size, although there were no significant changes to activation energy. Due to their observations, they suggest that the rate-determining step is C-H bond activation which requires an oxygen atom and a vacant site adjacent. With smaller crystallites, or lower oxygen content in PdO_x, the chance of such sites occurring decreases, which would explain the observed lower activity with particles of smaller sizes. From an XPS perspective, PdO_x/ZrO_2 catalysts are not ideal for quantitative oxidation state studies, due to the strong overlap between the Pd 3d (335, 340 eV binding energy) and Zr 3p (330, 344 eV) peaks. This overlap, coupled with the typically low loading of Pd, makes the Pd 3d signals hard to accurately resolve, and so it is not an appropriate support in this project, despite the promising activity.

Another group to study palladium on zirconia around the same time was Epling and Hoflund, also with the intention of studying pre-treatments and loading effects [60]. They determined that low temperature aging (110-280 °C) was preferable to high temperature aging (at 500-800 °C), but only where the desired reaction temperature was within the low temperature range. It is worth noting here that activity over most catalysts is low in the low temperature region, so the higher temperature aging is likely to be preferable. Of the reductive treatments, 250 °C was preferable to 400 °C in terms of the catalytic activity which it yielded. As Pd loading was increased there was a noted increase in activity, although above 10 wt. % the change is minimal. In addition, over 50 hour activity tests Pd/ZrO_2 showed no significant activity loss, whilst an equivalent Pd/Al_2O_3 catalyst decayed over this period. From their XPS analysis, it was stated that the Pd/ZrO_2 as prepared consisted of Pd, PdO and PdO_2. Treatment at 180 °C, where the reaction starts, caused partial reduction of some PdO back to Pd. With the nature of peaks in this region (as discussed above) and the quality of the data, it is hard to be certain that Pd(IV)/PdO_2 is truly present in any of the treatments. They also suggested a mechanism, by which the C-H bond breaks, with the carbon and a surface oxygen forming an adsorbed CO, which forms an intermediate carbonate before decomposing to CO_2, which it desorbs as. Further, they add that the presence of Pd metal could help, as the methane dissociatively adsorbs onto the Pd site before spilling over onto either palladium oxide or the zironcia (which is also slightly active as a catalyst for the reaction), where it can react to form CO_2.

Zeolites are aluminosilicate materials with microporous structures, meaning they contain pore channels on the micron scale. As any micro- or nano-structured materials will have a much higher surface area to volume ratio than non-structured materials, and this can be highly useful within catalysis. Maeda studied mordenite and ZSM-5 for this purpose [61]. Within their selection of catalysts, the best long term activity was found in a Pd/H-mordenite (with a Si/Al_2 ratio of 145) catalyst. They suggested that the porous stucture of the zeolite may have helped with the long term activity, as it helped to prevent significant sintering of the palladium nanoparticles. As with prior studies, palladium oxide was deemed to be the active species for methane oxidation, and they stated that the amount of active oxygen on the palladium surface was increased by use of zeolites as a support. Titration of acid sites in zeolites with sodium proved effective for Pd/zeolite catalysts in the research of Petrov. [62] T50 (the temperature at which 50% conversion is reached) differences of 50 °C or more were observed between the sodium-exchanged zeolite and the protonated form. The long term stability was also vastly improved, and significantly better than tested Pd/alumina catalysts.

Preparation and Precursor Effects

In 2006, Simplicio et al. published their discussion on the effects of palladium precursors and preparation route on the activity of Pd/Al_2O_3 catalysts [63]. The range of precursors selected was: $Pd(NO_3)_2$, $PdCl_2$ and $Pd(C_5H_7O_2)_2$, with intended Pd loadings of 3 wt. %. Two distinct preparation methods were used, the first one of which was impregnation which has been a widely used method for preparation of supported nanoparticles due to its simplicity. The other is referred to as the polyol method, which involves the low temperature dispersion of alumina in ethylene glycol, followed by addition of a solution of $Pd(C_5H_7O_2)_2$ in ethylene glycol, then separation and drying. The particle size was shown to vary significantly depending on the precursor used for impregnation, with the chloride salt yielding much larger particles (average diameter 60 nm) compared to the nitrate (average 12 nm) and the acetylacetonate yielding particles that were smaller still (average 7 nm). Using the polyol method gave larger particles than the impregnation method with the same precursor (11 nm compared to 7 nm). As with prior studies, it is stated that palladium was shown to be present as Pd, PdO and PdO_2 by XPS, for all precursors/methods. Studying the presented spectra and fitted peaks, some very unusual fits are seen, with ratios between Pd $3d_{5/2}$ and Pd $3d_{3/2}$ peaks that do not seem to fit the correct values. As such, the inclusion of the PdO_2 is again uncertain, and they do indeed suggest that this may result from well-dispered PdO particles instead, as also suggested previously by Voogt. [64] In terms of initial activity, the catalyst produced from acetylacetonate precursor (via impregnation) performed best, followed by the same precursor using the polyol method. The latter was very similar to the "impregnated nitrate", with the "impregnated chloride" having a much lower initial activity. The poor activity of catalysts synthesized from $PdCl_2$ is understood to arise from some chloride still being present on the catalyst surface despite calcination to 600 °C, as well as the large and poorly dispersed palladium particles that it produced.

In 2010 Shimizu et al. studied the possibility of preparing palladium nanoparticles in situ for methane oxidation [65]. $Pd(THD)_2$ (where THD is 2,2,6,6-tetramethyl-3,5-heptadione) was dissolved in toluene and injected as an aerosol into a laminar flow reactor (containing a typical reaction flow of methane, oxygen and nitrogen), with nanoparticle production verified by XPS and TEM of particles post-reaction. Ignition of methane was found to occur at 150 °C lower in the feed with the nanoparticles compared to without. It was found that the nanoparticle sizes varied with loading (as shown from more typical production methods), with diameters of up to 20-30 nm, depending on loading. They note that the heat released from the catalytic reaction at this lower temperature can bring the gas to a higher temperature which leads the gas phase reaction to occur also, leading to thermal runaway and then fuel ignition. As with previous studies, they found a key step to be the adsorption of oxygen onto the palladium surface, with the rate-limiting step being oxidative dissociation of methane on the Pd sites.

Chin et al. studied the effects of palladium cluster size on the thermodynamics of Pd to PdO phase transitions, to determine the potential impact of these factors for methane oxidation [66]. Their preparation involved impregnation of 0.6 wt. % Pd onto alumina, with treatments at 700, 750, 800, 850 and 900 °C to produce particle of different size & dispersion. For smaller clusters of palladium, they found that the Gibbs free energy of palladium oxide formation is more negative, compared to samples with larger clusters, increasing the tendency for bulk palladium oxidation. As the relative oxygen content increases there is an increase in methane activation, due to the increase in conversion from oxygen adatoms to O^{2-} and Pd^{2+} pairs. These ion pairs offer greater stability to the transition state as compared to the oxygen adatoms, allowing a four centre transition state to form.

Another potential palladium support which has been studied for methane oxidation is multi-walled carbon nanotubes (MWCNTs), which were studied by Gao et al. in 2016 [67]. The MWCNTs were used both fresh, and after treatment with nitric acid, with palladium added from its nitrate precursor using ultrasonic impregnation. The nitric acid treatment increases the amount of carbonyl and hydroxyl surface groups, and these aid the anchoring of Pd precursors to the support, which should improve the dispersion of the Pd across the MWCNTs. Their highest activity came from a catalyst on treated support which had been calcined and reduced post-preparation, whilst the worst activity came from a fresh catalyst, with neither of these post-treatments. They reason that this suggests that Pd(0) is the active species, in disagreement with many previous studies. The catalysts were tested under lean fuel conditions for up to 350 hours, at which point the best catalyst still retained over 90% conversion. The deactivation noted up to this stage seemed to be caused by Pd nanoparticle agglomeration, with particle size increasing from 3 to 10 nm on average. There was also possible partial oxidation of the support, which they expected to enhance the Pd agglomeration. They conclude that though MWCNTs are a promising support, Pd may have to be doped with another metal to improve the catalyst durability, especially in oxygen-rich conditions.

Tab. 1.1 summarises some of the literature discussed here, with various examples of Pd catalysts on alumina and other support materials. This highlights some of the key issues when comparing catalysts from different groups, namely the inconsistency of the experiments. Preparation methods, metal loading, nanoparticle size, gas feed composition, and pre-treatments all tend to vary between groups, making direct comparison of catalysts very difficult, outside of those within a single publication.

Support	Pd, % (Precursor)	Size	CH4:O2	H2O	Activity Notes	Ref
Al_2O_3	Pd, 0.5	-	1:60*	None	100% Conv. by 450 °C	[50]
Al_2O_3	PdO, 3.5	-	1:60*	None	-	[50]
Al_2O_3	Pd, 4 (NO)	2.6	1:20	None	T50 of 330 °C	[68]
Al_2O_3	Pd, 4 (NO)	2.6	1:20	2.7%	T50 of 380 °C	[68]
Al_2O_3	Pd, 1.95 (Cl)	2-8	1:4	None	-	[54]
Al_2O_3	Pd, 3.2 (Cl)	60	1:4	None	100% Conv. by 600 °C	[63]
Al_2O_3	Pd, 2.7 (NO)	12	1:4	None	100% Conv. by 500 °C	[63]
Al_2O_3	Pd, 2.6 (AA)	11	1:4	None	100% Conv. by 425C	[63]
Al_2O_3	Pd, 5.0 (NO)	-	1:25	None	T50 of 320 °C	[69]
Al_2O_3	Pd-Co, 5.0 (NO)	-	1:25	None	T50 of 350 °C	[69]
Al_2O_3	Pd/Co, 5.0 (NO)	-	1:25	None	T50 of 350 °C	[69]
$Ce_{0.2}Zr_{0.8}/Al_2O_3$	Pd, 1.0 (Cl)	-	1:4	None	100% Conv. by 450 °C	[70]
Al_2O_3	Pd, 1.0 (Cl)	-	1:2	None	Max of 30% Conv.	[42]
ZrO_2	Pd, 1.1 (Cl)	-	1:2	None	Max of 50% Conv.	[42]
ZrO_2	Pd, 5.0 (NO)	-	1:12	None	100% Conv. by 350 °C	[60]
MWCNT-D	Pd, 5.0 (NO)	1.5-5	1:50	None	100% Conv. by 340 °C	[67]
Silicalite-Cordierite	Pd, 0.19 (NHCl)	-	1:100	None	100% Conv. by 340 °C	[71]
Silicalite-Cordierite	Pd, 0.19 (NHCl)	-	1:10	None	100% Conv. by 370 °C	[71]
SiO_2	Pd-Co_3O_4, - (Cl)	-	1:20	None	100% Conv. by 420 °C	[72]
SiO_2	Pd-$NiCo_2O_4$, - (Cl)	-	1:20	None	100% Conv. by 370 °C	[72]
MCM-41	Pd, 1.0 (Cl)	-	1:4	None	100% Conv. by 475 °C	[73]
MCM-41	Pd(Plasma), 1.0 (Cl)	-	1:4	None	100% Conv. by 450 °C	[73]

Table 1.1: Table summarising various palladium nanoparticle based catalysts for complete oxidation of methane, from the literature. Where exact temperatures were not given, they are approximated based on the presented data. Where the loading or size are not stated, this is left as ”-”. Cl, NO, AA and NHCl refer to palladium chloride, nitrate, acetyl acetate and dichlorodiamine precursors respectively.

1.3.2 Platinum Catalysts

Platinum catalysts have been commonplace now for a long time, and find use across a wide range of processes. [74–77] Early work on platinum for methane oxidation comes from Firth, mentioned above, who showed that an increase in oxygen pressure decreased the rate of methane oxidation above platinum, an effect which was much more pronounced than for any other metal they studied (Pd, Rh, Ir). [51] Burch, who was earlier mentioned for research on Pd/Al_2O_3, has also studied Pt/Al_2O_3 systems for methane oxidation [78]. Catalysts were prepared at multiple loadings and treatment temperatures, with higher loaded samples having significantly lower metal dispersion, and nearly twice the particle size (1.9 nm for 2% loading compared to 4.4 nm for 10% loading of Pt on Al_2O_3). This meant that, despite having a five times greater loading, the effective amount of platinum surface atoms was only twice as large. They showed that the optimum active surface for methane oxidation is neither fully reduced platinum nor platinum oxide, but that it requires a surface with a mixture of adsorbed oxygen and methane to be effective. This would be consistent with a Langmuir-Hinshelwood mechanism, as opposed to the Mars van Krevelen mechanism which is understood to be the mechanism for methane oxidation on palladium.

Becker et al. studied methane oxidation over alumina-supported platinum using in situ x-ray absorption near-edge spectroscopy (XANES) [79]. They confirmed that an oxygen-rich platinum surface showed lower dissociative adsorption for methane, and thus a lower activity for methane conversion (compared to more oxygen-poor Pt surfaces). Due to this they speculate that such catalysts would likely need to be subject to hydrogen pulses to ensure the surface was reduced for efficient activity. This would not be ideal for scaled commercial use, as an ideal catalyst would be able to be installed and run in the exhaust feed as needed, without needing a pulsed gas feed to reduce it every few hours.

More recently, in 2014, Amin et al. studied the hysteresis in methane oxidation over Pt/Al_2O_3 catalysts [80]. They noted that, in both lean-fuel and stoichiometric feeds, a conversion hysteresis was displayed, with the conversion during extinction being higher than during ignition at a given temperature. This would theoretically mean that high conversion could be achieved at lower temperatures, though this does require initial high-temperature ignition, before a drop in temperature to exploit this effect. The achieved temperature difference was up to 50 °C in these studies, and could be maintained for tens of minutes.

Importantly, this effect was shown to also persist in wet reaction feeds. It is understood that this is related to a range of heat effects, such as the conduction of heat along the catalyst and the convective heat transfer of the inlet gas.

In general, platinum has not been as widely studied for complete methane oxidation as palladium, though there have been a number of papers published on the use of platinum as a catalyst for the related process of partial methane oxidation. [45, 81–83]

1.3.3 Bimetallic Catalysts

Bimetallic catalysts can generally be described as materials which contain two metals which are in some way active for the reaction. It is possible that both metals can be directly active for the reaction, or the presence of one improves properties of the other, increasing the overall activity. Bimetallic systems can take a range of forms, some of which are shown in Fig. 1.7. Bimetallic specifically describes alloyed systems, as shown, but it is often the case that samples which are described as bimetallic will actually be phase segregated, such that the surface comprises of individual nanoparticles of each metal, rather than alloyed nanoparticles. It is possible to have a two metal system where both bimetallic and monometallic particles exist, especially in cases where the mixture is rich in one of the two metals. It is also worth noting that phase segregated nanoparticles could form bimetallic particles upon high temperature annealing, due to the sintering which is often caused by heating. Core-shell nanoparticles have been produced with a range of metals for a variety of purposes, and in general it describes any system where one metal wholly encapsulates the other. Some research has been done where these core-shell structures have been doped, such that a small amount of the "core" metal appears in the shell, and a small amount of the "shell" metal appears in the core.

An early example of bimetallic Pd-Pt catalysts comes from Japan in 1993, where Toshima synthesised a range of colloidal dispersions of bimetallic clusters for the catalysis of the partial hydrogenation of 1,3-cylcooctadiene to cyclooctene [84]. Both metal precursors (hexachloroplatinic acid and palladium (II) chloride) were separately dissolved (in water and ethanol respectively), before being combined and refluxed, to yield the colloidal product. From TEM analysis, the average size of the bimetallic particles was shown to vary depending on the Pd:Pt ratio, although all were between 1.5-2.5 nm. In general, the average particle

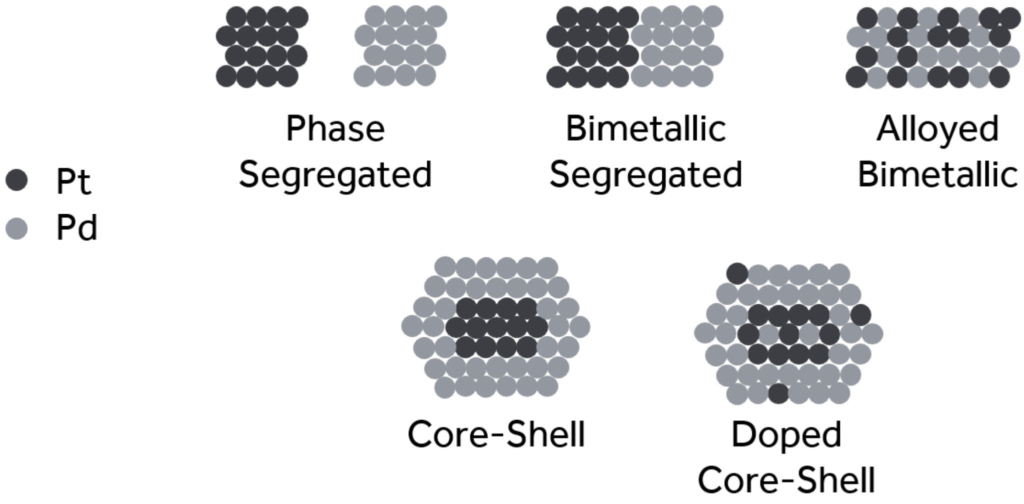

Figure 1.7: Graphical representation of a selection of the possible forms which can be taken by "bimetallic" PdPt Catalysts.

size decreased with increasing Pd:Pt ratio, although in very Pd-rich catalysts (such as Pd:Pt 10:1) that size increases again, and the monometallic particles are larger still. This leads to the suggestion that at highly Pd-rich ratios, it is possible that some particles are purely Pd rather than Pd-Pt bimetallic. Previously, the same group studied these samples using extended x-ray absorption fine structure (EXAFS) [85]. They concluded it was likely that their most active (Pd:Pt 4:1) catalyst formed a Pd shell around a Pt core, whilst a catalyst with a different loading ratio (Pd:Pt 1:1) showed a Pt core with discrete Pd islands on the surface, effectively the same as a core-shell model with an incomplete shell, due to the differing ratios between the metals.

In 1998, Vitos discussed the surface energy of metals, and used density functional theory to calculate that in the cases of the fcc (111), (100) and (110) surfaces palladium had a lower surface energy than platinum [86]. Following this work, in 1999, Ruban, Skriver and Norskov presented a database of segregation energies for binary metallic alloys [87]. They showed that if palladium is the host metal of platinum, there was a moderate antisegregation energy (0.19 eV), meaning that it was preferential for platinum to stay in the bulk, with palladium at the surface. This is consistent with the behaviour mentioned above from the work of Toshima, who showed the Pt formed the core and Pd formed the shell [85]. With the reverse instance, where platinum was the host to palladium, the segregation energy was 0.0 eV, so there was neither preferential segregation nor antisegregation.

Oetelaar et al. studied the surface segregation for Pd-Pt alloys, both as pure alloys, and on various supports including alumina. [88] Significant surface segregation was observed for the alloys, with the surface fraction of Pd increasing with increased temperature for alloys of various compositions, in both hydrogen and oxygen atmospheres. For alumina-supported Pd-Pt, however, there was minimal observed change in the surface fraction of Pd, after heating to 500 °C in either hydrogen or oxygen. In this case, the dispersion of the metal and the lack of bulk palladium are suggested as reasons for the segregation not being readily observed.

A number of groups have made bimetallic nanoparticles using either palladium or platinum, either with other platinum group metal such as ruthenium, or with other cheaper metals such as copper and nickel, which are discussed below. Ruthenium-platinum and ruthenium-palladium bimetallic colloids were prepared by Liu in 1999, as catalysts for the selective hydrogenation of ortho-chloronitrobenzene [49]. In both cases, addition of Pt or Pd generally increased the average particle size, with the Pd-Ru particles typically being larger than the Pt-Ru particles at equivalent PGM loading. Additionally, both were found to form core-shell structures with ruthenium cores, which is consistent with the calculations of Ruban, Skriver and Norskov [87]. Both bimetallic nanoparticles offered improvements to activity and selectivity, and were also more stable than the ruthenium monometallic particles which were prepared using the same method, which used $NaBH_4$ for the reduction of (mixed) metal salts.

Palladium-copper bimetallic methane combustion catalysts, supported on silica, were synthesized by Reyes in 2000 [89]. These were prepared by impregnation and the sol-gel method, depending on the loading of copper. With impregnated catalysts the activity decreased with increased copper loading, which is attributed to Pd-Cu interaction limiting the availability of the active Pd reaction sites. Impregnated catalysts suffered from sintering under the harsh aging conditions, whilst the opposite effect was noticed with sol-gel prepared catalysts.

Palladium-nickel nanoparticles with a variety of core-shell structures were prepared for use as catalysts of Sonogashira cross-coupling reactions by Son in 2004 [90]. In this instance, they discuss the view of “atom economy”, whereby catalysts are designed with a noble metal shell and a cheaper metal core in an attempt to be efficient with expensive materials. They designed discrete core-shell particles in both orientations, as well as mixed core-shell particles with a nickel-rich core and a palladium-rich shell. By comparison to equivalent palladium monometallic catalysts, the Pd-Ni nanoparticles showed superior activity, due to the larger number of particles resultant from the core-shell structure (as the same amount of Pd was used in each case).

Some of the first palladium bimetallic catalysts for methane oxidation were synthesized by Ishihara in 1993, where they found that the addition of NiO increased activity compared to monometallic palladium catalysts [91]. One of the first instances of platinum addition to alumina supported palladium nanoparticles was in 1999 by the Narui group in Japan [92]. In this case, the Pt:Pd atomic ratio was 0.2, and they were synthesized using the impregnation method from $Pd(acac)_2$ and $Pt(acac)_2$. In testing, after 6 hours (under 0.5% methane in air) the $PdO\text{-}Pt/Al_2O_3$ activity was still over 97%, whilst the PdO/Al_2O_3 activity had dropped to around 75%. The average particle sizes were similar for both Pd and Pd-Pt (8.0 and 6.5 nm respectively), however after the activity testing the monometallic particles saw an increase in average size (to 11.0 nm), whilst the Pd-Pt particles were slightly decreased on average (5.7 nm). In addition, the dispersion of Pd was better in the bimetallic catalyst, and was unchanged after testing, whilst the dispersion of the Pd monometallic catalyst decreased.

In 2006, Persson et al. prepared a range of $Pd\text{-}Pt/Al_2O_3$ catalysts, across a range of bimetallic ratios (from 80:20 to 33:67 of Pd:Pt), for methane combustion. [93] The catalysts here were also prepared using co-impregnation from nitrate precursors of both metals. The Pd-Pt catalyst with 80% Pd exceeded the activity of the monometallic palladium catalyst, whilst after these two examples the activity generally decreased with increasing Pt and decreasing Pd (with the exception that the Pt monometallic catalyst showed better activity than the 33% Pd bimetallic catalyst). They noted that the higher loadings of platinum lead to higher resistance to deactivation, and that therefore bimetallic catalysts with either 67% or 50% palladium were optimal. With more Pt content in the bimetallic samples, the Pd became more likely to exist as Pd(0) rather than Pd(II). It is likely that this leads to the low activity of the Pt rich catalysts, as PdO is understood to be a preferential catalyst to Pd for methane oxidation. Further work from the same group also looked into a range of other metals which could be combined with palladium for methane oxidation [94]. They showed that the degree of alloying depended on the second metal - with some forming phase separated particles (such as iridium or silver) and others forming bimetallic alloys (such as gold and platinum). These were all shown to have greater stability than the spinel-structured bimetallic oxide systems that the group synthesized (formed from nickel and cobalt). From this selection, Pd-Pt bimetallic catalysts were shown to combine the best activity with long term stability. As the intention for this group's research was for applications in gas turbines, they performed high pressure testing, with working pressures up to 15 bar, and confirmed that the Pd-Pt catalyst was stable and effective at this pressure.

In the same year, Lapisardi also presented research into the doping of platinum into alumina-supported palladium nanoparticles for methane oxidation [95]. They demonstrated that the addition of smaller amounts of platinum (below a 0.5 molar ratio of Pt:Pd) was beneficial for activity in lean conditions and more beneficial still within a wet reaction feed. A steam aging process (heating at 600 °C in an O_2-N_2 mixture containing 10% H_2O) was used to simulate long term reaction aging, after which the bimetallic catalyst still outperformed the Pd monometallic catalyst. They assert that the improved activity is due to Pt-Pd interactions.

Bimetallic nanocrystals of various compositions of Pd and Pt were studied by Goodman et al. [96] These nanocrystals were deposited onto alumina with a total weight loading of 0.5%, with the metals being well mixed within the nanocrystals. Whilst the best turnover frequency (TOF) was observed initially for a Pd monometallic catalyst, a bimetallic catalyst with Pt : Pd ratio of 1 : 4 showed the best resistance to hydrothermal aging. Their assertion for this is that Pt prevents the formation of bulk PdO. The stable and active phase they define for bimetallic catalysts is PtPd/Pd/PdO.

Satsuma et al. also studied the effects of the preparation method of Pd/Al_2O_3, which they alloyed with cobalt [69]. Cobalt was added in the same amount as palladium (over a range 0.5-5.0 wt. %), and the catalysts were prepared using co-impregnation, as well as sequential impregnation (where the Pd precursor was added to Co/Al_2O_3). For the catalysts with 0.5 wt. % loading (of each metal), the co-impregnated sample gave the best activity, ahead of the sequentially impregnated and a reference palladium monometallic catalyst. The co-impregnated and Pd monometallic were very similar at 1 wt. % loading, whilst at 3 and 5 wt. % loadings the best catalyst was the one prepared by sequential impregnation. They speculate that the sequential impregnation lead to less of a Pd-Co interface than the comparable co-impregnated sample. By comparison to the sequential preparation, the co-impregnation produced a higher dispersion of both Pd and Co.

In 2015, Abbasi studied both the effects of composition and catalytic pre-treatment for Pd-Pt bimetallic methane oxidation catalysts [97]. In dry conditions, the hydrothermally aged Pd-Pt catalysts showed an increase in T50 of 30 °C, which compared to changes of 73 °C for Pd monometallic and 66 °C for Pt monometallic catalysts. Both with and without pre-treatment, the order of activity was Pd > Pd-Pt > Pt. The aged Pd and Pd-Pt catalysts suffered similarly in wet conditions (T50 increased by 58 °C and 64 °C respectively compared to the dry aged test), meanwhile the Pt monometallic aged catalyst was better in the wet feed (lower T50 by 3 °C), although still comfortably the worst catalyst overall in terms of light off temperature (in these experiments, the wet feed contained 5% water). Interestingly they noted that methane conversion is not dependant on pressure over platinum catalysts, whilst for palladium containing catalysts there is a dependance on methane partial pressure. They do however show that this is not the case for wet feeds.

Osman et al. produced a range of Pd-Pt bimetallic catalysts supported on both alumina and ZSM-5 (an aluminosilicate zeolite), with addition of TiO_2 in some cases. [98] All catalysts in this study were prepared using the standard wet impregnation method, from a mixture of palladium (nitrate and chloride) and platinum (ammonia and chloride) precursor salts. They concluded that the acidity of the chosen support material is of huge importance, as the acidity increases the electrophilicity of the metallic palladium species which facilitated re-oxidation, which is possible due to the inclusion of an oxygen carrier in the form of TiO_2. They note however that where the acidity of the support (ZSM-5) is increased too far that the Pd becomes too electrophilic and the redox behaviour becomes less favourable, and so activity is lost. Most importantly, they show that with optimised support and reaction conditions, methane oxidation can be performed at only 200 °C which is lower than is usually reported.

More recently, in 2017, Martin et al. studied methane oxidation over bimetallic Pd-Pt/alumina using operando diffuse reflectance infrared Fourier transform spectroscopy and mass spectrometry (DRIFTS/MS). [99] They synthesized a bimetallic Pd-Pt catalyst composed of 2.4 wt. % total PGM (5:1 Pd:Pt) on alumina using wetness impregnation. Using TEM it was shown that both dry and wet aged (at 800 °C for 10 hours) samples yielded Pd-Pt particles of approximately 50-100 nm particle size, with additional Pd particles of

5-10 nm diameter. These Pd particles were smaller on average than in the fresh samples (treated to only 500 °C for 2 hours), whilst the Pd-Pt particles were not present at all in the fresh sample. It was shown that methane oxidation activity was best when PdO particles started to form on the outside of the Pd-Pt nanoparticles. As expected from the high temperature treatments, it was primarily Pd that formed the exposed surface, whilst Pt was mainly within the Pd-Pt particles. In the lower temperature treatment this effect was not seen. They concluded, in agreement with much of the prior Pd and Pd-Pt work, that the most active phase is the palladium oxide.

Also in 2017, Yashnik studied the effects of various catalyst poisons in the gas feed, and Pt addition, to Pd-Mn-hexaaluminate catalysts for methane oxidation [100]. In terms of activity and resistance to deactivation by both water and sulfur their best catalysts had a Pt:Pd ratio of less than 0.3, which is consistent with the range of "ideal" Pt:Pd ratios that have been demonstrated previously. At higher Pt loadings the effects were less notable. The improvement in these qualities at low Pt loading is attributed largely to the formation of the PdPt alloy, as with previous studies, although they note that the total catalyst should not be comprised of more than 50% PdPt alloy.

Outside of methane oxidation, Pd-Pt bimetallic nanomaterials have been produced for a range of other applications and with a range of novel structures. Lim et al. grew nanocrystals of bimetallic palladium-platinum alloys, using a simple co-reduction synthesis from standard metal salt precursors (K_2PtCl_4 and Na_2PdCl_4) [101]. Different shape nanocrystals were produced by varying the amount of PVP (poly (vinyl pyrrolidone)) added, and the way it was added. At the same time, hollow Pd-Pt nanocubes were being produced by Huang et al. [102], using iodide to give control over the shape of the nanostructures. They showed that hollow nanocube catalysts could be produced using Pd and Pt, which offers a potentially viable catalyst with a significant accessible surface area compared to previous solid nanocubes (in this case, the intended use being for formic acid oxidation electrocatalysis). In 2011, Wang produced Pt-on-Pd nanodendrites, which featured a platinum exterior around a palladium interior (the opposite orientation to that which would likely be best for methane oxidation, and which has been commonly seen for core-shell style catalysts) [103]. This was also achieved by a simple synthesis where the metal precursor salts were mixed with Pluronic P123, mixed and reduced, before being washed and isolated. This yields highly dispersed nanodendrites, with a diameter of less than 15 nm, with composition which is easily tunable by varying the Pd:Pt precursor ratio.

Various groups have reported the synthesis of bimetallic Pd-Pt nanoparticle catalysts, with some of these focused on methane oxidation. In general, the best catalysts have been shown to be palladium rich with some level of platinum doping, although the optimal level of doping has varied from group to group (though typically between 20-50 wt. %). Bimetallic catalysts can take a number of forms, and a variety of these have been prepared. True comparisons of bimetallic to core-shell are lacking for equivalent Pd-Pt ratios, though it is clear that both can be beneficial. Platinum is not, by itself, a strong catalyst for methane oxidation, so it is clear that there is a beneficial effect of Pt on the Pd which is improving activity and stability, though the exact nature of this is not confirmed. It has been widely accepted that the precursors can have a significant effect, and that using palladium or platinum chloride is detrimental for methane oxidation, as compared to nitrates or other typical precursors. This project will aim to determine optimal Pd-Pt ratios for methane oxidation, factoring in activity under varied conditions and atom efficiency and catalyst production cost.

1.4 Supports

When synthesizing heterogeneous catalysts, the support choice is just as important as the catalyst itself. The supports for transition metal catalysts are often oxides, such as alumina, silica, ceria, zirconia and more. [104–115] There are various reasons that supports are useful, with one significant reason being that they allow for a high level of metal dispersion, with the potential to produce very high surface area catalysts. It is generally accepted that ceria and zirconia are also beneficial because of their oxygen mobility, which aids in the oxidation process. This is one of the common ”metal-support interactions”, whereby the support can influence the behaviour of the metal. A major issue which can arise with supported metal nanoparticles is sintering, where the small particles will agglomerate into larger particles, typically induced by high temperatures. This reduces the active surface area of the catalyst, and typically therefore also the activity. Some supports, including ceria-zirconia, can actually show some activity for methane conversion, in addition to increasing the activity of the PGM loaded onto it. [116]

An early paper studying the support effect for Pd/Al_2O_3 catalysts for methane oxidation was published in 1996 by Muto et al. [117], who studied alumina, silica, and a number of silica-alumina mixed supports. All supports were impregnated using $PdCl_2$ to a loading of either 0.5 or 2.0 wt. %. For catalysts with a support comprised of alumina with silica deposited onto it (using chemical vapour deposition (CVD), from $Si(OCH_3)_4$), a loading of 5 wt. % of silica was found to give the best activity over a few hours, though its initial activity was poor compared to that of catalysts with higher silica loadings. Before testing, the Pd dispersion decreased with an increased silica loading, with an exception occurring between 15 and 20 wt. %, where there was a small increase. After testing, all dispersions had decreased significantly, but with the same trend showing, and the 5 wt. % catalyst (which showed the best activity) having the highest dispersion (15%). The exception to this trend is the non-silica loaded catalyst, which showed a significantly bigger dispersion decrease than any other catalyst (67% to 6.3%). This shows a benefit of silica addition using this method, as small amounts of silica prevent sintering occurring as severely. Overall, silica-only support gave the best activity, ahead of alumina, and the mixed supports. It is thought this is the case as silica interacts more weakly with palladium than alumina, which has been demonstrated for silica with other metals.

Yang et al. attempted to determine the active phase of palladium supported on alumina, zirconia, and a silica-stabilized zirconia [118]. In initial tests, the silica-stabilized zirconia showed the greatest activity, with zirconia performing better than alumina. For the zirconia only support, pre-treatment in hydrogen gave better activity than pre-treatment in air. When discussing alumina, their suggestion is that the palladium is in a partial oxide state initially, and it is this oxygen that the methane first reacts with, reducing the palladium to the metallic form. Due to this, they claim that the palladium is in a mixed partial oxide state during the reaction, as $Pd(0)/PdO_x$ (where $0 \leq x \leq 1$). They also attribute the higher performance and stability of the zirconia supports partially to its higher oxygen mobility compared to alumina. Alumina has a far higher thermal conductivity than zirconia, though it decreases heavily over the reaction temperature regime, which is not true of zirconia. It is suggested that because of this, small temperature changes will affect the catalysis above alumina supports much more than it will affect it on zirconia supports, with this explaining the comparatively enhanced stability of activity over zirconia.

Alumina remains a popular support, and Thevenin et al. have used lanthanum and barium to modify alumina, to use as a palladium support [119,120]. Ba and La were added to a total of 3 wt. %, with a Pd loading of 2.5 wt. %, with all catalysts prepared using the impregnation technique. For all catalysts, high temperature aging (1000 °C) lead to much larger particle sizes (80-100 nm compared to 5-10 nm for 500 °C calcination), whilst the surface areas also decreased. The change in surface area was most notable for pure alumina, with La-Al_2O_3 showing the least change. XPS analysis revealed that, after 500 °C calcination, all catalysts consisted of a mix of Pd(0) and Pd(II), and that Ba- and La-doped Al_2O_3 had fully oxidised Pd to Pd(II) after the 1000 °C treatment. The addition of both Ba and La has a negative effect on the activity, however, with undoped alumina showing the best activity for the 1000 °C treated catalysts. With the high temperature treatment, there is a migration of Al to the surface, and the Pd active sites become less accessible. There is also an issue with Ba and La seeming to inhibit the formation of the desired Pd mixed oxide state, which is known to be active for methane oxidation. It was noticed that larger Pd particles interact more with Ba and La than smaller Pd particles do. These supports have also been studied when doped with cerium (with cerium doping occurring before palladium impregnation). Cerium doping increased the surface area for alumina-only supported Pd (when aged at 1000 °C), but made minimal difference to the La- and Ba-doped alumina. There was no change to the Pd(0)/PdO ratio for Pd/Al_2O_3 when Ce was added, although it did enhance the reduction for the other doped supports. For both Ba- and La- doped supports, Ce addition increased the activity, whilst Ce addition to alumina decreased the activity. Yue took the modification of Pd/Al_2O_3 further, using ceria-zirconia mixtures [70]. They showed that addition of Ce-Zr was generally beneficial in terms of stability, with the optimal acitivty and thermal stability presented by the Pd/$Ce_{0.2}Zr_{0.8}$/Al_2O_3 catalyst. This was justified by XPS data showing that this Ce-Zr mix preserves Pd in a higher oxidation state and aids the re-oxidation of Pd(0) to PdO under reaction conditions, helping to aid the long term activity.

Schmal et al. introduced niobia as a potential support, both individually and with alumina, and compared it to the more well-studied alumina and zirconia [42]. Of the precursors they tested, palladium nitrate gave better activity than palladium chloride, which is consistent with other studies. Despite the nitrate precursor leading to less well dispersed Pd, the chloride remains on the surface and inhibits the reaction. Dispersion decreased in the order Al>Nb-Al>Nb, and the catalytic tests reflected this order also with alumina performing better than either niobia containing support. As in previous studies, the zirconia support initially showed lower activity than alumina, but was much more thermally stable, whilst the alumina-supported catalyst deactivates comparatively quickly.

In 2006, Persson et al. prepared a wide range of supports for Pd-Pt nanoparticles [121]. This included the commonly used alumina and zirconia, as well as $LaMnAl_{11}O_{19}$, Ce-ZrO_2 and Y-ZrO_2. Using the BET method, the surface areas for all other supports were significantly lower than for alumina (10-20 m^2g^{-2} compared to 91 m^2g^{-2}). CO uptake was significantly higher on zirconia than on any other catalyst. At low temperatures, PdPt/Al_2O_3 showed the best activity, whilst PdPt/Ce-ZrO_2 had better activity above 620 °C, and above 800 °C PdPt/$LaMnAl_{11}O_{19}$ was best. PdPt/Ce-ZrO_2 showed better re-oxidation of Pd than PdPt/Al_2O_3, a trait which has been noticed for Ce and Zr containing supports previously due to their high oxygen mobility.

Yoshida et al. synthesized a wide range of supported Pd nanoparticles, using ZrO_2, Al_2O_3, MgO, SiO_2, SiO_2-ZrO_2, SiO_2-Al_2O_3 and $SO_4{}^{2-}$-ZrO_2 as supports [122]. Whilst they note that the best activity at low temperatures (623-723K) is achieved over Pd/Al_2O_3 and Pd/SiO_2, the maximum activity is achieved (around 800K) with Pd/Al_2O_3 and Pd/Al_2O_3-SiO_2. By varying oxygen partial pressures over the catalysts (with methane constant), the reaction was determined to be 0-0.1 order with respect to oxygen. The effects of pre-treatment on these catalysts were studied, and for all pre-oxidised catalysts it was seen that the activity was at its maximum initially, before decreasing to a stable rate. Conversely, after pre-reduction, the catalysts generally started with low activity which increased over time. For Al_2O_3 and Al_2O_3-SiO_2 supported catalysts, activity for pre-reduced catalysts was still lower at the end of the test period (4 hours) than the pre-oxidised sample, though this was not true for the MgO supported sample. Analysis of the Pd dispersion showed no significant change for the MgO supported Pd after testing at a range of pressures, whilst Al_2O_3, Al_2O_3-SiO_2, SiO_2-ZrO_2 and ZrO_2 all showed significant decreases after testing. Oddly, the dispersion over SiO_2 increased with testing (the only support to show this effect), although the overall dispersion was still lower than nearly all other catalysts after testing.

The acidity of the support is often considered to be important, and as far back as 1960 alumina was described as having intrinsic acidity. [105] Hensen charactersied amorphous silica-alumina supports to understand their acidity. [123] It was shown that the silica-alumina contained a range of strong and moderate Bronsted acid sites, along with stronger and weaker Lewis acid sites. The presence of the strong Bronsted sites was linked to the reactivity (in this case, for n-heptane hydroconversion). Van den Brand studied the acid-base characteristics of alumina supports using XPS. [124] This involved pre-treating alumina in acid and base conditions, and whilst minor variations were observed between these in XPS, they were often around the level of the error in the experiment. Larger variation was noted when comparing different forms of alumina.

Willis et al. studied the particle size effects for PdO catalysts on alumina, silica, magnesia and a ceria-zirconia support. [125] Alumina-supported catalysts had the highest TOF for any given nanoparticle size, with 3-5 nm PdO being the optimal choice of particle size for most supports. This report also highlighted that avoiding water adsorption on the support is key. Strong particle size effects were also noted by Price et al. for Pd/alumina partial methane oxidation catalysts. [126] Better initial activity was observed over a catalyst with 10 nm palladium nanoparticles, as compared to those with 4-7 nm particles.

There has been a lot of study into catalyst supports for palladium for methane oxidation, primarily focused on alumina. Palladium, platinum, and bimetallic Pd-Pt catalysts will be prepared, starting with alumina as a support material. Following this, silica and two silica-alumina mixed supports will be studied with the same Pd, Pt and Pd-Pt loadings, with the aim to understand support effects on catalyst activity for complete oxidation of methane.

1.5 Catalyst Deactivation

Catalyst deactivation is a significant issue in the real world applications of catalysts. Initial activity tests are often (as in this project) done in ideal gas streams, which are largely devoid of potential catalyst poisons, such as those which would likely be present in the atmosphere that the catalyst would be expected to operate in industrially. It is important therefore that studies are done in gas streams with catalyst poisons, to understand whether the catalysts are commercially viable.

1.5.1 Water

One widely studied catalyst poison is water which, due to being a product of the complete oxidation of methane, is always present around operational catalysts. As such it is crucial that exposure to water does not inhibit the activity of the proposed catalysts. Cullis et al. noted that water caused deactivation of supported palladium catalysts (though not unsupported palladium catalysts), and suggested that this was caused by the formation of palladium hydroxide, as shown in Fig. 1.8. [127]

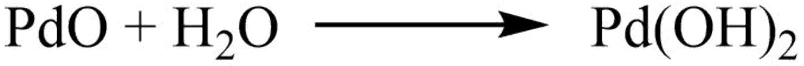

Figure 1.8: The reaction scheme, proposed by Cullis, for the deactivation of palladium oxide by water.

In 1995, Burch studied the effects of both water and carbon dioxide on a range of alumina and silica supported palladium catalysts [68]. For 4% Pd/Al_2O_3 the addition of 2.7% water to the gas feed caused significantly lower activity at low temperatures, but both achieved nearly 100% conversion around the same temperature. By switching the water supply on and off, it is shown that the effects are largely reversed once the water is no longer in the feed, especially at higher temperatures. The effect of addition of CO_2, even as 20% of the gas stream, is minimal by comparison. It is shown by switching the CO_2 supply on and off that the deactivation is reversible. They also studied the effects where both water and carbon dioxide are present. Where there is CO_2 in the feed, the addition of H_2O caused a further drop in activity, which then dropped significantly further when the CO_2 was switched off. When H_2O is also switched off, the activity is near-fully recovered. With the reverse order, where CO_2 is added to a feed with H_2O already present, there is no change in activity, although the conversion is already below 10% anyway in this case. Activity increases sequentially with the removal of H_2O and then CO_2 from the feed.

Van Giezen et al. also studied the effects of water and carbon dioxide, with gas feed loadings of up to 6% each, over a 7.3% Pd/Al_2O_3 catalyst [128]. They determined the reaction orders for the various feed gases, and found them to be: 1.0 for methane, 0.1 for oxygen and -0.8 for water. For their dry feed (1% CH_4 and 4% O_2) the activation energy was determined as 86 kJmol^{-1}, which compared to 151 kJmol^{-1} when 2% water was added to the feed. Ciuparu et al. looked at water deactivation on both zirconia and alumina supported palladium catalysts [129]. They found that the water does not influence the catalytic activity for the metal particles, but does cause deactivation of the metal oxide particles, which is consistent with the proposed deactivation scheme.

Kikuchi et al. looked at a range of oxide supports, which were Al_2O_3, SnO_2 and Al_2O_3-36NiO [130]. With increasing water concentration, the activity of the Pd/Al_2O_3 catalyst decreased continuously. For the SnO_2 and Al_2O_3-36NiO supported catalysts, there was an initial drop in activity with water, but minimal change with increases of water at higher concentrations. All were shown to recover their activity when the water in the feed was switched off, confirming previous studies which showed the effects to be reversible. Zhang et al. studied the effects of water on the PdO (101) surface [131], where they showed that chemisorbed water prevented methane adsorption onto the PdO surface.

A recent study of water deactivation was done by Monai et al. over Pd@CeO2/Si-Al_2O_3. They show a low temperature deactivation, and show that after deactivation at 600 °C the catalyst needs to be heated over 700 °C to be regenerated. They demonstrate the build up of hydroxyl groups on the surface, and postulate that this prevents oxygen spillover from CeO_2 onto Pd, which prevents Pd from re-oxidising to its active state, thus deactivating the catalyst. The effects of ceria doping were studied by Alyani. [132] This showed that ceria addition to Pd on alumina led to smaller amounts of H_2O adsorption, and a higher rate of H2O desorption, which combined give a less inhibiting effect of water.

Recently, Velin et al. studied the water inhibition effect using in situ diffuse reflectance infrared Fourier transform spectroscopy (DRIFTS). [133] They show two differing routes for the hydroxylation of alumina, which is stated to be responsible for the detrimental effects of water on Pd/alumina catalysts. This included the water dissociation on alumina, primarily an issue in the wet condition. Additionally there is the spillover of hydroxyls to the Pd-Al boundary, a site which understood to be important for methane oxidation. DRIFTS was also employed to study surface hydroxyls by Ciuparu. [134] The build up of hydroxyls on alumina was shown to be promoted by the presence of PdO, as a bare alumina showed significantly lower hydroxyl presence, as compared to a PdO/alumina catalyst. Additionally, the benefit of the higher oxygen mobility in supports such as ceria was shown, with this contributing to greater de-hydroxylation and greater catalyst activity in wet conditions as a result. Digne et al. performed density functional theory (DFT) calculations to understand the behaviour of hydroxyls on alumina surfaces, and the acid/basic properties of the alumina. [135, 136]

Work by Losch et al. focused on the hydrophobic/hydrophilic nature of the support, as a way to optimise catalyst functionality in wet operation conditions. [137] Their optimal catalyst was supported on a mesoporous zeolite beta, with a Si/Al ratio of 40. Water temperature programmed desorption (TPD) experiments showed that this support desorbed significantly less water than alumina, or other tested zeolites, within the relevant temperature range. With only 0.5 wt.% loading, this catalyst reached 50% conversion by 355 °C. This testing was conducted with a methane:oxygen:water ratio of 1:8:8.4, which is fairly low relative oxygen and water levels, as compared to some typical reaction feeds. However, it still shows the significant benefits of using a more hydrophobic support.

Work by Gholami et al. concluded that there are three effects of water presence that lead to lower activity: water adsorption; palladium hydroxide formation; and water-assisted sintering of palladium. [138] The latter is only relevant at higher temperatures, and is irreversible, whilst the water adsorption and hydroxide formation are reversible.

Doping Ba into Pd/alumina was studied as a method of reducing water inhibition by Friberg. [139] There was a notable benefit when the catalysts were regenerated at lower temperatures (below 600 °C). The benefit was not seen to be directly related to an increase in oxidation of methane, and no differences in water adsorption/desorption were seen.

In real conditions water will not be the sole potential poison, and will appear with other gases such as SO_2 and/or NO. A combined study of NO and H_2O by Olofsson showed a promotional effect of NO, which was proposed to be the result of NO and OH reacting, reducing the hydroxyl presence on the surface, and reducing the deactivation by water as a result. [140]

Whilst there have clearly been a range of studies on the effects of water as a catalyst poison for monometallic catalysts, there is very little study on water as a poison for bimetallic catalysts. This project aims to improve the understanding of the effects water has on these types of catalysts. It also will aid understanding as to whether the addition of Pt to Pd can help to prevent water poisoning, and why this effect arises if so.

1.5.2 Sulfur

Another poison which has been discussed for methane oxidation catalysts is sulfur, both from SO_2 and H_2S. Yu et al. studied the poisoning effect of H_2S on PdO/Al_2O_3 [141]. They demonstrated that the poisoning effect was as a result of the formation of palladium sulfide at low temperatures, and then the formation of aluminium sulfate at high temperatures, a reaction which they claim is promoted by the PdO. The surface area of the catalyst decreases with increased poisoning temperature. After regeneration at 600 °C, some of the activity was regained, but conversion was still worse compared to the fresh catalyst.

Mowery studied the effects of SO_2 in the gas feed for both PdO and Pd/Al_2O_3 [142]. It was demonstrated to cause deactivation in dry reaction feeds, with these effects worsened in wet feeds. In the wet feed, the deactivation was attributed (by in situ infra red spectroscopy (IR)) to the formation of $PdSO_4$ and $Al_2(SO_4)_3$, similarly to the work of Yu. [141] They show that the addition of water leads to an inhibition of spillover of SO_2 from PdO to alumina, leading to a greater formation of $PdSO_4$ and therefore greater deactivation. $PdSO_4$ is also produced on the unsupported palladium sample.

Later, Jones et al. studied the effects of sulfur poisoning over Pd, Pt and Rh supported on alumina [143]. Their poisoning mixture contained a total of 10 ppm of sulfur, and was comprised of a mix of ethyl mercaptan (ethanethiol), methyl mercaptan (methanethiol), carbonyl sulfide and hydrogen sulfide. Of the three, they showed that the Pd catalyst was affected the least, and is easier to regenerate compared especially to Pt, with Rh showing an intermediate behaviour.

Monai, who had previously studied water posioning, has more recently studied sulfur poisoning (by SO_2) for their catalysts based on $Pd@Ce_xZr_{1-x}O_2$ [43]. They too attributed the deactivation to the formation of $PdSO_4$ forming from the active PdO phase. At higher temperatures (over 500 °C), they noted spillover of SO_2 onto the support. $Pd@ZrO_2$ catalysts showed the best resistance to sulfur poisoning, along with having the easiest regeneration.

The relative sulfur resistance of Pt and Pd was compared by Sharma. [144] Pt was seen to be significantly less poisoned than Pd under relevant reaction conditions. This was assigned to the greater likelihood of oxide presence for Pd than Pt. Palladium sulfate and adsorbed sulfur species were favoured, whilst platinum sulfate did not occur.

Bounechada et al. investigated the effects of sulfur dioxide on platinum catalysts supported on alumina, ceria and silica. [145] Sulfur was found to enhance methane oxidation for Pt/alumina, but inhibit activity for Pt/silica. This inhibition on silica was explained by the sulfur dioxide competing with methane for oxidation, whilst new active sites at the metal-support interface caused the benefit for the alumina sample. On ceria there is an initial activity enhancement with sulfur dioxide addition, but after longer term exposure the effect becomes detrimental, with the latter attributed to the formation of bulk sulfate species. The effects of sulfur dioxide on ceria-supported platinum were also studied by Kylhammar et al. who primarily used in situ FTIR. [146] Their findings agree with those of Bounechada, with initial promotion but long term inhibition of methane oxidation, again assigned to the build up of sulfates on ceria, which inhibits the oxygen mobility between ceria and platinum, forcing the platinum to remain in an unfavourably oxidised form.

As with the water section discussed previously, there is very little research into sulfur deactivation of Pd-Pt bimetallic catalysts. If these catalysts are to be relevant commercially, then there needs to be a better understanding of the deactivation which can be caused by the gas feeds in which they will need to operate.

2 Experimental

2.1 Preparation

2.1.1 Powder Catalysts - Incipient Wetness Impregnation

Label	Pd:Pt (wt. %)	Support	Variants
AL1	0:5	γ-Al_2O_3	Dry F500 F800 SCAT F900
AL2	1:4	γ-Al_2O_3	Dry F500 F800 SCAT
AL3	2.5:2.5	γ-Al_2O_3	Dry F500 F800 SCAT F900
AL4	4:1	γ-Al_2O_3	Dry F500 F800 SCAT
AL5	5:0	γ-Al_2O_3	Dry F500 F800 SCAT F900
AL6	4:0	γ-Al_2O_3	Dry F500 F800 SCAT
AL7	2.5:0	γ-Al_2O_3	Dry F500 F800 SCAT F900
AL8	1:0	γ-Al_2O_3	Dry F500 F800 SCAT
AL9	0:4	γ-Al_2O_3	Dry F500 F800 SCAT
AL10	0:2.5	γ-Al_2O_3	Dry F500 F800 SCAT F900
AL11	0:1	γ-Al_2O_3	Dry F500 F800 SCAT
AL12	2.5:2	γ-Al_2O_3	Dry F500 F800 SCAT
AL13	2.5:3	γ-Al_2O_3	Dry F500 F800 SCAT
AL14	0:5	SiO_2	Dry F500 F800 SCAT
AL15	2.5:2.5	SiO_2	Dry F500 F800 SCAT
AL16	4:1	SiO_2	Dry F500 F800 SCAT
AL17	5:0	SiO_2	Dry F500 F800 SCAT
AL18	0:5	$40SiO_2$-$60Al_2O_3$	Dry F500 F800 SCAT
AL19	2.5:2.5	$40SiO_2$-$60Al_2O_3$	Dry F500 F800 SCAT
AL20	4:1	$40SiO_2$-$60Al_2O_3$	Dry F500 F800 SCAT
AL21	5:0	$40SiO_2$-$60Al_2O_3$	Dry F500 F800 SCAT
AL22	0:5	$10SiO_2$-$90Al_2O_3$	Dry F500 F800 SCAT
AL23	2.5:2.5	$10SiO_2$-$90Al_2O_3$	Dry F500 F800 SCAT
AL24	4:1	$10SiO_2$-$90Al_2O_3$	Dry F500 F800 SCAT
AL25	5:0	$10SiO_2$-$90Al_2O_3$	Dry F500 F800 SCAT

Table 2.1: Table showing the Pt and Pd loading for each catalyst, along with the variants prepared.

For all powder catalysts prepared within this project, incipient wetness impregnation (also referred to as dry impregnation) was used. This consisted of adding metal precursor(s) -

palladium (IV) nitrate and platinum (IV) nitrate - to a powdered oxide support (alumina, silica and silica-alumina). [147] For bimetallic catalysts, the precursors were mixed before addition to the support. After addition and mixing, the samples were dried at 120 °C for 4 hours to remove the nitrates from the precursor. The samples were then calcined at 500 °C for 2 hours in a static air ager. All heat treating was performed on samples in ceramic boats.

Small amounts of all samples were then treated at 800 °C in the same way, with a selection also treated at 900 °C to study the effects of high-temperature aging (both also performed for 2 hours in static air). Heat treated samples will be referred to as F500, F800, or F900, to reflect these temperatures. Activity tested samples will be referred to as SCAT. All prepared samples are shown in Tab. 2.1. All F800, F900 and SCAT versions were prepared from F500 samples, unless otherwise stated. All F500 samples were also pelletized for activity testing (and thus all SCAT samples are pellets rather than powders). Generally pellets will break down after months of storage, so samples were re-pelletized before testing if they had not been used for longer than this.

Throughout this thesis, the loadings of platinum and palladium are generally reported as weight percentages (wt.%) with respect to their support material. This is the standard reporting method for heterogeneous catalysts, but it is important to note this when considering multiple metals, and differing supports. The 2.5Pd-2.5Pt catalyst, for example, has 2.5 wt.% of each palladium and platinum. These metals, however, vary significantly in atomic weight, at 106.42 u for Pd and 195.08 u for Pt respectively. This means that, for a typical batch of catalyst which uses 20 g of alumina, there would be $2.83\text{x}10^{21}$ atoms of palladium, but only $1.54\text{x}10^{21}$ atoms of platinum, giving an atomic ratio of Pd : Pt of 1.83 : 1 for a catalyst with equal weight loadings of each metal. This is similarly a consideration when comparing catalysts supported on silica and alumina. Whilst 20 g of both would typically be used here, the molar masses again vary significantly (60.08 for SiO_2 and 101.96 for Al_2O_3). This, combined with the above, means that the metal : support atom ratio varies significantly. Per atom of active metal, the amount of support molecules can therefore be as low as 42 (Pd/Al_2O_3) or as high as 130 (Pt/SiO_2) within these parameters (based on 2.5 wt.% catalysts).

2.1.2 Single Crystals

For the single crystal studies, a Re0001 single crystal was used as a substrate for deposition. This is used because the lattice parameters of the crystal and deposited palladium and platinum are very similar [148]. The nearest neighbour distances are 2.75, 2.77 and 2.74 $\AA$ for Pd, Pt (both face-centred cubic(fcc)) and Re (hexagonal close-packed (hcp)) respectively. [149] Thin layers of palladium and platinum were deposited using an Oxford Instruments EGN4 evaporator. Palladium was evaporated at approximately 27 W and 11 nA, whilst platinum required 40 W and 11 nA. Over distances around 10 cm these conditions gave 1 ML of PGM after approximately 5 minutes. The crystal was typically heated to approximately 150 °C during deposition, whilst cleaning was typically performed by a high temperature (1500 °C+) flash. In some cases, where this temperature was not reachable (such as at the Materials Science beamline at Elettra), it has been found that (so long as there is a small amount of PGM on the surface) any carbon, oxygen and palladium can be removed by a cleaning cycle of 10 minutes in oxygen ($1\text{x}10^{-7}$ mbar) at 700 °C followed by 10 minutes in UHV at 500 °C. And example of the removal of Pd by this process is shown in Fig. 2.1. For removal of platinum, currently the crystal needs to be flashed to approximately 2000 °C, so it was not possible to remove this from the Re(0001) crystal during the beamtime at Materials Science, Elettra.

2.1.3 Thin Oxide Film Supported Model Systems

Spin Coating Process

3-micron γ-alumina powder was purchased from Alfa-Aesar. The powder was mixed with a solvent (variously water, ethanol or methanol) and spin coated onto (approximately) 1cm^2 silicon wafers (phosphorous doped, with or without a thin gold layer on the reverse side). Exact values for spin speed, acceleration, etc varied, and will be summarised in the relevant results section.

Anodization Process

A platinum electrode of approximately 25 mm x 4 mm was used. Aluminium pieces (0.5 mm thickness, 25 mm x 25 mm, Goodfellow) were cut to approximately 25 mm x 6 mm. Initially, pieces were not washed before anodization. Approximately 5 mm of the aluminium was kept

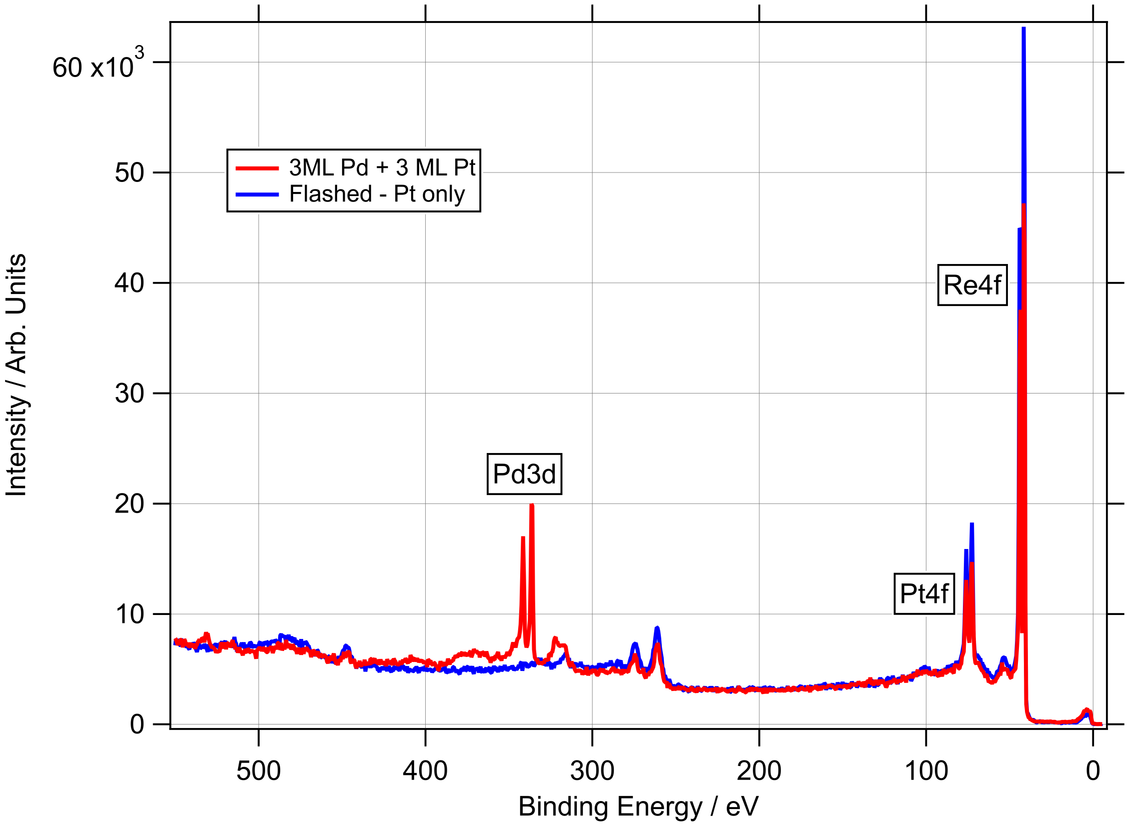

Figure 2.1: Survey XPS spectra from before and after a 1200 °C flash of thin films on a Re(0001) single crystal. Spectra recorded at 650 eV photon energy.

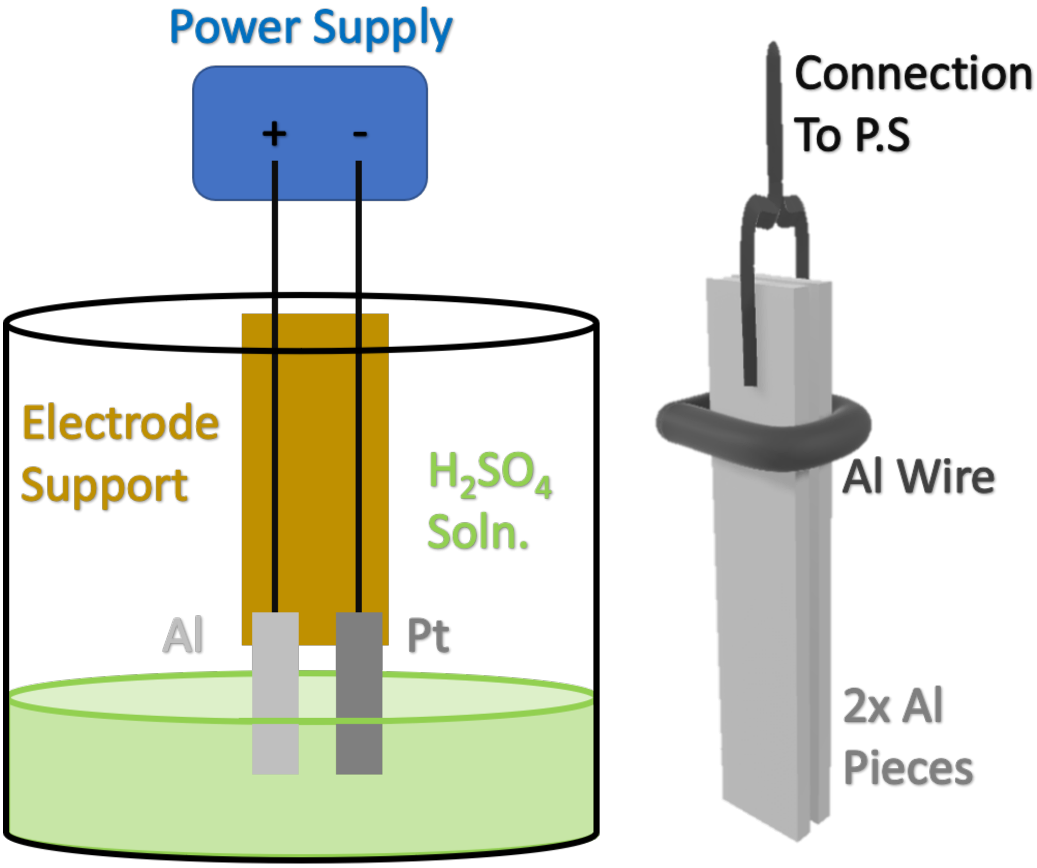

Figure 2.2: A diagram showing the setup used for anodization of aluminium pieces. Left: diagram showing overall process set up. Right: diagram showing the two aluminium pieces being held back to back by an aluminium wire wrapped around them. Components not shown to scale.

out of the sulfuric acid solution, to allow for the connection to the power supply, giving an oxidised area of approximately 80 mm^2. Two strips of aluminium were placed back to back to ensure anodization only occurred on one side of each piece. The pieces were held together with a twisted aluminium wire, and connected to the electrochemical set up, as shown in Fig. 2.2. After the anodization process, films were cleaned by sequential sonication treatments in water and ethanol. Exact parameters used for the anodization process are summarised in section 5.2.2. The sulfuric acid solution had a concentration between 0.2-1.3 moldm^{-3}, with a total volume of up to 3 mL. The current used was between 0.001-0.03 A, for a total anodization time of 600-3600 s.

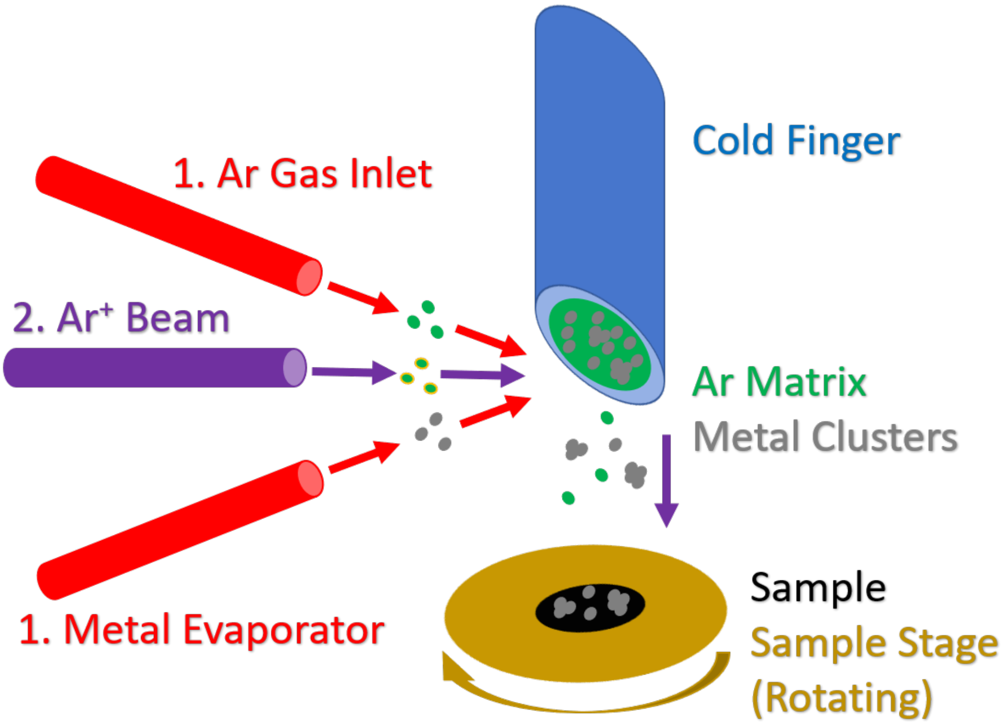

Figure 2.3: A diagram showing the setup of the Matrix-Assisted Cluster Source used during this project, at Swansea University.

2.1.4 Cluster Source Nanoparticle Deposition

A new approach to the preparation of nanoparticles for catalysts without the use of solvents is the use of a matrix assisted cluster source (MACS). General operation of this instrument to prepare nanoparticles is described by Palmer and Xu. [150, 151] A diagram showing the simplified process is presented in Fig. 2.3. Nanoparticles of palladium were deposited onto various flat oxide surfaces, prepared as described above. Palladium was evaporated in an argon environment (approx. 10^{-6} mbar), with the result being a matrix of palladium and argon formed on a cold plate. This was then bombarded with high energy argon ions, with the palladium clusters breaking away and falling onto the sample plate, which is continually rotated to ensure an even coverage. The sample plate can hold multiple wafers at a time, ensuring consistency between a number of samples. A copper TEM grid is also placed on the rotating plate, along with the samples, such that the deposited clusters can be analysed.

2.2 Analysis

2.2.1 X-Ray Photoelectron Spectroscopy (XPS)

Principles of XPS

X-ray photoelectron spectroscopy (XPS) is an analytical technique offering surface sensitive characterisation of all elements aside from hydrogen and helium (due to their lack of core electrons). [152] XPS is based on the fundamental principles of the "photoelectric effect". This was first observed by Heinrich Hertz in 1887, who noticed that when illuminated by ultraviolet light, the voltage required to cause a spark (in a spark gap generator) changed. [153] Later studies by Philipp Lenard and J.J. Thomson explained that electrons can be released from a metal surface under illumination. [154] In 1905, Albert Einstein theorised that light was composed of tiny particles of light which each contained an amount of energy which was dependant on the frequency of the electromagnetic radiation. [155] He assumed that when a material was exposed to radiation, a photon could penetrate that material and transfer its energy. This energy, diminished by a material specific work function (ϕ), would be transferred to an electron in the material. This, less the binding energy (E_b) of the electron, becomes the kinetic energy (E_{kin}) of the emitted electron. The equation describing the relationship between the incident radiation and the binding energy of the released electrons is stated in Eqn. 2.1, where h is Planck's constant, ν is the frequency of the incident x-ray.

$$h\nu = E_{kin} + E_b + \phi \tag{2.1}$$

The binding energy of an electron is an element specific property, and as such XPS can be used for elemental analysis. Further, the oxidation state can be determined for many elements, due to slight shifts in the binding energy (E_b) caused by differing chemical environments. For reference purposes, databases of binding energies are available, which generally include information about a wide range of possible compounds of each element. A diagram showing the basic process of the emission of a core electron to the vacuum, is presented in Fig. 2.4.

Emitted electrons will travel a distance known as the inelastic mean free path (IMFP), which is defined as the distance an electron can travel before its intensity decays to 1/e of its initial energy. The IMFP is dependant on the kinetic energy of the electron (with a

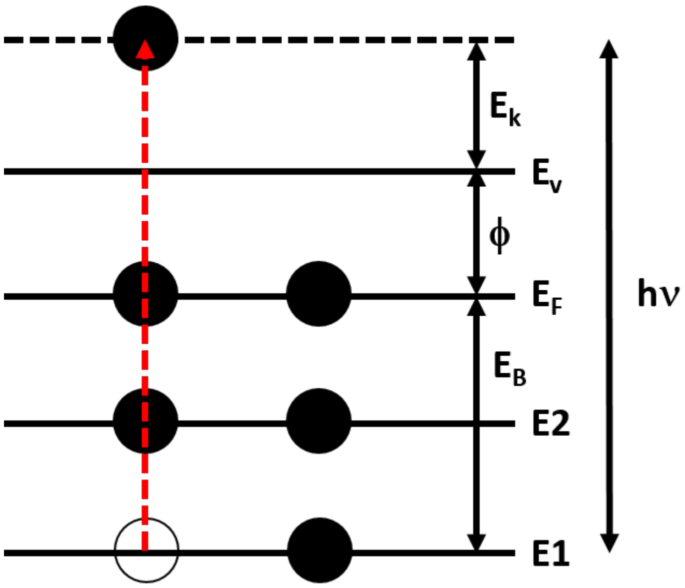

Figure 2.4: Diagram showing the electron emission process, where E_v, E_f, E1 and E2 represent the vacuum, Fermi, primary and secondary core energy levels respectively. E_K, and E_B represent the kinetic and binding energies of the emitted electron. ϕ represents the work function of the material, and hν is the energy of the incident x-ray.

typical value of up to 10 nm through solid materials). These emitted electrons travel from the sample through the electron optics section will focus the emitted electron beam into the hemispherical analyser. The hemispherical analyser consists of a positive inner plate and negative outer plate (in terms of relative potential), which ensures only electrons of the desired energy (E_{kin}) are passed to the detector. In Eqn. 2.2, e is the charge on an electron, ΔV is the difference in potential between the inner and outer plates, and R$_1$ and R$_2$ are respectively the radii of the inner and outer hemispheres.

$$E_{kin} = e\Delta V \left(\frac{R_1 R_2}{R_2^2 - R_1^2} \right) \tag{2.2}$$

Shown in Fig. 2.5 is a simplified diagram of the key elements of an x-ray photoelectron spectrometer.

Lab Sources

X-ray lab sources follow the basic process of x-ray fluorescence. A source of electrons is used, such as a heated tungsten wire or LaB$_6$, which emits electrons towards the anode, across a large potential difference. Upon bombardment, the anode will emit characteristic x-rays.

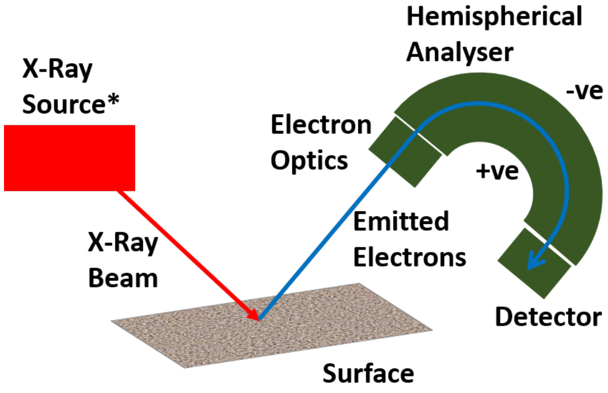

Figure 2.5: Diagram showing the important sections of an ultra-high vacuum x-ray photoelectron spectrometer.

Some commonly used lab source anodes include Mg Kα with an energy of 1253.6 eV and Al Kα with an energy of 1486.6 eV. All laboratory XPS data within this work was recorded using an Al Kα source.

Synchrotron Sources

In a synchrotron, electrons are emitted from an electron gun, and accelerated (to around the speed of light) around a ring by a series of accelerators. When they reach this speed they are injected into the main ring, where they are bent around the ring by magnets, whereby the resulting emitted radiation is channelled into individual beamlines. The beam of incoming radiation is then tuned by a series of mirrors before reaching the end station, where it is used for sample analysis.

There are a range of key advantages of synchrotron radiation over lab sources. For one, there is a much higher brilliance of the beam (a much higher photon intensity), which can allow for a much faster rate of data acquisition. Additionally, synchrotron radiation spans a wide range of photon energies, which can be tuned via the use of a monochromator. This allows us to maximise the photoionisation cross-section (the probability of an electron being emitted) for given elements, increasing signal and potentially further reducing analysis time required. There are databases of cross-sections, so photon energy can be tuned to the composition of the sample. This allows for more effective depth profiling of the materials, as the higher photon energies will cause electrons to be emitted with higher kinetic energy, allowing them to travel further.

Ultra-High Vacuum (UHV-XPS)

Since its inception, XPS has primarily been operated under ultra-high vacuum (UHV, typically $<10^{-9}$ mbar) conditions, as is consistent with other surface science techniques (such as electron microscopy). This has generally been of use as it ensures the likelihood of emitted electrons being scattered before reaching the analyser is greatly reduced, and as such the intensity of the signal is greater. The signal intensity (I) is related to the electron travel distance, d, the pressure, p, and the cross-section of the scattering, σ by Eqn. 2.3. [156]

$$I \sim e^{-(\sigma d p)} \tag{2.3}$$

Further, it is of benefit in keeping the surface clean of contaminants. This ensures the surface (and resultant spectra) are consistent across the analysis time, and are indeed representative of the intended, ideal surface. Indeed, the sticking probability is directly related to the pressure and the rate of monolayer formation. [157] This is particularly relevant to the model systems researched in this project, where analysis will be run over many hours, and so ideally there should be minimal carbon build up on the surface over the reaction time. UHV conditions in XPS are achieved by the combination of turbo molecular pumps and ion pumps, which pump gaseous molecules out of the chamber. For typical UHV chambers, it will be necessary to bake-out the chamber after it has been opened (for sample changing, etc) which requires the chamber to be covered and heated to over 100 °C to remove water and other contaminants.

Near Ambient Pressure (NAP-XPS)

NAP-XPS allows for the collection of XPS data whilst the sample is exposed to an atmosphere (currently up to 10-100 mbar, depending on the set up). This is possible due to a differential pumping system between the experimental chamber and the analyser, which ensure electrons from the surface still reach the analyser whilst the gas is removed. [158] An example of this system, as used at ”VerSoX” (Diamond Light Source beamline B07-C) is shown in Fig. 2.6. Whilst this pressure range is not equivalent to that used in a conventional catalytic reactor - 1 bar in our set up at Johnson Matthey, but often above 1 bar for other reactions - it is generally enough to see reaction progress, as monitored by a mass spectrometer connected in the first differential pumping stage of the analyser.

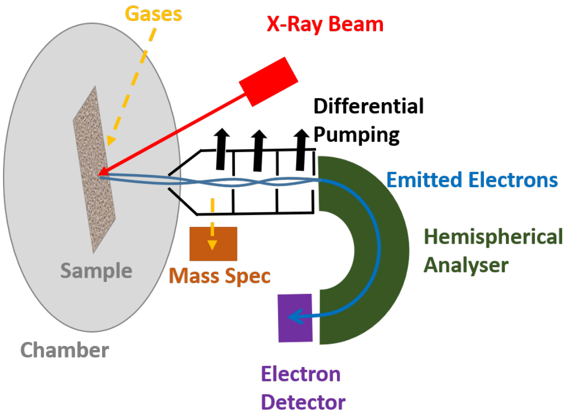

Figure 2.6: Diagram showing the important details of the NAP-XPS "Tea Pot" endstation at the B07 beamline at Diamond Light Source. Components not to scale.

The construction and functionality of the VerSoX beamline at Diamond Light Source is described in detail by Held et al. [159]. Additional NAP-XPS experiments were performed at beamlines with differing experimental set ups to VerSoX. These were the HIPPIE beamline at MAX IV, and X07DB NanoXAS at Swiss Light Source, which are described by Schnadt et al. and Novotny et al. respectively. [160, 161].

Spin-Orbit Splitting

Most of the elements of interest in this project (Pd, Pt and Al) have orbitals which show spin-orbit splitting. This feature, which is a splitting of a peak to two peaks, arises where an orbital has an angular momentum quantum number (l) > 0. This arises due to the coupling of the electron spins with the orbital angular momentum, and gives two states with total angular momentum quantum numbers (J) of l±0.5, with a fixed peak to peak area ratio, as shown in Tab. 2.2. For a given element and peak, there is a characteristic splitting between the two peaks. For example, the gap between Pd $3d_{5/2}$ and Pd $3d_{3/2}$ is approx. 5.26 eV, whilst the difference between Pt $4f_{7/2}$ and Pt $4f_{5/2}$ is only 3.35 eV.

Chemical Shifts

The binding energy (E_b) is dependant on a range of chemical properties including: the core level it is removed from; the oxidation state of the atom it is removed from; and the chemical and physical environment of the atom. For an emitted electron the binding energy is defined

Subshell	l	J	Peak area ratio
p	1	3/2, 1/2	2:1
d	2	5/2, 3/2	3:2
f	3	7/2, 5/2	4:3

Table 2.2: Table of angular momentum quantum numbers for the p, d and f sub-shells, along with the peak-to-peak area ratios.

as the difference in energies of the initial state electron N wavefunction and the final state electron N-1 wavefunction, as shown in Eqn. 2.4 [162].

$$E_b = E^{N-1} - E^N \tag{2.4}$$

Whilst core shell electrons are not directly involved in chemical bonding, they are affected by changes in valence electron shell structure. As oxidation state increases, the number of valence shell electrons will decrease, and as such the attraction between the nucleus and the emitted electron will increase. This is reflected in the XPS spectra as a shift to higher binding energy of the electron, as it is emitted with a lower kinetic energy, compared to an equivalent electron from an equivalent atom from a non-oxidised sample. A relevant example of this shifting is palladium, where the Pd $3d_{5/2}$ peak shifts from 335.0 eV as Pd(0) to 336.3 (as Pd^{2+} in PdO) to 337.9 (as Pd^{4+} in PdO_2) [163]. Therefore, to be able to accurately assign the peaks to the correct oxidation state, it is important to record high resolution spectra.

Another type of chemical shift which is often observed is surface core level shift (SCLS). As the surface atoms are less coordinated than the bulk atoms, the valence bandwidth is narrower, which increases the density of states. Depending on the valence band filling and therefore the band centre position, the binding energy can increase (if more than half is filled) or decrease (if less than half is filled). These shifts will typically be smaller than the shifts caused by a change in oxidation state, and are likely to be less than 1 eV.

XPS Sample Preparation

Samples were prepared for UHV-XPS by applying powdered catalyst to carbon tape, which was attached to a stub and inserted into the spectrometer. In the case of pelletized samples (for example, those which had already undergone catalytic activity testing), the pellets were crushed to avoid excessively thick layers, and the significant charging that would have resulted.

Samples for NAP-XPS were prepared by a number of methods. The first was spray coating, where the catalyst was mixed with water and adhesive (Disperal P3, a form of alumina), with the ratio 1 : 10 : 30 (adhesive : catalyst : water), which was spray coated onto (phosphorous-doped) silicon wafers. This method deposited a few milligrams of sample onto the wafer (approx. 1 cm^2), which is theoretically good for ensuring a good signal, but also leads to significant charging issues. In theory this could also be tuned to give a thinner layer, but even reducing thickness this way proved to give significant charging.

The second method was grinding, whereby the catalyst sample was placed onto a silicon wafer, with another wafer pressed and ground against it, leaving a thin layer of catalyst. The grinding method gave a thinner layer, which is more beneficial for reduction of charging (discussed below) but can be worse for signal, especially when studying low loadings of metal (such as the 1 wt. % Pt or Pd which have been prepared). Due to charging issues experienced using P-doped silicon, these wafers were replaced with silicon wafers with a thin gold layer on the reverse side, to improve conductivity.

With both of these methods proving problematic with regards to sample charging under the x-ray beam, a new approach had to be used. The sample mixtures were prepared as per the spray-coating method, but then simply dropped onto the wafers using a pipette. The wafer is then heated to 120 °C to remove the water. Depositing just a few drops provides less than 1 mg of sample, in an often inconsistent layer, but does normally provide a thin enough area of sample which exhibits minimal sample charging during analysis. This method was also used without the addition of P3, as it was feared that the presence of this additional aluminium species could cause confusion during the interpretation of the aluminium spectra.

XPS Analysis

X-ray photoelectron spectroscopy (XPS) was to be used in the two forms previously described: Near ambient pressure (NAP) and ultra high vacuum (UHV). Following general wide survey scans the key areas (with binding energies in eV) which were scanned were: Al 2p-Pt 4f (65-85); C 1s (275-295); O 1s (520-540); and Pd 3d-Pt 4d (305-350). This was to be used to determine the elemental composition of the samples, along with the chemical states for each element. The quoted binding energies are the typical values, but higher values were needed for samples with significant levels of charging. Pt 4f would ordinarily be the only platinum region studied, however it overlaps nearly completely with the Al 2p peak, so the Pt 4d is recorded instead. For single crystal and metallic foil work, where aluminium is not present, the Pt 4f is used. The cross sections for the relevant elements are shown in Fig. 2.7. At lower photon energies, the Pt 4d has a much lower cross section than the Pt 4f, but at higher energies the cross sections are comparable.

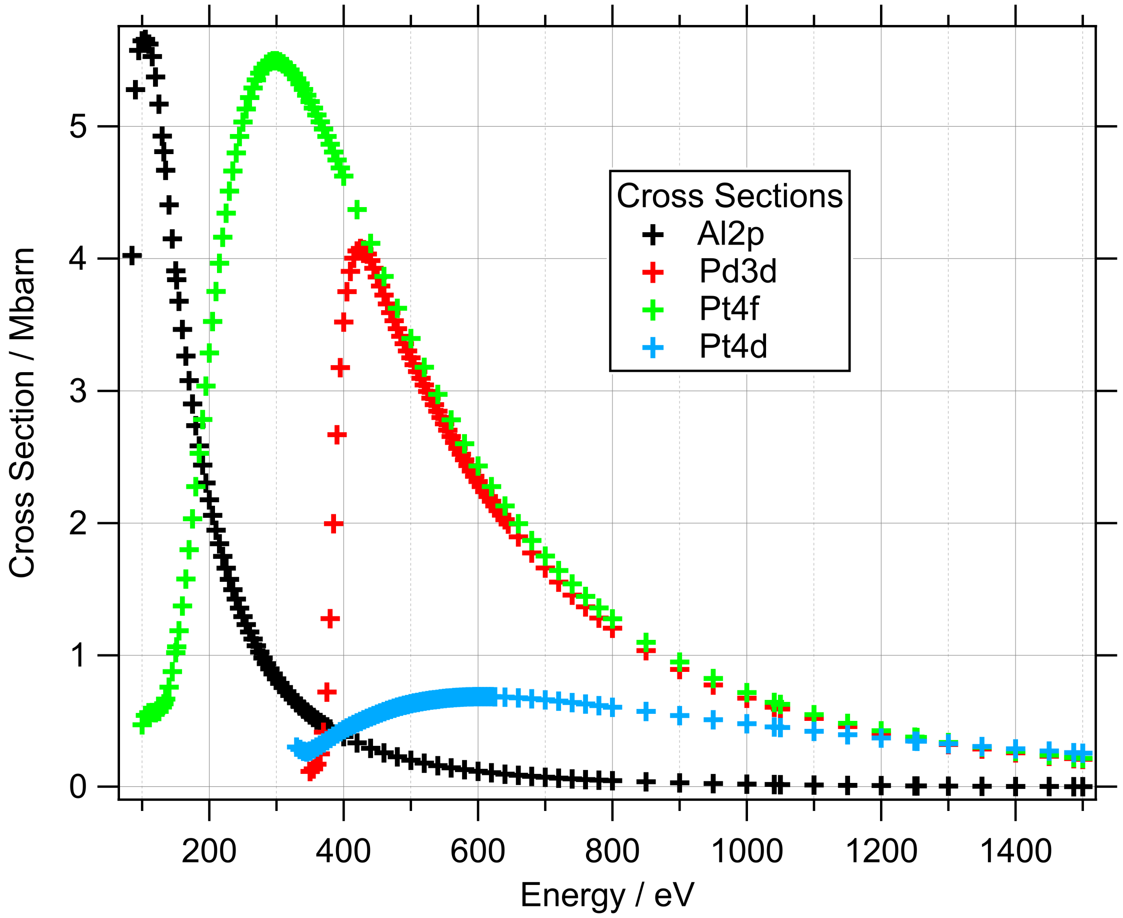

Figure 2.7: Photoionization cross section data for Al 2p, Pd 3d, Pt 4f and Pt 4d.

A consideration which arises for XPS analysis at synchrotron sources is photon energy. With the use of a monochromator, synchrotrons will allow for the selection of a wide range of energies for XPS measurements (varying by facility, but typically within the range of 200-1500 eV). This can be used to vary the information depth of the analysis, with lower photon energies being much more surface sensitive. However, for a given sample some photon energies will be unusable due to the presence of Auger electron peaks. These occur at a fixed kinetic energy, and therefore the binding energy they appear at is dependant on the photon energy of the x-ray source. For our typical alumina supported samples, a range of photon energies (1350, 900, 700 and 450 eV) were selected where no Auger peaks are in areas of interest. For most of the presented synchrotron analysis, 1350 eV was used as the photon energy. All of the laboratory UHV-XPS presented used a photon energy of 1486.6 eV (Al Kα).

Charging

For the alumina supported samples, the issue of charging arises, due to alumina being an insulating material. Charging is the phenomenon where, due to repeated electron emission, a positive charge is built up on the sample. As the sample is non-conductive (or only partially conductive in some instances) the positive charge cannot be removed. This positive charge will increase the attraction to the remaining core electrons, and so the kinetic energies of these core electrons decreases which, according to Eqn. 2.4, corresponds to an increase in apparent binding energy. There are a few ways that charging can be dealt with, depending on sample and equipment set-up. To reduce the chances of charging being an issue for insulating samples in this project, the preparation method attempts to ensure a very thin layer of catalyst is deposited on the conductive wafer support. This ensures any charging effects are minimised, typically to < 10 eV for our samples. For some examples, where a pellet is a preferred sample form, it is not so practical to minimise thickness in this way. For these cases there are additives which can be used in sample preparation, such as carbon powder or tantalum mesh, which can increase the conductivity, however these may not be useful depending on the composition/catalytic analysis that needs to be performed. In some cases it will not be practical to use the above examples, and the materials will need to be used as-prepared. For laboratory UHV-XPS a flood gun is often used, which bombards the sample with low energy electrons/ions to neutralize the positive charge. If it is not possible to use any of the above methods (and often even if they are used), it will be necessary to correct the acquired spectra. For the powder samples in this project this is typically done by measuring the Al 2p peak alongside the regions of specific interest, and shifting all spectra by the difference of the Al 2p peak from the correct value (typically used as 74.6 eV for Al 2p in Al_2O_3). For the model catalysts the Fermi edge can instead be measured and used in the same way, corrected to 0.0 eV.

An example of the charging experienced over the time of a measurement is shown in Fig.

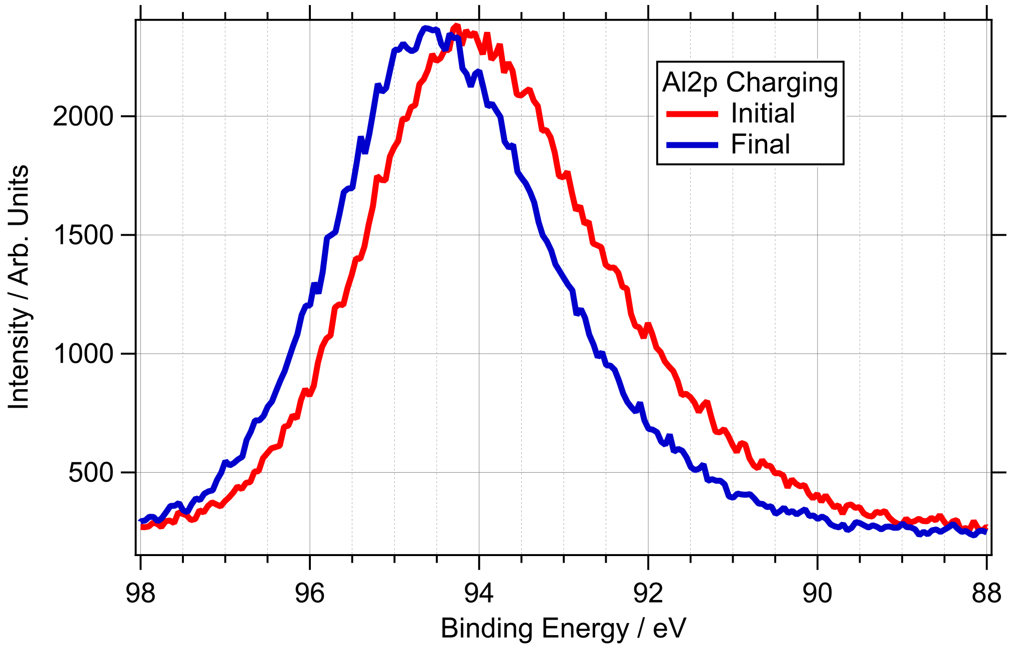

Figure 2.8: An example of the change in Al 2p peak position due to charging during XPS analysis.

2.8, which shows Al 2p spectra at the beginning and end of a set of measurements. The time difference between these two spectra was 57 minutes. The shift in the main Al 2p peak, as determined by peak fitting, was +0.62 eV. On the scale of differences in oxidation states for metals, this is quite significant, so this must be accurately measured and compensated for.

Processing

After charge corrections have been made, data will be first processed by normalization, which divides through all data points by the y value of the background. After this, the background is removed, using either a linear or Shirley background depending on which is more appropriate for the spectrum. Overall, this ensures comparability between spectra, and is routinely performed for laboratory and synchrotron XPS data shown throughout this work.

Fitting

For all NAP-XPS measurements, Al 2p scans were performed before and after each Pd 3d scan. Due to the charging over the time of a single palladium spectrum (often 30 minutes or more), it is important to have a reliable calibration. In some cases, where charging over time was larger, Pd 3d scans were run for 15 minutes, with Al 2p scans between each one, with more repetitions of this process.

An example of the process is shown in Fig. 2.9, which shows 2 fitted Al 2p peaks, and the fitted Pd 3d peak performed between them. This example is the ”vacuum RT” (labelled either UHV RT, or Vac RT) measurement from the 4.0Pd-1.0Pt sample (before the stoichiometric wet experiment).

The first part of the fitting concerns the Al 2p peaks, shown in Fig. 2.9a. 2 peaks are used for this, with relative freedom on the parameters. The peaks are restricted to ensure they are the same width, which is typically between 2 and 3 eV, though in certain cases can be up to 3.5 eV where charging is particularly problematic. Once the fit has produced a good match, the position and area of each peak is analysed, and key data is taken, this is: Al2pA position, Al2pA/Al2pB area ratio, and Al2pA-Al2pB energy difference. As the measurements are taken before & after the palladium spectrum, the average of the two values is taken for each parameter. The Al2pA position is used to determine the binding energy offset. Al 2p should appear at 74.6 eV in alumina, so the difference between the Al2pA peak and this value determine the necessary ”shift”, which is applied to the Pd 3d peak before fitting. In the example shown, the initial Al2pA position is 111.31 eV, and the final is 112.45 eV. This gives a ”shift” value of -37.28 eV for Pd 3d. The area ratios are 5.38 and 4.91 for the initial and final spectra respectively, with an average value of 5.14 used. For the area ratios, a small variation is permitted during the fit (typically under 5%), due to the potential variation in true value. The gaps between peak centres for Al2pA and Al2pB were 2.64 and 2.90, giving and average used value of 2.77 eV. As above, a small variation is permitted in the fit, due to the difference in values. The peak widths were 2.956 eV and 3.000 eV (limited) for the two Al 2p spectra, giving a usable width of 2.978 eV for Pd 3d.

In total, eight peaks are fitted to each Pd 3d spectrum, covering Pd(0) and Pd(II) states for Al2pA and Al2pB, with Pd 3d$_{5/2}$ and Pd 3d$_{3/2}$ split peaks for each. The Pd 3d$_{3/2}$ peaks are directly linked to the Pd 3d$_{5/2}$ peaks by their area and peak position. The Pd 3d$_{3/2}$ peak has an area of 0.67 times that of the Pd 3d$_{5/2}$ peak, and is 5.26 eV higher on the binding energy scale.

Once a suitable fit has been produced, with the areas and positions of peaks verified to ensure there are no fitting errors, the relative areas can be analysed. The peak areas for the Pd(II) 3d$_{5/2}$ and Pd(0) 3d$_{5/2}$ are both used to determine the ”percentage Pd(II)”, which is

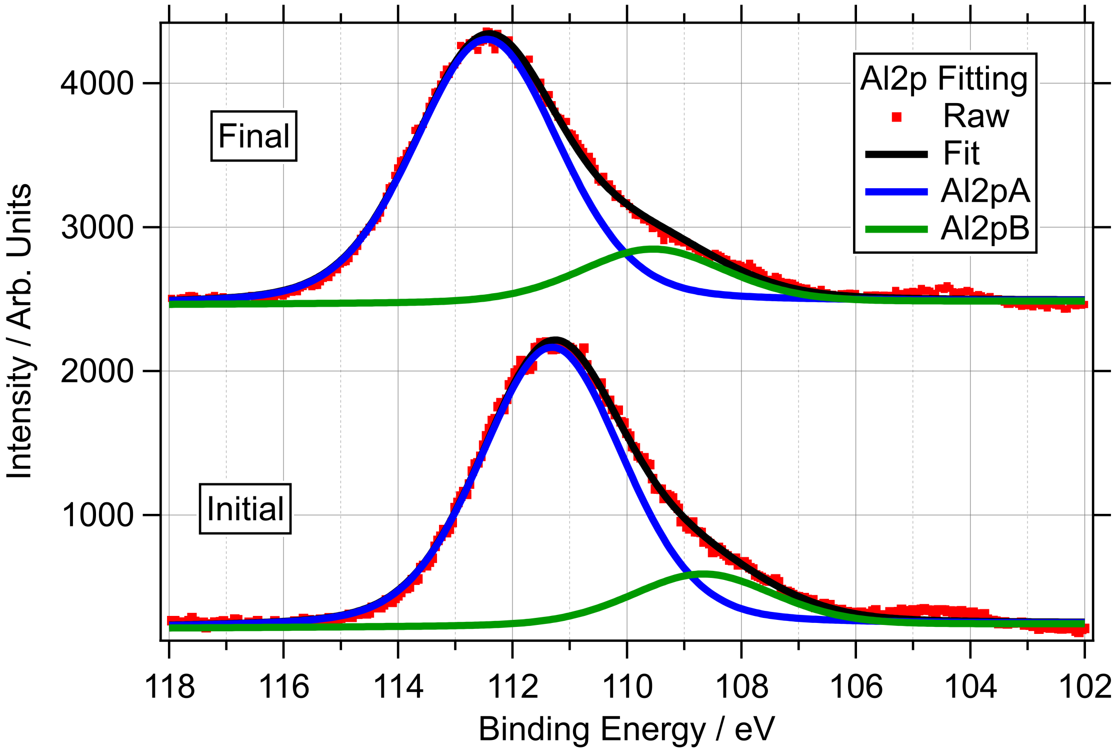

(a) Al 2p spectra with raw data, individual fitted peaks, and composite fit.

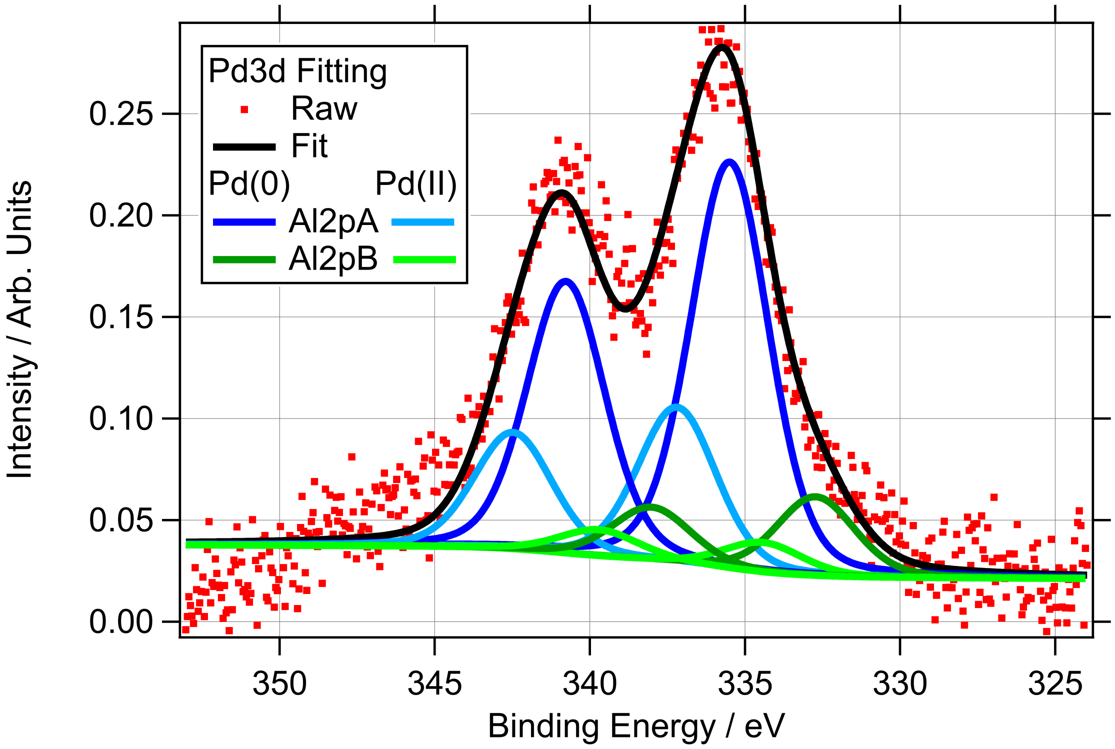

(b) Pd 3d spectra with raw data, individual fitted peaks, and composite fit.

Figure 2.9: Examples of fitting process for Pd 3d peaks, showing Al 2p peaks used for determination of fitting parameters.

the percentage of the total Pd that is oxidised.

2.2.2 Synthetic Catalytic Activity Testing (SCAT)

Each catalyst sample was pressed, crushed and sieved to between 250 and 355 μm. The resulting pellets of each sample (0.4g) were exposed to a gas flow within the rig, with the gas composition varied. A temperature ramp was performed across a range of 150 - 590 °C, at a ramp rate of 15 °C per minute (Some runs were terminated before 590 °C, if the conversion had reached 100%). For the initial testing, prepared catalyst pellets were subjected to three consecutive testing runs. The gas compositions for these runs were, respectively: 0.1 % CH_4 and 1 % O_2; 0.1 % CH_4 and 12 % O_2; and 0.1 % CH_4, 12 % O_2 and 10 % H_2O, with the balance comprised of N_2 in all cases. In later examples, catalysts were subjected to two consecutive ramps, in 0.1 % CH_4 and 0.2 % O_2; and 0.1 % CH_4, 0.2 % O_2 and 10 % H_2O. Additional experiments were performed where a ramp was paused, to study specific features of the previously observed reaction curves. A Fourier-transform infrared spectrometer (FT-IR) was used to monitor the gas streams, and could be switched to analyse either the inlet (reactants) or outlet (products). Initially, a measurement is recorded of the inlet, to ensure the correct level of methane (and water, where used) is present and stable before beginning the reaction. A separate oxygen meter was used to check the oxygen presence, as this is not detected in the FT-IR. Due to the nature of this device the data are not recorded, and so are not presented here. The product gas stream was analysed by FT-IR to determine the efficiency of the conversion, which is measured by the change in the methane signal throughout the reaction. Signals for CO_2 and H_2O (complete oxidation products) along with CO (partial oxidation product) were measured to ensure the selectivity was as desired.

An example of the reaction data collected by FT-IR is presented in Fig. 2.10. The decrease in methane can clearly be seen, along with the production of both complete oxidation products in the correct stoichiometric ratio (ending with approx. 1000 ppm of carbon dioxide and 2000 ppm of water respectively). The trace for carbon monoxide is also shown, though no meaningful quantity of this is ever detected, showing the catalyst to be totally selective towards complete oxidation products.

Due to the noisy nature of the carbon dioxide and water detection in the FT-IR, the methane trace is used as an indicator for reaction progress. For presented catalytic data, the

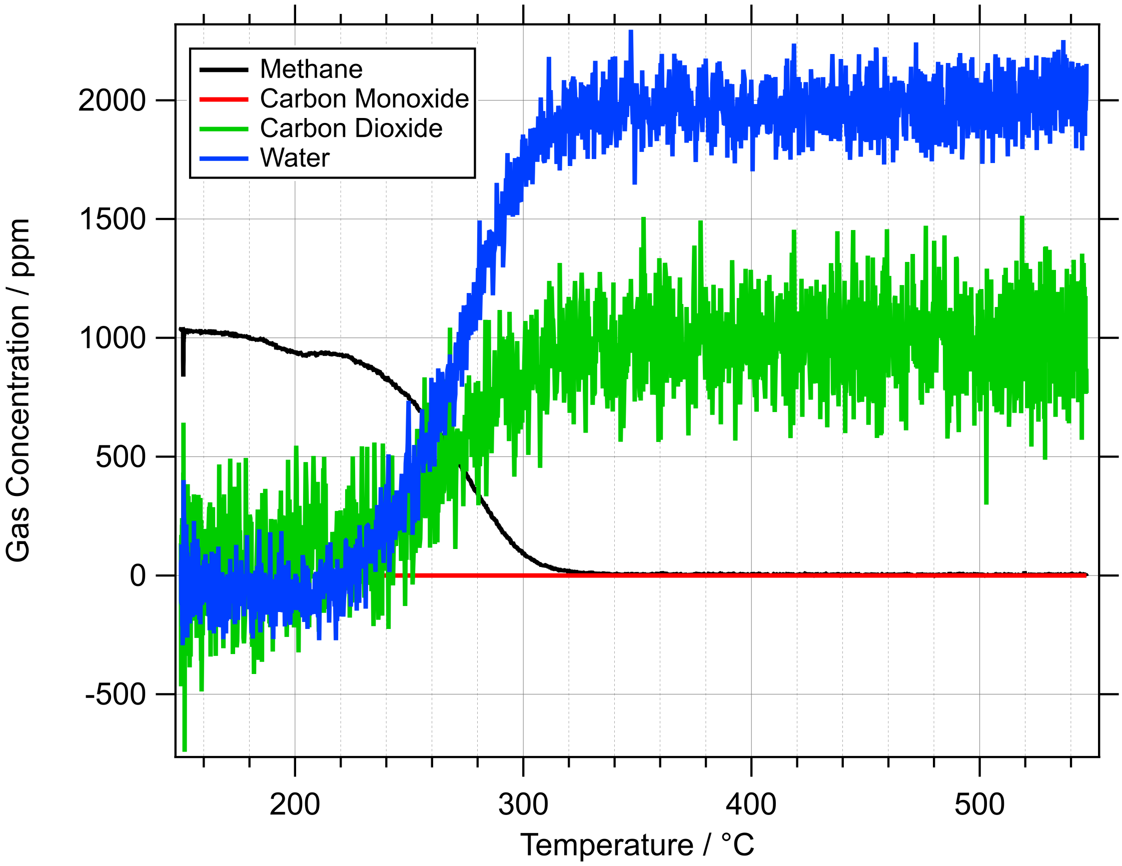

Figure 2.10: An example of the FTIR data recorded for conversion of methane to carbon dioxide and water, for a 5.0Pd/Al_2O_3 catalyst under oxygen rich dry conditions. Carbon monoxide is included, to show no partial conversion is taking place.

"methane conversion" is the inverse of the methane presence curve, calculated by subtracting the real value of methane at a given point from the initial stable value, typically around 1000 ppm (0.1 %).

After catalysts had been tested, samples of the pellets were retained for further analysis, to study the effects of catalytic testing on the catalysts.

2.2.3 Transmission Electron Microscopy (TEM)

Transmission electron microscopy (TEM) is a technique that was employed to determine particle sizing of the catalyst nanoparticles. Samples were prepared for TEM by grinding the powdered catalyst between two glass slides, before being dusted onto a holey carbon coated copper grid. All TEM analysis was performed at Johnson Matthey on a JEM 2800 (Scanning) Transmission Electron Microscope at 200 kV and using C2 aperture (um) 70 and 40. Dark field (z-contrast) imaging in scanning mode using an off-axis annular detector.

Compositional analysis by x-ray emission detection in the scanning mode.

Particle size analysis performed on TEM images using FIJI (a version of ImageJ with various tools included). Images were analysed variously using automatic threshold application and manual particle analysis, with average values presented to limit errors from either method. Automatic threshold application tends to merge particles, and pick up smaller particles which are simply the result of noise, whilst manual particle selection tends towards a larger average particle size, due to the ease of noticing and selecting these particles. In general, where manual selection was performed, a minimum of 50 particles was generally used. It was important to try and select as many particles as possible from an image, to ensure the average was being determined from the largest available data set.

A key technique coupled to the TEM is energy-dispersive x-ray spectroscopy (EDX). This technique allows for elemental composition analysis over a small area, which can be mapped onto the images collected in the TEM measurements. In these experiments, it can therefore be used to study the composition of bimetallic particles.

2.2.4 CO Chemisorption

CO chemisorption was used to determine the metal dispersion and surface area for each catalyst, using a Micromeritics AutoChem II 2920. For CO Chemisorption analysis, the powdered catalyst (0.2g) was packed into a tube, where it was initially reduced to ensure all platinum and palladium was in its metallic state, before carbon monoxide was pulsed. The pulsing was repeated until no change in adsorption was noted, and as such the surface was determined to be saturated.

For the data analysis, the total area under the peak for each pulse is taken, and summed, to yield a total cumulative quantity of CO adsorbed. This can then determine the total metallic surface area of the sample. From this, combined with the total loading and mass of the used sample, the average particle size, and therefore the dispersion, can be determined. This determination assumes particles to be hemispheres on the support surface, and does not consider the potential variation in particle size, giving only a singular average value. As such, this is not an ideal tool for determining accurate particle size, as compared to TEM. However, this allows for much faster measurements meaning more samples can be quickly analysed to determine general trends across a series. Interesting samples can then be studied in a more detailed way with TEM and EDX.

2.2.5 Inductively coupled plasma mass spectrometry (ICP-MS)

ICP-MS is another technique which was used, to provide information about the amounts of platinum and palladium in the samples. This was used only on initial samples, to verify that the preparation had been executed correctly, with the samples having the desired metal loadings.

2.2.6 Temperature programmed reduction (TPR)

TPR is a technique which provides data about the reducibility of the samples. For this work, it gives an insight into the state of the metal nanoparticles on the catalyst surface. The powder sample (0.2g) is placed into a tube and nitrogen and hydrogen is flowed across the sample, across a temperature ramp from -90 °C to 700 °C. The hydrogen reacts with oxygen from the sample to produce water, with the produced water measured.

2.2.7 Powder x-ray diffraction (XRD)

XRD is a technique which has been used to study the phases present for both support material and nanoparticles. Powdered samples were packed into flat plate sample holders, with experiments performed on a Bruker D8 Advance, using Cu Kα radiation. The scans were performed between 10 and 130 °, with steps of 0.044 °, at ambient temperature.

3 Alumina supported catalysts

Material in this chapter has been published as: Alexander Large, Jake Seymour, Wilson Quevedo Garzon, Kanak Roy, Federica Venturini, David C Grinter, Luca Artiglia, Emily Brooke, Martha Briceno de Gutierrez, Agnes Raj, Kevin R J Lovelock, Roger A Bennett, Tugce Eralp-Erden and Georg Held. Operando Characterisation of alumina-supported bimetallic Pd-Pt catalysts during methane oxidation in dry and wet conditions. *Journal of Physics D: Applied Physics*, 54:174006, 2021.

3.1 Introduction

The first stage of this project was to produce gamma-alumina supported nanoparticle catalysts. As a support it offers many benefits: it is inexpensive, easy to handle, non-toxic, stable to high temperatures and very well characterised. Many PGM catalysts have previously been prepared using alumina, including various catalysts used for methane oxidation, meaning it was a natural starting point for this research.

Alumina-supported catalysts were produced for this project in a number of stages. Initially, a batch of 5 catalysts with a total loading of 5 wt. % were prepared. These were: 5.0Pd, 4.0Pd-1.0Pt, 2.5Pd-2.5Pt, 1.0Pd-4.0Pt, and 5.0Pt. This was a basic sample set of catalysts to allow for a study of the changes in physical properties and catalytic activity with varied sample composition. The total weight loading was maintained at 5%, with monometallic and bimetallic catalysts prepared to give a good base set to work from.

Additional batches of alumina-supported catalysts were prepared after this. The second batch comprised of 4.0, 2.5 and 1.0 wt. % catalysts of both Pd and Pt, to form monometallic comparison samples. Not only do these samples allow for the study of the effects of PGM loading, but they would also provide a benchmark by which the bimetallic catalysts could be measured.

The final alumina-supported batch of catalysts comprised only two samples: 2.5Pd-2.0Pt and 2.5Pd-3.0Pt. With this small variation in Pt loading, we intended to be able to monitor the effects of Pd:Pt ratio, without significantly affecting the Pd loading or overall particle size. There was a consideration to make even more minor adjustments at this stage (2.4Pd-2.6Pt or similar), but it was preferable to keep the Pd loading consistent as this is the most active component. Equally, with the expected variations being small, varying the Pt loading by 20% up or down gave a good chance that observed differences would be reliable.

3.2 Palladium on alumina

3.2.1 Preparation & Characterisation

This section will discuss the four monometallic Pd/Al_2O_3 catalysts that were produced, with weight loading percentages of 5.0, 4.0, 2.5 and 1.0. In each case, initial batches of 20 g were prepared, with an additional batch of 5.0 Pd due to the increased amount of characterisation performed on this sample.

The variation in sample appearance is shown in Fig. 3.1, for fresh and 500 °C calcined samples. The catalysts with a higher palladium loading take on a darker brown colour. The calcination at 500 °C increases the darkness of the colour for all catalysts.

Loading / wt. %	500 °C / nm	800 °C / nm	900 °C / nm	500 °C T / nm
5.0Pd	14.7	16.5	28.0	18.0
4.0Pd	19.1	11.1	18.2	17.0
2.5Pd	15.4	6.3	12.3	13.2
1.0Pd	5.0	5.2	8.5	4.2

Table 3.1: Average particle sizes in nm for monometallic Pd/Al_2O_3 catalysts at various calcination temperatures, and after catalytic testing (500 °C T). All determined by CO chemisorption.

Inductively-coupled plasma mass spectrometry (ICP-MS) showed the 5.0Pd sample contained 3.89% palladium before calcination, and 4.39% after 500 °C calcination. This increase can largely be assigned to the removal of nitrates leftover from the precursor. Given the general observed variation from the expected value, this is a reasonable result. In both cases, the platinum content was below the minimum measurable value of 0.01%, so was deemed to be nil, as expected. Average particle size data for all Pd monometallic catalysts, as determined

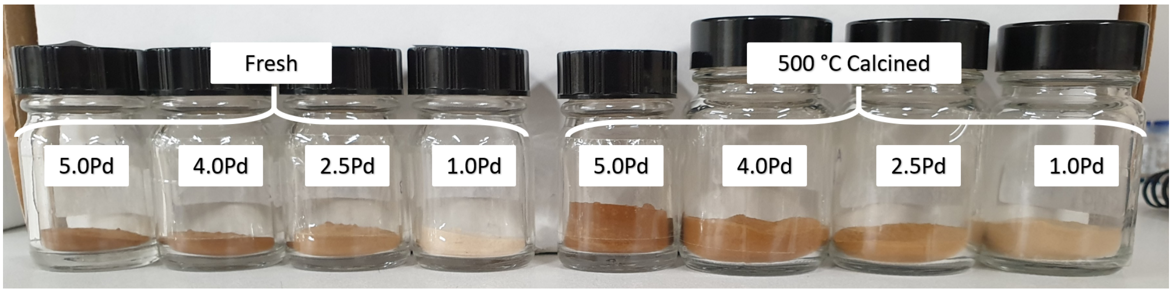

Figure 3.1: Picture showing (left four) fresh and (right four) 500 °C treated samples for (from left) 5.0Pd, 4.0Pd, 2.5Pd and 1.0Pd.

by CO chemisorption, is presented in Tab. 3.1. Over the tested temperature range, 500 to 900 °C, there is some sintering observed for 5.0Pd, with a particle size increase of 14.7 to 28.0 nm. For catalysts with lower loadings, however, there is less observed sintering, with both 4.0Pd and 2.5Pd showing negative changes in particle diameter over this range. 1.0Pd does show significant sintering between 800 and 900 °C, but still retains the smallest particle size, due to the very low loading.

Particle size analysis was also performed on select TEM images, and yielded an average size of Pd particles of 12 ± 5 nm, for 5.0Pd after 500 °C calcination. Energy dispersive x-ray spectroscopy (EDX) maps for 5.0Pd catalysts calcined at 500 °C and 800 °C are presented in Fig. 3.2. In both cases, large variations can be seen in Pd particle size. This is expected, due to the preparation method not being designed to provide particle size control. The maps clearly show the increase in the presence of larger Pd particles with higher temperature calcination as expected, however there are still many visible smaller particles, explaining the relatively small difference in average particle size as shown in the CO chemisorption experiments.

Pd 3d laboratory XPS spectra are shown in Fig. 3.3 for all monometallic Pd catalysts after treatment at 500 °C, 800 °C, and after catalytic testing. In this figure, spectra have been adjusted such that the Pd $3d_{5/2}$ peaks are of equal intensity to highlight the similarity in oxidation. From this, it can be clearly seen that after the standard 500 °C calcination treatment, there is no significant difference in Pd oxidation states with varied loading. Given the Pd $3d_{5/2}$ peak position, at around 337 eV, the Pd in all samples is presumed to be primarily Pd(II). There is a slight relative broadening for the 1.0Pd sample, though this is very minor, and would not effect the assigned oxidation state.

Treatment at 800 °C makes minimal difference for most compositions, although there is a

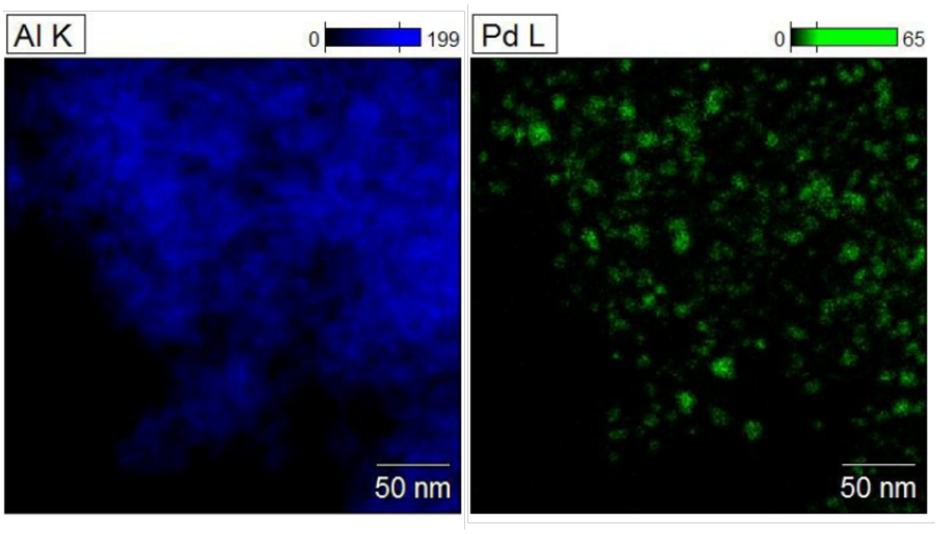

(a) 5.0Pd 500 °C

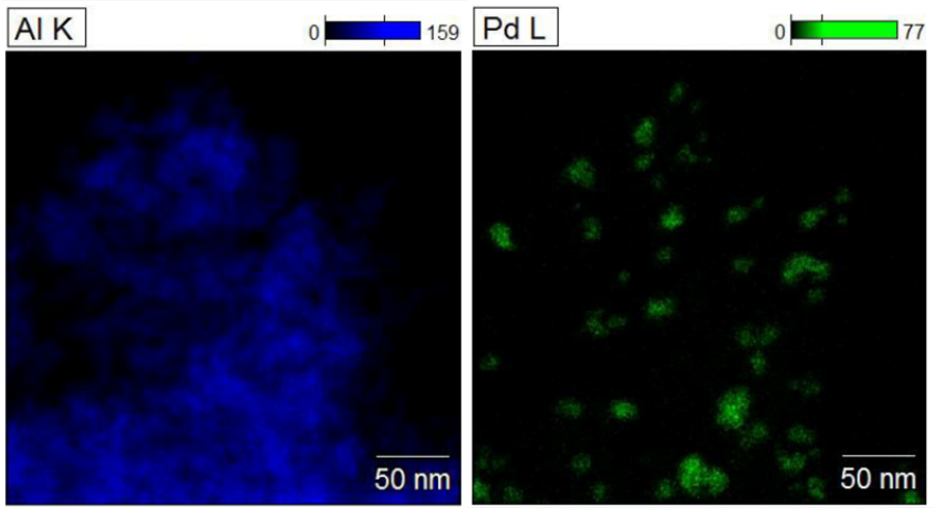

(b) 5.0Pd 800 °C

Figure 3.2: EDX maps for aluminium and palladium on 5.0Pd catalysts calcined at 500 and 800 °C. Images have had brightness and contrast increased for clarity.

slight additional broadening for 1.0Pd. This calcination does not lead to a significant change in particle size for 1.0Pd, so the increase in relative intensity is presumed to be due to a higher presence of oxidised palladium.

Fig. 3.4 shows the carbon and nitrogen contamination on a typical sample after various stages of preparation. The carbon can be seen to continually decrease with increased calcination temperature, as shown in Fig. 3.4a. The tested catalyst shows significantly lower carbon levels than the 500 °C catalyst, which is the version used for testing. Nitrogen is expected as a contaminant in the fresh sample, as some nitrates will remain from the palladium and platinum precursor nitrate solutions. This is seen in Fig. 3.4b, which shows the minimal level

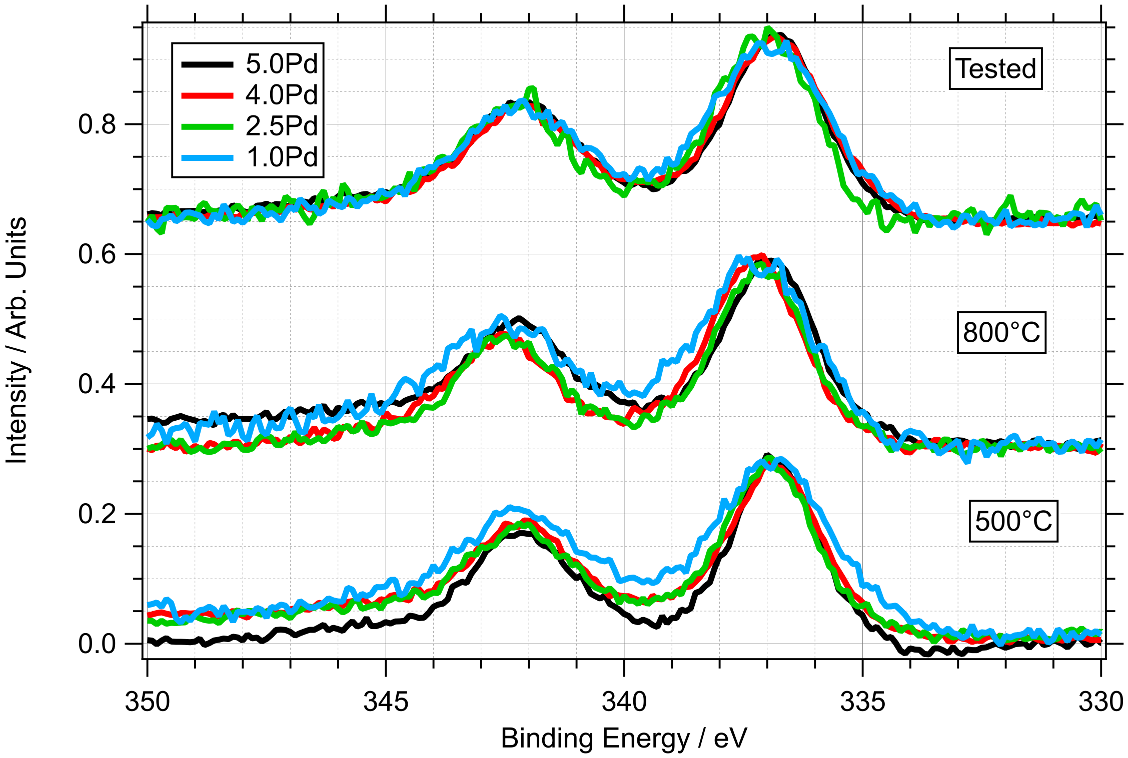

Figure 3.3: Pd 3d region XPS spectra of 5.0Pd, 4.0Pd, 2.5Pd and 1.0Pd catalysts after treatment at 500 °C, 800 °C, and after catalytic testing. Tested catalysts had previously been treated at 500 °C. All spectra recorded on a laboratory system with 1486.6 eV photon energy, under ultra-high vacuum conditions at room temperature. All corrected to Al 2p at 74.6 eV. All Pd $3d_{5/2}$ peak intensities aligned to the same value for a given condition for clarity of presentation.

of nitrogen observed after 500 °C calcination. No significant changes in N 1s are observed between 500 °C and higher temperature calcinations, so these are not presented.

Catalytic testing (through the initial cycle of three consecutive ramps under gas composition with CH4 : O2 : H2O ratios of 1 : 10 : 0, 1 : 120 : 0 and 1 : 120 : 100) was performed on samples previously treated at 500 °C. There is no notable change to the Pd 3d peaks for any monometallic catalyst after the testing cycle. This, combined with the minimal changes in average particle sizes, indicates that there is minimal surface restructuring caused by exposure to reaction conditions.

Temperature programmed reduction (TPR) experiments were performed on 5.0Pd and 2.5Pd samples, after calcination at 500, 800 and 900 °C, with all data shown in Fig. 3.5. For the 500 °C comparison, 2.5Pd is shown to be significantly more reducible, with the main reduction peak present around 26 °C, compared to 38 °C for 5.0Pd. However, for 2.5Pd there seems to be minimal change in the TPR profile across the three calcination temperatures, save

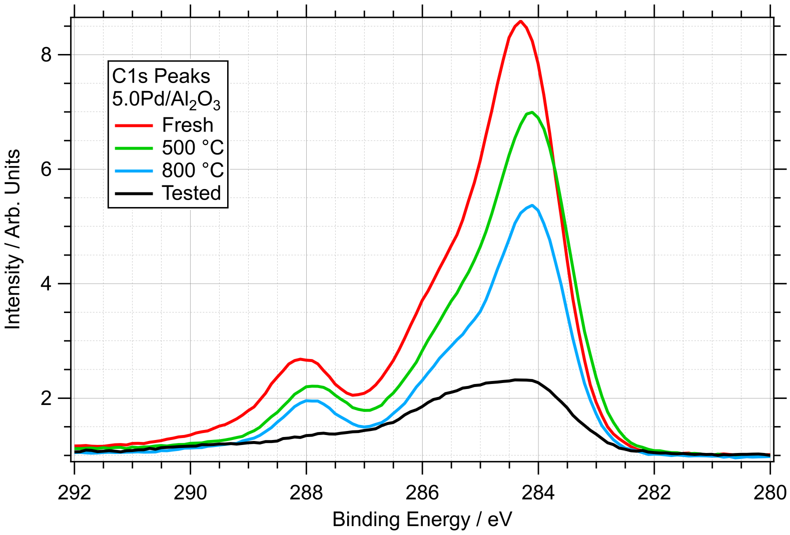

(a) C 1s peaks

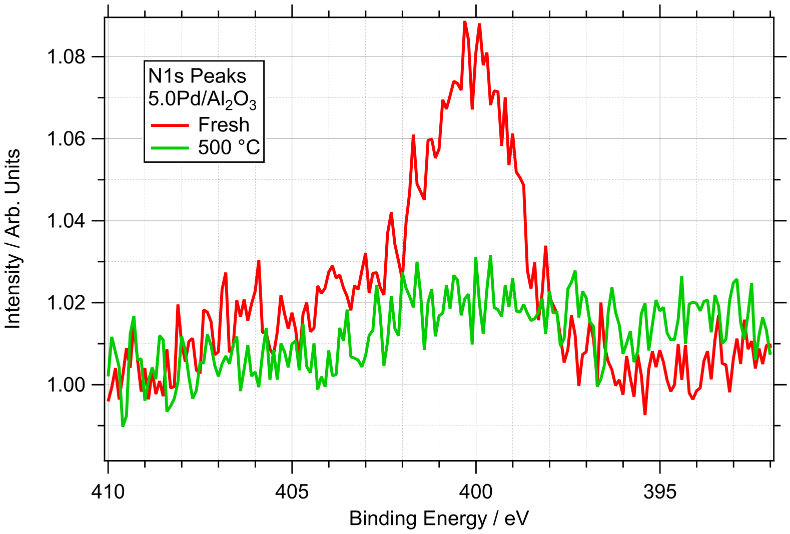

(b) N 1s peaks

Figure 3.4: C 1s and N 1s region XPS data showing contamination levels for a 5.0Pd catalyst after various treatments.

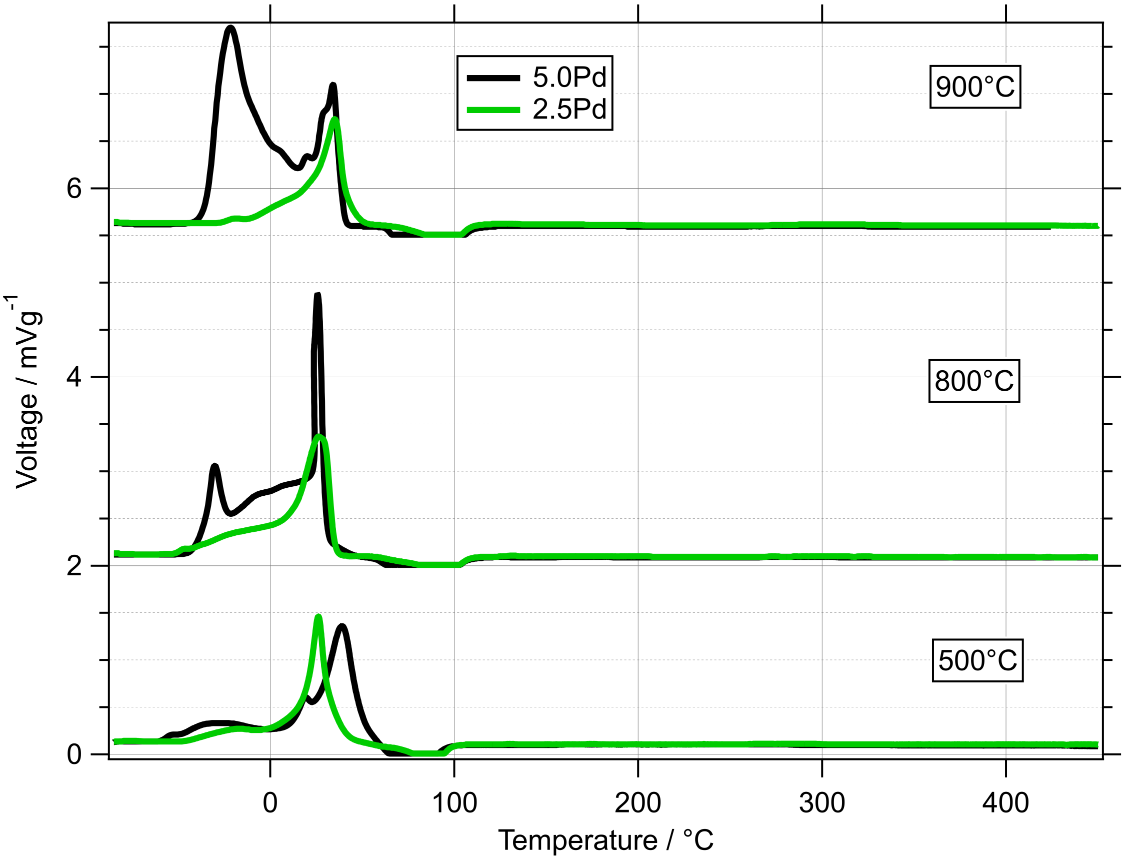

Figure 3.5: TPR data for 5.0Pd and 2.5Pd catalysts after treatment at 500 °C, 800 °C and 900 °C. 800 °C data offset by +2.0 mVg^{-1}, 900 °C data offset by +5.5 mVg^{-1}.

for slight changes in the sub-zero peaks. For 5.0Pd, an increase in calcination temperature lead to a decrease in the temperature of primary reduction, to the extent where - for the 900 °C calcined sample - the main reduction happens below 0 °C.

Loading / wt. %	T50 Dry	T50 Wet	ΔT50	TOF Dry	TOF Wet
5.0Pd	269	379	110	2.96×10^{-2}	1.49×10^{-2}
4.0Pd	272	380	108	4.38×10^{-2}	2.61×10^{-2}
2.5Pd	287	401	114	3.75×10^{-2}	1.19×10^{-2}
1.0Pd	302	426	124	1.94×10^{-2}	5.73×10^{-3}
5.0Pd 900 °C	317	437	120	1.52×10^{-2}	3.68×10^{-3}
5.0Pd Stoic.	283	382	99	1.94×10^{-2}	1.16×10^{-2}

Table 3.2: T50 data and turnover frequencies for all Pd monometallic conditions. 500 °C treated and oxygen excess conditions unless otherwise noted. TOF values determined at 250 °C and 350 °C for dry and wet conditions respectively.

Activity testing data for all monometallic palladium catalysts are shown in Fig. 3.6. Tab. 3.2 summarises the T50 values (the point at which 50% conversion is reached) along with the turnover frequencies for each catalyst, as determined at 250 °C (dry) or 350 °C (wet).

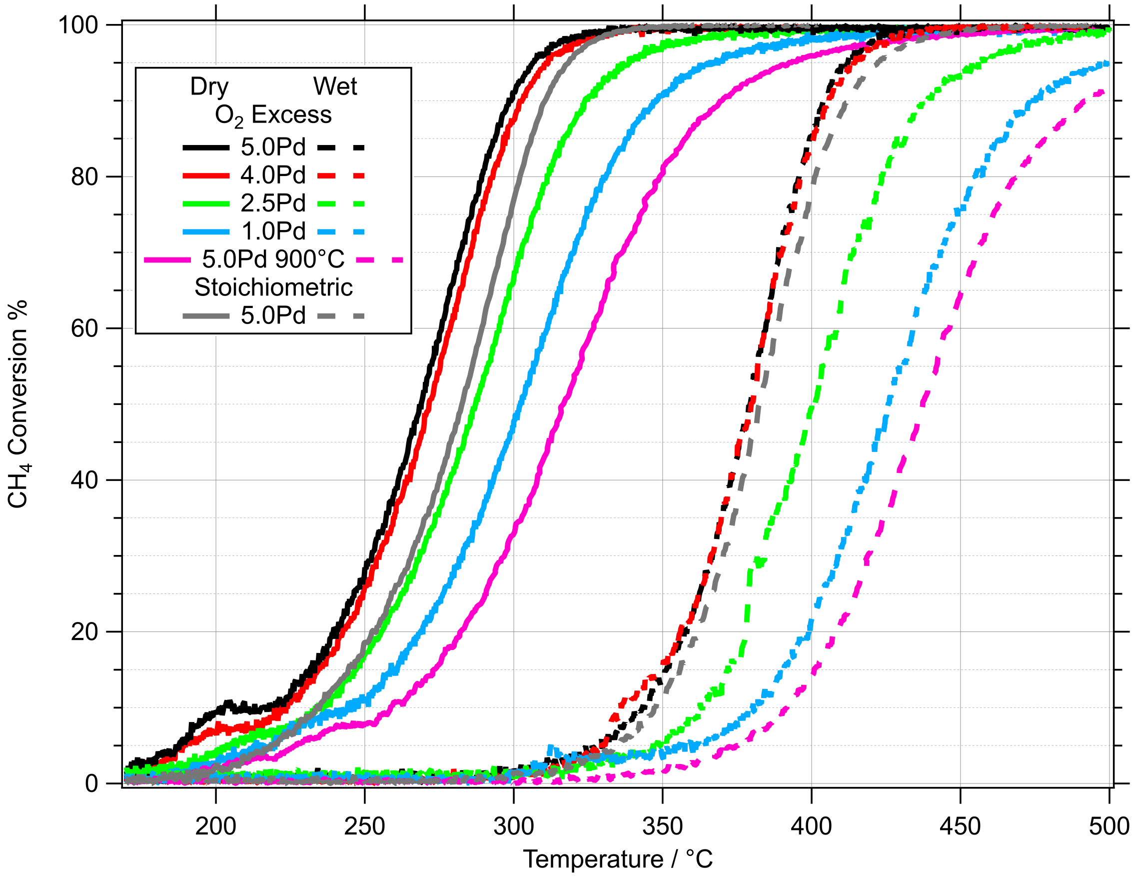

Figure 3.6: Activity testing data for all Pd monometallic catalysts. "O_2 Excess" condition dry (0.1% CH_4 and 12% O_2) and wet (0.1% CH_4, 12% O_2, and 10% H_2O). "Stoichiometric" condition dry (0.1% CH_4 and 0.2% O_2) and wet (0.1% CH_4, 0.2% O_2, and 10% H_2O). In all cases, nitrogen is used to balance total pressure.

TOF values for oxygen excess conditions are also presented in Fig. 3.7.

Clearly, a decrease in Pd loading leads to a decrease in activity under dry or wet oxygen excess conditions. This is consistent with the prior reports that the presence of water in the gas feed has a large negative effect on palladium catalysts for methane oxidation. [68, 129–133, 164] Additionally, there is bigger ΔT50 (the difference in T50 between dry and wet conditions) for 1.0Pd than any other Pd monometallic catalyst, indicating that the water presence has the largest effect on this sample. Given the lower amount of Pd to deactivate and the consistent water level, this is to be expected.

After calcination at 900 °C, the 5.0Pd catalyst is significantly worse than after the 500 °C calcination, with T50 values around 50 °C higher in dry or wet conditions. These T50 values for the 900 °C 5.0Pd catalyst are even higher than those of the 1.0Pd calcined at only 500 °C. The turnover frequency is nearly halved by the calcination (2.96×10^{-2} compared

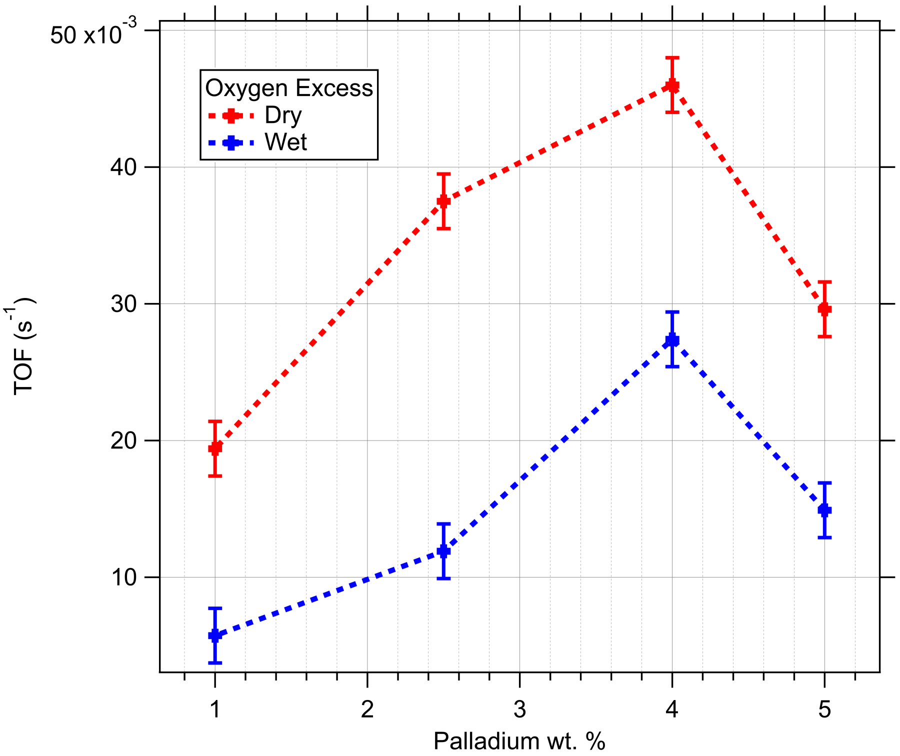

Figure 3.7: Turnover frequencies for all Pd monometallic catalysts under "O_2 Excess" condition dry (0.1% CH_4 and 12% O_2) and wet (0.1% CH_4, 12% O_2, and 10% H_2O) conditions. TOFs determined at 250 °C and 350 °C for dry and wet conditions respectively. In all cases, nitrogen is used to balance total pressure.

to 1.52×10^{-2}) in dry conditions, and in wet conditions it is four times lower (1.49×10^{-2} compared to 3.68×10^{-3}). This is primarily attributed to the major increase in particle size, and the resulting decrease in active surface area for the reaction.

Reducing the oxygen flow such that methane and oxygen are stoichiometric leads to a slightly worse activity in dry and wet conditions, with the difference smaller in wet conditions. The turnover frequency decreases by around 33% with the decreased oxygen in dry conditions, and by around 22% in wet conditions. As a result of this finding, it can be suggested that water inhibition is a larger effect in more oxygen rich gas conditions.

When comparing turnover frequencies of Pd catalysts of varied loading, the best catalyst is 4.0Pd, in both dry and wet conditions. In dry conditions, the turnover frequency decreases in the order 4.0Pd > 2.5Pd > 5.0Pd > 1.0Pd. This varies slightly in wet conditions, with 5.0Pd > 2.5Pd.

3.2.2 Near-ambient pressure XPS of Pd/Al_2O_3 catalysts under methane oxidation conditions

A core aim of this project was to study the surface chemical behaviour of catalysts under reaction conditions using near-ambient pressure x-ray photoelectron spectroscopy (NAP-XPS). This section presents NAP-XPS data for a 5.0Pd catalyst, recorded under various reaction conditions, to mimic the gas ratios used in activity tests as described previously. The 5.0Pd catalyst was selected as the one monometallic palladium catalyst to be studied using NAP-XPS due to the generally good catalytic activity, coupled with the higher loading which would theoretically minimize the experiment time.

All Pd 3d spectra recorded during NAP-XPS experiments are presented in Fig. 3.8 and Fig. 3.9 for stoichiometric and oxygen rich gas conditions respectively. This is summarised in Fig. 3.10, which overlays the Pd (II) % (as determined by NAP-XPS) with the catalytic activity for various reaction conditions.

Initial measurements were generally made under "UHV RT" conditions, which typically refers to a condition of a pressure below 1×10^{-7} mbar and a temperature of below 50 °C, with the exact values varying slightly between experiments, due to the difficulty in cooling the sample down after high temperature experiments, due to the lack of active cooling. In 3 of 4 "UHV RT" measurements, the Pd can be seen to be predominantly reduced. The exception to this is shown in Fig. 3.8b, where the Pd(II)% is 60%. This followed on from the "Stoic. Dry" experiment shown in Fig. 3.8a, and whilst it appears to be more oxidised than is typical, the measurements at increased temperature show the Pd still readily oxidises and reduces. Given this, and the fact that the laboratory UHV XPS typically showed the palladium to be fully oxidised, this is not considered to be an issue.

Under oxygen excess conditions (methane : oxygen of 1 : 120), the palladium is fully oxidised at all temperatures, in both dry and wet reaction mixtures. This is shown in Figs. 3.9a and 3.9b respectively. When measuring in stoichiometric gas conditions, there is more interesting variation in oxidation states. During the lowest temperature measurements, which are taken below the point at which the catalyst is significantly active, Pd is present as approx. 80% Pd(II) under dry conditions (Fig. 3.8a). This is decreased slightly for the low water (1 : 2 : 2) condition, and more dramatically, to around 40% Pd(II), for the very wet (1 : 2 : 100) feed (Figs. 3.8b and 3.8c respectively). This indicates that, without a

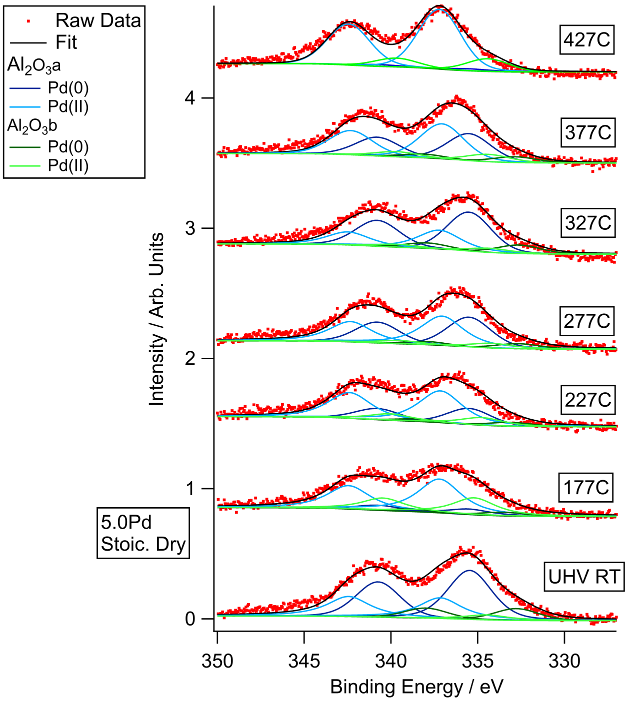

(a) Stoic. Dry

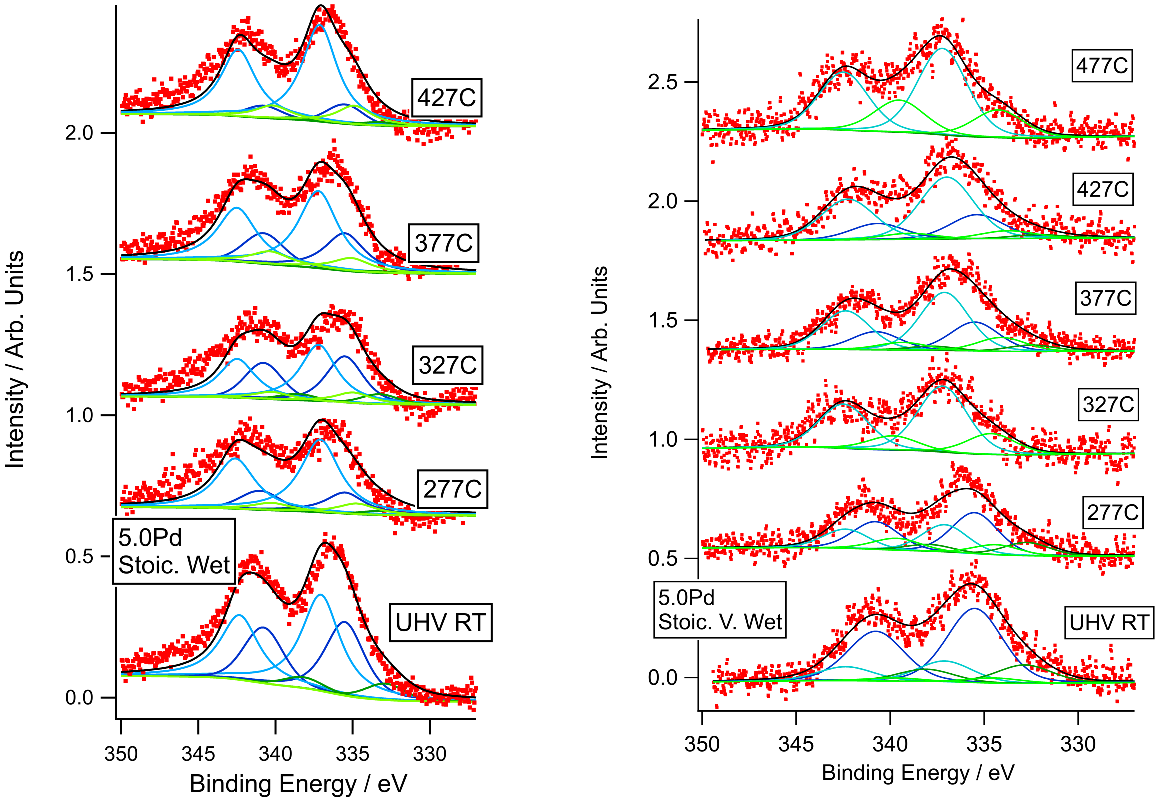

(b) Stoic. Wet

(c) Stoic. Very Wet

Figure 3.8: Pd 3d region NAP-XPS data for 5.0Pd catalyst under all tested stoichiometric conditions. All spectra recorded using 1350 eV photon energy.

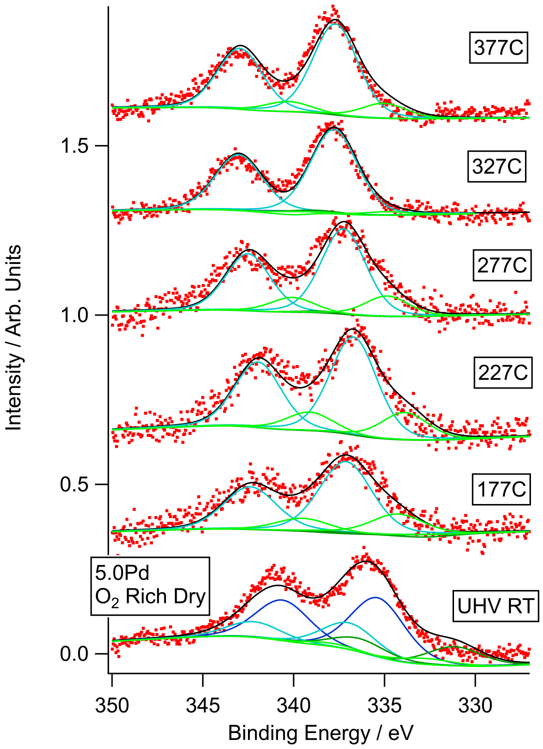

(a) Oxygen Rich Dry

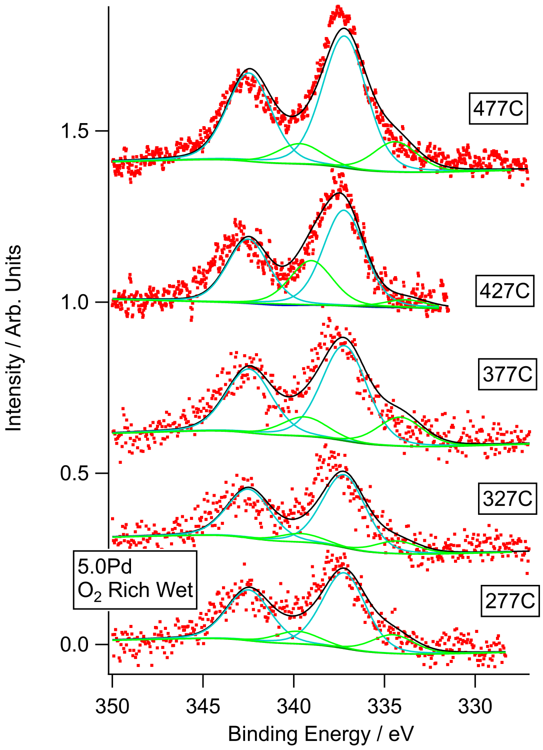

(b) Oxygen Rich Wet

Figure 3.9: Pd 3d region NAP-XPS data for 5.0Pd catalyst under all tested oxygen rich conditions. Key is consistent with Fig. 3.8. All spectra recorded using 1350 eV photon energy.

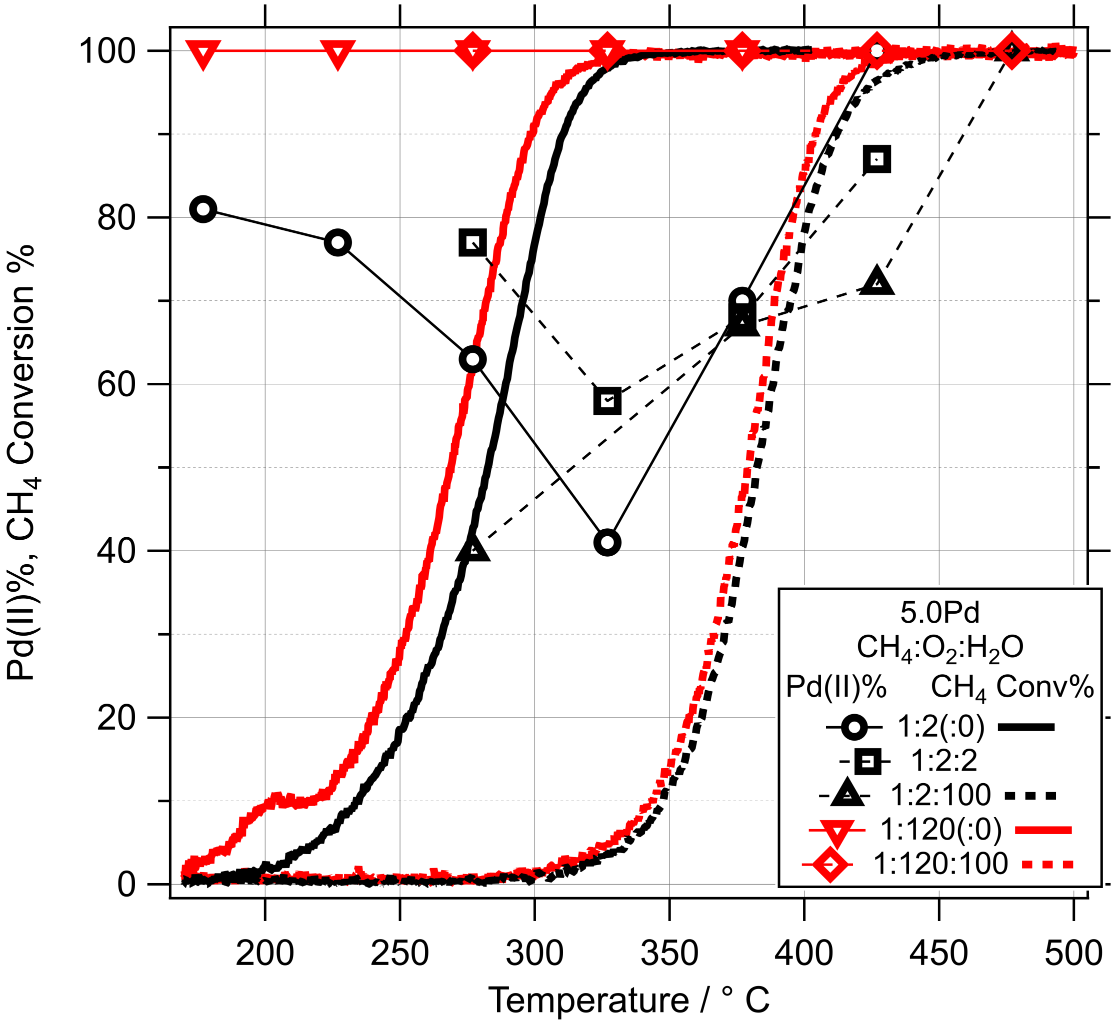

Figure 3.10: NAP-XPS data overlaid with catalytic activity data for 5.0Pd catalyst, recorded under various dry and wet conditions. All spectra recorded using 1350 eV photon energy.

reaction progressing, the increase in water in the feed has a negative effect on preserving the palladium in an oxidised state. As the reaction progresses in the dry condition, there is a gradual decrease in Pd(II), down to 40% at around 95% methane conversion (327 °C). Above this temperature/conversion, there is a continual re-oxidation, and the Pd is fully oxidised in the measurements at 427 °C.

It is well established that a presence of Pd(II) is necessary to drive the reaction on Pd/Al_2O_3 catalysts, but the exact extent to which Pd oxidation is optimal is yet to be determined. [55, 59, 165] From this comparative analysis, when operating in more oxygen rich dry conditions the Pd is fully oxidised, compared to between 40-80% in the stoichiometric condition, and the T50 is 14 °C lower. This may suggest that the 100% Pd(II) presence is preferable. However, in wet conditions, there is a T50 difference of only 3 °C, but at the point closest to T50 (377 °C), the very wet condition (1 : 2 : 100) sees Pd at <70% Pd(II). This indicates that the significant presence of Pd(0) in this case (30%) is preferable to the palladium being fully oxidised, in a 5.0Pd catalyst.

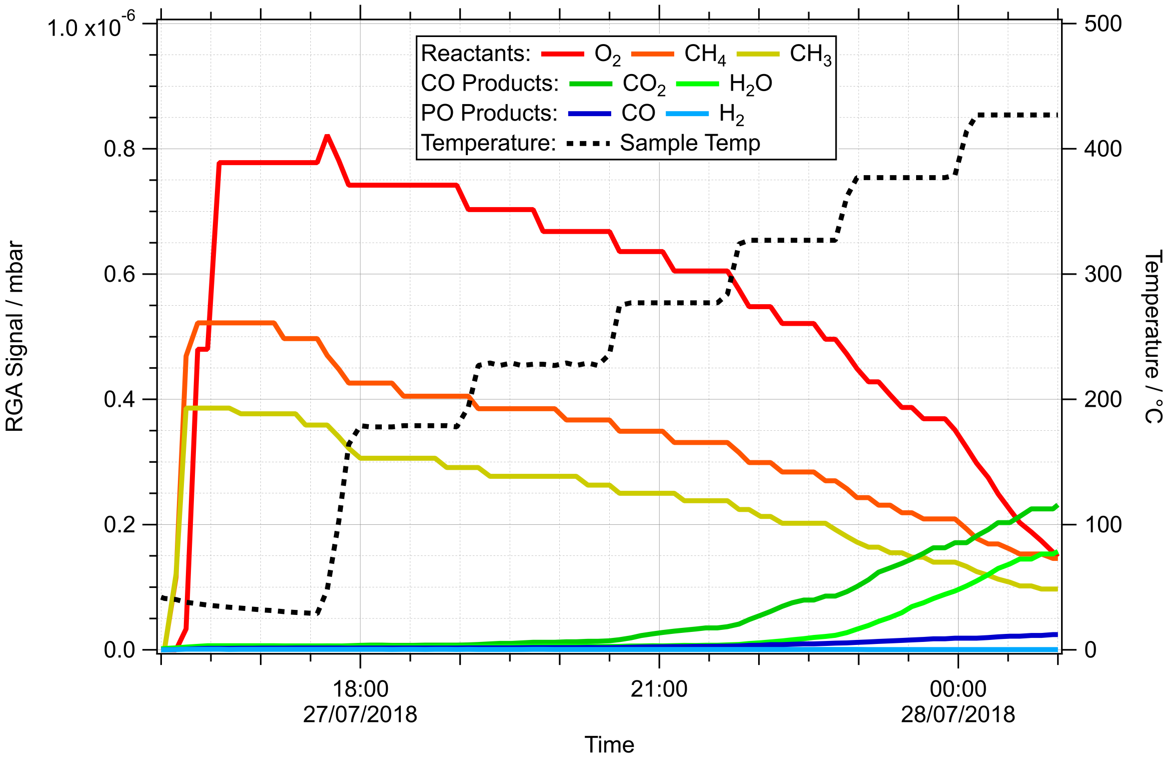

Figure 3.11: Mass spectrometry data recorded on the first pumping stage of the differential pumping system of the VerSoX beamline at Diamond, during NAP-XPS measurements of a 5.0Pd/Al_2O_3 catalyst under dry stoichiometric methane oxidation conditions.

For an early NAP-XPS experiment with a higher amount of powder catalyst (and therefore worse charging), the mass spectrometry data recorded showed a meaningful presence of complete methane oxidation products. This is shown in Fig. 3.11. This figure shows all reactants, including the CH_3 fragment, which is necessary to identify methane as the 16 mass peak can also be assigned to oxygen. The complete methane oxidation products - carbon dioxide and water - are monitored, along with hydrogen and carbon monoxide (the undesired partial oxidation products). This set of data is from a 5.0Pd/Al_2O_3 catalyst under dry stoichiometric methane oxidation conditions. This shows the gradual increase in carbon dioxide and water formation with increasing temperature. The trace for CO can also be seen to increase, but this is more likely due to the fact that this fragment can appear due to the higher presence of CO_2. CO is part of the cracking pattern of CO_2. The lack of hydrogen formation at any temperature indicates that the CO trace is unlikely to be due to the formation of CO by the catalyst.

3.2.3 Palladium on alumina Summary

When analysing only Pd/Al_2O_3 catalysts, 4.0Pd seems to be optimal in many regards. The activity is very strong, and turnover frequencies are higher than those of 5.0Pd in both dry and wet conditions. From a commercial point of view, retaining nearly all of the activity whilst reducing the palladium loading by 20% is very positive, especially if this was to be produced on a large scale. 500 °C is preferable for calcination compared to the higher temperatures tested, as the sintering suffered at 800-900 °C is too large to retain good activity. Palladium catalysts performed more strongly in oxygen rich than stoichiometric conditions. Given that exhaust feeds are closer to the oxygen rich condition tested (albeit with many more minor gases), this is not of concern.

Deactivation in water is a key issue here, and it was noted that the effect was significant for Pd monometallic catalysts, with a DT50 of over 100 °C for all monometallic catalysts in oxygen rich conditions. There was a slight relative improvement with a stoichiometric gas mixture, although the 5.0Pd catalyst was marginally worse in this condition generally as compared to the oxygen rich condition.

NAP-XPS showed significant variations in Pd oxidation state with change in gas composition and temperature. Whilst oxygen rich conditions allowed Pd to be preserved fully as Pd(II) throughout, under stoichiometric conditions there were large changes. Increasing water content lead to a more reduced Pd pre-reaction, but also to a smaller drop in oxidation state at mid-reaction temperatures. When heated high enough beyond 100% conversion, 5.0Pd tended towards 100% Pd(II) in all conditions, indicating that these variations are only relevant in the lower temperature/conversion range. In only 1 case did the catalyst not reach 100% Pd(II) by the highest tested temperature, and this was the $1:2:2$ stoichiometric wet condition, in which the experiment ended at 427 °C. Given the change that was seen at lower temperatures, and the behaviour in the other wet condition, it is expected the Pd would have been fully oxidised if it had been heated to and measured at 477 °C.

Overall, the stoichiometric conditions gave a less oxidised catalyst, and resulted in worse activity compared to oxygen rich conditions. This would be in general agreement with previous suggestions that a significant amount of Pd(II) sites are needed. The difference in activity was smaller in wet conditions, though the difference in oxidation state was largely similar, indicating that this is not the only relevant factor here.

3.3 Platinum on alumina

3.3.1 Preparation & Characterisation

A total of four monometallic Pt/Al_2O_3 catalysts were produced, with weight loading percentages of 5.0, 4.0, 2.5 and 1.0. All underwent initial calcination at 500 °C, with additional treatments performed at 800 and 900 °C to study the effects of heat treatment on particle size.

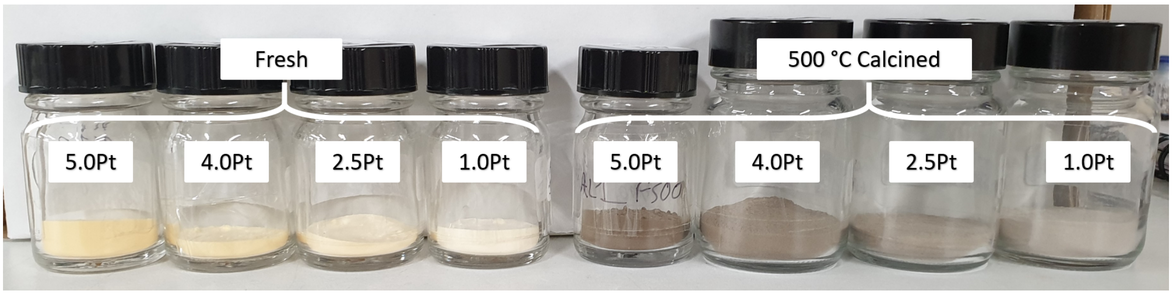

(a) Picture showing (left four) fresh and (right four) 500 °C treated samples for (from left) 5.0Pt, 4.0Pt, 2.5Pt and 1.0Pt.

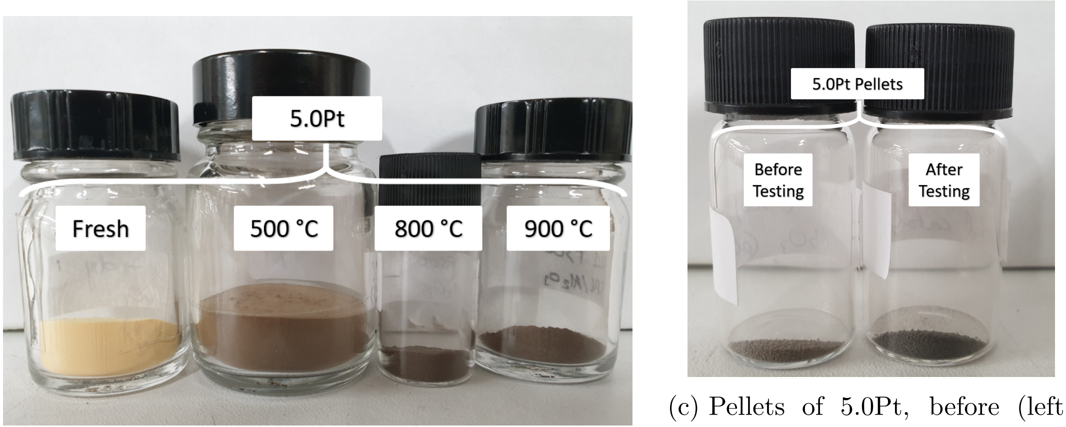

(b) From left: 5.0Pt fresh, 500 °C, 800 °C and 900 °C

(c) Pellets of 5.0Pt, before (left) and after (right) standard catalytic testing.

Figure 3.12: Images of various monometallic platinum samples.

The variation in sample appearance with varied loading is shown in Fig. 3.12a for fresh and 500 °C calcined samples. The fresh samples are a pale yellow, whilst the 500 °C aged samples are a brown-grey. In all cases, a lower Pt loading leads to a more pale sample colour, with the fresh 1.0Pt sample looking similar to bare alumina. Changes in appearance with increased calcination temperature, from 500 °C to 900 °C, are shown in Fig. 3.12b. There is a substantial change between the fresh sample and the 500 °C calcined sample, with a progressive darkening of the sample with higher calcination temperature. Images of pellets used for catalytic testing are shown in Fig. 3.12c, showing the sample darkening after a standard testing cycle.

Loading / wt. %	500 °C / nm	800 °C / nm	900 °C / nm	500 °C T / nm
5.0Pt	2.6	57.0	75.9	3.1
4.0Pt	2.6	52.6	29.9	4.4
2.5Pt	2.4	58.6	44.2	4.1
1.0Pt	2.4	37.3	28.6	3.7

Table 3.3: Average particle sizes for monometallic Pt/Al_2O_3 catalysts at various calcination temperatures, and after catalytic testing (500 °C T). All determined by CO chemisorption.

ICP-MS analysis of a 5.0 Pt catalyst gave a platinum content of 3.81% before calcination, and 4.46% after 500 °C calcination. In both cases, the palladium content was below 0.01% (the minimum reading from the instrument) and therefore assumed to correctly be nil.

Particle size data is presented for all Pt catalysts in Tab. 3.3. After the standard preparation, with 500 °C calcination, there is only a minor variation in particle size with loading, of 2.5 nm ± 0.1 nm. This is very different to the trend observed for Pd, where the 1.0Pd catalyst had an average particle size of 5.0 nm, compared to 14.7 nm for 5.0Pd. The Pt particle sizes for 500 °C catalysts are much smaller than those observed for Pd. In part this can be assigned to the lower number of atoms present for a given weight loading, with equivalent loadings have 1.83 Pd atoms for each Pt atom. However, catalysts with equivalent amounts of atoms still tend to be larger for Pd than Pt, so total atom loading is not entirely responsible for this. Auvray has recently shown it is possible to achieve better dispersion of platinum nanoparticles using microwave heating. [166] The nature of the heating - faster and more homogeneous as compared to a typical resistive oven heating - was key in producing more dispersed platinum.

Whilst high temperature calcination consistently leads to a large increase in particle size, there is very little consistency to the extent of this growth. After 800 °C treatment, the 5.0, 4.0 and 2.5Pt catalysts all have an average size of 55.6 nm ± 3.0 nm. 1.0Pt is much smaller at 37.3 nm, though this is generally to be expected given the significantly lower loading. Typically a higher calcination temperature would lead to a higher particle size, especially with platinum which undergoes significant sintering in this temperature range. However, for all catalysts other than 5.0Pt, the average particle size after treatment at 900 °C was lower than after the 800 °C treatment. As the 800 and 900 °C treatments are not sequential, but

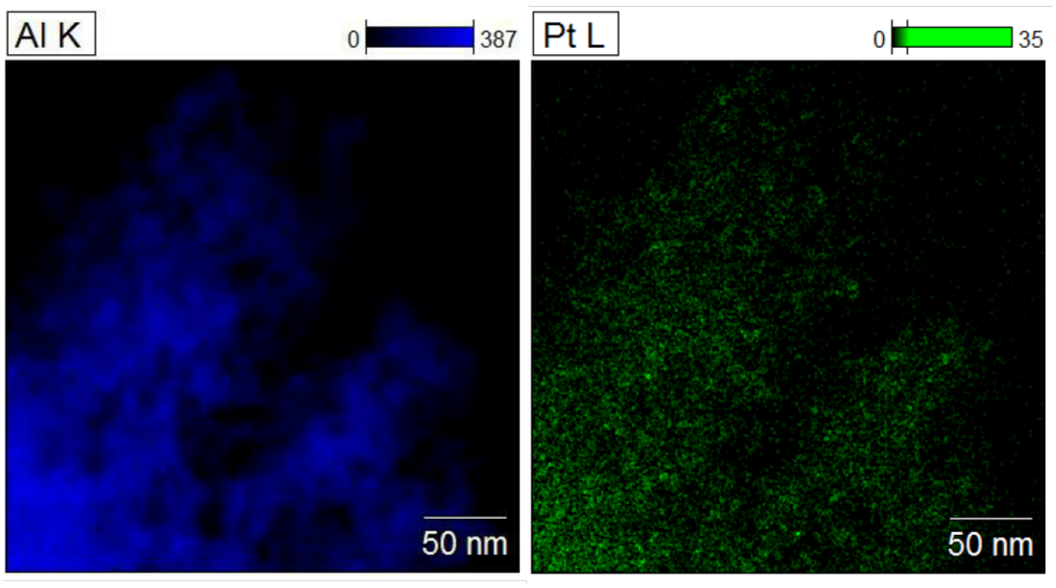

(a) 5.0Pt 500 °C

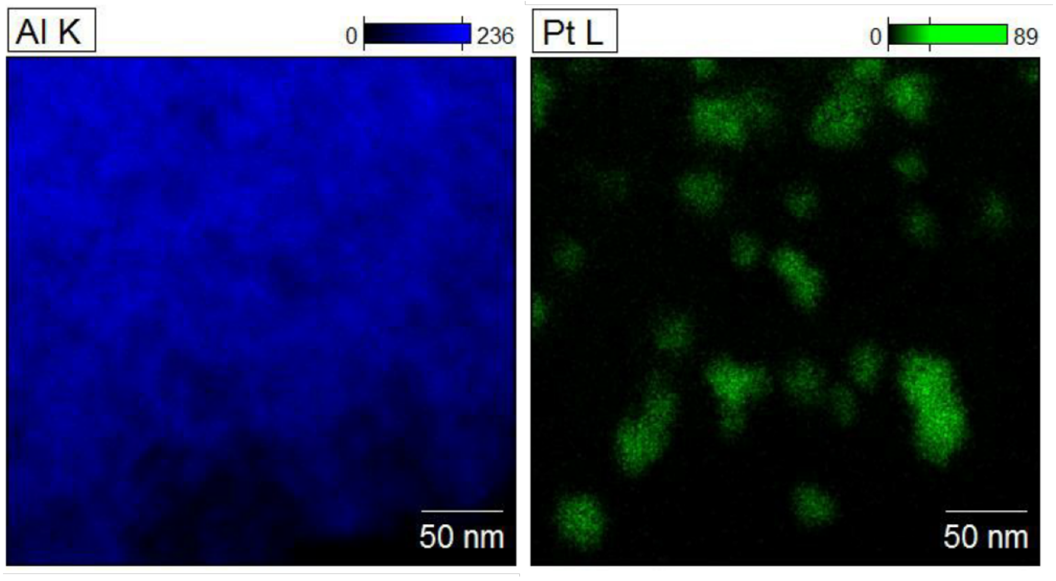

(b) 5.0Pt 800 °C

Figure 3.13: EDX maps for aluminium and platinum on 5.0Pt catalysts calcined at 500 and 800 °C. Images have had brightness and contrast increased for clarity.

instead are performed on different batches of 500 °C treated sample, it is likely not a case of particles breaking down, but simply of them not agglomerating to the same extent. All monometallic platinum catalysts showed significant growth after catalytic testing, though to a much smaller extent than the high temperature calcinations. There was no clear ordering to the extent to which this happened, with 5.0Pt growing to 3.1 nm, whilst 4.0Pt increased to 4.4 nm. This increase was not observed consistently for Pd, with 3 samples decreasing (by small amounts) in size, and only one increasing.

Other particle size analysis was performed through TEM. Fig. 3.13 shows EDX maps of 5.0Pt catalysts calcined at 500 °C and 800 °C, in which the increase in Pt particle size can be very clearly seen. With there being a large amount of tiny particles after treatment at 500 °C, the particles can be difficult to distinguish from the background. This is much clearer for the 800 °C sample, where particles are typically much larger. There is still a wide range of particle sizes, with particles between 5-50 nm.

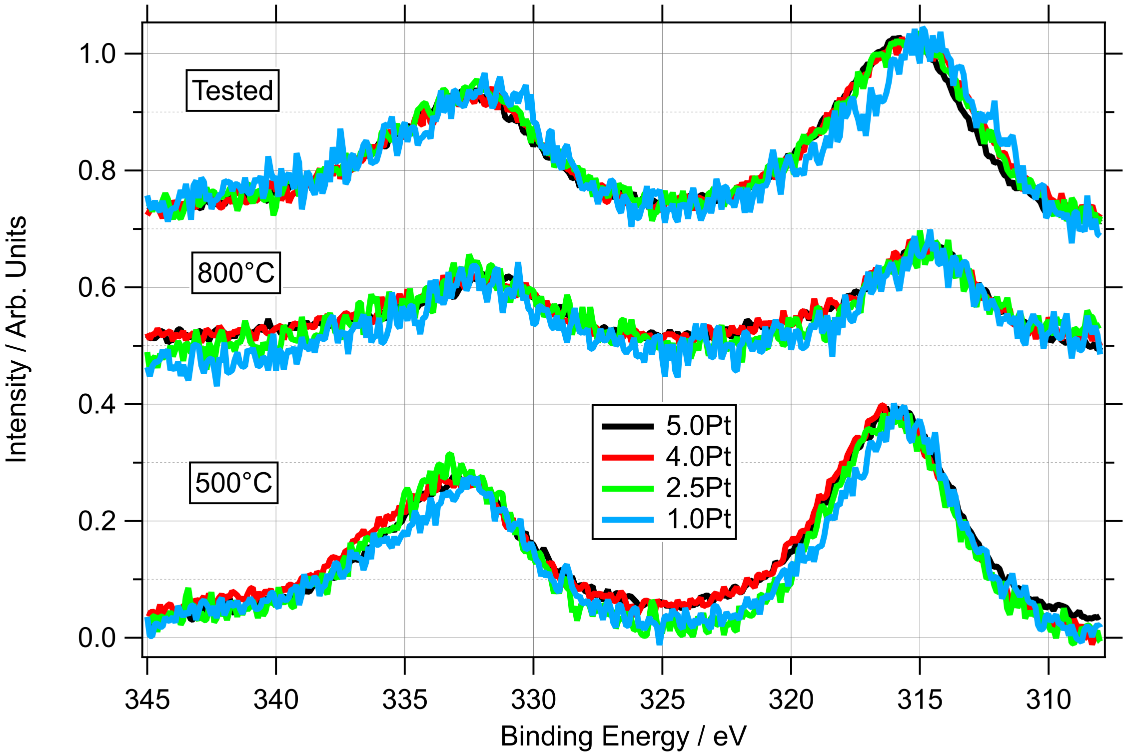

Figure 3.14: Pt 4d region XPS spectra of 5.0Pt, 4.0Pt, 2.5Pt and 1.0Pt catalysts after treatment at 500 °C, 800 °C, and after catalytic testing. Tested catalysts had previously been treated at 500 °C. All spectra recorded with 1486.6 eV photon energy, under ultra-high vacuum conditions at room temperature. All corrected to Al 2p at 74.6 eV. All Pt $4d_{5/2}$ peak intensities aligned to the same value for a given condition for clarity of presentation.

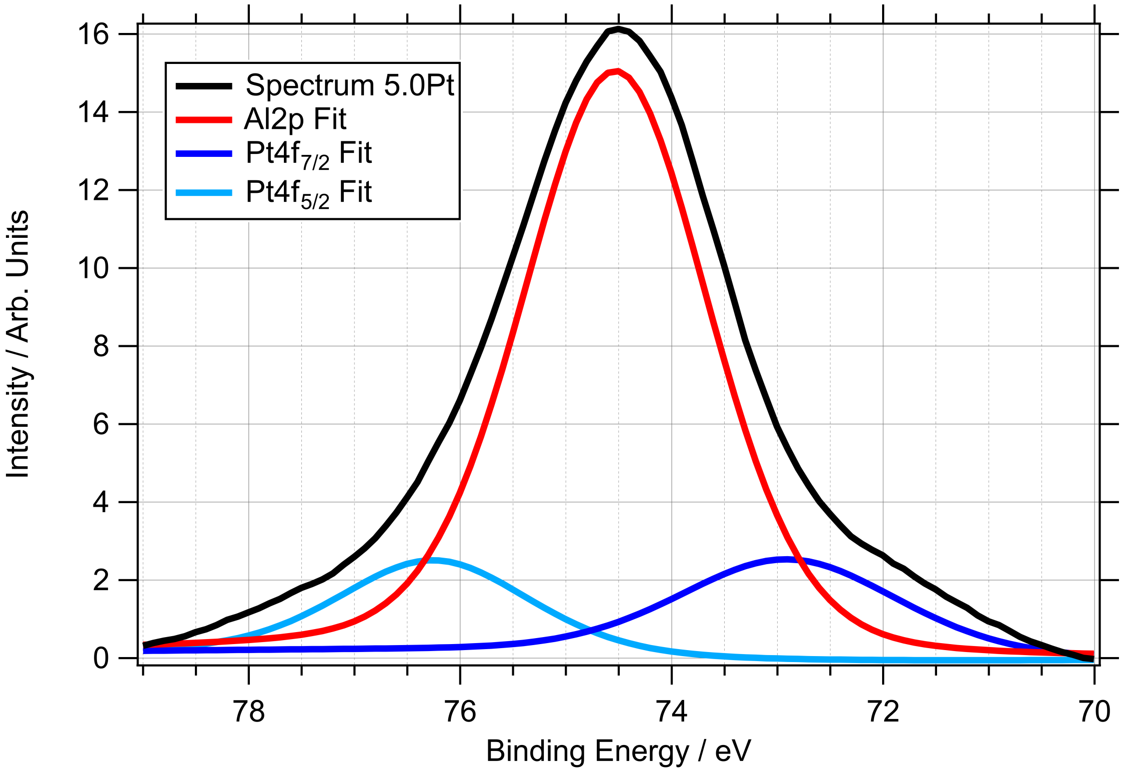

Figure 3.15: Pt 4f and Al 2p region XPS spectra of 5.0Pt after treatment at 500 °C, including fitted spectra for Al 2p, Pt 4f$_{7/2}$ and Pt 4f$_{5/2}$ peaks.

Laboratory XPS analysis of all four Pt catalysts - after treatment at 500 °C, 800 °C, and after testing - is shown in Fig. 3.14. The spectra are rescaled to better display variations in binding energy. For both the 500 °C and tested (also 500 °C) samples, 1.0Pt appears to be very slightly shifted to lower binding energy than the other loadings (within which there is no difference). In the case of 1.0Pt "Tested", the Pt 4d$_{7/2}$ peak appears to be more significantly split into two peaks, though this is the only sample where this occurs. Given that this is the sample with the lowest loading, and so the noisiest spectrum when rescaled, it is possible this is not a feature representing a different species, especially when the overall width is unaffected.

When studying platinum with XPS, it is typical to use the 4f peaks due to their greater cross-section. However, these peaks overlap significantly with the Al 2p peak. A loading of 5 wt.% of platinum on alumina relates to a atomic ratio of Al : Pt of 38.3 : 1. Whilst platinum has a higher cross section at typically used energies, it is not enough to overcome this issue. An example of a spectrum from this region is shown in Fig. 3.15, which includes fitted alumina and platinum peaks. The Pt 4f peaks have a combined area approximately

2.8 times smaller than the Al 2p peak. This makes meaningful fitting of the Pt 4f region difficult, especially for catalysts with the lower loadings of platinum.

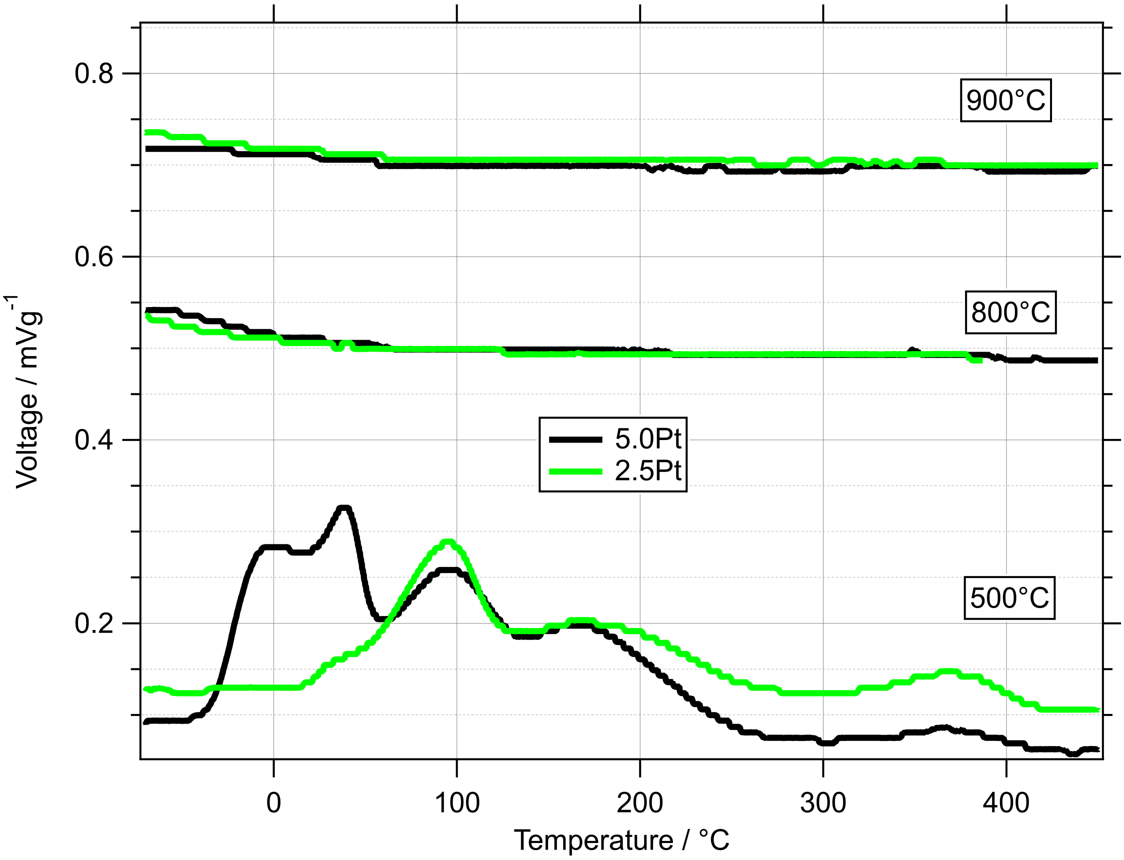

Figure 3.16: TPR data for 5.0Pt and 2.5Pt catalysts after treatment at 500 °C, 800 °C and 900 °C. 800 °C data offset by +0.4 mVg^{-1}, 900 °C data offset by +0.6 mVg^{-1}.

TPR data for 5.0Pt and 2.5Pt catalysts after various heat treatments are shown in Fig. 3.16. When comparing the 500 °C treated sample above 60 °C, the reduction peaks are similar for both 2.5Pt and 5.0Pt. 5.0Pt, however, has a large reduction feature between -10 and 30 °C. Given the lack of differences observed from other forms of analysis, the variation in TPR profiles is difficult to understand, but it does indicate a more reducible sample, with a higher relative presence of Pt(II) or Pt(IV).

There is no significant observed reduction behaviour after treatments at 800 or 900 °C. In these cases, the particles are much larger, with the samples having a significantly smaller total surface area as a result. With the XPS for these samples showing a more reduced sample, it can be assumed that there is minimal oxidised platinum remaining after the high temperature treatments.

As expected, a higher loading of platinum lead to a better catalyst, in terms of activity in

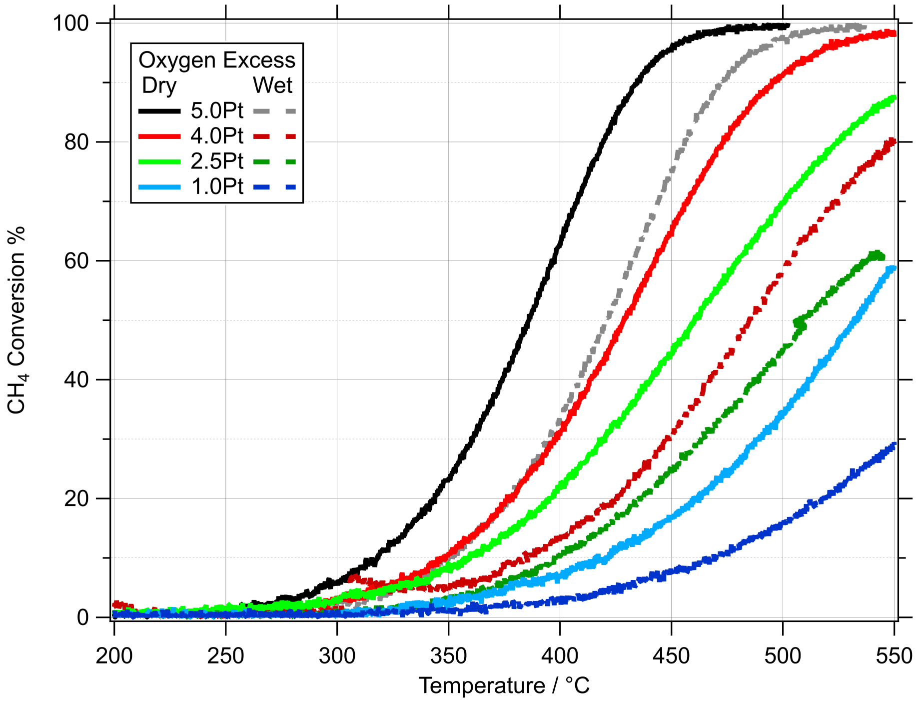

(a) Varied loading

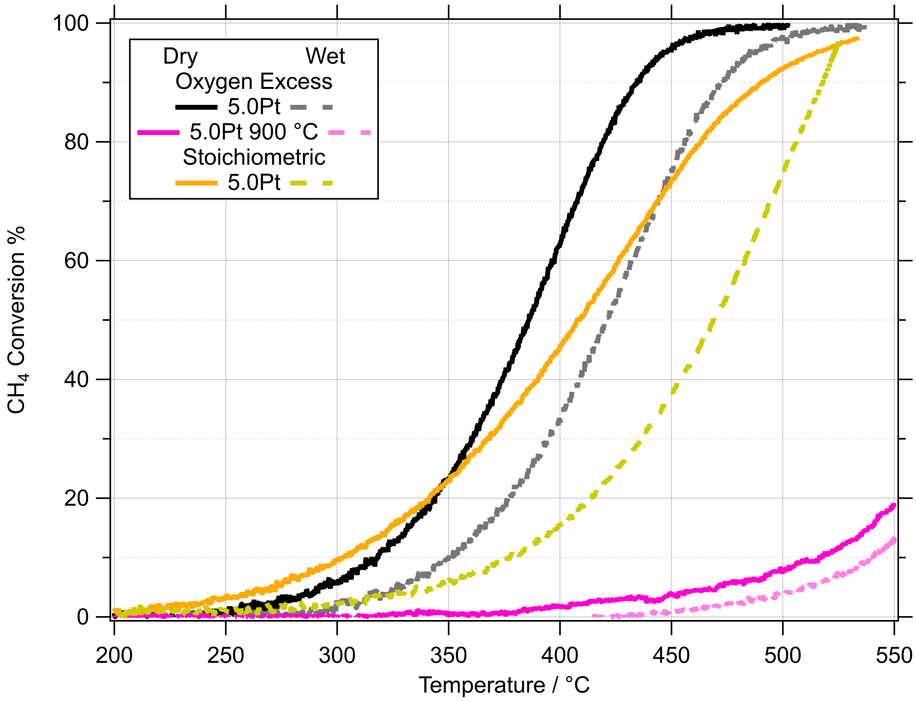

(b) Varied treatment and gas

Figure 3.17: Activity testing data for all Pt monometallic catalysts. "Oxygen Excess" condition dry (0.1% CH_4 and 12% O_2) and wet (0.1% CH_4, 12% O_2, and 10% H_2O). "Stoichiometric" condition dry (0.1% CH_4 and 0.2% O_2) and wet (0.1% CH_4, 0.2% O_2, and 10% H_2O). In all cases, nitrogen is used to balance total pressure.

dry or wet conditions, as shown in Fig. 3.17. The DT50 values are significantly lower than for the Pd monometallic catalysts (average value 46 °C for Pt vs 114 °C for Pd), showing

Loading / wt. %	T50 Dry	T50 Wet	DT50	TOF Dry	TOF Wet
5.0Pt	386	421	35	2.01×10^{-3}	3.37×10^{-3}
4.0Pt	429	485	56	1.08×10^{-3}	2.08×10^{-3}
2.5Pt	461	508	47	1.58×10^{-3}	2.01×10^{-3}
1.0Pt	532	-	-	-	1.65×10^{-3}
5.0Pt 900 °C	-	-	-	-	-
5.0Pt Stoic.	408	469	61	3.23×10^{-3}	3.63×10^{-4}

Table 3.4: T50 data and turnover frequencies for all Pt monometallic conditions. 500 °C treated and oxygen excess conditions unless otherwise noted. TOF values determined at 300 °C and 350 °C for dry and wet conditions respectively.

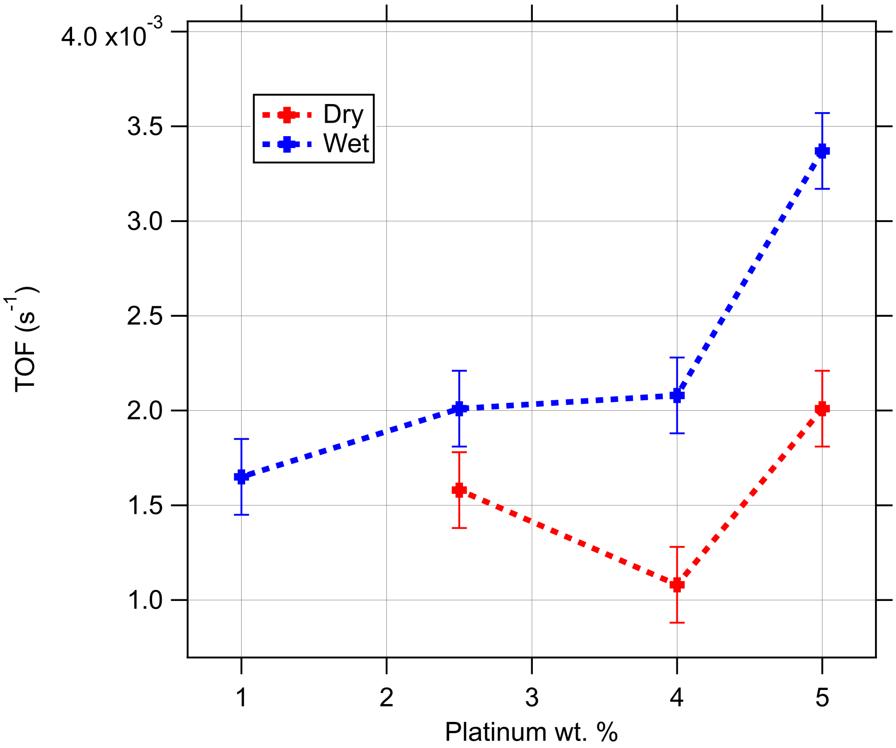

Figure 3.18: Turnover frequencies for all Pt monometallic catalysts under "O_2 Excess" condition dry (0.1% CH_4 and 12% O_2) and wet (0.1% CH_4, 12% O_2, and 10% H_2O) conditions. TOFs determined at 300 °C and 350 °C for dry and wet conditions respectively. In all cases, nitrogen is used to balance total pressure. 1.0Pt did not show any conversion at the measured point, so is not included.

that the effects of water are less significant for Pt. Whilst they are less affected by the presence of water, they are also less effective catalysts than the Pd monometallic samples, even in wet conditions. 4.0Pt, 2.5Pt and 1.0Pt failed to reach 100% conversion by 550 °C under oxygen rich wet conditions. When studying 5.0Pt in varied oxygen dry conditions, it is notable that it lights off earlier under stoichiometric conditions. However, it struggles to achieve higher activity with the limited oxygen, with a T50 22 °C higher than under oxygen excess. Under wet conditions the gap is larger, but there is no observed early light off. Overall this is indicative of platinum requiring a higher oxygen content in the gas feed to be effective, something which was not observed for palladium. Calcination at 900 °C caused a large degree of sintering, from 2.6 to 75.9 nm. Due to the resulting low amount of surface sites, it is no surprise that it is very poor as a catalyst, failing to reach 20% conversion in dry or wet conditions by 550 °C.

Turnover frequencies are calculated at different temperatures in dry conditions compared to Pd, to ensure the activity is high enough to measure. For platinum, the conversion used to determine TOF is taken at 300 °C (dry) or 350 °C (wet). In wet conditions, the TOF is seen to increase with increased Pt loading. Whilst this is the overall trend for dry conditions also, the 4.0Pt has a lower TOF than 2.5Pt. In both cases this shows significant variation from Pd, where 4.0Pd gave the optimal TOF. Given the differences in amount and size of particles, this difference is to be expected.

3.3.2 Near-ambient pressure XPS of Pt/Al_2O_3 catalysts under methane oxidation conditions

Despite the issues already noted with studying Pt on an alumina support using NAP-XPS, experiments were attempted, to see if meaningful data could be gained, to provide insight into the behaviour of platinum catalysts.

NAP-XPS data recorded under dry stoichiometric conditions are shown in Fig. 3.19. This shows the variations in platinum 4d and aluminium 2p peaks across the tested temperature range. Al 2p spectra are corrected and rescaled in Fig. 3.19b to show the consistency, and to confirm that the variations in platinum peak position are genuine shifts. The Pt $4d_{5/2}$ peak shifts with gas introduction, by around +1.7 eV, which is likely indicative of a change from Pt(0) to Pt(II). At 227 °C and 327 °C, this peak can be seen at around 313.5 eV, which is notably lower than the expected value for metallic platinum (typically 314.6 eV). The Al 2p spectra for these are consistent with those recorded under the other conditions, so this is not an energy correction issue. At most other temperatures under reaction conditions, the Pt 4d peaks are largely consistent with the one recorded under UHV RT conditions. Wet condition measurements were not completed for this sample.

Mass spectrometry data from the dry stoichiometric NAP-XPS experiment for 5.0Pt is presented in Fig. 3.20. This shows the presence of all reactants and (partial and complete) methane oxidation products. The increase in carbon dioxide and water formation with each increase in temperature is clear, though there is still a high methane presence by the end of the experiment (at 477 °C). As with the observation for the 5.0Pd catalyst previously, only complete oxidation is clearly observed. "CO" appears to increase, but this is more likely due to cracking of some of the formed carbon dioxide, as the hydrogen signal does not increase significantly at any stage.

Due to the poor activity of platinum for methane oxidation, the greater interest in palladium or bimetallic catalysts, and the limited availability of beamtime, no further NAP-XPS experiments were performed with monometallic platinum samples.

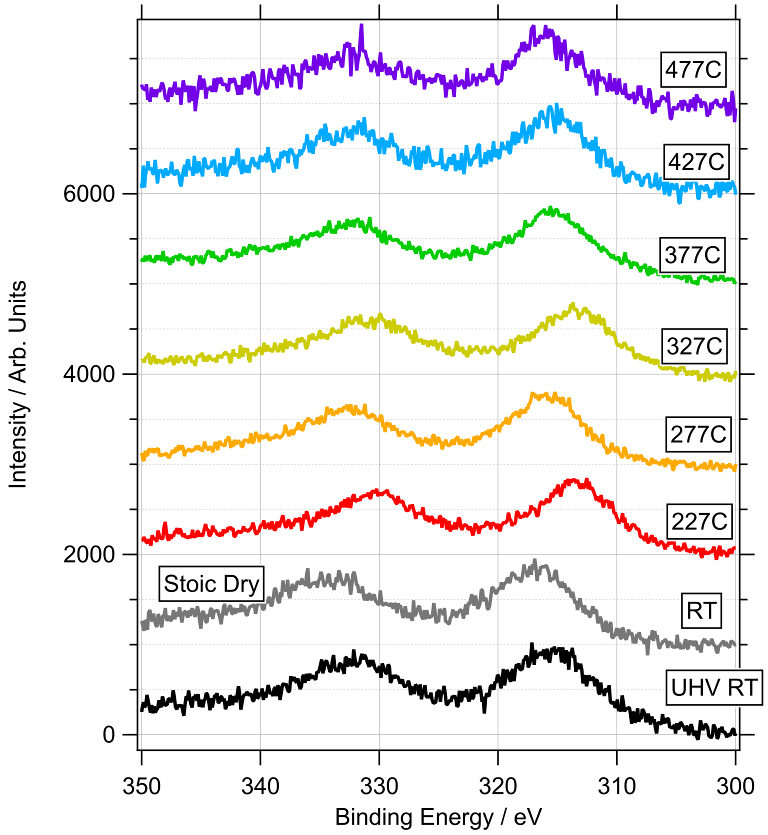

(a) Pt 4d spectra

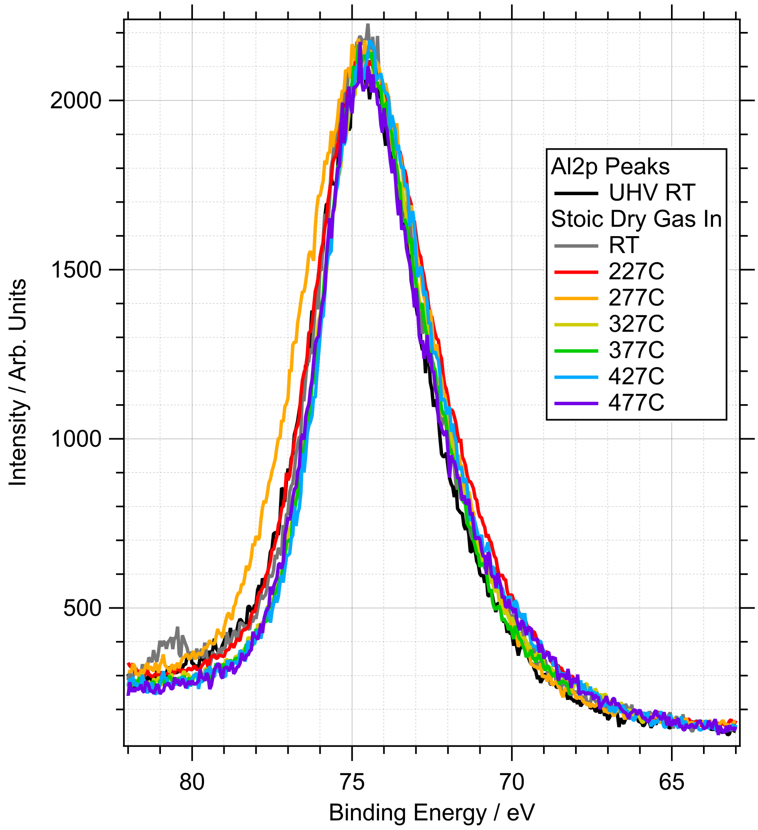

(b) Al 2p spectra

Figure 3.19: NAP-XPS spectra for a 5.0Pt catalyst recorded under dry stoichiometric methane oxidation conditions. All spectra recorded using 1350 eV photon energy.

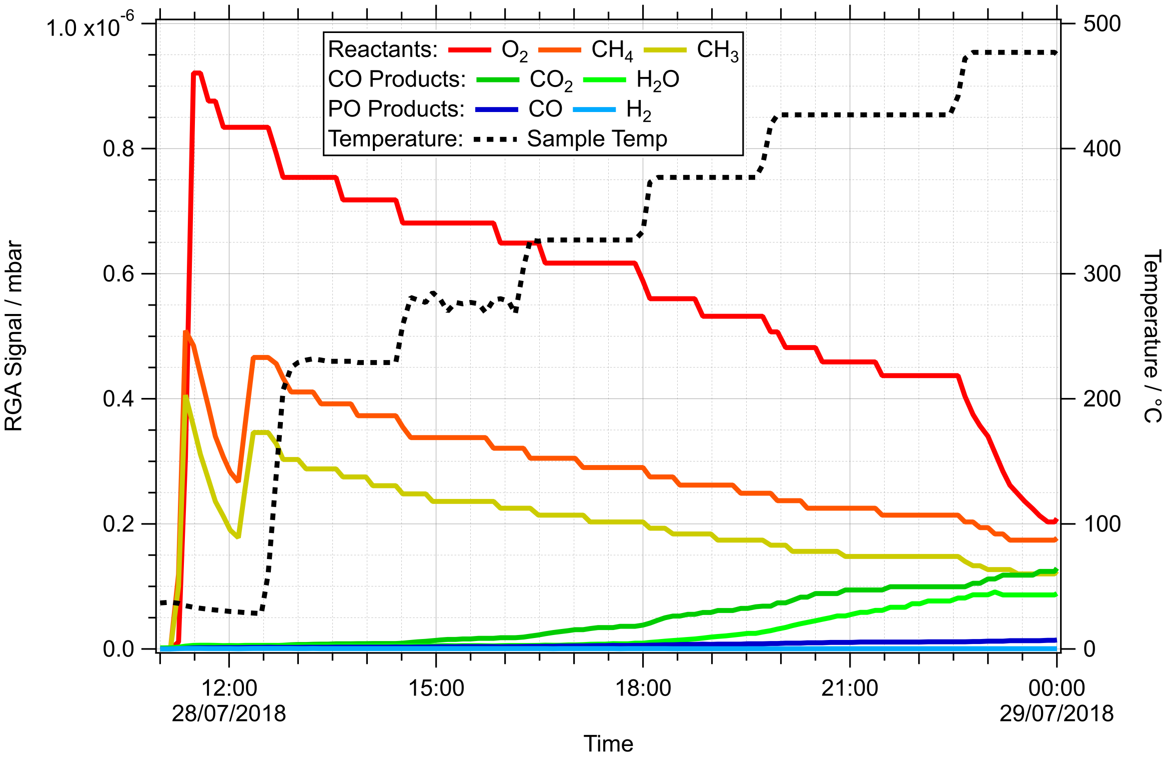

Figure 3.20: Mass spectrometry data recorded on the first pumping stage of the differential pumping system of the VerSoX beamline at Diamond, during NAP-XPS measurements of a 5.0Pt/Al_2O_3 catalyst under dry stoichiometric methane oxidation conditions.

3.3.3 Platinum on alumina summary

Platinum catalysts were largely studied here to provide explanation for effects which may be seen for bimetallic catalysts. The observed lower level of deactivation in the presence of water is a key positive for platinum catalysts, though the overall activity for methane oxidation is not ideal.

The particle sizes obtained for platinum catalysts were typically smaller after low temperature treatments, as compared to palladium. This trend was reversed however after high temperature calcination, as platinum undergoes much more significant sintering.

3.4 Monometallic catalysts summary

When comparing alumina-supported platinum and palladium catalysts for complete oxidation of methane, the differences are very clear. Palladium catalysts consistently show superior activity, even in wet reaction conditions. Various catalytic activity plots are shown in Fig. 3.21, to allow comparison of equivalent Pd and Pt catalysts. Figs. 3.21a and 3.21b show the dry testing data for 5.0Pd and 5.0Pt respectively, under each of the three methane:oxygen ratios used. Palladium performs better in feeds with a higher oxygen concentration. Platinum, however, has unusual behaviour in regards to oxygen content. 1:2 and 1:10 give initially similar behaviour, but the activity in 1:2 conditions does not match that of the other mixtures even by T20. T90 is very similar for 1:10 and 1:100, and at around 430 °C, is around 60 °C lower than that in 1:2. This shows that for initial activity and ignition the lower oxygen content is preferred, but that a higher oxygen concentration is needed to maintain higher conversions. 5.0Pd catalysts are significantly more effective than 5.0Pt catalysts under dry or wet, stoichiometric (see Fig. 3.21c) or oxygen excess (see Fig. 3.21d) conditions.

Whilst it is important to remember that all catalysts are referred to in weight loading, and as such a 5.0Pt catalyst contains less atoms of PGM than a 5.0Pd catalyst, the activity difference is not down to this. This can be seen by comparison of a 2.5Pd catalyst to a 5.0Pt catalyst - a situation where there are more Pt atoms than Pd - and this is shown in Fig. 3.21d. In this case, the 2.5Pd is significantly better in dry conditions than the 5.0Pt (T50 difference of approx. 100 °C). In wet conditions they are much more similar, with the 5.0Pt catalyst better at up to 20% conversion (approx. 375 °C). Above this, the 2.5Pd sample is superior, with a difference in T90 of over 30 °C.

The data for samples treated at 900 °C are shown in Fig. 3.21e. The significant sintering suffered by platinum after this treatment makes them very ineffective catalysts, due to the much smaller remaining surface area.

Platinum does show some positives - the limited extent of deactivation in wet conditions is very promising - but the activity is still never favourably comparable to Pd. It can be concluded that simply exchanging Pd for Pt should not be able to provide a benefit under any of the tested conditions, so any improvements noted for bimetallic Pd-Pt catalysts will depend on the form taken by the nanoparticles, and the interaction between the metals.

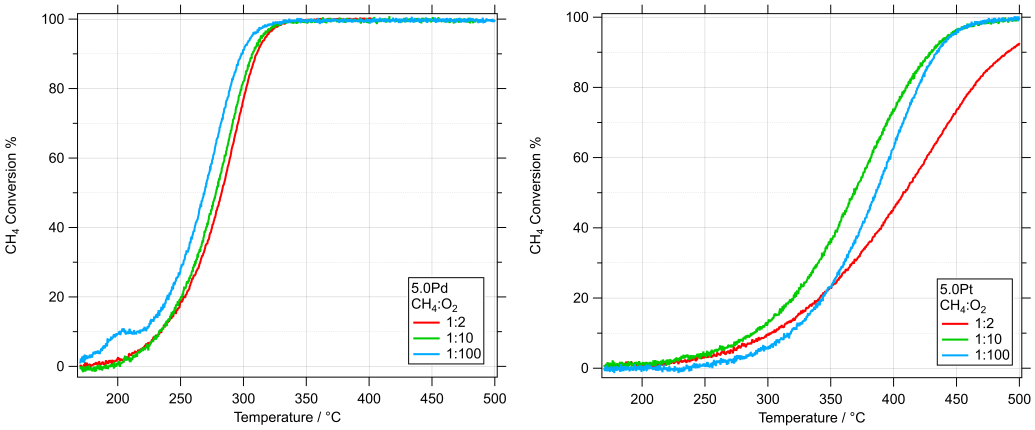

(a) All 5.0Pd (b) All 5.0Pt

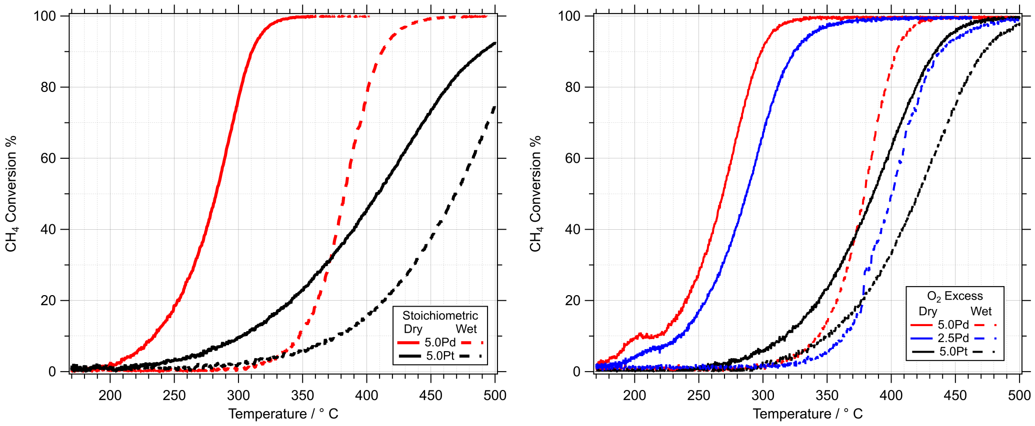

(c) Stoichiometric (d) Oxygen Excess

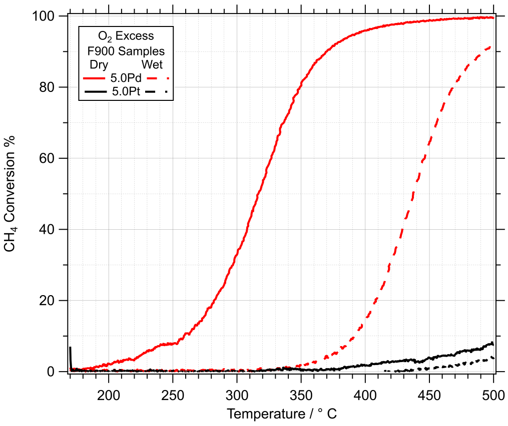

(e) 900 °C Calcined

Figure 3.21: Synthetic catalyst activity testing data for various Pd and Pt monometallic catalysts under various methane oxidation conditions.

3.5 Palladium-Platinum on alumina

3.5.1 Preparation & Characterisation

Loading / wt. %	500 °C	800 °C	900 °C	500 °C T
4.0Pd-1.0Pt	14.4	20.0	29.1	15.8
2.5Pd-2.0Pt	10.6	25.1	35.6	10.6
2.5Pd-2.5Pt	10.5	31.4	52.7	11.6
2.5Pd-3.0Pt	9.0	31.9	38.6	8.2
1.0Pd-4.0Pt	4.0	41.8	50.3	4.3

Table 3.5: Average particle sizes for bimetallic Pd-Pt/Al_2O_3 catalysts at various calcination temperatures, and after catalytic testing (500 °C T). All determined by CO chemisorption.

With palladium catalysts showing consistently good activity across varied conditions, and platinum catalysts showing a greater resistance to deactivation in wet conditions, a series of bimetallic catalysts was prepared to explore the synergy between these two metals. The catalysts in this series range from Pd-rich (4.0Pd-1.0Pt) to Pt-rich (1.0Pd-4.0Pt) with various intermediate examples. Three bimetallic catalysts were prepared with 2.5Pd in each, with varied platinum loadings of 2.0, 2.5 and 3.0 respectively. Whilst these catalysts differ in total weight loading, they allowed us to monitor the effects of simple addition of platinum, rather than Pd-Pt exchanging. It was preferable to make variations to only 1 metal, as the exchange would not make it clear which part(s) was causing the change(s).

ICP-MS measurements were peformed for 4.0Pd-1.0Pt, 2.5Pd-2.5Pt and 1.0Pd-4.0Pt "fresh" and 500 °C calcined catalysts. These data are summarised in Tab. 3.6. The ratios between the weight percentages of palladium and platinum are shown for each case, with minimal variations between the fresh and calcined catalysts. This shows the preparation process to be reliable, as the achieved ratios are reasonably close to the intended values in all cases.

The particle sizes, as shown in Tab. 3.5, show a largely expected variation between Pd-rich and Pt-rich samples. After 500 °C treatment only, there is a general trend for larger particles with a higher Pd : Pt ratio, with the exception of 2.5Pd-2.0Pt and 2.5Pd-2.5Pt, which have a very similar average size. This trend remains post-catalytic testing, with only minor variations (approx. ± 10%).

After higher temperature treatments, there is always an increase in average size, with higher Pt-loaded catalysts undergoing more dramatic increases. This is consistent with the

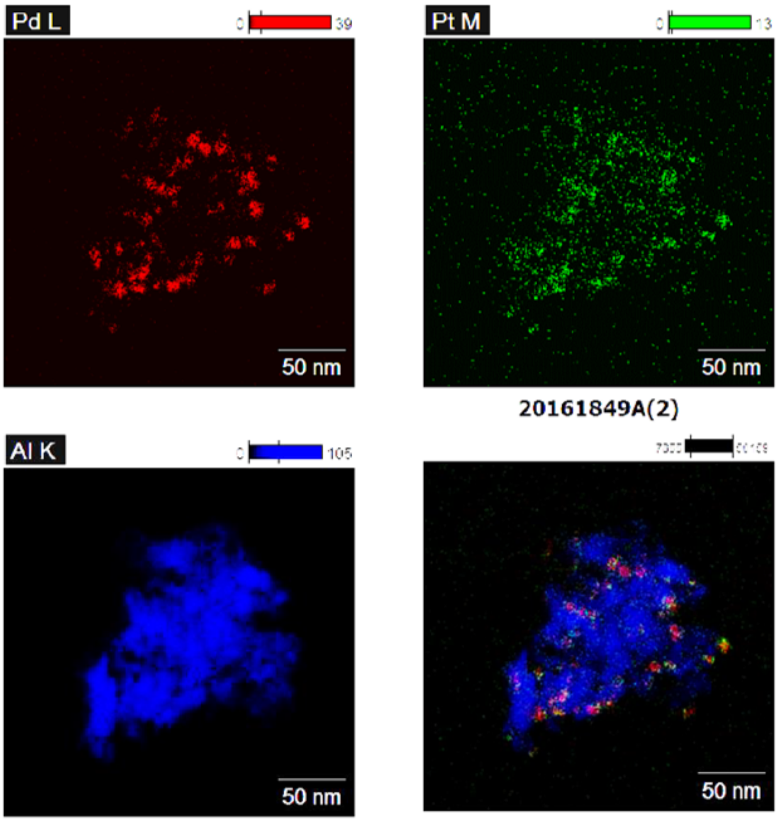

(a) 4.0Pd-1.0Pt 500 °C

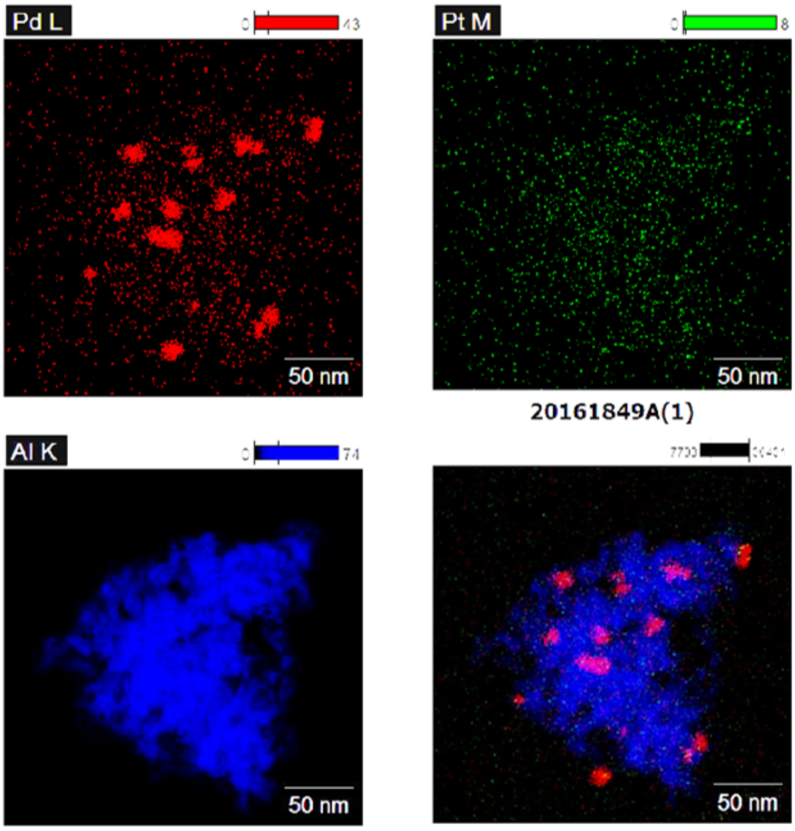

(b) 4.0Pd-1.0Pt 800 °C

Figure 3.22: TEM images with EDX maps for bimetallic catalysts after 500 °C or 800 °C calcination.

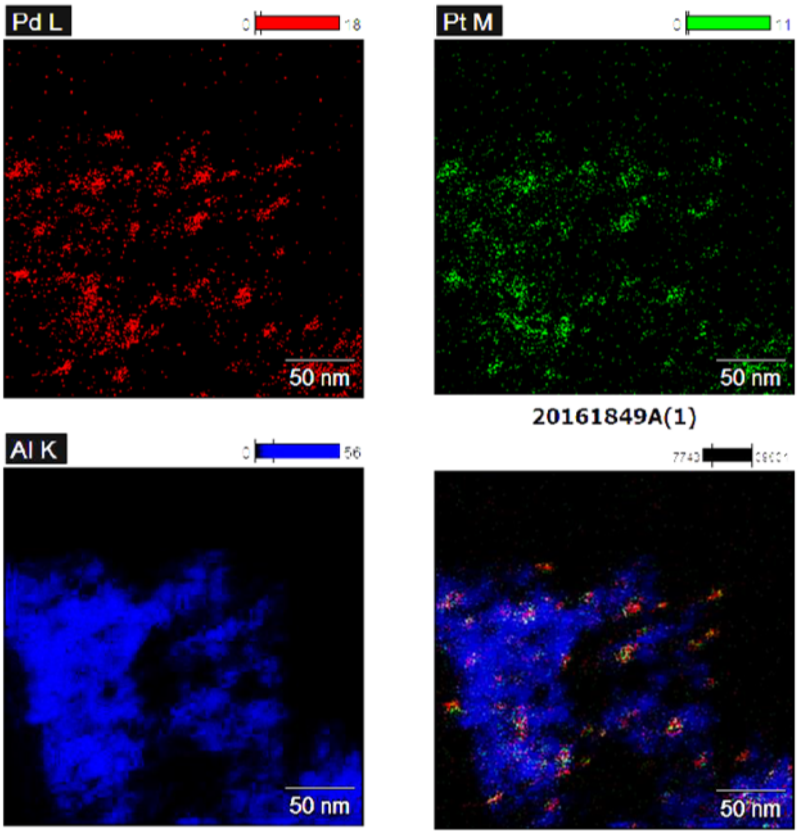

(a) 2.5Pd-2.5Pt 500 °C

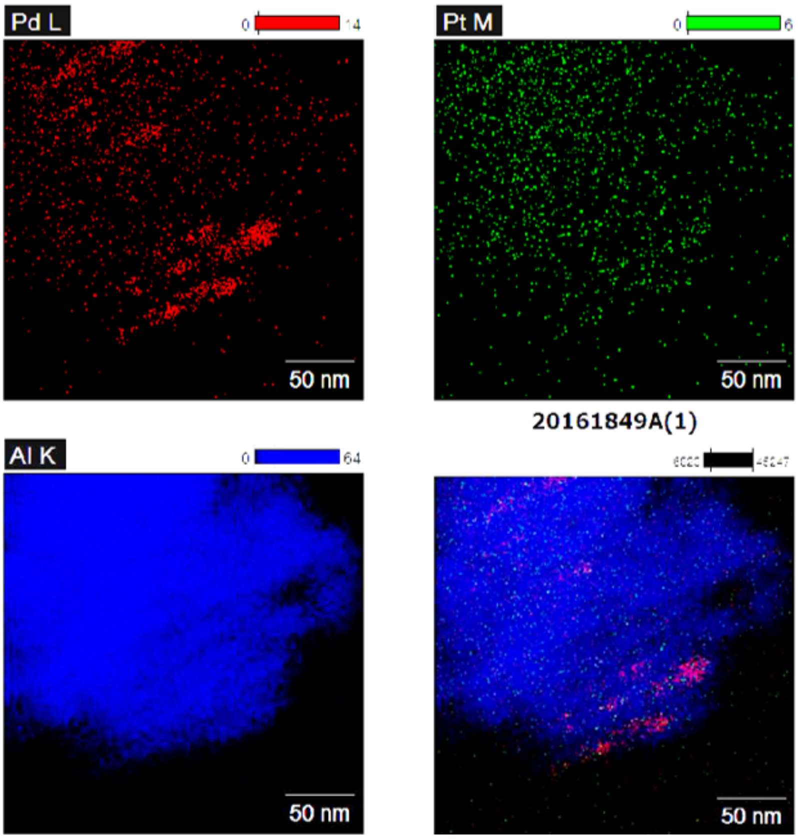

(b) 2.5Pd-2.5Pt 800 °C

Figure 3.23: TEM images with EDX maps for bimetallic catalysts after 500 °C or 800 °C calcination.

Composition	Fresh Pd %	Fresh Pt %	Fresh Ratio	500 °C Pd %	500 °C Pt %	500 °C Ratio
4.0Pd-1.0Pt	3.11	0.83	3.75 : 1	3.48	0.92	3.78 : 1
2.5Pd-2.5Pt	1.97	1.99	0.99 : 1	2.18	2.21	0.99 : 1
1.0Pd-4.0Pt	0.76	3.11	0.24 : 1	0.87	3.58	0.24 : 1

Table 3.6: Platinum and palladium percentage data for fresh and 500 °C calcined bimetallic catalysts as determined by ICP-MS, including ratios of weight percentages.

monometallic data, where Pt catalysts increased in size significantly more than Pd catalysts. When comparing 500 °C and 900 °C treated samples, 4.0Pd-1.0Pt increases from 14.4 nm to 29.1 nm (a 102% increase) whilst 1.0Pd-4.0Pt increased from 4.0 nm to 50.3 nm (a 1257% increase). Unusually, the catalyst with the largest average particle size after 900 °C treatment was 2.5Pd-2.5Pt, at 52.7 nm. This was significantly greater than that of the similarly loaded 2.5Pd-2.0Pt and 2.5Pd-3.0Pt, which were 35.6 and 38.6 nm respectively. Whilst the 2.5Pd-2.5Pt was prepared at a different time to the other two 2.5Pd-based bimetallic catalysts, there should not be any specific issues with the alumina or metal precursor batches used. There should be minimal differences in the physical preparation - initial calcinations would have been performed with different numbers of samples (5 total for 2.5Pd-2.5Pt, 2 total for the others), but all 900 °C treatments were performed at the same time. The time difference between preparation and CO chemisorption measurements will have varied between the two, but any change over time would be expected to be minimal, and not give the differences observed here. A repeat measurement of the 2.5Pd-2.5Pt sample some time later gave a value of 49.9 nm, which is reasonably consistent with the initial value.

TEM images and EDX maps are shown in Fig. 3.22 and 3.23 for 4.0Pd-1.0Pt and 2.5Pd-2.5Pt catalysts respectively, after treatment at both 500 °C and 800 °C. In the case of both 500 °C treated samples, it is fairly clear that Pd and Pt largely appear in the same locations, with minimal presence of monometallic particles. In all images, there is a large amount of background noise, generally visible as single pixel dots, due to the length of data collection as a result of the low loadings.

Line scans taken over individual particles in 4.0Pd-1.0Pt 500 °C and 800 °C samples are shown in Fig. 3.24. For the 500 °C sample 3 Pd-Pt particles are shown across 2 maps, in Figs. 3.24a and 3.24b, and in all cases there is no clear ordering of Pd and Pt relative to each other, confirming there is no continuous structuring (such as core-shell). Given the

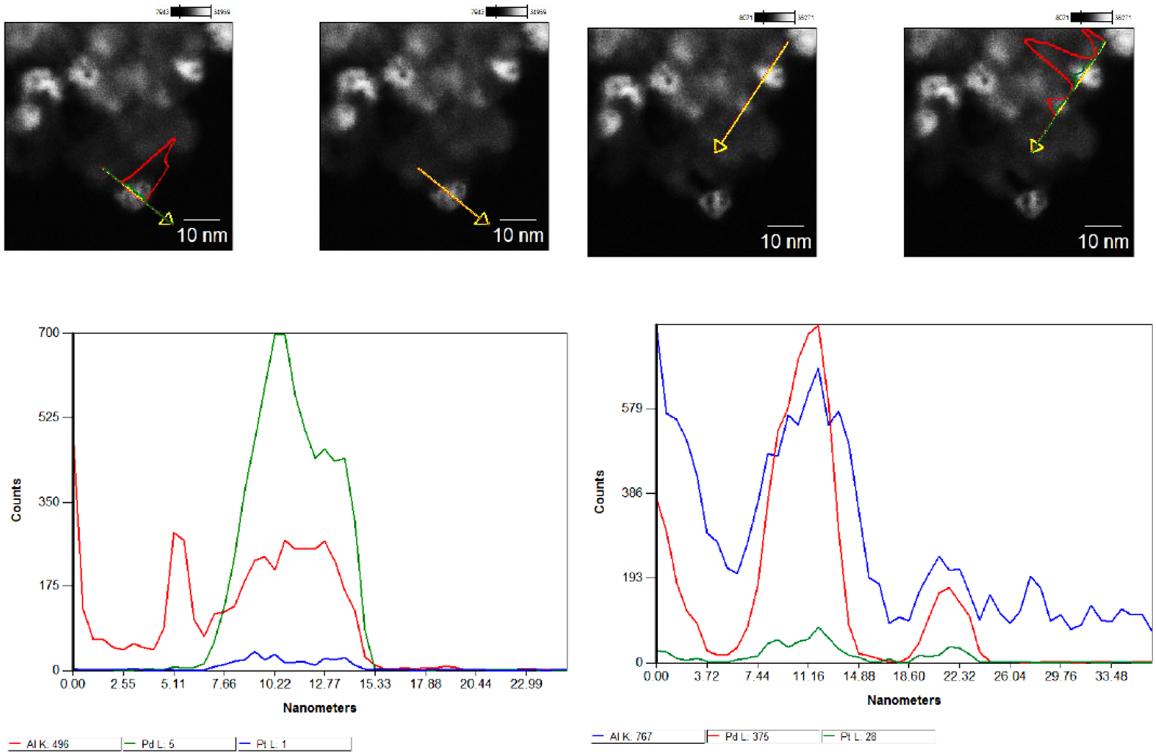

(a) 4.0Pd-1.0Pt 500 °C spot 1

(b) 4.0Pd-1.0Pt 500 °C spot 2

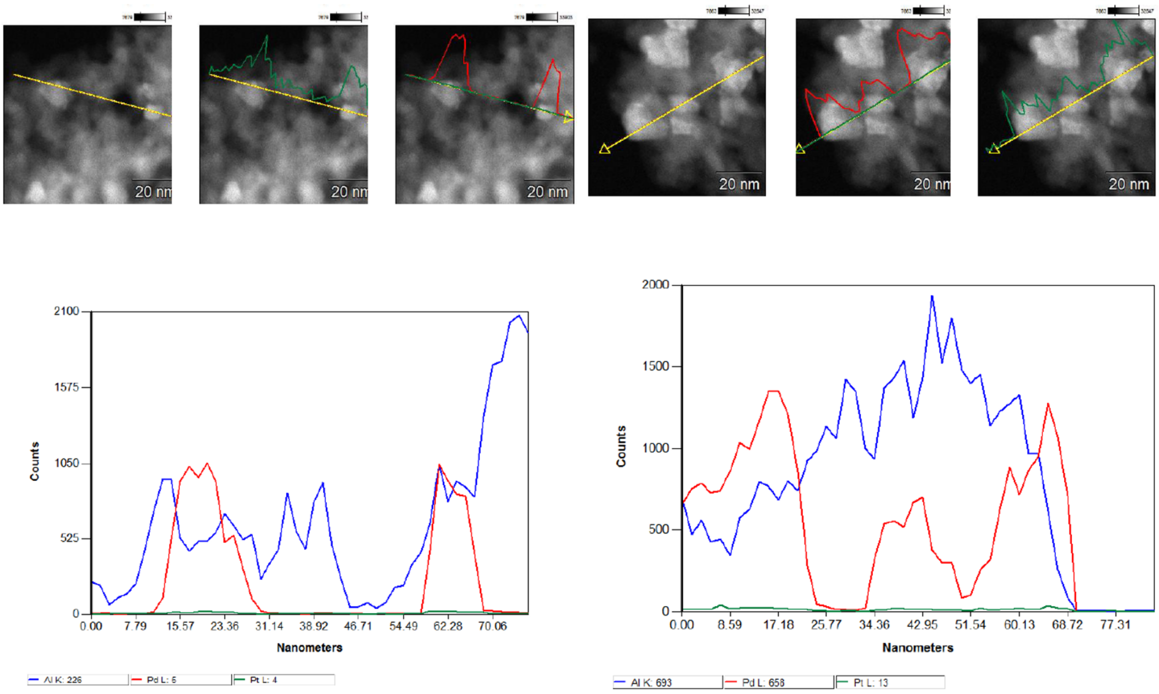

(c) 4.0Pd-1.0Pt 800 °C spot 1

(d) 4.0Pd-1.0Pt 800 °C spot 2

Figure 3.24: Maps taken in two different spots of 4.0Pd-1.0Pt catalysts after 500 °C and 800 °C treatment using TEM & EDX. Note that the line colours are not consistent across all graphs.

preparation method, no specific ordering was expected, and this provides confirmation of this. In the case of spot 1, shown in Fig. 3.24a, there is a Pd enrichment on one side of the particle. This is not observed in either of the other particles, suggesting that the composition is not overly consistent on a particle-by-particle basis. In all studied spots, the observed Pd : Pt ratio is similar.

Two line scans were also performed for a 4.0Pd-1.0Pt sample after a higher temperature treatment at 800 °C. These particles also show no preferential structuring, although it is notable how much lower the counts for platinum are compared to the 500 °C sample.

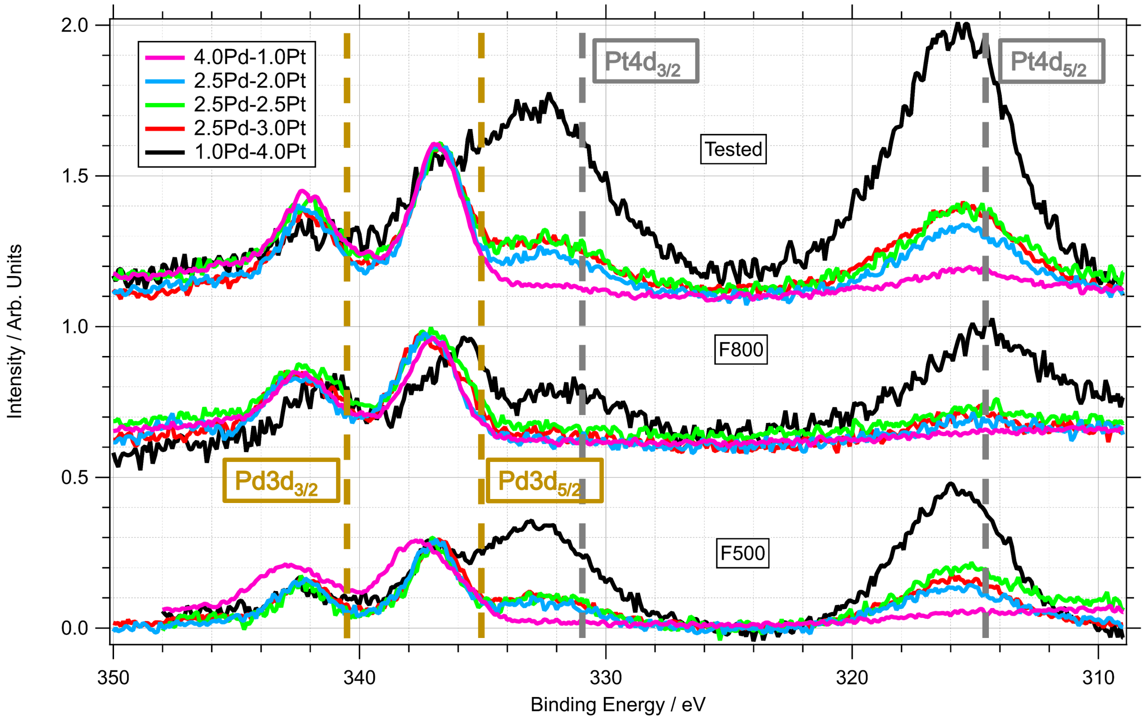

Figure 3.25: Pt 3d and Pt 4d region XPS spectra of all bimetallic catalysts after treatment at 500 °C, 800 °C, and after catalytic testing. Tested catalysts had previously been treated at 500 °C. All spectra recorded with 1486.6 eV photon energy, under ultra-high vacuum conditions at room temperature. All corrected to Al 2p at 74.6 eV. All Pd $3d_{5/2}$ peak intensities aligned to the same value for a given condition for clarity of presentation. Vertical dashed lines indicate typical expected positions for metallic palladium and platinum.

Palladium 3d and platinum 4d region XPS data for all bimetallic catalysts after 500 °C and 800 °C treatments, along with tested versions, are shown in Fig. 3.25. The Pd : Pt ratio decreases between the 500 °C and 800 °C samples, which is consistent with the observations from the EDX line scans. This may be indicative of platinum moving into the bulk of the larger particles with increasing calcination temperature. The Pd 3d peaks for 4.0Pd-1.0Pt are significantly broader than any other samples after 500 °C treatment, indicating a generally more oxidised palladium is present. After higher temperature treatments, Pd seems to be consistently oxidised in most samples. An exception is 1.0Pd-4.0Pt after 800 °C calcination. In this case, Pd appears to be split between a reduced and oxidised species. This is not the case for this sample after the 500 °C calcination, nor after catalytic testing, although in the latter case the Pd 3d peaks are not as well resolved. For this case, there is also a significant change in Pd : Pt ratio with the 800 °C treatment. In the 500 °C spectrum, the Pt peaks are notably larger than the Pd peaks, but this is reversed after the higher temperature treatment. This could be more evidence for particle restructuring, as the relative intensities would change in this way in a case where Pt migrated towards the core. The EDX for this shows a very small amount of platinum, so it is hard to gain much information on structure in that case.

Comparison of hydrogen TPR are shown in Fig. 3.26, divided into two sub-figures for clarity. Fig. 3.26a shows the TPR profiles for the three original Pd-Pt catalysts after 3 different calcination treatments. For 500 °C treated samples, 1.0Pd-4.0Pt is the most readily reduced, with the main peak coming well below 50 °C. 4.0Pd-1.0Pt follows this, with the least readily reduced sample being 2.5Pd-2.5Pt, giving no overall trend across the set. After higher temperature calcinations, the 1.0Pd-4.0Pt sample shows very little reduction behaviour, which is partially consistent with its more reduced appearance from the XPS data. For both 800 °C and 900 °C calcined samples, a greater peak is seen for 4.0Pd-1.0Pt than 2.5Pd-2.5Pt, indicating a greater presence of more oxidised samples in these cases.

Fig 3.26b shows the TPR profiles for all catalysts containing 2.5Pd. For all the 500 °C calcined samples the main peak intensity is somewhat similar, though there is a significant low temperature reduction for 2.5Pd-2.0Pt, whilst 2.5Pd-2.5Pt shows its only reduction feature at the highest temperature of the set. Overall there is no trend observed with regards to platinum loading in these samples. After higher temperature treatments, the greatest reduction is seen for 2.5Pd, indicating that this sample retains the most oxidised Pd after these calcination processes.

Activity testing data is presented graphically in Fig. 3.27 and 3.28, with T50 and TOF values included in Tab. 3.7. Fig. 3.27a shows all 5 bimetallic catalysts tested under dry and wet oxygen rich conditions. In both cases, the 4.0Pd-1.0Pt catalyst is superior, albeit the

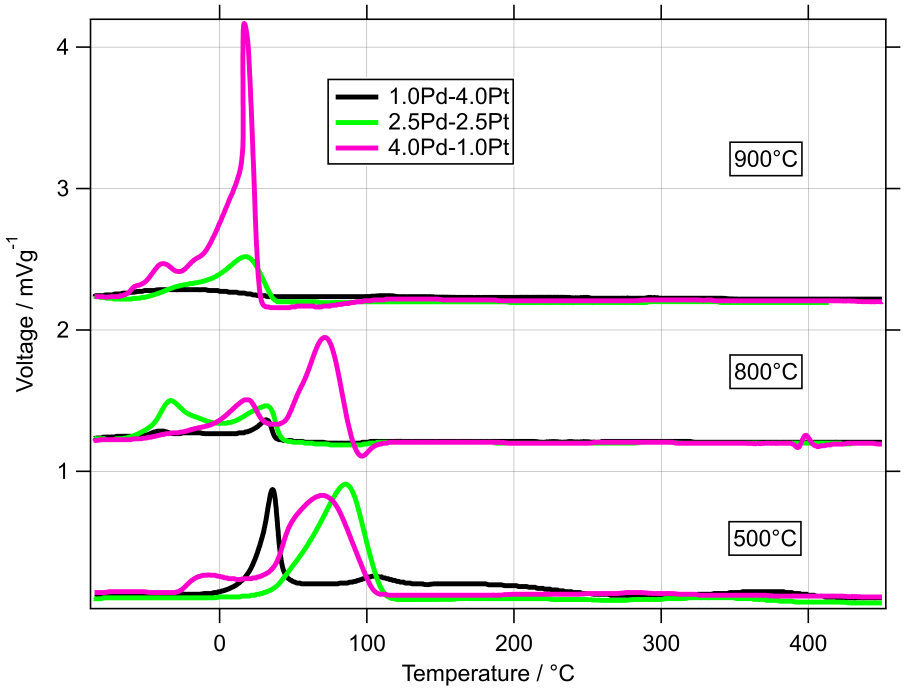

(a) 4.0Pd-1.0Pt, 2.5Pd-2.5Pt and 1.0Pd-4.0Pt catalysts

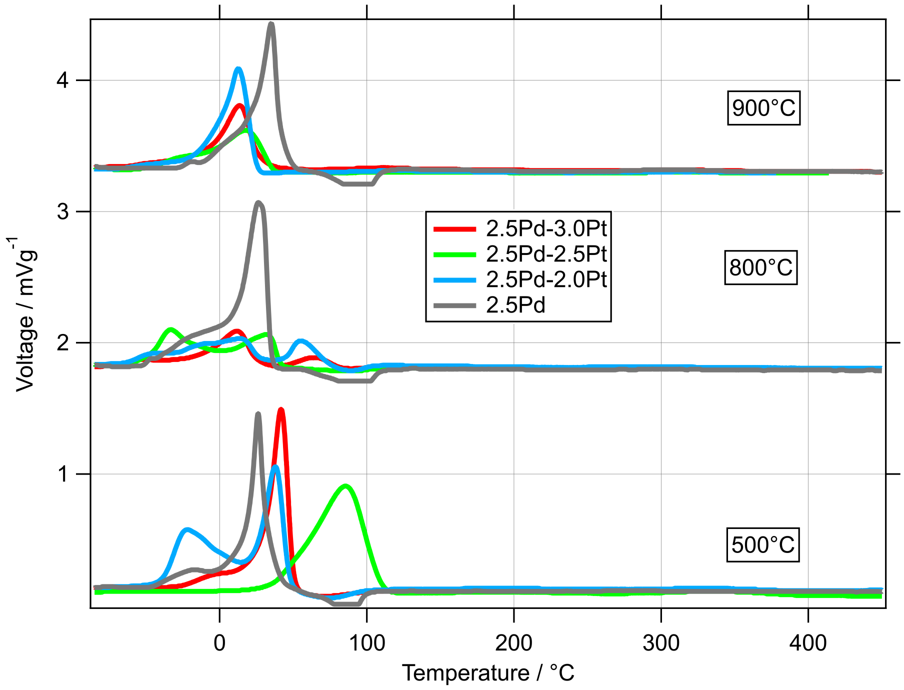

(b) All 2.5Pd based catalysts

Figure 3.26: TPR data for bimetallic catalysts after treatment at 500 °C, 800 °C and 900 °C. 800 °C data offset by +1.1 mVg^{-1}, 900 °C data offset by +2.1 mVg^{-1}.

extent of this is limited in the wet conditions. The three bimetallic catalysts based on 2.5Pd all perform very similarly under dry or wet conditions. In both cases, the higher Pt loading leads to a slightly better performance, although the T50 values show only small differences,

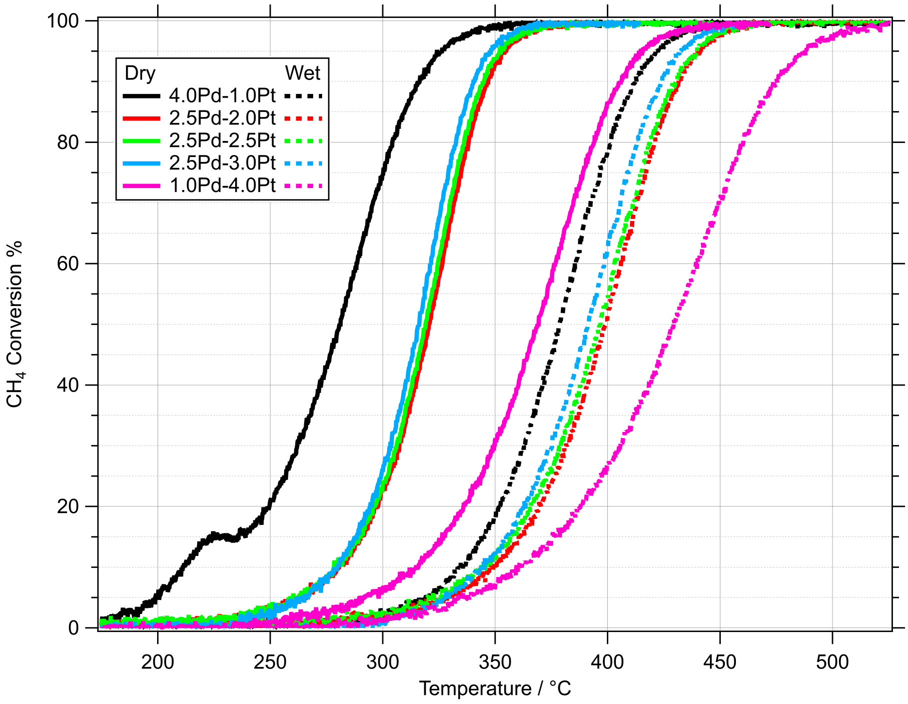

(a) All Bimetallic 500 °C

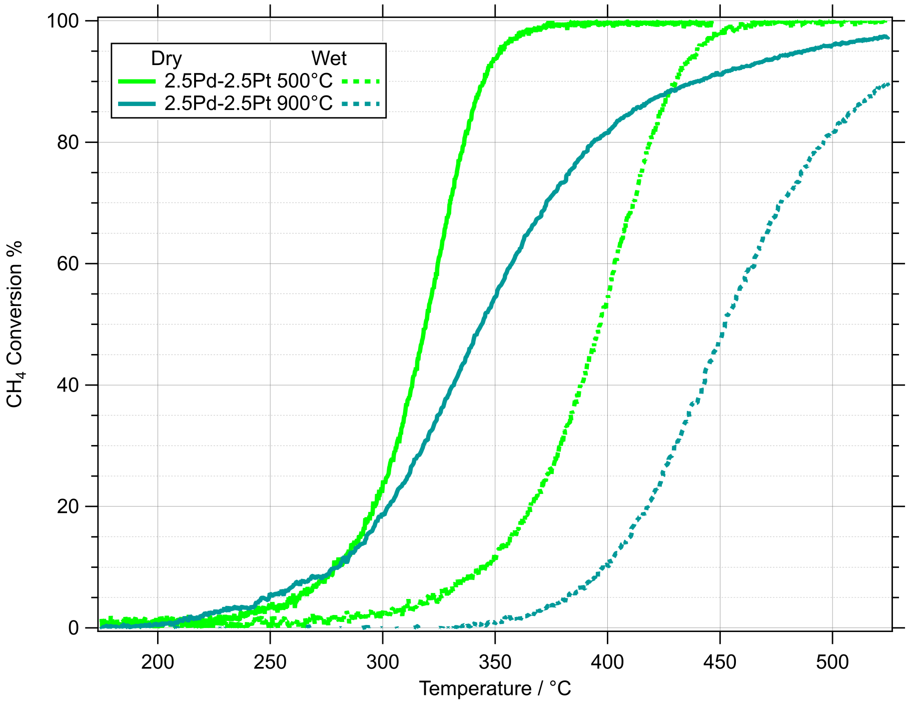

(b) 2.5Pd-2.5Pt after 500 °C and 900 °C

Figure 3.27: Compilation of activity tests for bimetallic catalysts dry and wet oxygen rich conditions.

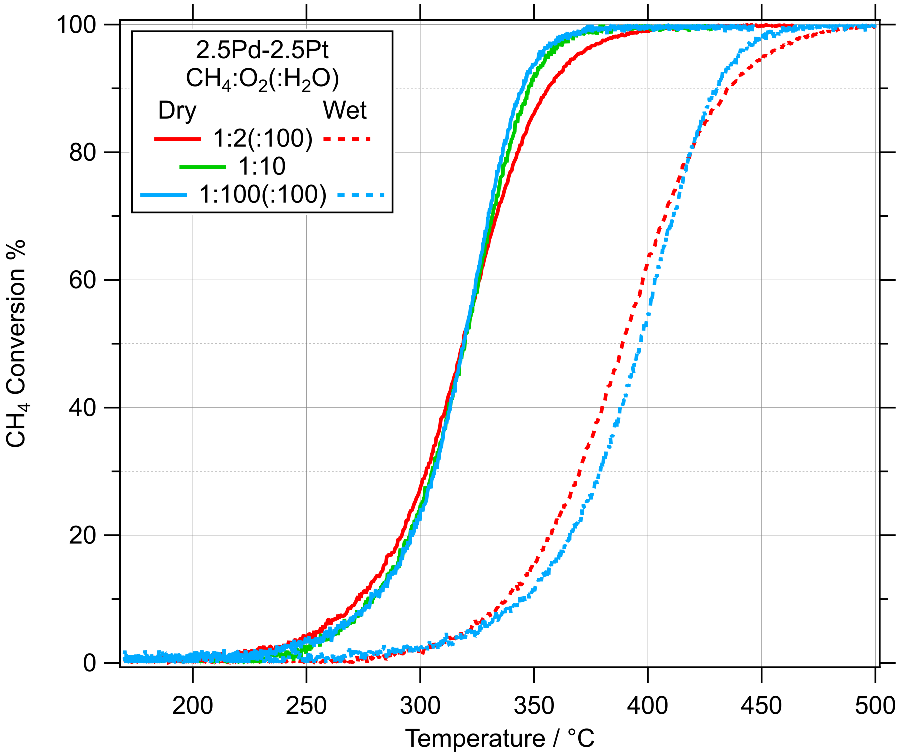

(a) 2.5Pd-2.5Pt

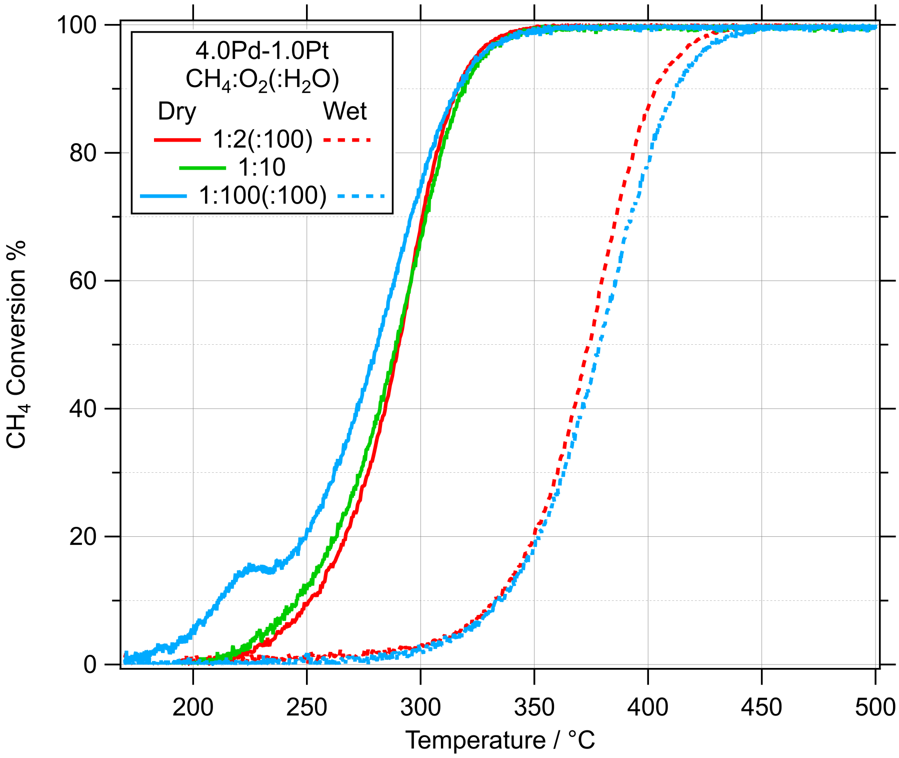

(b) 4.0Pd-1.0Pt

Figure 3.28: Compilation of activity tests for bimetallic catalysts under various conditions.

321 to 316 °C in dry, 399 to 391 °C in wet. In both dry and wet, the 1.0Pd-4.0Pt catalyst is significantly worse than all other compositions. Given the low activity of platinum and the low loading of palladium this is hardly surprising. This composition primarily exists to better understand the effects of combining the 2 metals.

Fig. 3.27b shows a comparison between 2.5P-2.5Pt catalysts calcined at 500 °C and 900 °C. The average particle sizes of these catalysts are, as shown previously in Tab. 3.5, 10.5 nm and 52.7 nm respectively. It is surprising, then, that under dry conditions, the initial activity is very similar. However, after 290 °C, the activity of the 900 °C calcined catalyst fails to keep pace with the 500 °C calcined version, failing to reach 100% conversion before 500 °C. By comparison, this happens well below 400 °C for the 500 °C sample. In wet conditions, the initial similarity is lost, with the 900 °C sample being consistently worse, but again further worsening at higher conversions, only reaching around 90% conversion by 500 °C.

Figs. 3.28a and 3.28b show the effects of oxygen concentration on the methane conversion activity for 2.5Pd-2.5Pt and 4.0Pd-1.0Pt catalysts respectively. For 2.5Pd-2.5Pt, the stoichiometric gas feed gave better conversion at low temperatures in both dry and wet conditions. However, in both cases, the catalysts reach 100% conversion at lower temperatures in oxygen rich conditions than for stoichiometric. The point at which this switches varies depending on water, around 50% or 320 °C in dry, to 90% and 420 °C in wet. In dry conditions, the difference between the 1:10 and 1:100 conditions is minimal across the full range of conversions. The 4.0Pd-1.0Pt sample shows very different behaviour to this. In dry conditions, the oxygen rich feed shows better conversion at low temperatures, but very similar to the stoichiometric and 1:10 feeds at high conversion, with all reaching 90% conversion at around 315 °C. In the presence of water the catalyst light off is very similar in both rich and stoichiometric conditions, but the stoichometric feed allows the catalyst to reach full conversion slightly before the rich condition.

Across the four tested conditions for the pair of catalysts, only minimal differences are seen in regards to the temperature at which full conversion is reached. Whilst the rich feed is more representative of typically expected conditions, this provides reassurance that these catalysts could continue to function effectively in more oxygen lean gas feeds.

Loading / wt. %	T50 Dry	T50 Wet	DT50	TOF Dry	TOF Wet
4.0Pd-1.0Pt	281	379	98	2.35×10^{-2}	2.00×10^{-2}
2.5Pd-2.0Pt	321	399	78	3.52×10^{-3}	1.09×10^{-2}
2.5Pd-2.5Pt	319	397	78	3.00×10^{-3}	1.07×10^{-2}
2.5Pd-3.0Pt	316	391	75	1.32×10^{-3}	9.13×10^{-3}
1.0Pd-4.0Pt	369	429	60	4.97×10^{-4}	3.29×10^{-3}
2.5Pd-2.5Pt 900 °C	344	452	108	2.63×10^{-2}	4.97×10^{-3}
4.0Pd-1.0Pt Stoic.	290	375	85	1.05×10^{-1}	2.24×10^{-2}
2.5Pd-2.5Pt Stoic.	319	389	70	3.86×10^{-3}	1.48×10^{-3}

Table 3.7: T50 data and turnover frequencies for all Pd-Pt bimetallic catalysts. 500 °C treated and oxygen excess conditions unless otherwise noted. TOF values determined at 250 °C and 350 °C for dry and wet conditions respectively.

3.5.2 Near-ambient pressure XPS of Pd-Pt/Al_2O_3 catalysts under methane oxidation conditions

Primary NAP-XPS experiments focused on 5 gas conditions, the same as those shown previously for 5.0Pd. These are: stoichiometric dry, stoichiometric wet, stoichiometric very wet, oxygen rich dry, and oxygen rich wet. The Pd 3d spectra are shown for 4.0Pd-1.0Pt in Figs. 3.29 and 3.30 for stoichiometric and oxygen rich conditions respectively. These show how the relative presence of Pd(0) (BE: 335.0 eV) and Pd(II) (BE: 336.7 eV) changes over the course of the reaction for each different condition. Initial vacuum measurements typically show a higher presence of Pd(0). Under stoichiometric conditions, an increase in Pd(II) is observed with increasing temperature, though the maximum level varies dependant on the gas condition used. With increasing water presence, the final state contains more Pd(0), indicating that the water presence is inhibiting the Pd(II). Under oxygen rich conditions, the Pd is fully Pd(II) in the majority of measurements, with only a minor presence of Pd(0) at the lower temperatures. Above 227 °C in the dry, and 327 °C in the wet, there is no presence of Pd(0). This is similar to the behaviour seen for 5.0Pd, where the catalyst is always fully oxidised. In most cases, the completed fits (solid black line) gave good agreement with the experimental data (red dots). There are a few exceptions in these experiments, where it was not possible to perfectly match the experimental data. Notably in oxygen rich dry conditions, the measurements at 277 °C and 327 °C show Pd $3d_{5/2}$ peaks at a higher binding energy than the typical value for Pd(II), at around 336.7 eV binding energy. The difference is well below 1 eV, and the peaks fairly sharp, so it is unlikely to be due to any presence of Pd(IV), or any other higher state. Whilst peak positions are kept heavily restricted in the fits in order to ensure consistency between different fits, it is possible that Pd(II) could appear at this higher energy. Given that the fits here represent 100% Pd(II) anyway, it is unlikely that this variation significantly affects the results here. The Al 2p peaks for these temperatures, and those below/above have been compared, and show no significant variation, confirming the corrections are not an issue here.

The NAP-XPS data for 4.0Pd-1.0Pt are summarised, together with the catalytic activity data, in Fig. 3.31. This clearly shows the plateau effect in Pd(II) that is seen in stoichiometric reaction conditions: once full conversion is reached, the Pd(II)% levels off, rather than increasing to 100% as was observed for 5.0Pd. This plateau level decreases with increased wa-

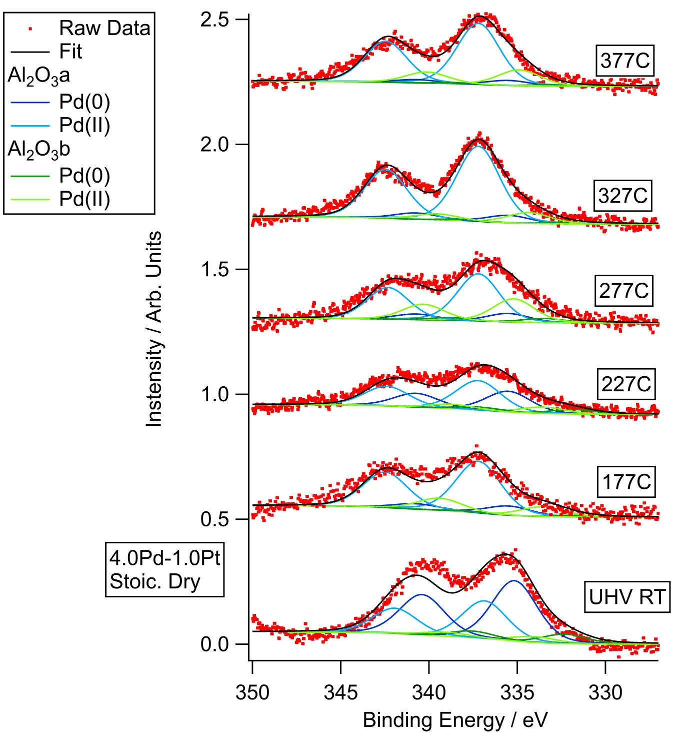

(a) Stoic. Dry

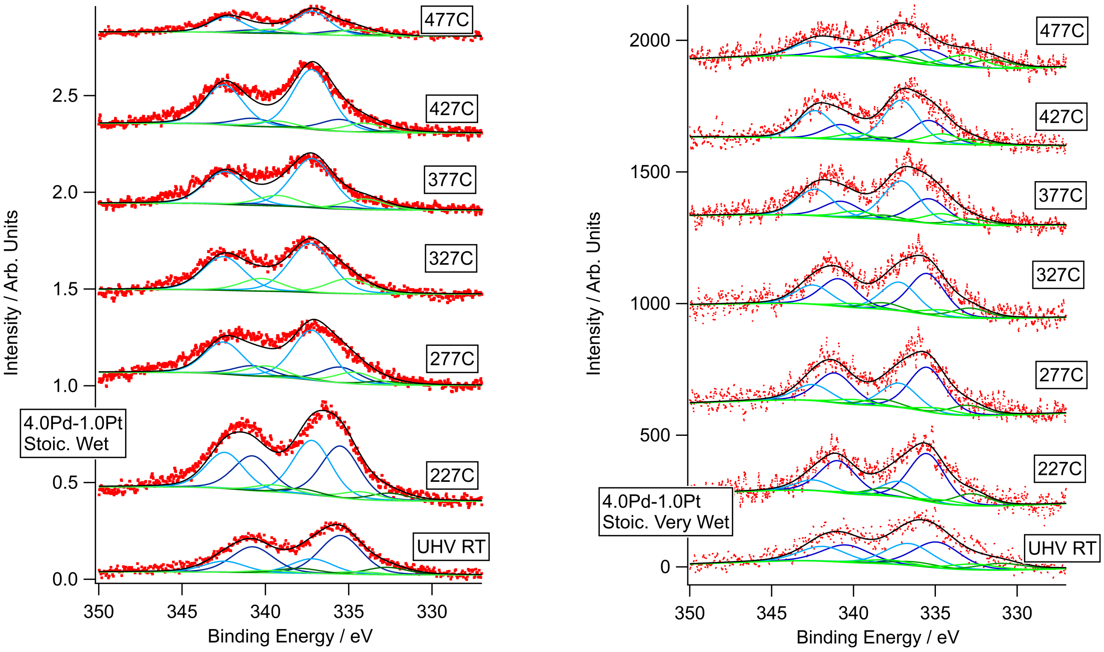

(b) Stoic. Wet

(c) Stoic. Very Wet

Figure 3.29: Pd 3d region NAP-XPS data for 4.0Pd-1.0Pt catalyst under all tested stoichiometric conditions. All spectra recorded using 1350 eV photon energy.

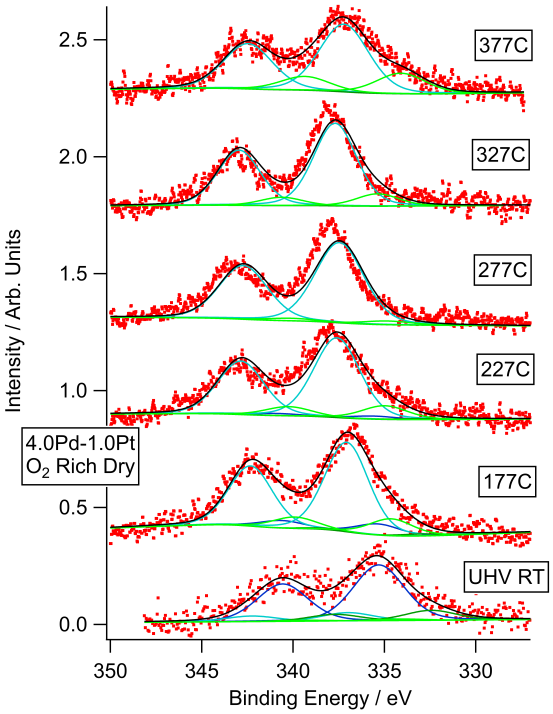

(a) Oxygen Rich Dry

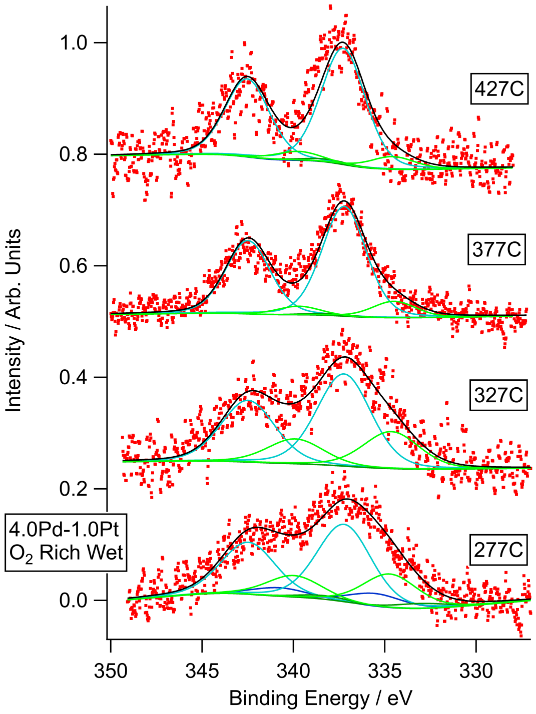

(b) Oxygen Rich Wet

Figure 3.30: Pd 3d region NAP-XPS data for 4.0Pd-1.0Pt catalyst under all tested oxygen rich conditions. Key is consistent with Fig. 3.29. All spectra recorded using 1350 eV photon energy.

ter presence in the feed: from 92% in dry, to 83% in wet, to 60% in very wet conditions. This is the most direct evidence we have that the increased water presence negatively impacts the presence of Pd(II). However this does not have a negative impact on activity as had been expected. Comparing the two conditions in which water is present at 100 times greater amount than methane (stoichiometric very wet, oxygen rich wet), the catalyst is active at slightly lower temperatures in the stoichiometric condition, despite the significantly lower level of palladium oxidation observed. In the dry condition the gap between the Pd(II)% for the two oxygen levels is smaller, with the stoichiometric condition initially showing worse activity. By 90% conversion however, they are very similar, with stoichiometric being marginally better, where the Pd still has a small presence - less than 10% - of Pd(0). Overall, this is good evidence that the presence of Pd(0) is beneficial for methane oxidation. Whilst Pd(II) still makes up the majority of the Pd for most measured conditions at reaction temperatures, the Pt presence does seem to enable some of the Pd to stay reduced. The difficulty in measuring a platinum signal in XPS for these catalysts makes it unclear the exact origin of this benefit. It is possible that the platinum presence in the nanoparticle surface prevents the water from sticking directly to the palladium, and blocking the more active reaction sites.

Measurements under the same conditions were also performed for a 2.5Pd-2.5Pt catalyst, and are shown in Figs. 3.32 and 3.33 for stoichiometric and oxygen rich conditions respectively. Under stoichiometric dry conditions, the palladium is fully oxidised to Pd(II) at 3 of the 4 temperatures measured. It is less easily oxidised under either stoichiometric wet conditions, but it is still primarily Pd(II) at most temperatures in either case. Oxygen rich data show a similar trend, with the Pd rarely being fully oxidised. The only point at which it appears to be fully oxidised is in oxygen rich wet conditions, at 377 °C. In this case, the water had run out during the measurement, but this was not noticed until the temperature had been increased to 427 °C for the next measurement. Given the nature of the experiment, and the hysteresis often observed on methane oxidation catalysts, it was decided that decreasing the temperature to measure again would not give accurate data. Whilst this data point is therefore not representative for this condition, it does show that a partially oxidised catalyst can readily become fully oxidised, where the presence of water is removed. This is consistent with some of the other results, showing a higher relative Pd(II) presence in dry conditions than wet, at a given temperature.

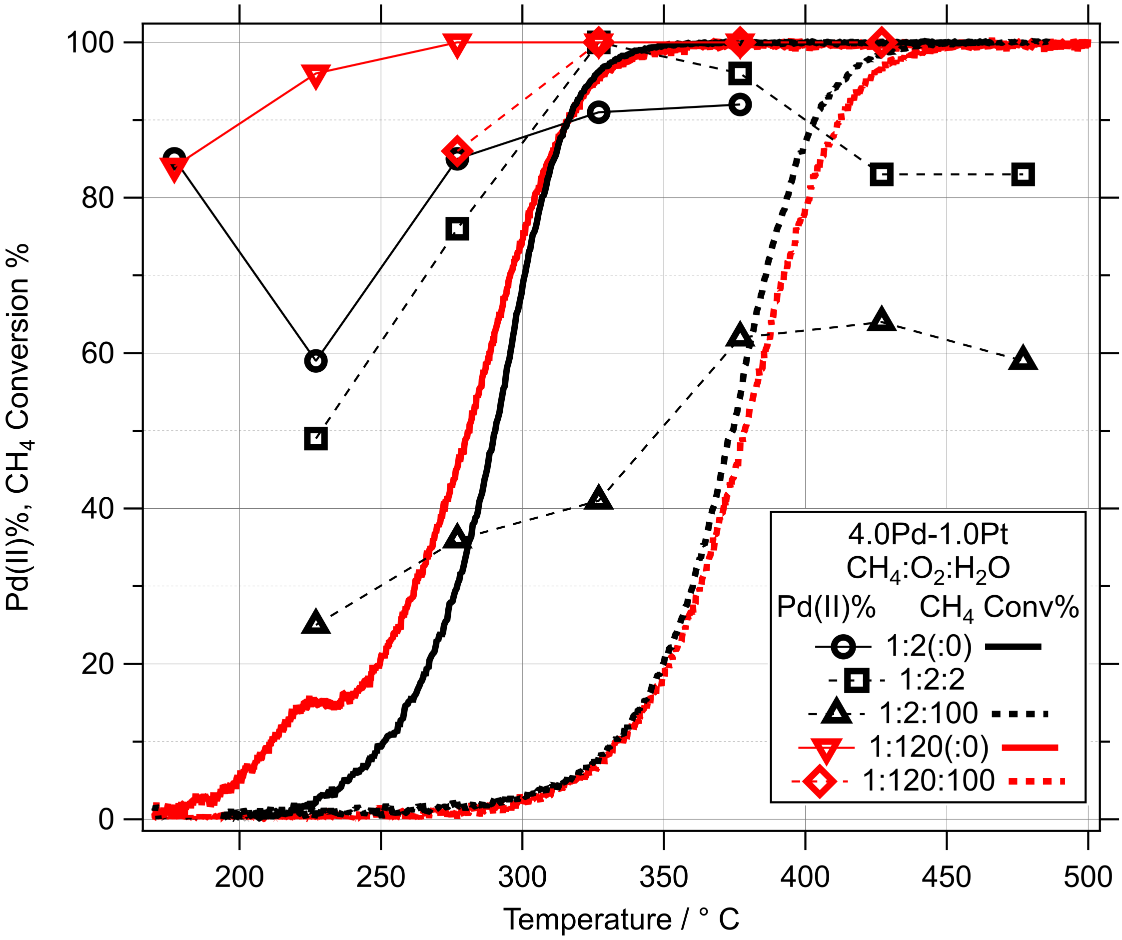

Figure 3.31: NAP-XPS data overlaid with catalytic activity data for 4.0Pd-1.0Pt catalyst, recorded under various dry and wet conditions.

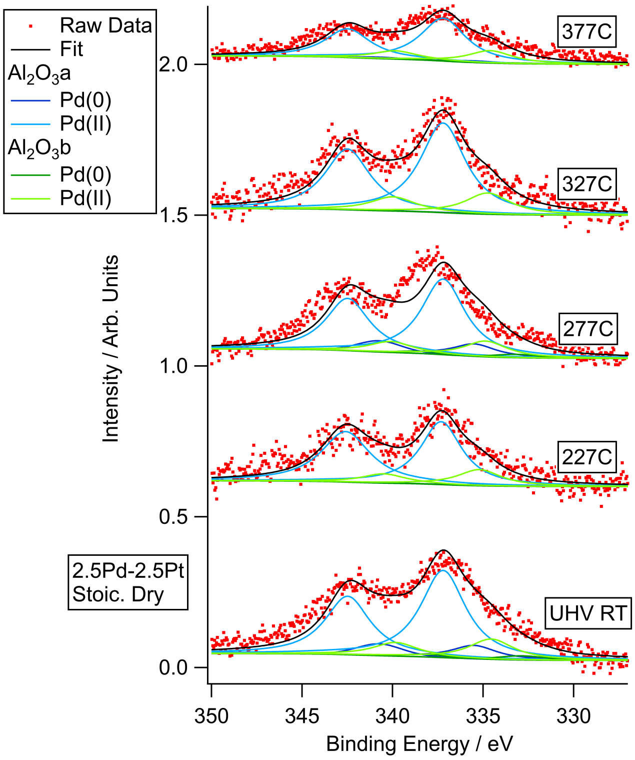

(a) Stoic. Dry

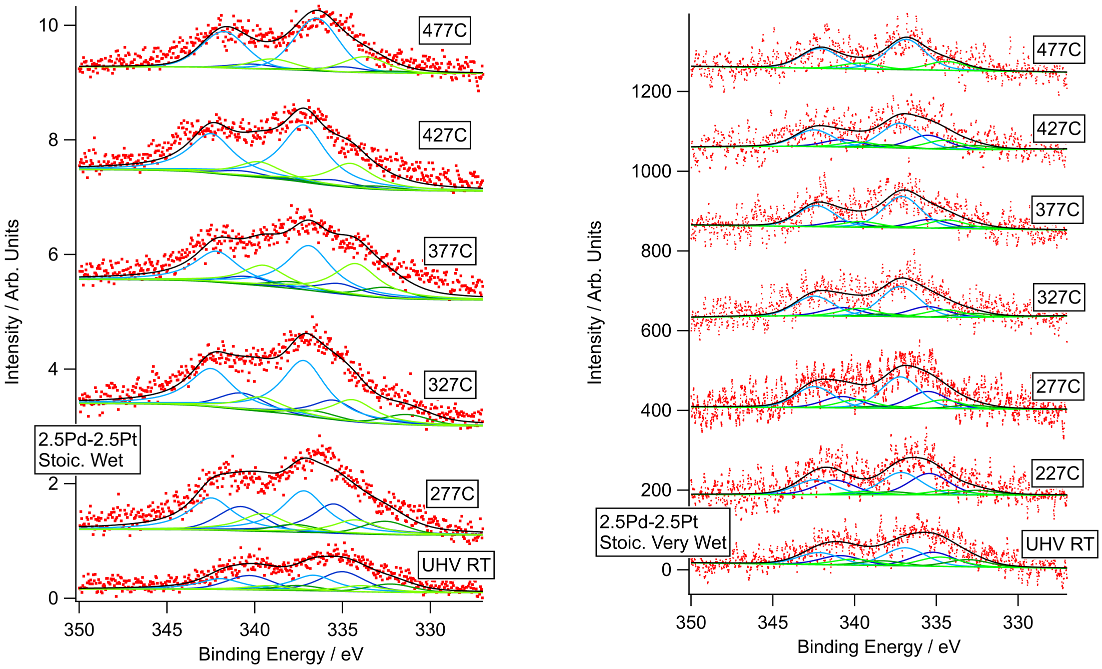

(b) Stoic. Wet

(c) Stoic. Very Wet

Figure 3.32: Pd 3d region NAP-XPS data for 2.5Pd-2.5Pt catalyst under all tested stoichiometric conditions. All spectra recorded using 1350 eV photon energy.

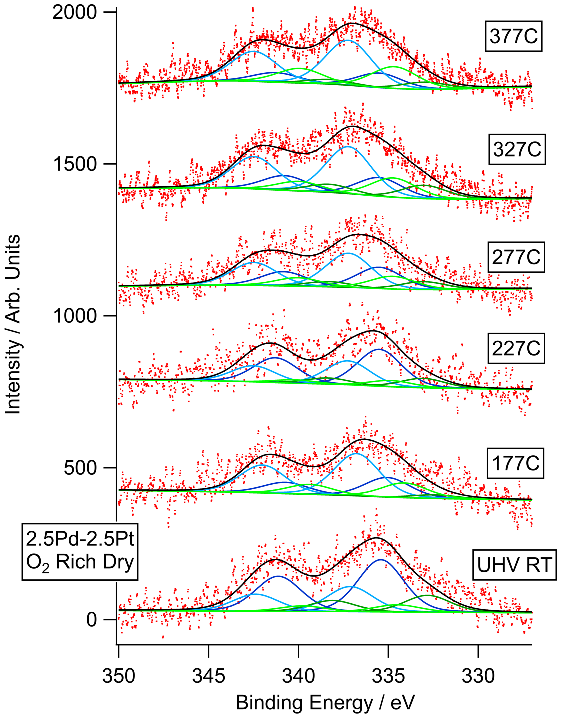

(a) Oxygen Rich Dry

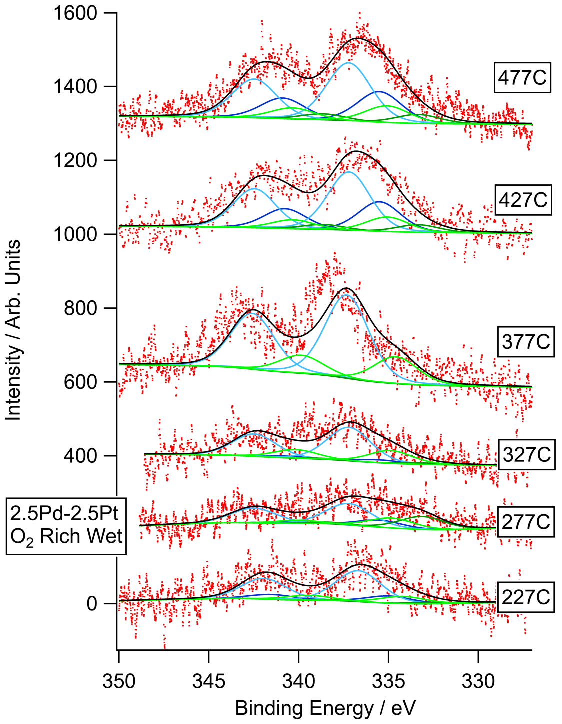

(b) Oxygen Rich Wet

Figure 3.33: Pd 3d region NAP-XPS data for 2.5Pd-2.5Pt catalyst under all tested oxygen rich conditions. Key is consistent with Fig. 3.32. All spectra recorded using 1350 eV photon energy.

As with 4.0Pd-1.0Pt, in some rare cases the raw data appear to show the Pd $3d_{5/2}$ peak at a higher binding energy than the fit. In these cases, the fit is already largely Pd(II), so it is again not considered to be an issue. Some of these measurements had a more significant variable charging of alumina, as seen by the larger green peak presence - most clear for stoichiometric wet conditions at 377 °C onwards. Whilst efforts are generally made to avoid sample spots with varied alumina presence, it was not always possible due to time constraints, so this sample had to be measured in this position. The Al 2p data is used to give the fit ratios between the blue (Al_2O_3a) and green (Al_2O_3b) peaks, so it can be confirmed that this unusual peak fit is a genuine result of the unusual alumina behaviour.

All of the NAP-XPS and activity data for 2.5Pd-2.5Pt are summarised in Fig. 3.34. The behaviour here is far more varied than for 4.0Pd-1.0Pt or 5.0Pd. The oxygen rich conditions now no longer lead to a fully oxidised sample, and where they appeared to, this is due to an issue in the dosing (as described previously). In dry conditions, the Pd is much more oxidised under stoichiometric conditions than oxygen rich, with approx. 95% and 75% Pd(II) respesctively at 377 °C. The oxygen rich wet condition typically shows Pd to be more heavily oxidised than the oxygen rich dry condition, which is again unlike the previous data. This may be due to the increased Pt presence, though which this would cause this significant and unexpected variation is hard to explain without being able to collect Pt core level data.

Fig. 3.35 shows an issue which was noted for the 2.5Pd-2.5Pt catalyst under oxygen rich wet condition. Initial spectra were recorded normally, as shown by the black spectra, with aluminium showing an offset of around 15 eV. During a Pd 3d spectrum, labelled "Scan 3" on Fig. 3.35b, a significant shift occurs. An Al 2p spectrum recorded after this is shown as "Scan 4" in Fig. 3.35a. The aluminium can be seen to shift to a lower binding energy by around 9 eV. The pressure and temperature were constant at this point, with no notable external inputs that would have caused this change. It is possible the sample shifted slightly, meaning the spot being analysed changed, though there is no clear reason for this. After this, it was deemed to be necessary to re-align the sample, to ensure a good and reliable spot was used for the final measurements at 427 and 477 °C. This is shown as the "final spot", which showed a significantly lower charging level, and a good enough signal to proceed.

Upon fitting this data (see Fig. 3.36), a major change was noted during the spot change. The fitted composite of the initial spot data gave a Pd 3d region which was assigned entirely

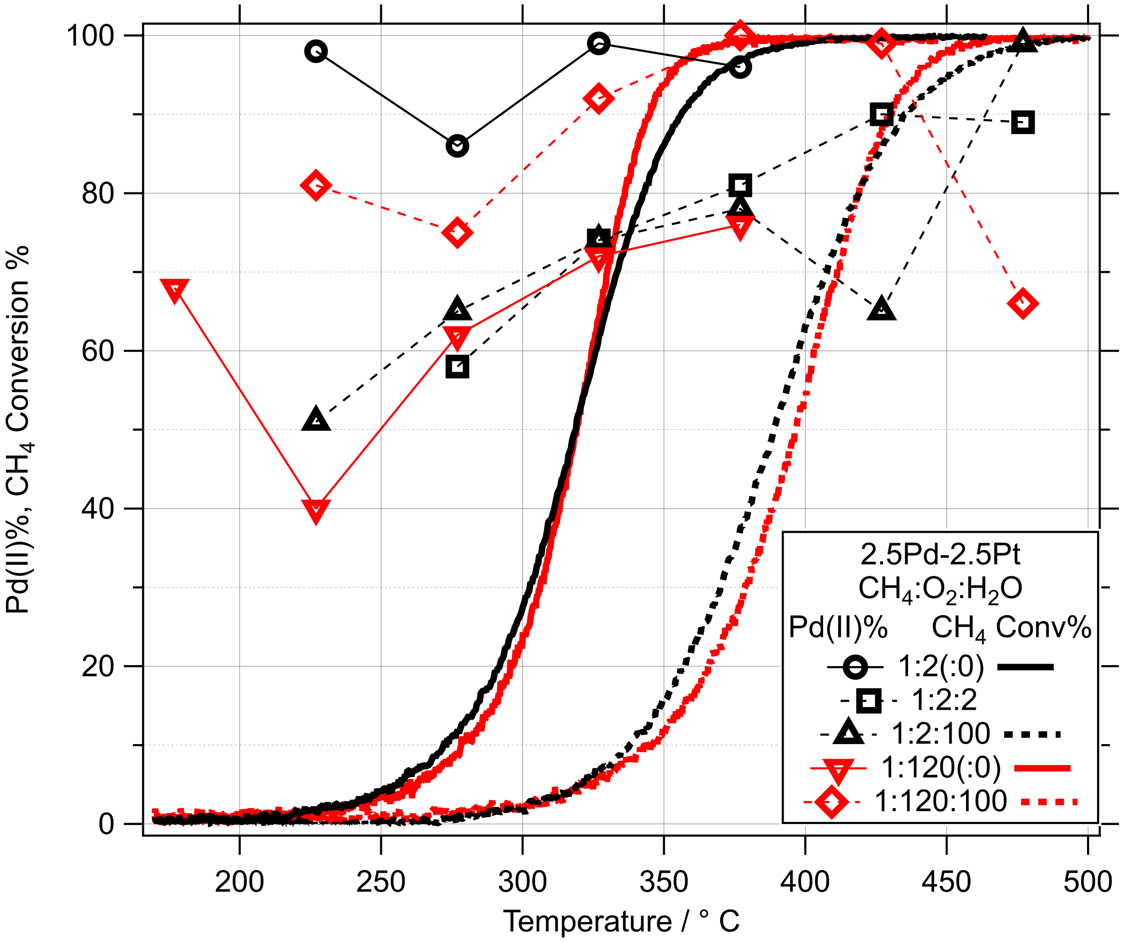

Figure 3.34: NAP-XPS data overlaid with catalytic activity data for 2.5Pd-2.5Pt catalyst, recorded under various dry and wet conditions.

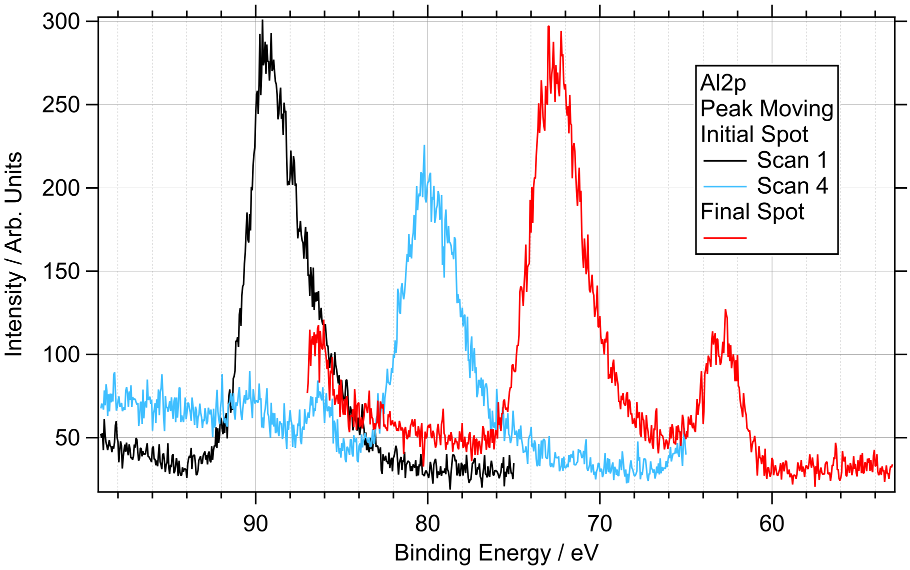

(a) Al 2p Peaks

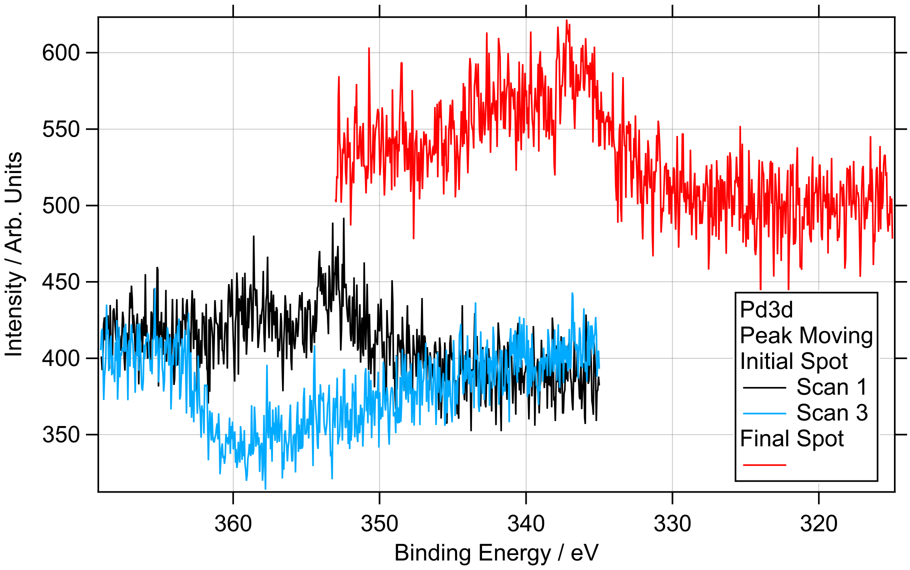

(b) Pd 3d Peaks

Figure 3.35: Pd 3d and Al 2p region NAP-XPS data for a 2.5Pd-2.5Pt catalyst, showing the changes observed over the course of an experiment, with the moving of spots. All data recorded at 427 °C under oxygen rich wet conditions. Spectra are not corrected with respect to binding energy. All spectra recorded using 1350 eV photon energy.

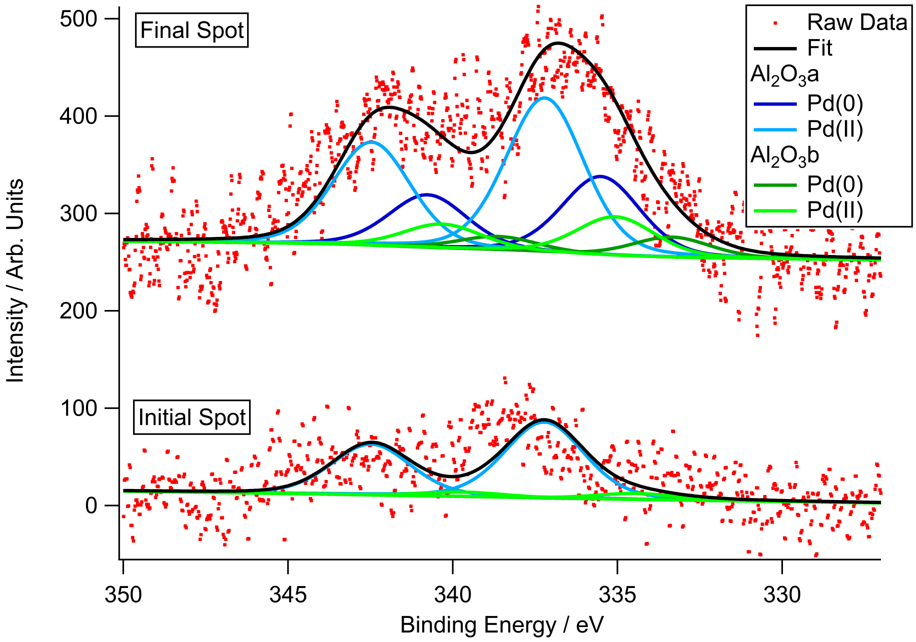

Figure 3.36: Pd 3d region NAP-XPS data for a 2.5Pd-2.5Pt catalyst, showing the changes observed over the course of an experiment, with the moving of spots. All data recorded at 427 °C under oxygen rich wet conditions. All spectra recorded using 1350 eV photon energy.

as Pd(II). The final spot, however, showed a mixture of Pd(0) and Pd(II). From an analysis point of view this could be a concern, as multiple individual Pd 3d spectra are typically recorded over an hour or more, to give a good enough combined spectrum for fitting. If it is the case that there are significant changes to the palladium over this time, that would make the overall fit an average, rather than truly representative of the oxidation state at this stage. It is worth noting that there was around 3 hours between the last "initial" measurement and the first "final" measurement. During this time the sample was continuously kept at temperature, in the gas feed, so it is possible that changes were caused by this. Typically, samples are not maintained at a fixed temperature & pressure for more than 2 hours, as this is all that is normally needed for a set of measurements. In the combined graphics, the initial spot data is the one included, hence it is shown to be 99% Pd(II). Fig. 3.34 shows the combined results of the data fitting, and it is notable that here the 477 °C measurement in wet oxygen rich conditions represents no change from the "final" spot measurement at 427 °C (both around 65-66% Pd(II)).

Mass spectrometry data from a 2.5Pd-2.5Pt catalyst under dry stoichiometric methane oxidation conditions are included in Fig. 3.38. This shows the production of carbon dioxide

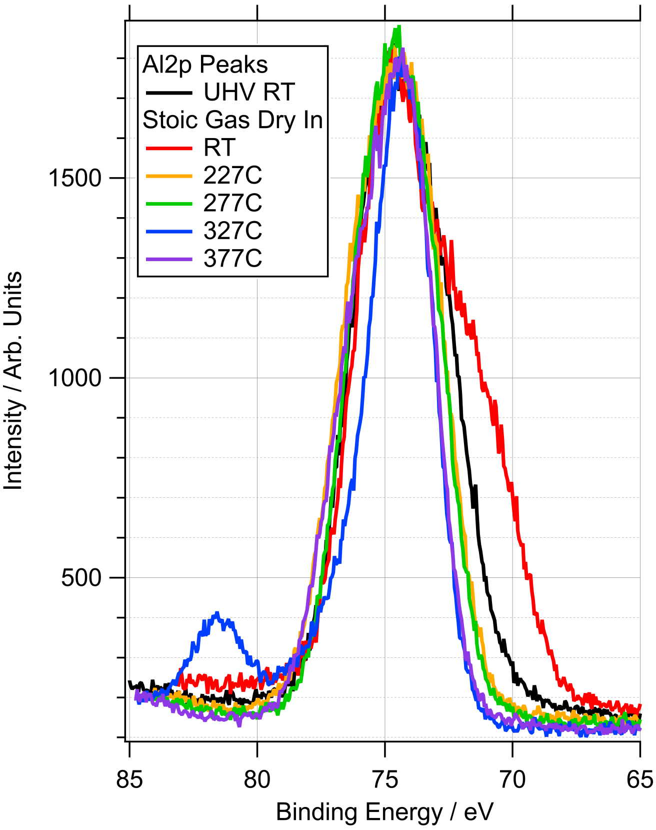

(a) Dry stoichiometric

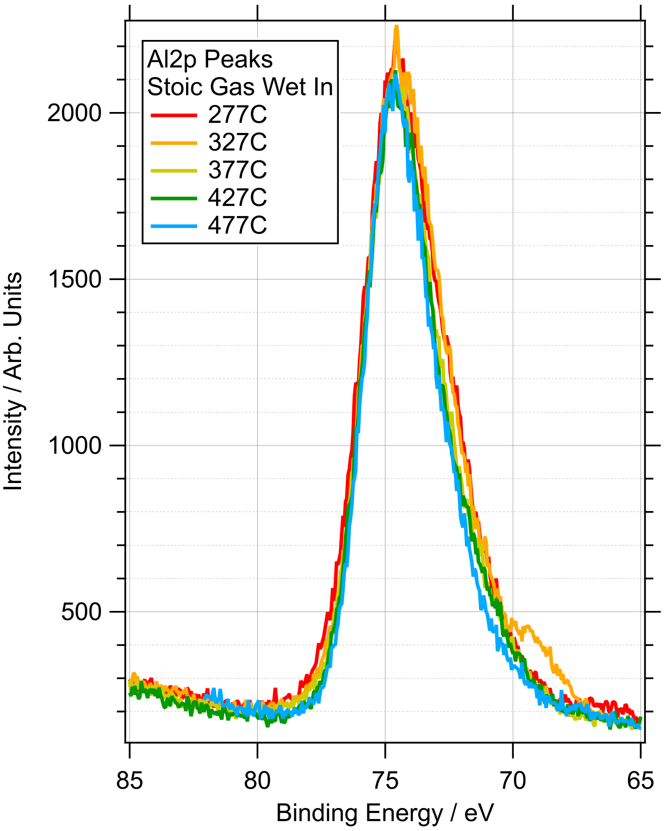

(b) Wet stoichiometric

Figure 3.37: Al 2p region NAP-XPS spectra recorded for a 2.5Pd-3.0Pt catalyst under dry and wet stoichiometric methane oxidation conditions. All spectra recorded using 1350 eV photon energy.

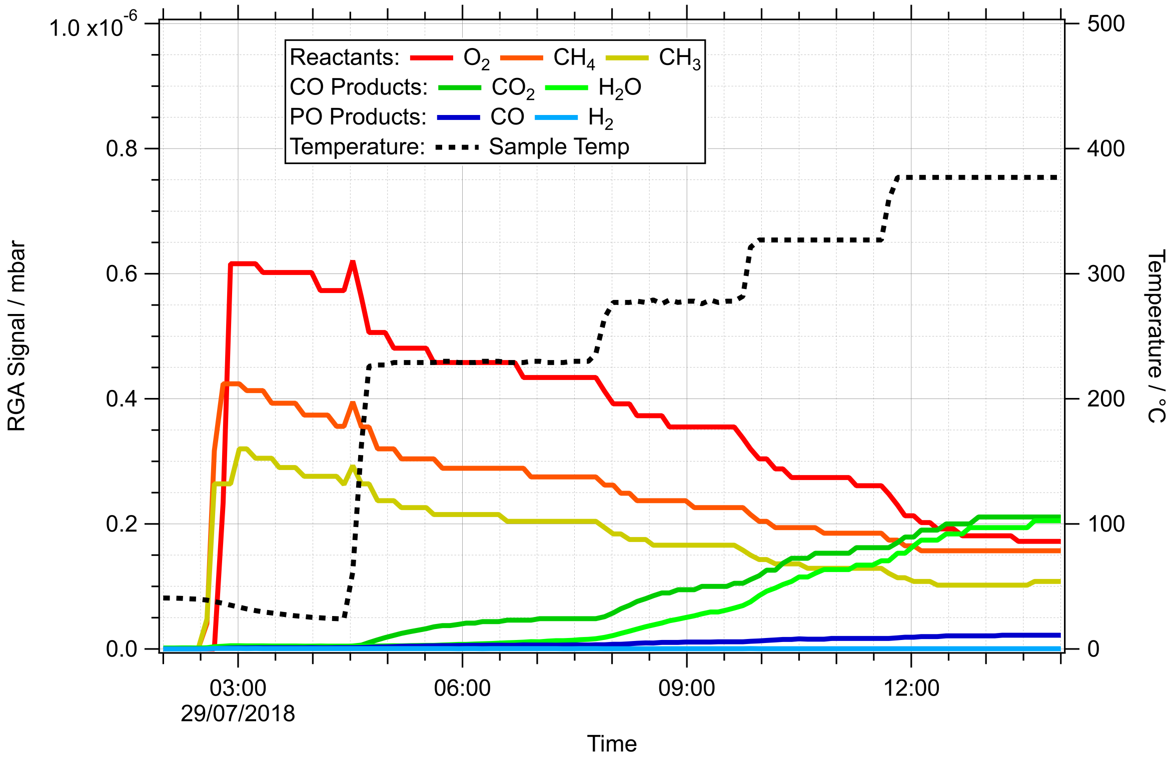

Figure 3.38: Mass spectrometry data recorded on the first pumping stage of the differential pumping system of the VerSoX beamline at Diamond, during NAP-XPS measurements of a 2.5Pd-2.5Pt/Al_2O_3 catalyst under dry stoichiometric methane oxidation conditions.

and water, with this sample showing a higher yield of both intended products than either the 5.0Pd or 5.0Pt samples which have been shown previously. This is more likely due to the amount of physical sample present, due to the variations in the amounts deposited by the spray coating method, rather than because of any variation in activity, especially as this catalyst is less active in these conditions than the 5.0Pd. As with those samples, there is no clear evidence for partial oxidation taking place, as there is no hydrogen formation.

3.5.3 Palladium-Platinum on alumina summary

A total of 5 bimetallic catalysts were produced to study the effects of exchanging palladium for platinum, and of varying the platinum loading. Co-impregnation led to catalysts comprising mixed Pd-Pt particles, with minimal evidence for individual monometallic nanoparticles in catalysts of any composition. The mixed metal nanoparticles showed no clear, consistent structuring, as was expected from the preparation method.

Catalytic activity tests showed the most active catalyst in dry or wet conditions was 4.0Pd-1.0Pt. Of the three 2.5Pd-based Pd-Pt catalysts, the one with the highest Pt loading (3.0Pt) was most active in both dry and wet conditions, though the margins between it, the 2.5Pd-2.5Pt and 2.5Pd-2.0Pt were minimal, and would not realistically justify the additional expense that would be caused by the higher platinum content.

Higher platinum content generally leads to a smaller level of deactivation in wet conditions, but the overall activity is still worsened by the decrease in palladium.

NAP-XPS experiments provided some insight into potential reasons for variations in activity. The oxidation state of palladium in the 4.0Pd-1.0Pt catalyst was highly variable with reaction condition. In oxygen rich, dry or wet conditions, it was nearly always fully oxidised. In stoichiometric conditions much more variation was observed, with a higher water presence leading to a more reduced catalyst. With the variation in oxidation state in different wet conditions, it can be suggested here that it is not optimal to have only Pd(II) present, but rather that both Pd(0) and Pd(II) sites are needed for optimal activity.

2.5Pd-2.5Pt catalysts were typically more oxidised under stoichiometric conditions, but less oxidised under the oxygen rich atmospheres. This indicates a strong effect from this higher platinum presence, an effect which will be more closely studied in the later chapters, where platinum is better able to be studied.

3.6 Additional Experiments

In each chapter, I will discuss some experiments which had been planned, but which were made either impractical or impossible by the restrictions present throughout much of 2020 and early 2021. Others were rejected for different practical reasons, which will be discussed below. These could also provide the basis for any future work which would follow within this project area.

One plan to prepare a sample with equivalent atomic percentage loading of each palladium and platinum - as no other catalysts prepared had equal atomic amounts (as all ratios were determined in weight %). These would then have been characterised, activity tested, etc, in the same way as the other catalysts described previously.

With some of the high temperature calcinations showing unusual variations, such as higher temperature treatments of Pt giving smaller particle sizes, repetitions of this would have been ideal. Separate batches of a given catalyst would be subjected to the same cycle of calcination, then studied using CO chemisorption, to see if they produced equivalently sized particles. Whilst some CO chemisorption measurements were repeated where unusual data was recorded, this was often after the passing of a significant amount of time (due to instrument accessibility) and so it can not be assumed there were no real physical changes over this time. In an ideal situation, these would be repeated as soon as possible after, to verify whether the unusual trends were genuine.

Another new preparation focused on a variation in support material. For previous samples, we have used a generic gamma alumina, with an approx. grain size of 100 μm. For preparations of "realistic model" samples (discussed in a later chapter), 3 μm gamma alumina had been sourced. The intention was to use this for the model samples, but also to prepare powder catalysts using this in the way described previously, to give a more direct comparison for our new models, and also to test how the alumina grain size affects the activity.

A final new catalyst preparation would have seen the same bimetallic ratios used as were focused on previously, 4.0Pd-1.0Pt and 2.5Pd-2.5Pt. Instead of the precursors being initially mixed, however, they would be sequentially added, with the sample being calcined before the addition of the second metal. The expectation is that this would give us either discrete islands of Pd and Pt, clusters of Pd and Pt in contact but not well mixed, or some mixture of the two. In any of these cases, a difference in nanoparticle structure would provide inevitable changes in activity, which could have allowed us to better understand the role of platinum, which was especially interesting in wet conditions.

Stoichiometric activity tests were planned to be carried out for more samples, especially the 4.0Pd, 2.5Pd-2.0Pt and 2.5Pd-3.0Pt, to provide a better understanding of how the Pt loading affects the activity under these conditions.

Additional wet activity tests had been planned with a lower water presence in the gas feed. Previously, water was either not included, or present as 10% of the feed, and we had intended to use lower percentages to study the effects that the level of water had on the catalyst activity. In addition to the reasons for the other experiments not taking place, this proved difficult due to the limitations of the water pumping system, which was designed to deliver much higher amounts of water. Prior studies had shown that in some cases the activity decreases strongly with increased water presence, and our NAP-XPS data showed clear changes in surface Pd oxidation with water presence, so we have strong reasons to believe these experiments would have shown interesting variations.

A NAP-XPS experiment which could have given additional information would have been to study the 4.0Pd catalyst under various conditions, to see if there was any variation in palladium oxidation state with varied loading, given the observed differences in activity between 5.0Pd and 4.0Pd being small.

3.7 Discussion & Conclusions

Comparisons of bimetallic catalysts with monometallic catalysts containing the same amounts of Pd or Pt are shown in Fig. 3.39. Fig. 3.39a shows 2.5Pd, 2.5Pt and all 2.5Pd based bimetallic catalysts, as tested under oxygen rich conditions.

In dry conditions, the 2.5Pd catalyst shows significantly better activity than all others, up to very high conversions (approx. 97%), after which it is more equal to all of the Pd-Pt bimetallic samples. In wet conditions, however, the 2.5Pd is continually worse than any of the Pd-Pt samples from low to full conversion. Within the group of bimetallic catalysts, the higher loading of Pt is beneficial in both dry and wet conditions. In dry conditions this is a particularly curious effect, as the catalysts with Pt are shown to, generally, be worse than Pd only, yet despite this a higher Pt presence is preferential. Whilst the differences are minor, the trend is clear in both conditions, and shows that the presence of Pt in certain Pd : Pt ratios is beneficial. The 2.5Pt catalyst is significantly worse than any of the other catalysts in dry or wet conditions.

Fig. 3.39b presents the same comparison for the Pt-rich bimetallic catalyst 1.0Pd-4.0Pt and it's relevant monometallic samples. When compared to the 2.5Pd catalyst series presented previously, it is remarkable to note the difference between the 1.0Pd and 1.0Pd-4.0Pt catalyst in dry conditions, with a temperature delta of more than 50 °C at most conversions. In wet conditions, however, the bimetallic samples once again show their use, with the 1.0Pd-4.0Pt reaching a higher conversion than 1.0Pd by 500 °C. Whilst an increase in conversion of only 2-3% may not be worth the increased expense of adding 4.0 wt.% platinum, it is interesting to note that the beneficial effects of platinum addition are still true for this composition in wet conditions. Under dry conditions, the Pt only catalyst is once again not worth considering, due to the much lower activity at all temperatures. In wet conditions however, it has a similar activity to 1.0Pd up to around 10% conversion. After this it fails to progress well, and does not even reach 60% conversion before 500 °C.

Fig. 3.39c compares 4.0Pd-1.0Pt with 4.0Pd and 1.0Pt. Whilst the 1.0Pt catalyst predictably shows minimal activity, the behaviour of the Pd and Pd-Pt samples is more interesting. In dry conditions, 4.0Pd is marginally better than 4.0Pd-1.0Pt, with a difference of 10-15 °C at high conversions. In wet conditions, the bimetallic is initially marginally better, but above 50% conversion (around 375 °C), this switches, and the 4.0Pd is marginally better at high conversions.

Fig. 3.40 shows specific condition comparisons using NAP-XPS and activity data for 5.0Pd and 4.0Pd-1.0Pt. The stoichiometric testing data, shown in Fig. 3.40a, shows that in dry conditions, the catalysts are similarly oxidised initially, and undergo reductions to differing extents. Both also show progressive re-oxidation, increasing to 100% Pd(II) with 5.0Pd, and to a plateau around 90% for 4.0Pd-1.0Pt. The activity of the two catalysts in this condition is very similar, with 5.0Pd only marginally better than 4.0Pd-1.0Pt. When water is added to this feed, 4.0Pd-1.0Pt is less oxidised at all temperatures as compared to 5.0Pd, although typically by less than 10%, excluding the final 477 °C measurements. The 4.0Pd-1.0Pt catalyst is slightly preferable in these conditions, lighting off and reaching 100% conversion at slightly lower temperatures. With the Pd being similarly oxidised in both catalysts, it must be assumed that this is not the sole cause of the variation in activity, though it could be considered that the higher level of oxidation in 5.0Pd is disfavoured. The comparable oxygen rich data is shown in Fig. 3.40b. Studying the dry condition, 5.0Pd is clearly superior, showing the largest margin of any conditions between these 2 catalysts. Initially the 5.0Pd is more oxidised, but after 277 °C they are both equally oxidised. In the wet condition, the activity is better initially for 4.0Pd-1.0Pt, but quite after 50% conversion

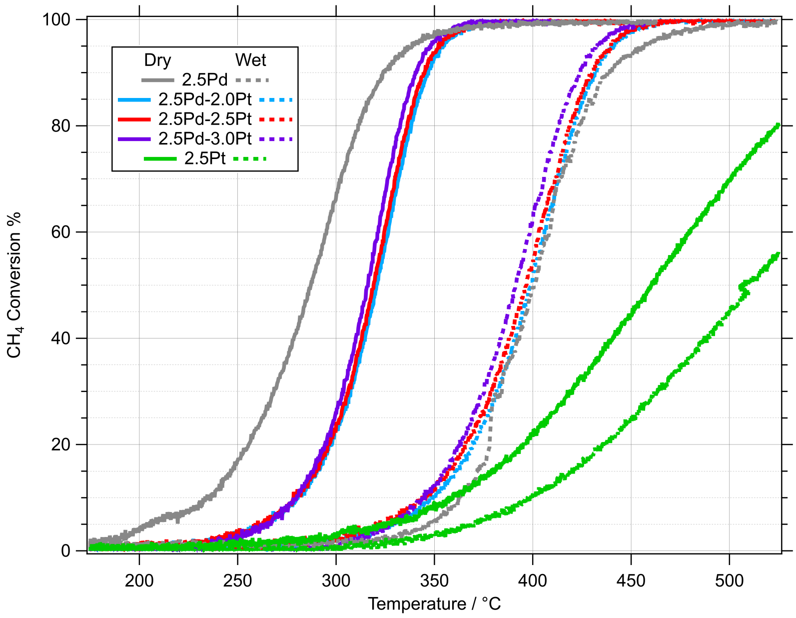

(a) All 2.5 wt.% based catalysts

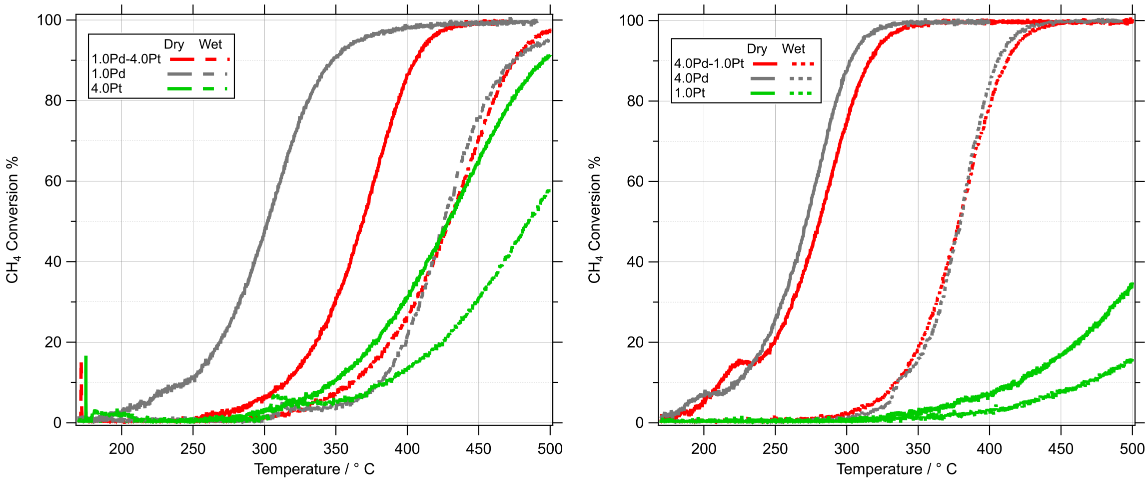

(b) 1.0Pd-4.0Pt, 1.0Pd and 4.0Pt

(c) 4.0Pd-1.0Pt, 4.0Pd and 1.0Pt

Figure 3.39: Comparisons of activity of bimetallic and monometallic catalysts of equivalent compositions. All recorded in oxygen excess conditions.

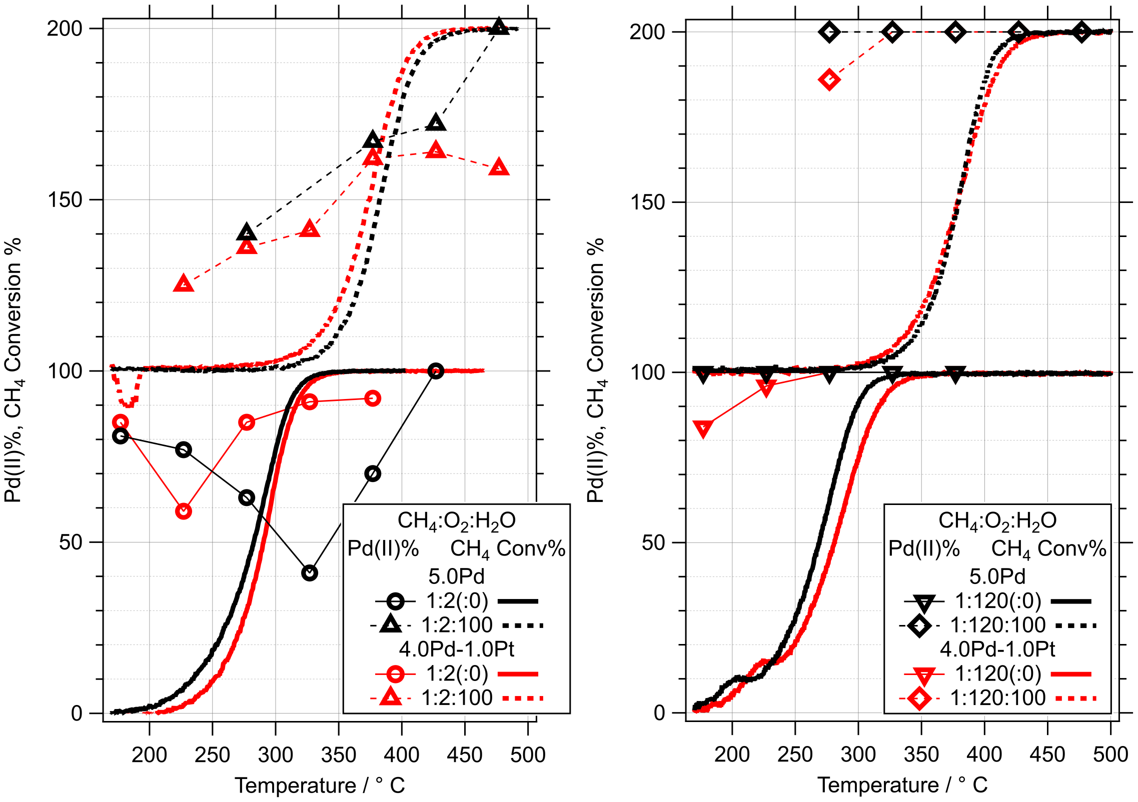

(a) Stoichiometric (b) Oxygen Rich

Figure 3.40: Overlaid NAP-XPS and activity data for 5.0Pd and 4.0Pd-1.0Pt catalysts under various conditions. Wet condition data are offset by 100% on the y-axes.

this is inverted. It is notable that the 4.0Pd-1.0Pt catalyst has less oxidised Pd at the lowest measured temperature - just before light off - which may be another indication of a lower oxidation state being beneficial for activity, similar to what was suggested for the stoichiometric wet conditions.

There is no definitive agreement in the literature as to the optimal surface states for palladium for methane oxidation, with both PdO and Pd being deemed beneficial in different situations. [57–59] Our findings largely agree with this, with the optimal state appearing to be a combination of Pd(0) and Pd(II), based on the activity differences observed.

When comparing bimetallic catalysts to monometallic, there are a number of important factors to consider. Whilst the prices of noble metals are typically variable, it is consistently the case that palladium is more expensive than platinum. As of October 14th 2020, the price is 2.68 times greater for palladium, gram for gram. With platinum containing 1.83 times more atoms per gram, palladium is only 1.46 times more expensive, atom for atom. However, these forms of metal are not practical starting points for catalyst production. When comparing typically available nitrate solutions, atom for atom, palladium is roughly 2.5 times the cost of platinum. With the preparation of bimetallic catalysts not being appreciably more expensive than that of monometallic catalysts (the minor additional time of measuring out one addition solution is insignificant on the time scale of the complete preparation process), it is clear that there is a financial benefit to the replacement of small amounts of palladium with equal amounts (atomically or by weight) of platinum. Switching from 5.0Pd to 4.0Pd-1.0Pt represents a cost saving of around 15% as a result.

It is clear that the operational conditions have a major effect on whether Pd or Pd-Pt is preferable. We have shown that, under any dry condition, there is no benefit to the bimetallic catalysts. There is an added expense, with commonly a decrease in activity.

In many senses, it is arguable that it is preferable to use a 4.0Pd catalyst over any others. The TOF is the highest of any Pd catalyst, in both dry and wet conditions. Due to this, and the benefit of reducing Pd content by 20%, it is clearly preferable to 5.0Pd. Additionally, it behaves very similarly to the 4.0Pd-1.0Pt in wet conditions, but again represents a less expensive catalyst.

4 Silica and silica-alumina supported catalysts

4.1 Introduction

Changing the active metal, or doping in additional metals, is a common approach when attempting to increase the activity of a catalyst. Another standard way forward is to vary the support material. Supports other than alumina have been widely studied for methane oxidation, including silica, zirconia, and ceria. [116,129,167–170] Zirconia is a difficult support to study low loadings of palladium nanoparticles on via XPS, due to the overlap of the Pd 3d and Zr 3p regions.

In this section, we study the variations in catalyst behaviour when the same amounts of platinum and palladium are deposited onto silica, and two silica-alumina mixed oxide supports. Silica is a very common and inexpensive oxide support material, which is different enough structurally to alumina to provide an interesting contrast. The two Al-Si supports, with varied Al : Si ratios, allow us to further understand why each oxide may be beneficial. These supports will be referred to throughout as: Si (SiO_2), 60-40 ($60Al_2O_3$-$40SiO_2$) and 90-10 ($90Al_2O_3$-$10SiO_2$), in addition to Al (Al_2O_3).

The Pd-Pt compositions selected for this are more limited than for alumina, but should still give us enough insight into the effect of support variation. The 4 selected catalysts were: 5.0Pd, 4.0Pd-1.0Pt, 2.5Pd-2.5Pt, and 5.0Pt. All four of these were prepared on alumina supports in the previous chapter of this work. This provides us with references for monometallic catalysts, and enough information on different bimetallic ratios.

4.2 Palladium, Platinum and Palladium-Platinum on silica and silica-alumina

4.2.1 Preparation & Characterisation

Support	Loading / wt. %	Size 500 °C / nm
SiO_2	5.0Pd	16.6
SiO_2	4.0Pd-1.0Pt	12.6
SiO_2	2.5Pd-2.5Pt	12.0
SiO_2	5.0Pt	9.2
$60Al_2O_3$-$40SiO_2$	5.0Pd	11.5
$60Al_2O_3$-$40SiO_2$	4.0Pd-1.0Pt	8.9
$60Al_2O_3$-$40SiO_2$	2.5Pd-2.5Pt	6.1
$60Al_2O_3$-$40SiO_2$	5.0Pt	2.3
$90Al_2O_3$-$10SiO_2$	5.0Pd	9.8
$90Al_2O_3$-$10SiO_2$	4.0Pd-1.0Pt	7.6
$90Al_2O_3$-$10SiO_2$	2.5Pd-2.5Pt	7.1
$90Al_2O_3$-$10SiO_2$	5.0Pt	25.2
Al_2O_3	5.0Pd	14.7
Al_2O_3	4.0Pd-1.0Pt	14.4
Al_2O_3	2.5Pd-2.5Pt	10.5
Al_2O_3	5.0Pt	2.6

Table 4.1: Average particle sizes for catalysts after calcination at 500 °C. All determined by CO chemisorption.

Particle size data are tabulated in Tab. 4.1, and presented graphically in Fig. 4.1. The general trend for three of the support materials is that an increased Pd loading and decreased Pt loading leads to a larger particle size. For $90Al_2O_3$-$10SiO_2$ this is true generally, but the 5.0Pt catalyst has a much higher average particle size than expected, at 25 nm compared to 2-10 nm for the other 5.0Pt samples. Within specific metal ratios, there is no particular ordering in particle size with regards to the supports. When only considering Pd-containing samples, SiO_2 and Al_2O_3 both tend to give larger average particle sizes than either of the mixed supports.

UHV laboratory XPS data is presented for all relevant catalysts in Fig. 4.2. This shows Pd 3d & Pt 4d, Al 2p and Si 2p region data in Figs. 4.2a, 4.2b and 4.2c respectively. In all cases, this data is grouped initially by support.

The loading variations seen for Pd and Pt are not entirely as expected. For SiO_2 and $90Al_2O_3$-$10SiO_2$, the Pd 3d : Pt 4d ratio largely changes as expected, but for $60Al_2O_3$-

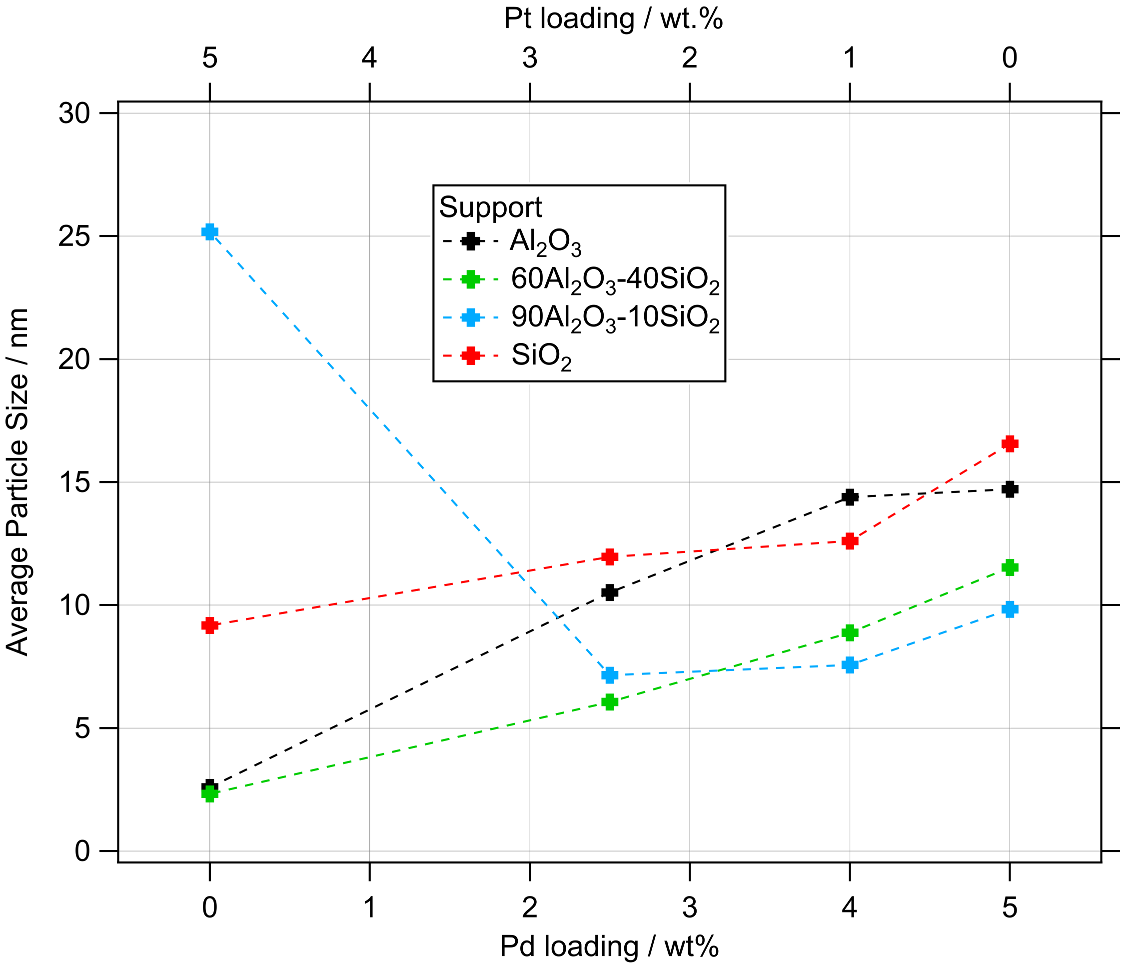

Figure 4.1: Average particle sizes for catalysts after calcination at 500 °C. All determined by CO chemisorption.

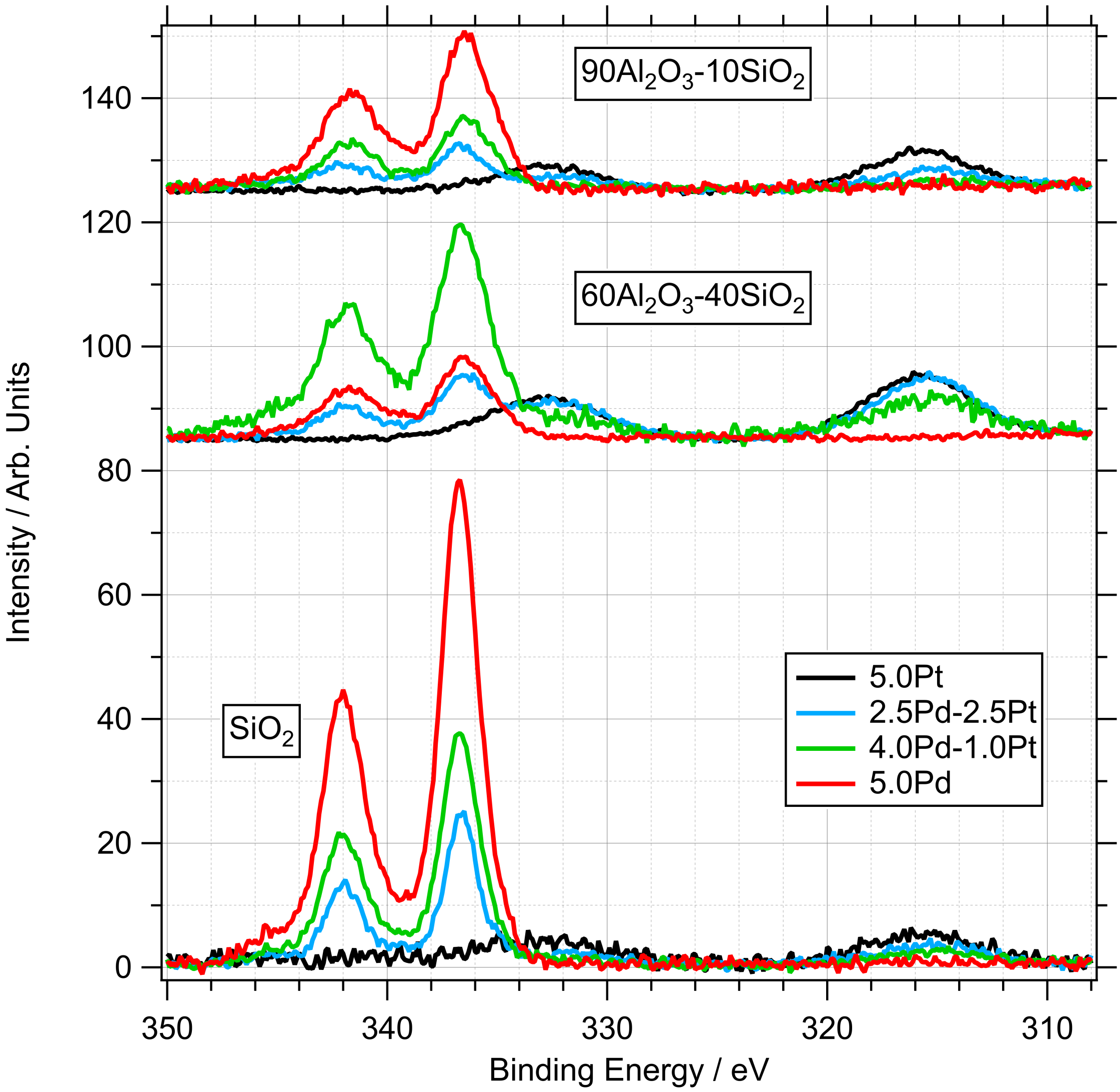

(a) Pd 3d & Pt 4d

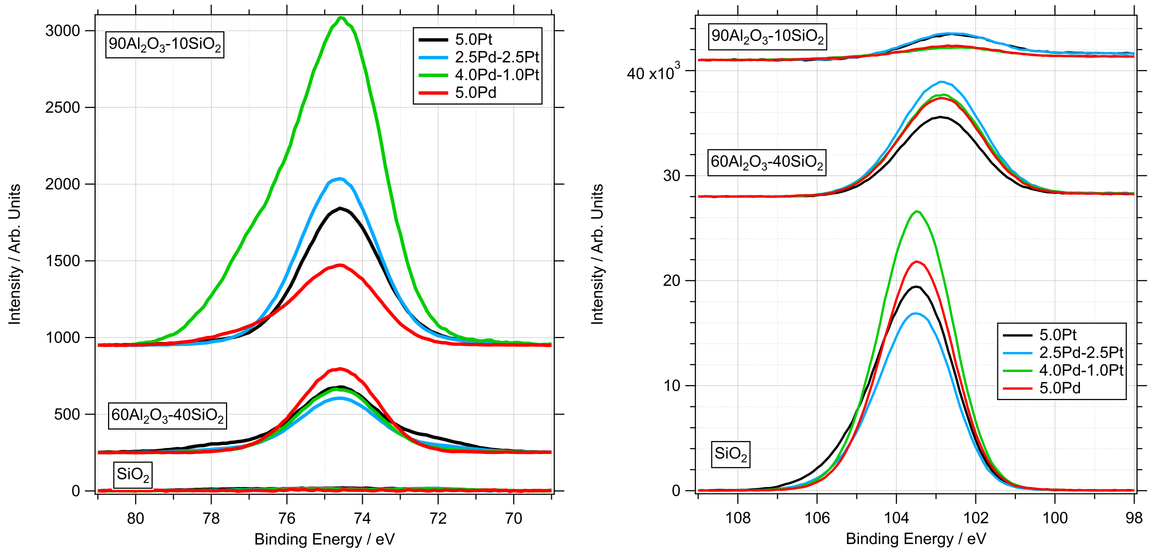

(b) Al 2p (c) Si 2p

Figure 4.2: XPS data for support and nanoparticle regions for all silica and silica-alumina supported catalysts, all after calcination at 500 °C. All spectra recorded using 1486.6 eV photon energy.

40SiO_2 there is an unusual variation. The highest Pd 3d signal is seen for 4.0Pd-1.0Pt, and not 5.0Pd. The Pd 3d signal in 5.0Pd is comparable to that in 2.5Pd-2.5Pt, when support peaks are also factored in. The peak positions seem to be broadly unaffected by loading or support in all samples, with Pd primarily appearing as Pd(II), around 336.5 eV, in all samples where it is present.

Where alumina was present in the support, this is used to calibrate the binding energy scale of the XPS spectra, with all adjusted such that the Al 2p peak is at 74.6 eV. In the case of the four SiO_2 samples this is not possible, so these are instead calibrated such that the Si 2p peak sits at 103.5 eV, as is typical for silica. The Si 2p peak in silica is notably shifted as compared to that in either of the silica-alumina species, where it appears around 102 eV. [171] The consistent Pd 3d and Pt 4d peak positions indicate that this is not an error, and that the silicon is taking a different state in these mixtures, compared to it's pure oxide form. A peak around 102 eV for silica would typically be representative of an aluminosilicate, indicating the Al-Si supports take this form.

Catalysts with 4.0Pd-1.0Pt on three different supports were studied using XRD, to confirm the support phase, and to try and identify the nanoparticle phase. This is shown in Fig. 4.3, and shows that the palladium phase is consistent across all three supports, as PdO Palladinite. Platinum is only well observed on the 60Al_2O_3-40SiO_2 support, with the Pt peaks seeming to show a significantly lower amount of platinum than intended.

Tab. 4.2 shows the T50 and turnover frequency data for 5.0Pd, 4.0Pd-1.0Pt and 2.5Pd-2.5Pt catalysts on all 4 support materials. Generally the ΔT50 is seen to decrease with increased Pt loading/decreased Pd loading - with the exception of silica. In this case, the ΔT50 for 2.5Pd-2.5Pt is unexpectedly high at 106, compared to 75, 84 and 78 for the three other supports.

The activity data are shown graphically in Figs. 4.4 and 4.5, which show the data by support and loading respectively. Activity testing data for silica-supported catalysts are shown in Fig. 4.4a, which shows that 5.0Pd is the best catalyst in dry oxygen rich conditions. 4.0Pd-1.0Pt behaves similarly in either stoichiometric or oxygen rich dry conditions, with a switch over around 75% conversion. In wet conditions, the 5.0Pd catalyst behaves very similarly to the 4.0Pd-1.0Pt catalyst. The 4.0Pd-1.0Pt catalyst is very similar in either oxygen rich or stoichiometric wet conditions. The 2.5Pd-2.5Pt catalyst is significantly worse

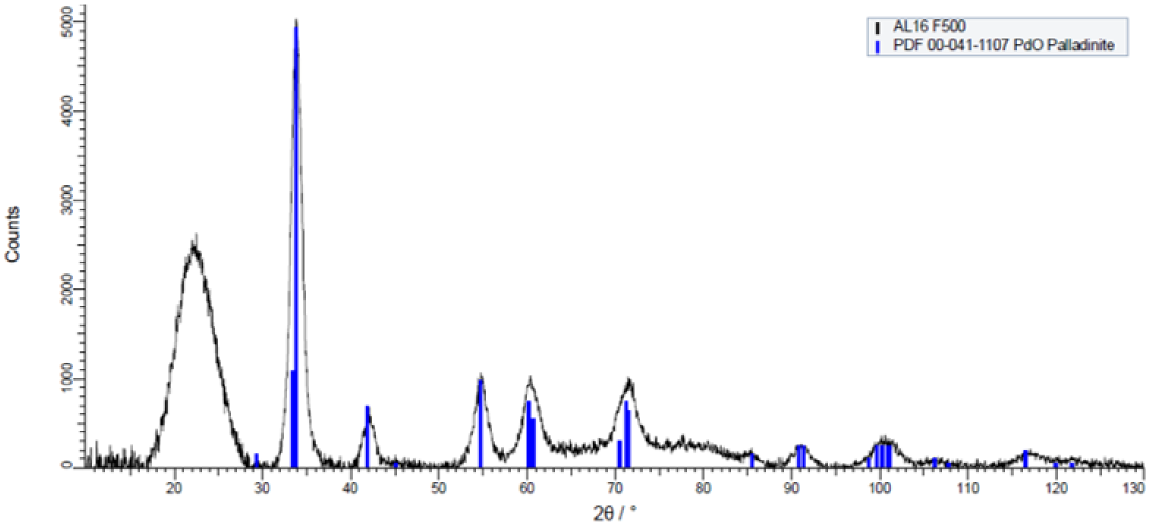

(a) 4.0Pd-1.0Pt/SiO_2

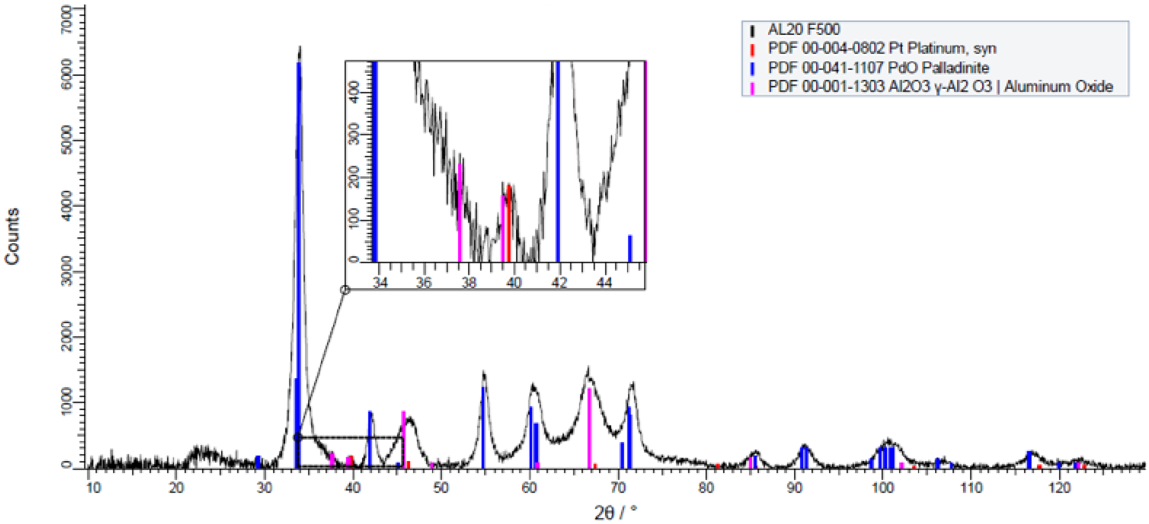

(b) 4.0Pd-1.0Pt/$60Al_2O_3$-$40SiO_2$

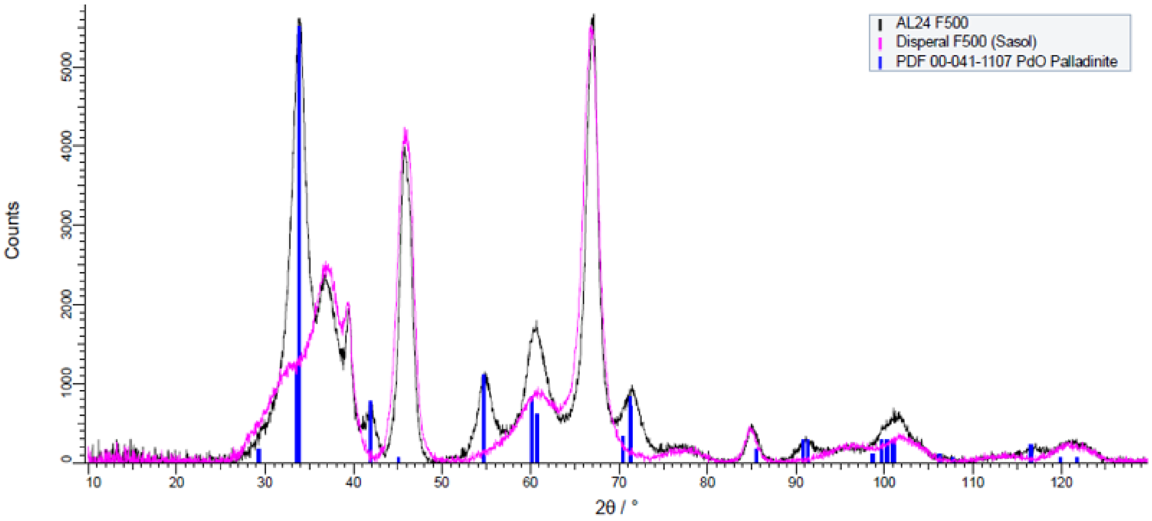

(c) 4.0Pd-1.0Pt/$90Al_2O_3$-$10SiO_2$

Figure 4.3: XRD patterns for three 4.0Pd-1.0Pt catalysts of different support materials.

Support	Loading / wt. %	T50 Dry	T50 Wet	ΔT50	TOF Dry	TOF Wet
SiO_2	5.0Pd	271	381	110	$x\times10^{-2}$	$x\times10^{-2}$
SiO_2	4.0Pd-1.0Pt	282	385	103	$x\times10^{-2}$	$x\times10^{-2}$
SiO_2	2.5Pd-2.5Pt	348	454	106	$x\times10^{-2}$	$x\times10^{-2}$
$60Al_2O_3$-$40SiO_2$	5.0Pd	285	403	118	$x\times10^{-2}$	$x\times10^{-2}$
$60Al_2O_3$-$40SiO_2$	4.0Pd-1.0Pt	292	393	101	$x\times10^{-2}$	$x\times10^{-2}$
$60Al_2O_3$-$40SiO_2$	2.5Pd-2.5Pt	332	407	75	$x\times10^{-2}$	$x\times10^{-2}$
$90Al_2O_3$-$10SiO_2$	5.0Pd	264	378	114	$x\times10^{-2}$	$x\times10^{-2}$
$90Al_2O_3$-$10SiO_2$	4.0Pd-1.0Pt	271	370	99	$x\times10^{-2}$	$x\times10^{-2}$
$90Al_2O_3$-$10SiO_2$	2.5Pd-2.5Pt	305	389	84	$x\times10^{-2}$	$x\times10^{-2}$
Al_2O_3	5.0Pd	269	379	110	2.96×10^{-2}	1.49×10^{-2}
Al_2O_3	4.0Pd-1.0Pt	281	379	98	2.35×10^{-2}	2.00×10^{-2}
Al_2O_3	2.5Pd-2.5Pt	319	397	78	3.00×10^{-3}	1.07×10^{-2}

Table 4.2: T50 data and turnover frequencies for all silica and silica-alumina supported catalyst under various conditions. 500 °C treated and oxygen excess conditions unless otherwise noted. TOF values determined at 250 °C and 350 °C for dry and wet conditions respectively.

than either other composition in dry or wet conditions.

The same general trends are seen in dry conditions for both of the mixed silica-alumina supports. In wet conditions for either mixed support, the 4.0Pd-1.0Pt catalyst is preferable to the 5.0Pd. The 2.5Pd-2.5Pt shows higher activity than 5.0Pd at very low conversions, but worse above 20-40%.

Activity tests for catalysts with a loading of 4.0Pd-1.0Pt on various supports are shown in Fig. 4.5a and 4.5b for oxygen rich and stoichiometric conditions respectively. Under dry or wet oxygen rich conditions, the $90Al_2O_3$-$10SiO_2$ supported catalyst was optimal. The Al_2O_3 and SiO_2 samples were very similar in either dry or wet, whilst the $60Al_2O_3$-$40SiO_2$ performed the worst. The 4.0Pd-1.0Pt catalyst on $90Al_2O_3$-$10SiO_2$ was not tested under stoichiometric gas conditions, due to time constraints. Of the three 4.0Pd-1.0Pt catalysts tested in stoichiometric conditions, the silica was preferable in the dry, whilst the alumina performed better in the wet.

The data for 5.0Pd samples are shown in Fig. 4.5c. Again, under dry conditions, the $90Al_2O_3$-$10SiO_2$ is optimal, although the margin between this and both Al_2O_3 and SiO_2 is minimal. In wet conditions the difference is even smaller, with all having a T50 within 3 °C of each other.

Overall, this shows that the SiO_2 and Al_2O_3 supported catalysts often behaved very sim-

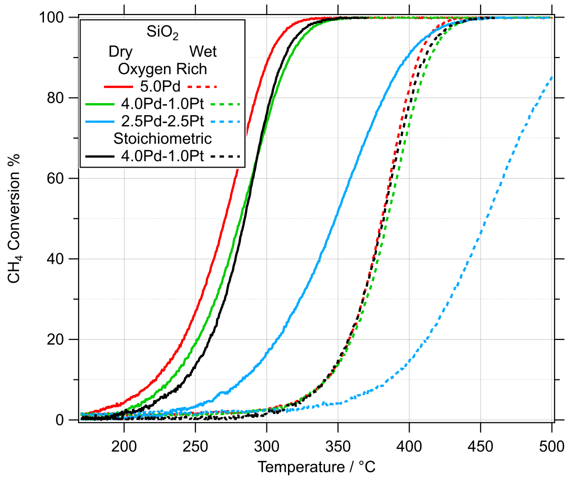

(a) SiO_2 supported

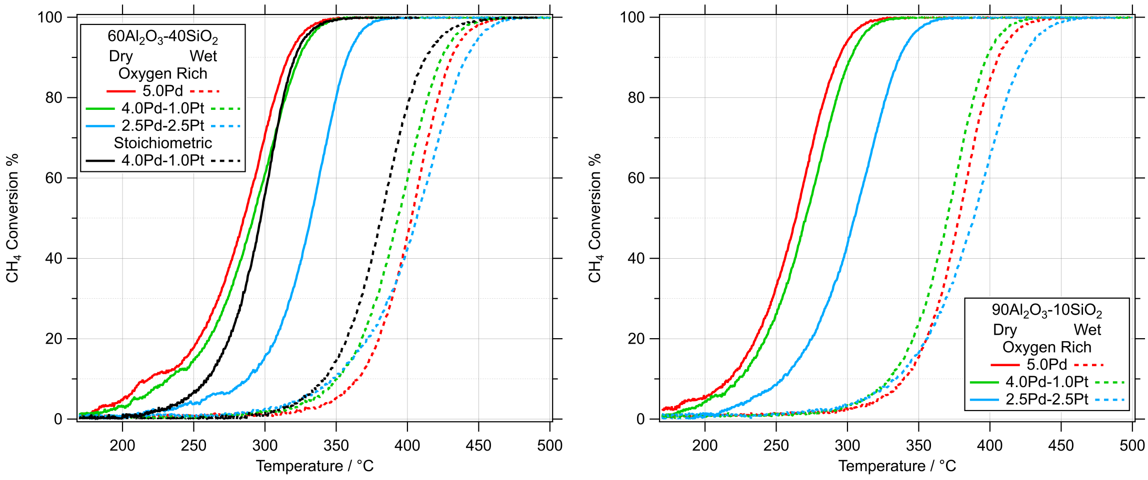

(b) $60Al_2O_3$-$40SiO_2$ supported

(c) $90Al_2O_3$-$10SiO_2$ supported

Figure 4.4: Catalytic activity tests under oxygen rich and stoichiometric dry and wet conditions for Pd and Pd-Pt catalysts on various silica and silica-alumina supports.

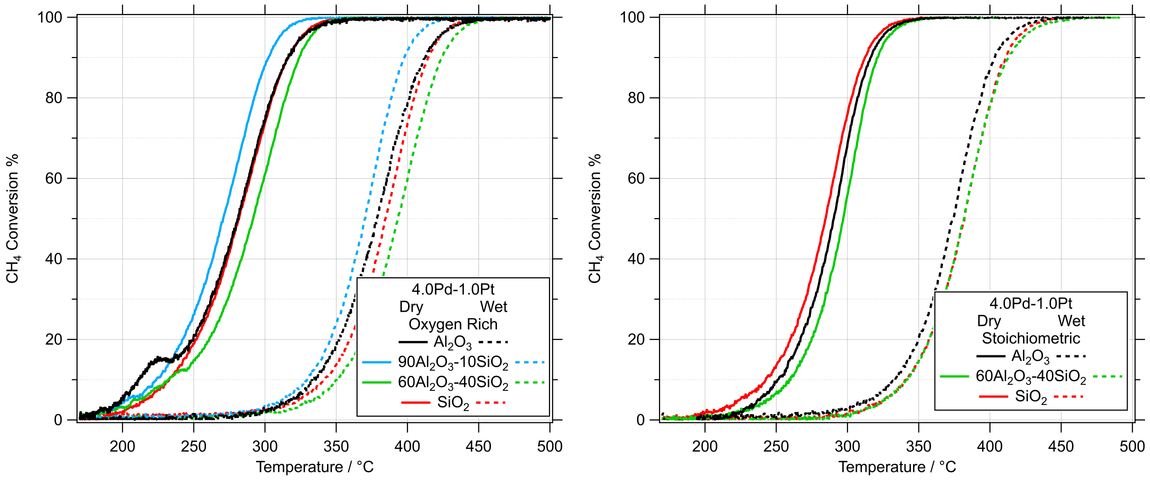

(a) 4.0Pd-1.0Pt Oxygen Rich

(b) 4.0Pd-1.0Pt Stoichiometric

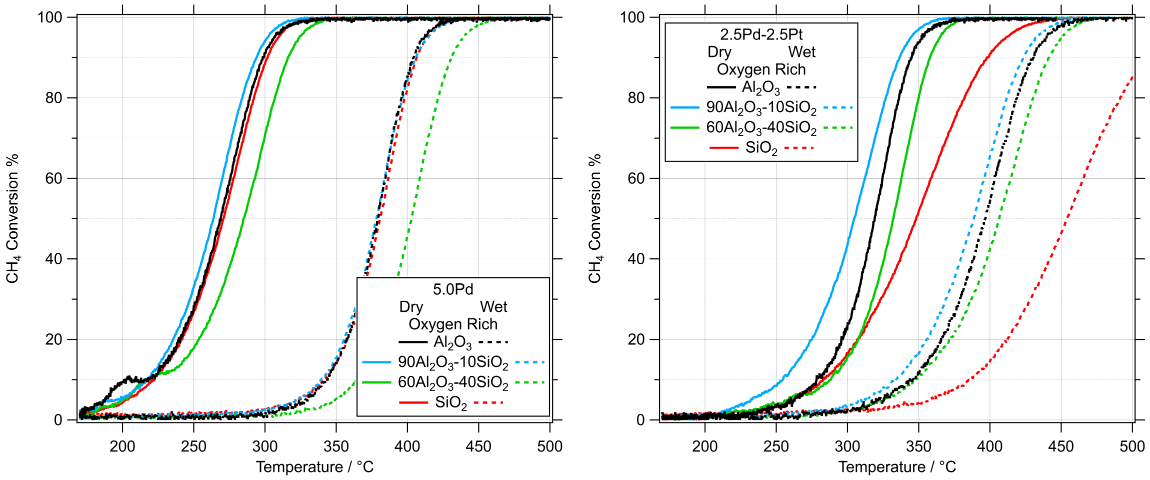

(c) 5.0Pd Oxygen Rich

(d) 2.5Pd-2.5Pt Oxygen Rich

Figure 4.5: Catalytic activity tests under oxygen rich and stoichiometric dry and wet conditions for Pd and Pd-Pt catalysts on various silica, alumina and silica-alumina supports.

ilarly, regardless of loading of Pd and Pt. In terms of the light off temperatures, $90Al_2O_3$-$10SiO_2$ was the best support for any loading of particles that was tested, under dry or wet conditions. The other mixed silica-alumina support, $60Al_2O_3$-$40SiO_2$, was the worst with most metal compositions in most gas conditions.

The 2.5Pd-2.5Pt data are shown in Fig. 4.5d, which shows similar general trends to other supports, with the 90-10 mixed support giving the best activity. For this Pd-Pt loading, however, the silica support is the weakest in both dry and wet conditions, by a significant margin.

The similarity between silica and alumina is unexpected. In a number of cases, the curves virtually sit exactly over one another, showing the same light off and gradient throughout, despite the differing physical supports. Despite this, the 2.5Pd-2.5Pt catalysts show vastly different behaviour on these supports, with the silica supported sample being inferior.

Equally, the variation in silica-alumina supports is unexpected, with 90-10 proving to be the best, and 60-40 the worst of the 4 tested support materials.

4.2.2 Near-ambient pressure XPS of Pd and Pd-Pt supported on SiO_2 and Al_2O_3-SiO_2

NAP-XPS data for two 5.0Pd catalysts on different supports are shown in Fig. 4.6. These experiments were only performed under dry methane oxidation conditions.

For 5.0Pd/SiO_2, the palladium is mainly reduced under vacuum conditions at room temperature. Once gas is introduced and the sample is heated to reaction temperatures, the sample is predominantly Pd(II) at all temperatures except 227 °C and 477 °C. 5.0Pd/40SiO_2-60Al_2O_3 is also predominantly Pd(II) at room temperature in vacuum. However, unlike for the silica supported catalyst, there is a significant amount of metallic palladium present at all reaction temperatures tested. This behaviour is much more similar to that of the alumina-supported sample under these conditions. This is another case of alumina and silica supported catalysts giving surprisingly similar data.

The NAP-XPS data for the 4.0Pd-1.0Pt/SiO_2 catalyst are shown in Fig. 4.7, for stoichiometric dry and wet conditions. In both experiments, the palladium is predominantly metallic under room temperature/vacuum conditions, before the ramps are started. For the dry condition, the palladium appears to be fully oxidised at all reaction temperatures. In the case of the later data points (especially 427 °C), the raw data are shifted slightly to the high binding energy side of the maximum fitted position of Pd(II). Whilst it is possible that this is representative of Pd(IV), we believe this to be unlikely, as was discussed in the alumina section. The behaviour is largely similar in the wet stoichiometric condition, but there is a continual small presence of Pd(0) throughout.

NAP-XPS spectra for a 4.0Pd-1.0Pt/40SiO_2-60Al_2O_3 catalyst are shown in Fig. 4.8 under dry and wet stoichiometric conditions. By comparison to the silica-supported catalyst, and the 5.0Pd on this support, the behaviour is largely similar, with a significant presence of both Pd(0) and Pd(II) at most temperatures measured. These data indicate that the support is more relevant than the Pd : Pt ratio with regards to the palladium oxidation state under these stoichiometric reaction conditions. Similarly, the 10SiO_2-90Al_2O_3 supported 4.0Pd-1.0Pt catalyst is predominantly Pd(II) at higher temperatures under dry or wet conditions. There are significant amounts of Pd(0) seen, especially in dry conditions at lower temperatures.

The NAP-XPS data are presented together with activity testing data in Figs. 4.10 and 4.11 for 5.0Pd and 4.0Pd-1.0Pt catalysts, respectively. In certain cases, the reaction condition

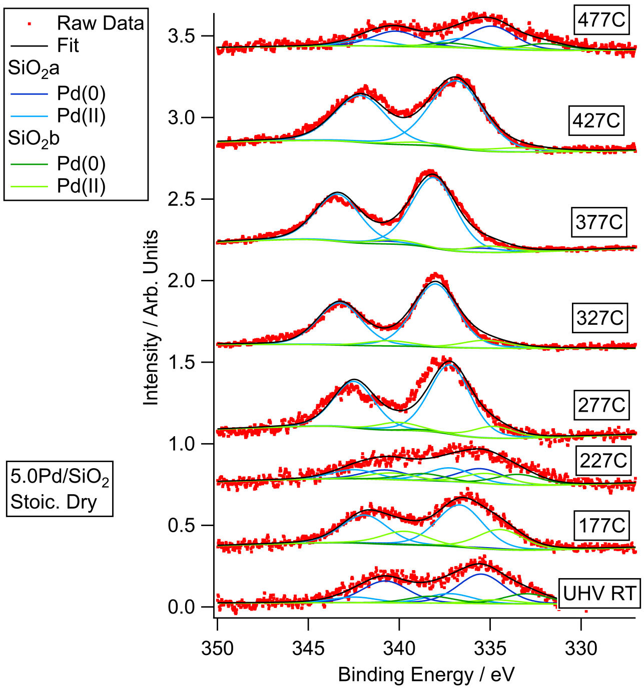

(a) Dry stoichiometric

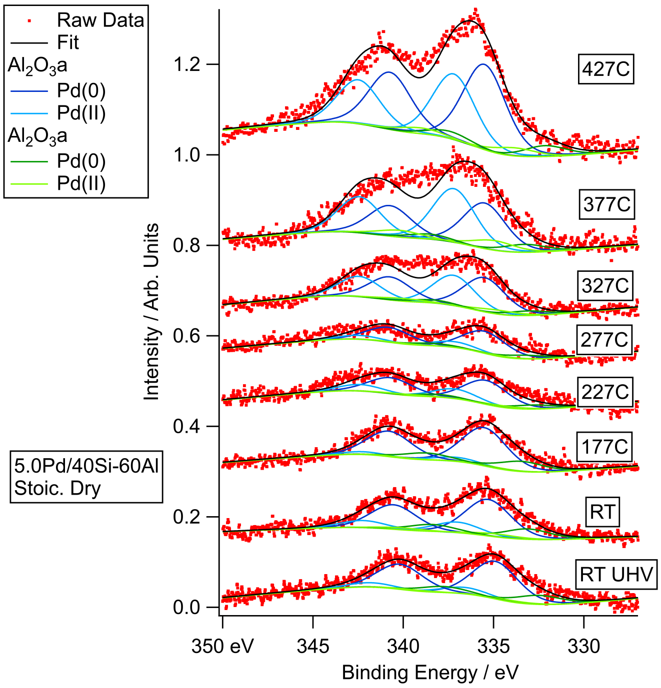

(b) Dry stoichiometric

Figure 4.6: Pd 3d region NAP-XPS spectra recorded for 5.0Pd catalysts on SiO2 and 40Si-60Al under dry stoichiometric methane oxidation conditions. All spectra recorded using 1350 eV photon energy.

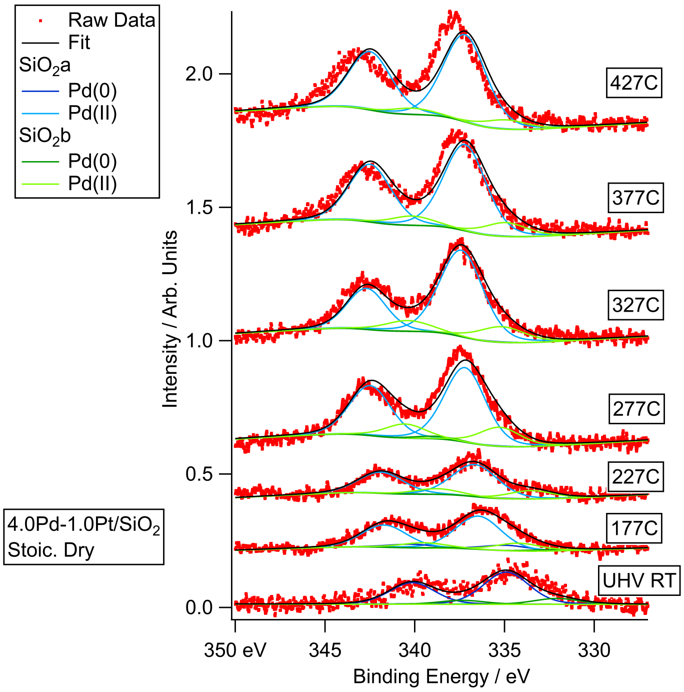

(a) Dry stoichiometric

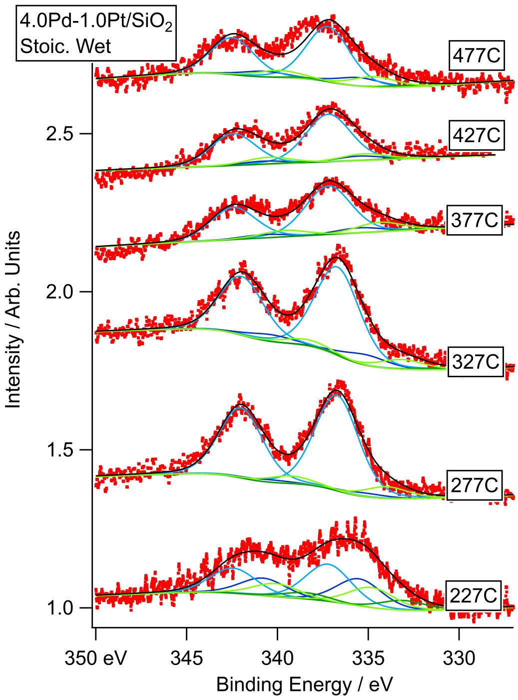

(b) Wet stoichiometric

Figure 4.7: Pd 3d region NAP-XPS spectra recorded for 4.0Pd-1.0Pt/SiO$_2$ catalyst under dry and wet stoichiometric methane oxidation conditions. All spectra recorded using 1350 eV photon energy.

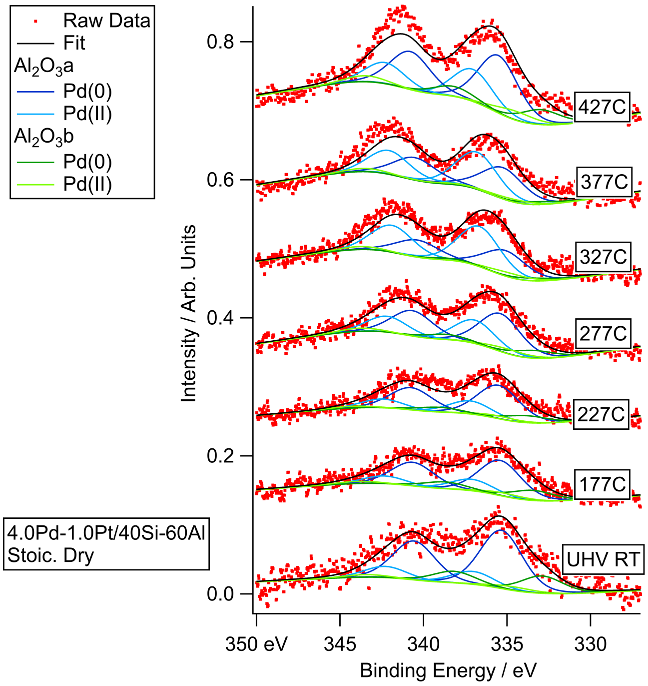

(a) Dry stoichiometric

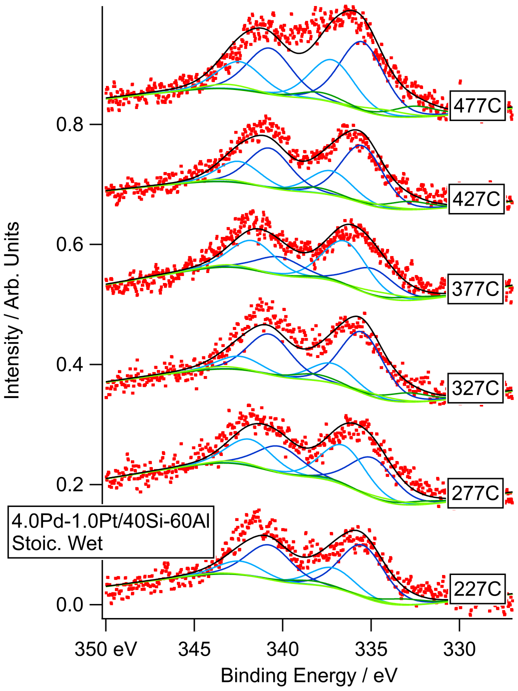

(b) Wet stoichiometric

Figure 4.8: Pd 3d region NAP-XPS spectra recorded for 4.0Pd-1.0Pt/40SiO_2-60Al_2O_3 catalyst under dry and wet stoichiometric methane oxidation conditions. All spectra recorded using 1350 eV photon energy.

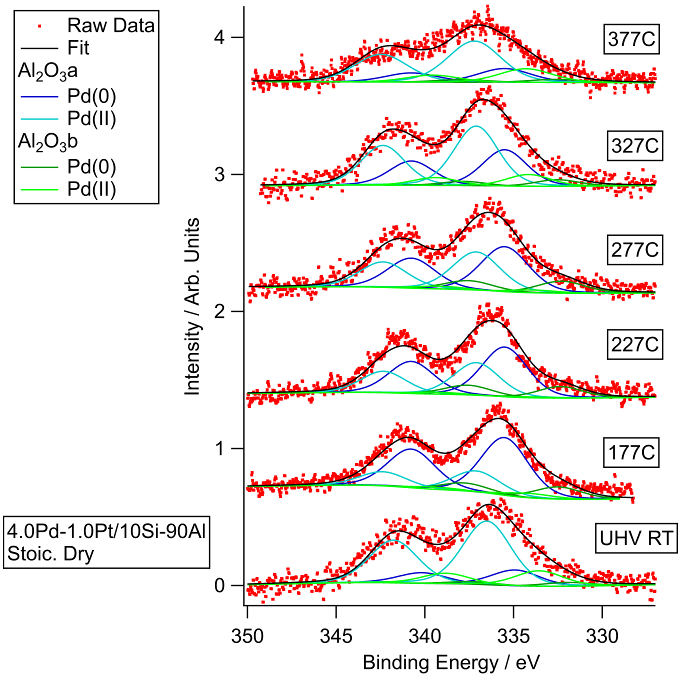

(a) Dry stoichiometric

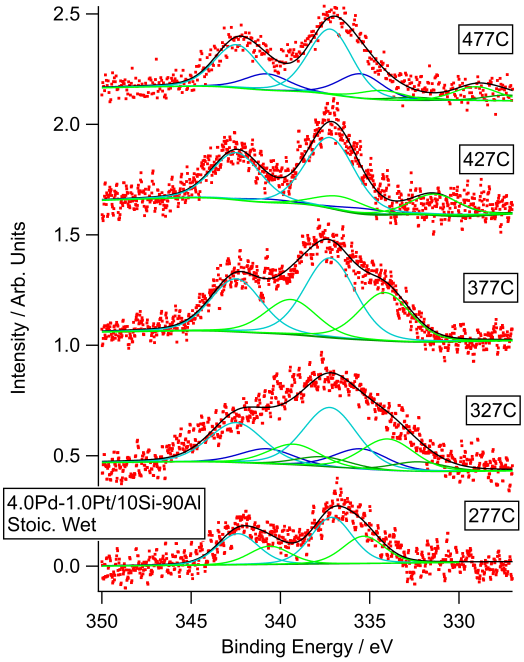

(b) Wet stoichiometric

Figure 4.9: Pd 3d region NAP-XPS spectra recorded for 4.0Pd-1.0Pt/10SiO_2-90Al_2O_3 catalyst under dry and wet stoichiometric methane oxidation conditions. All spectra recorded using 1350 eV photon energy.

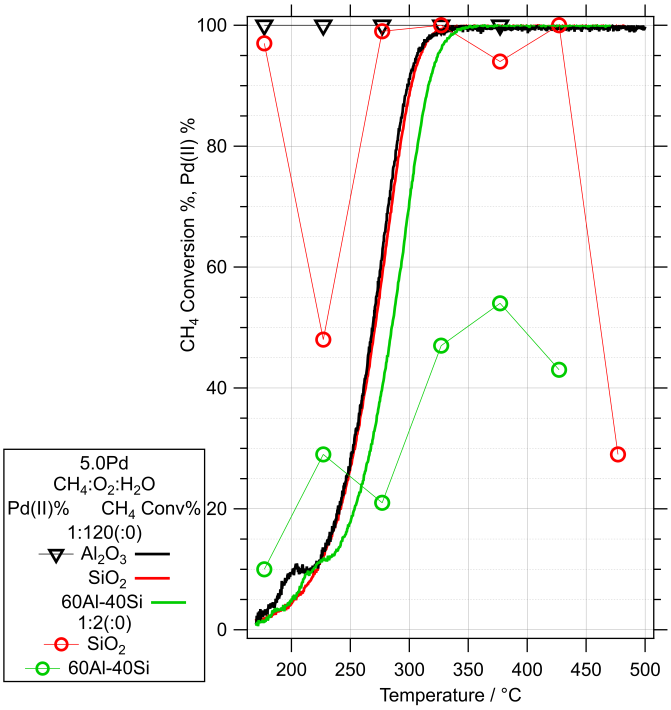

Figure 4.10: Pd(II)% as determined by NAP-XPS overlaid with catalytic testing data for 5.0Pd on various supports.

shown does not match with the NAP-XPS measurements performed. No stoichiometric activity data were recorded for 5.0Pd catalysts (with the exception of alumina), so the oxygen rich data activity are presented alongside the stoichiometric NAP-XPS data.

For both compositions and conditions, the Pd supported on the 60-40 mixed support is the least oxidised, typically remaining below 60% Pd(II) during reactions. These catalysts are also typically the least active of any tested support. Pure silica and alumina generally gave very similarly oxidised palladium in each case, which is reflected in the very similar activity - an unusual result as typically catalysts using these two supports behave very differently. [117] The correlation seems to break down with the 90-10 mixed support, as it outperforms the other supports, but the difference in palladium oxidation is inconsistent. In dry conditions, the palladium is similarly oxidised to that on the other mixed support, but with markedly better activity. In wet conditions, the palladium is similarly oxidised to that on both alumina and silica, with the activity being similar as a result. However, this was not tested under all conditions, so proper conclusions regarding catalysts on this support cannot be drawn.

Overall, this suggests that the oxidation of the palladium nanoparticles does still play a role here, but that it is not the most significant factor when comparing catalysts with different supports. $90Al_2O_3$-$10SiO_2$ looks like a very promising support for Pd or Pd-Pt catalysts for

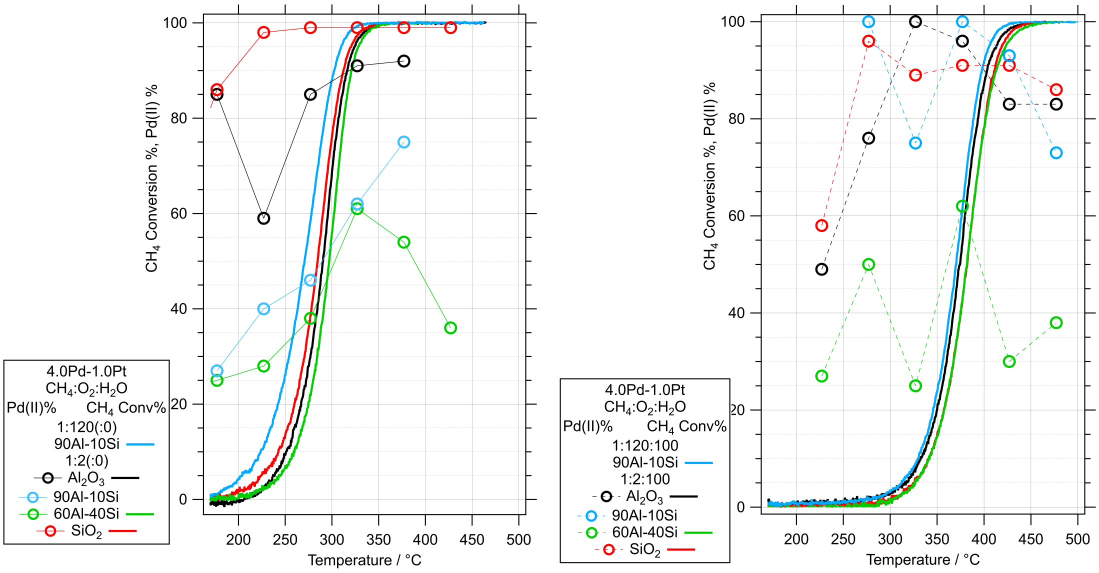

(a) 4.0Pd-1.0Pt Dry

(b) 4.0Pd-1.0Pt Wet

Figure 4.11: Pd(II)% as determined by NAP-XPS overlaid with catalytic testing data for 4.0Pd-1.0Pt on various supports.

methane oxidation in oxygen rich conditions, outperforming the typical alumina support in gas mixtures with or without water.

4.3 Additional Experiments

There were plans to collect significant amounts of additional data for this section, on silica and silica-alumina supported catalysts, in spring-summer 2020. Many of these were cancelled due to the Covid-19 pandemic, and the resulting lockdown. These additional experiments, with the reasoning behind them, are included below.

TEM imaging and EDX mapping of bimetallic, silica and silica-alumina supported catalysts. In the previous chapter, data is presented for various alumina supported catalysts, where we show the size, composition and distribution of nanoparticles on the support. We performed these experiments with various calcination temperatures and Pd : Pt ratios, and generally found the particles in bimetallic catalysts to be a non-ordered mix of palladium and platinum. This was seemingly unaffected by increased calcination temperature, or by varying Pd : Pt ratio. We had intended to perform this type of experiment again on our catalysts supported by silica and silica-alumina. Given the variations in activity that are observed with different supports, despite a generally similar particle size, we had hoped that these measurements may show a differing particle structure.

Catalytic testing was performed for various alumina-supported catalysts under stoichiometric reaction conditions. This provided some interesting data, with the NAP-XPS measurements often showing more variation than those performed under oxygen rich conditions. The intention was to complete additional stoichiometric tests for the Pd and Pd-Pt catalysts on silica and silica-alumina, but there was no possibility to access the reaction rigs which were used for all other catalytic tests. In some cases, other instruments would have been available, but with limited experimental time and the general difficulty of in person training during this period, they were not used.

Given the low level catalytic activity seen over some support materials, and the small activity variations observed between the catalysts, there was an intention to test the catalytic behaviour of the bare supports. This would have followed the same process as the other tests - the support would be calcined at 500 °C, pelletized and subjected to the usual set of ramps - just without the additional of PGM precursors. This would have given a baseline for each, and may have helped to explain some of the observed differences.

4.4 Discussion & Conclusions

Four support materials have been studied, to understand the effect of supports on Pd-Pt catalysts for the complete oxidation of methane. Pd-Pt ratios and percentage weight loadings were kept consistent across all supports, to ensure samples were as comparable as possible.

In regards to methane oxidation activity, $90Al_2O_3$-$10SiO_2$ supported catalysts were consistently better than catalysts supported on the other materials tested. Whilst the differences were often small, below 20 °C difference in T50, the consistent nature of the differences gave assurance that this catalyst support material is preferable. All supports still showed significant levels of deactivation in wet conditions, with ΔT50 of 99 °C or higher for all 5.0Pd and 4.0Pd-1.0Pt catalysts. 2.5Pd-2.5Pt catalysts on both mixed supports had lower ΔT50, consistent with alumina-supported catalysts.

NAP-XPS was conducted for some of these catalysts in select conditions. $90Al_2O_3$-$10SiO_2$ and $60Al_2O_3$-$40SiO_2$ supported 4.0Pd-1.0Pt catalysts consistently showed a presence of both Pd(0) and Pd(II), whilst SiO_2 or Al_2O_3 supported catalysts were typically more heavily oxidised. The NAP-XPS seemed to correlate well with the activity data, based on our previous expectations, with the exception of the $60Al_2O_3$-$40SiO_2$ support, which performed unexpectedly poorly. For support variation, it can be concluded that NAP-XPS can provide a useful insight into the nanoparticles on the surface, but that there are still larger factors at play in determining the effectiveness of the catalysts, such as the physical structure and acidity of the support.

When considering different supports, it is easy to simply report the weight percentage loading, but that does not tell the whole story. As mentioned previously, the differences in the molecular weight of alumina and silica mean that, for a given 20 g batch of catalyst prepared of a single mass, there will be significantly more molecules of silica than alumina (2.0×10^{23} compared to 1.2×10^{23}). However, this means there are more atoms of aluminium than silicon, ultimately giving different molecular and atomic ratios of Pd : Si and Pd : Al. With that said, with grain size varying heavily even within batches, and only general averages such as "100-150 μm" given, the actual relationship between surface support sites and PGM nanoparticles is very unclear, but can not be discounted when considering the variations in support.

5 Realistic model catalysts

5.1 Introduction

A real issue facing the in situ study of heterogeneous catalysts is the ability to study a catalyst in a form close its ordinary operational form. For the catalysts discussed in previous chapters, they would ordinarily be made into a slurry and coated onto a monolith, effectively a tube with many inner channels, with catalyst coated onto the walls of these channels, to maximise the surface area to volume ratio. [172–174]

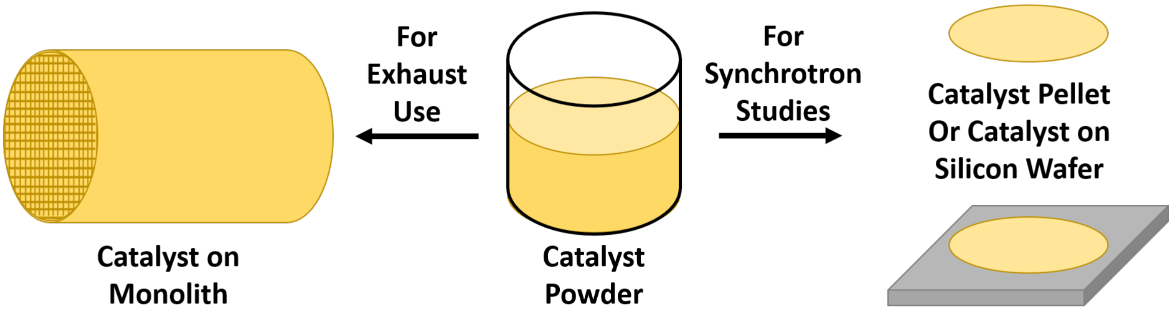

Figure 5.1: Diagram showing the comparative forms of a catalyst as prepared and studied in this work.

For practical measurement purposes this is an item significantly too large to perform NAP-XPS on, and so using a small fragment of the monolith may seem sensible. However, this can often still be impractically thick (and, as such, suffer from significant charging) as well as being structurally very different. A typical format for studying catalysts of this type is to press powders into a pellet, to ensure the sample is thin enough to not charge, whilst having enough sample to ensure good gas conversion is observed. These are often modified using metallic mesh or carbon powder to improve conductivity, but this makes the form even further removed from the functional catalyst. Coating samples onto a conductive substrate (as we have done with the silicon wafer) offers a similarly low-charging method of analysis, but again at a cost of unrealistic form. In these cases, not only is the sample physically very different to a real exhaust catalyst, but they can be inconsistent thickness from one sample to another - or even on different areas of a single sample - leading to further potential inconsistencies when measured. Examples of the forms mentioned here are shown in Fig. 5.1.

Because of the issues mentioned here, it was desirable for us to produce a sample which was similar structurally to a real catalyst - γ-alumina with nanoparticles of PGMs - but which were also a controllable and repeatable thickness. This requires two stages of model sample production. The first is to produce a repeatable, flat, γ-alumina substrate, thin enough to be conducting when deposited onto a conductive substrate. The second is to decorate this with PGM nanoparticles, of a similar size and relative loading to a powder catalyst.

5.2 Model alumina supports

5.2.1 Spin-coating

Spin coating is a method which can be used to produce a thin, dispersed layer of a sample onto a substrate. A mixture is deposited onto a substrate, which is spun at a high speed. Varying the solvent, acceleration rate, spinning speed and spinning time can lead to variation in thickness of the film produced. Many groups have successfully prepared thin films of metal oxides using spin coating. [175–178]

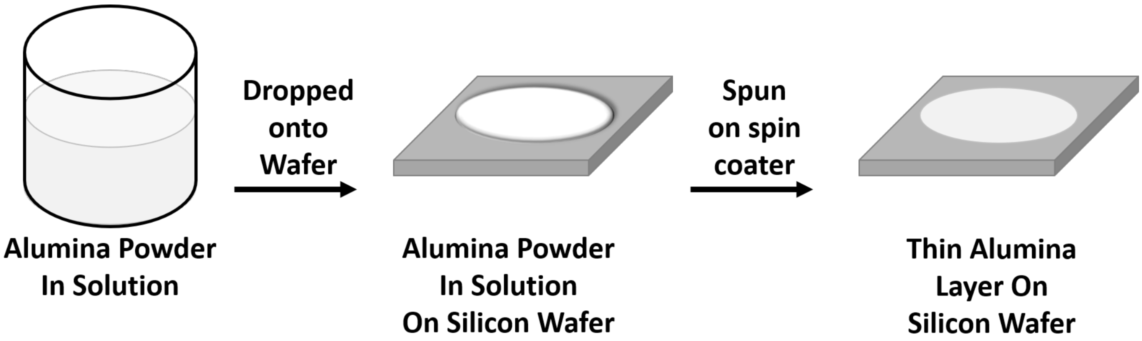

Figure 5.2: Diagram showing the comparative forms of a sample through the spin coating process.

Spin coating was briefly tried as a method to deposit the standard powder catalysts onto silicon wafers, but given the large grain size of alumina used (typically 100-150 μm), this yielded layers too thick to be of significant use.

Spin coating of aluminium hydroxide was considered, as this can be converted to different phases of alumina by calcination. [179] This was also rejected due to the particles sizes involved, and the desire to have a layer of minimum possible thickness.

For the spin coated alumina substrates, the primary powder used was a 3 μm γ-alumina. Using these smaller particles would allow for the production of a thinner and more conductive layer. A full table of the substrates prepared via the spin coating method is included in Tab. 5.1.

Water, ethanol and methanol were all tried as solvents for dispersing the alumina. Solution concentrations varied from 5-97 mgml^{-1}, with dosage amounts varying between 0.04-0.40 ml. Spin speed was varied between 750 and 3000 rpm. Acceleration was generally 30 rpm/s, but values of up to 180 were also used. Total spin time varied from 60-240 s. A simplified diagram showing the form of the sample through this process is shown in Fig. 5.2.

Various silicon wafers were used for deposition. Initial experiments used the phosphorous-doped silicon (referred to hereafter as P-Si), as a less expensive initial test substrate. After this, gold-coated silicon wafers (referred to as Au-Si) were used.

Thickness was determined based on the approximate surface area of the wafers used, and the total mass deposited. Given the low amounts of material added and the general inaccuracy of the balances used, some "thickness" values appear negative. The thicknesses determined are not considered as individually reliable, but generally they show a thickness typically of 1-3 microns. The equation used to determine the thickness is shown in Eqn. 5.1, where m$_{final}$ and m$_{initial}$ are the masses of the wafer after and before the alumina is deposited, ρ is the density of the alumina added, and A is the area covered by the alumina.

$$Thickness = (m_{final} - m_{initial})/(\rho \times A) \tag{5.1}$$

5.2.2 Anodization

The anodizing of aluminium is a commonly used practical method. [180] Tuning of experimental parameters such as temperature and potential can allow the tuning of material properties. [181–184] It is often used for decorative purposes, as varying the anodizing conditions can produce a vast range of colours. This can be seen in a wide range of industries, from jewellery to automotive parts. Sulfuric acid is widely used as the anodizing electrolyte, and is used here. [185]

Label	Powder	Solvent	Conc mgml^{-1}	Dose ml	Accel rpms^{-1}	Speed rpm	Time s	Wafer	Thickness μm
1	Al_2O_3	H_2O	96.8	0.32	30	1000	120	P-Si	1.37
2	Al_2O_3	H_2O	96.8	0.35	30	1700	120	P-Si	1.59
3	Al_2O_3	H_2O	48.0	0.34	30	1000	120	P-Si	1.88
4	Al_2O_3	H_2O	48.0	0.31	150	1000	120	P-Si	0.95
5	Al_2O_3	H_2O	48.0	0.26	150	1000	240	P-Si	4.49
6	Al_2O_3	H_2O	19.9	0.22	30	1000	120	P-Si	0.44
7	Al_2O_3	H_2O	19.9	0.21	30	3000	120	P-Si	0.79
8	Al_2O_3	H_2O	19.9	0.20	30	750	120	P-Si	2.55
9	Al_2O_3	H_2O	19.9	0.19	30	1000	90	Au-Si	1.86
10	Al_2O_3	H_2O	19.9	0.22	30	1000	120	Au-Si	0.20
11	Al_2O_3	H_2O	19.9	0.09	30	1000	60	Au-Si	1.58
12	Al_2O_3	H_2O	19.9	0.05	30	1000	60	Au-Si	1.58
C1	$Al(OH)_3$	H_2O	19.7	0.20	30	1000	60*	Au-Si	3.10
C2	$Al(OH)_3$	H_2O	5.0	0.21	30	1000	60*	Au-Si	0.13
C3	$Al(OH)_3$	H_2O	5.0	0.20	30	3000	60*	Au-Si	1.79
C4	$Al(OH)_3$	H_2O	5.0	0.40	30	3000*	60*	Au-Si	3.06
C5	$Al(OH)_3$	H_2O	5.0	0.39	30	3000	60*	Au-Si	3.72
3-1	3μm-Al_2O_3	H_2O	10.1	0.20	30	2000	60	Au-Si	1.99
3-2	3μm-Al_2O_3	H_2O	10.1	0.11	30	2000	60	Au-Si	0.50
3-3	3μm-Al_2O_3	H_2O	5.0	0.10	30	2000	60	Au-Si	1.00
3-4	3μm-Al_2O_3	H_2O	10.1	0.11	30	3000	60	Au-Si	1.50
3-5	3μm-Al_2O_3	H_2O	10.1	0.10	30	3000	60	Au-Si	0.00**
3-6	3μm-Al_2O_3	H_2O	10.1	0.07	120	3000	60	Au-Si	-1.00**
3-7	3μm-Al_2O_3	H_2O	10.1	0.15	30	3000	60	Au-Si	1.99
3-8	3μm-Al_2O_3	H_2O	10.1	0.12	30	3000	60	Au-Si	1.00
3-9	3μm-Al_2O_3	EtOH	7.8	0.09	30	3000	60	Au-Si	0.50
3-10	3μm-Al_2O_3	EtOH	7.8	0.07	120	3000	60	Au-Si	-1.50**
3-11	3μm-Al_2O_3	EtOH	7.7	0.04	80	3000	60	Au-Si	-0.50**
3-12	3μm-Al_2O_3	EtOH	7.8	0.04	180	3000	60	Au-Si	1.50
3-13	3μm-Al_2O_3	MeOH	8.4	0.05	120	3000	60	Au-Si	-1.00**
3-14	3μm-Al_2O_3	MeOH	8.4	0.05	120	3000	60	Au-Si	-1.00**

Table 5.1: Details of all alumina substrates prepared via the ”spin coating” method. Thickness values labelled with ** are considered to be invalid, as they are either zero or negative.

Labels	H2SO4 ml	Conc moldm-3	Current A	Time s	Size mm x mm	Cleaned?	Charging eV
14, 15	3	1.26	0.019	300	4 x 15, 4 x 15	No	1.9
16, 17	3	1.26	0.032	300	4 x 18, 4 x 18	No	1.1
18, 19	0.5	0.22	0.007	1200	4 x 16, 4 x 15	Yes	0.4
20, 21	0.5	0.22	0.01	600	4 x 15, 4 x 15	Yes	0.3
22, 23	0.5	0.22	0.003	2400	5 x 18, 5 x 19	Yes	0.6
24, 25	0.5	0.22	0.003	1200	4 x 18, 4 x 21	Yes	-
26, 27	0.5	0.22	0.001	600	4 x 12, 4 x 12	Yes	-
28, 29	0.5	0.22	0.003	2400	4 x 20, 4 x 20	Yes	-
30, 31	0.5	0.22	0.005	3600	4 x 20, 4 x 21	Yes	-
32, 33	0.5	0.22	0.003	900	4 x 15, 4 x 16	Yes	-

Table 5.2: Details of all alumina substrates prepared via the back-to-back "anodization" method. In all cases, the volume of water used was 40 mL. Charging is determined based on the Al 2p peak position in lab XPS scans. Where this value is given as "-", no data was collected.

Using sheets of aluminium means that, in principal, samples of any size, shape or thickness could be produced to best fit different experimental set ups, without needing to significantly vary the method of production.

Producing a substrate by converting the surface layer of an aluminium sheet to alumina ensures that the bulk of the sample will be conductive (as it will remain as metallic aluminium) and so will be viable for study under NAP-XPS conditions.

The method required using 2 aluminium pieces back-to-back, to prevent a build up of alumina on both sides of an individual piece. Initial experiments did not do this, and produced unusable substrates, so are not discussed here. Tab. 5.2 shows all of the "back-to-back" samples, with 2 pieces produced for each condition. Charging refers to the relative position of the Al 2p peak observed when studying the samples with a standard laboratory UHV XPS spectrometer. The lowest charging was achieved by the shortest anodization time, a total of 10 minutes, with decreased currents and sulfuric acid concentration also proving useful to reduce charging. For all XPS studied samples, however, the charging was below 2 eV, which is useful for synchrotron studies - though it must be noted that these were collected on a laboratory instrument with a flood gun for charge compensation.

5.3 Model palladium nanoparticles

Once a flat substrate was reliably produced, we needed to reliably deposit nanoparticles of consistent size and distribution onto them. An initial consideration for this was to simply deposit a palladium or platinum precursor (such as the nitrate solutions used for the powder catalysts) directly onto the surface and annealing them. This would keep the method of production as similar as was reasonably practical to that of the powder catalysts. However, accurately controlling the loading and distribution with this method is difficult. Whilst mixing of the precursor and a large volume of powder can give good dispersion, this method would have required a very small volume of precursor to be loading onto a small flat area, and it would not be possible to guarantee good dispersion in this way. As a key point of using model catalyst systems is to have well defined and controlled systems, it was decided that this method should not be used. Reverse micellar methods were also considered for use, as it is a common method for production of fine palladium or alloy nanoparticles. [186, 187]

A cluster source was used as the source of palladium nanoparticles. This allowed us to deposit a consistent amount onto multiple substrates at one time (due to the large rotating plate in the instrument), and gave good control over particle loading by varying the deposition time. Whilst it was not employed on the cluster source used here, other cluster source instruments can also allow for particle size and shape control, which is another useful step in controlling the consistency of samples. The cluster source used was based at Swansea University. [150, 151]

Palladium cluster depositions were performed on both spin coated and anodized substrates, to give a range of options.

Fig. 5.3 shows the comparison of Pd 3d and Al 2p peaks measured for the cluster source produced sample compared to a typical powder catalyst sample. Analysis of the relative peak areas show the loading of palladium on the anodized sample to be approx. 78% of that on the 5.0Pd powder sample. This was achieved with the 5 minute deposition cycle. Given the approximate nature of the calculations, along with Pd not having been deposited from this system before, this was considered to be a success, and showed that these samples can easily and rapidly be produced with a desirable loading.

TEM images were taken of copper TEM grids which were on the deposition plate during each palladium deposition cycle. Analysis of the particles in these images gave average

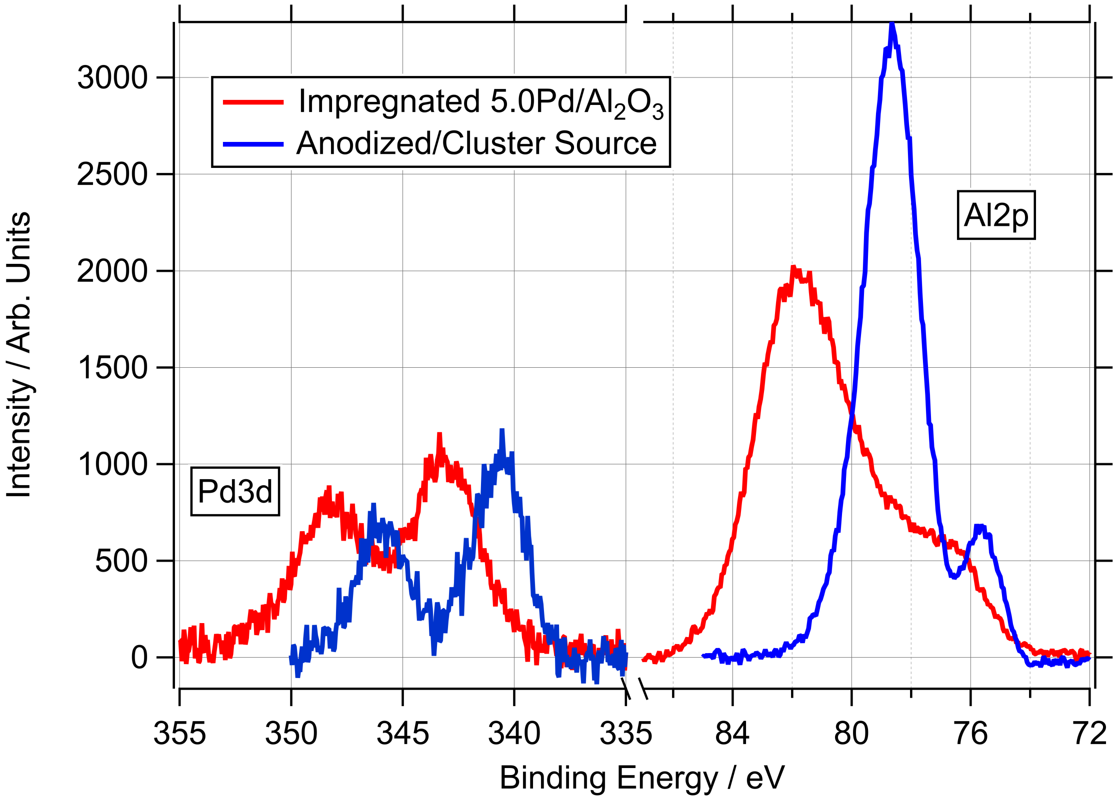

Figure 5.3: Al 2p and Pd 3d region XPS data for a typical powder 5.0Pd/Al$_2$O$_3$ sample and a sample with cluster source produced Pd nanoparticles on an anodized aluminium support. Recorded under vacuum at room temperature. Spectra are not corrected with respect to binding energy. Powder data recorded with 1486.6 eV photon energy, anodized sample data with 1350 eV photon energy.

particles sizes (± SD) of 0.97 ± 0.95 nm and 1.09 ± 0.83 nm for the 1 and 5 minute depositions respectively. The similarity between these is expected, as the particle size should not be significantly affected by the longer deposition time. With the samples not being heated at any stage, no additional agglomeration was expected or observed. In both cases, particle size analysis was completed using more than 300 particles.

The key issue currently with this method is the palladium nanoparticle size and size distribution. The 5.0Pd/Al$_2$O3$_3$ powder catalyst (after calcination at 500 °C) had an average particle size of 12 ± 5 nm (as determined by TEM). The particles produced via the cluster source are significantly smaller, with a greater standard deviation in particle size, relative to the average. The clusters produced in this experiment were at the limit of what could reasonably be deposited. With some size-selected methods it is possible to produce larger particles, but this comes at the cost of much greater preparation time, as it rejects the majority of produced clusters. Even with this, routinely producing clusters of greater than

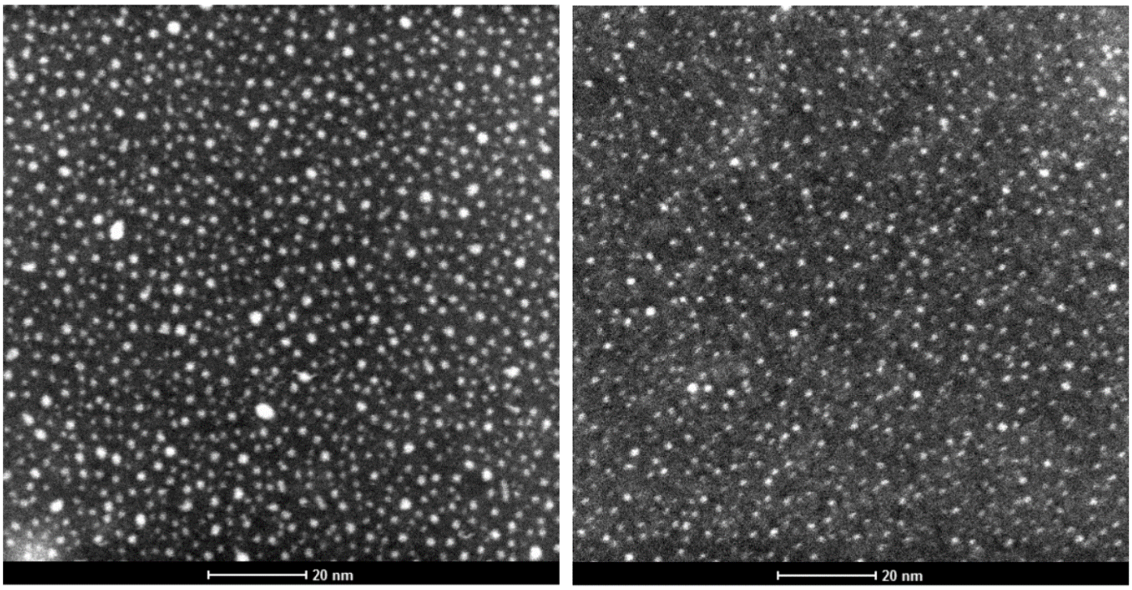

Figure 5.4: TEM images of Pd clusters deposited onto copper TEM grids during 1 minute (left) and 5 minute (right) depositions of palladium clusters.

10 nm is difficult. It is possible that, with high enough temperature calcination, it may be possible to produce larger nanoparticles on the surface after cluster deposition, but this was not attempted.

5.4 NAP-XPS of anodized sample

The sample produced via anodization and cluster source deposition was tested at the VerSoX beamline at Diamond, to ensure it was stable under heating and under the XPS beam, before further experiments.

An example of the XPS survey spectra taken before, during, and after heating to 500 $°C$ in 2 mbar of helium is shown in Fig. 5.5. Minimal variation in aluminium or palladium is seen through these, excluding due to the additional attenuation under helium as compared to vacuum conditions. These spectra are uncorrected, showing minimal charging, with peaks only being 6-7 eV from their natural positions. This is sustained over reasonable measurement times (more than an hour in total), confirming samples of this nature are stable enough for further study.

With the success of this sample during initial tests, it was taken to a beamtime on the X07DB NanoXAS beamline at Swiss Light Source. During initial measurements some con-

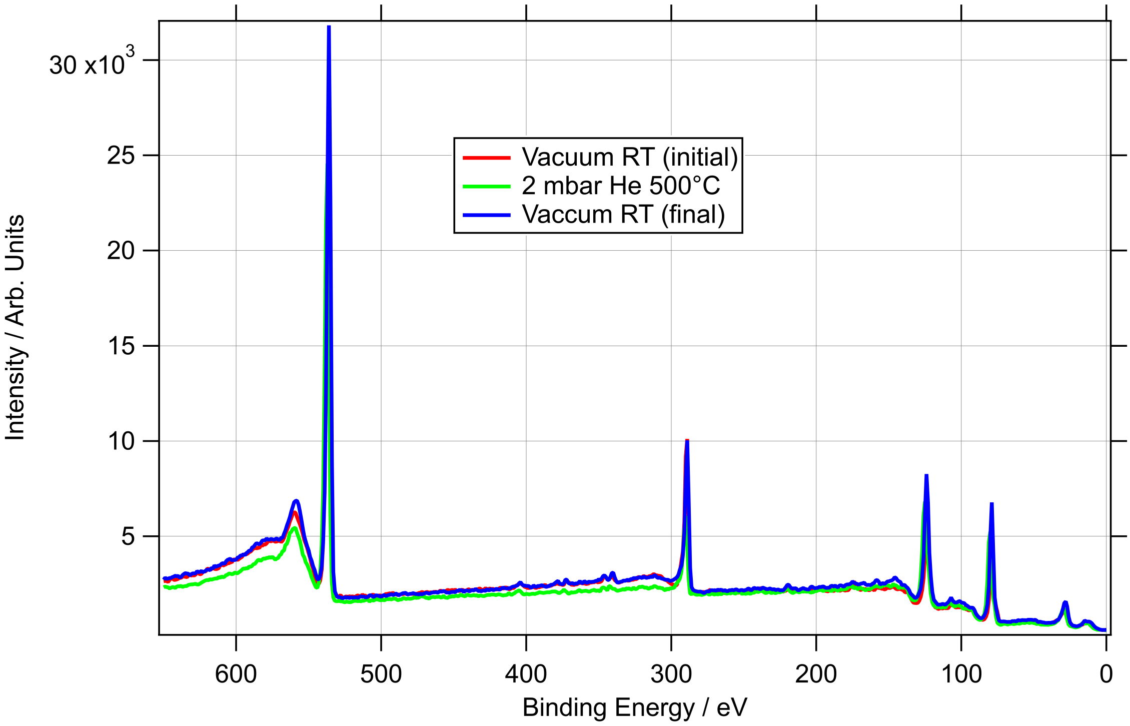

Figure 5.5: Survey XPS spectra for the sample with cluster deposited Pd on an anodized alumina substrate. Spectra taken at room temperature in vaccum, then 500 $°C$ in 2 mbar of helium, then again in vaccum at approx. 50 $°C$. Spectra are not corrected with respect to binding energy.

tamination was observed, so the sample was heated to clean the surface. An issue with the sample and thermocouple mounting led to the (laser) sample heater heating the sample to a high temperature very rapidly, much higher than the 500 °C which had been intended, at which point the surface appeared to distort. No good measurements were gained after this, with the assumption that the alumina film layer and the palladium deposited onto it had been removed/damaged by this process. Whilst the exact temperature the sample reached is unclear, it was sufficient to weld the aluminium onto the copper support plate, suggesting over 650 °C was reached.

5.5 NAP-XPS of spin-coated sample

One spin coated sample with deposited palladium clusters was also studied using NAP-XPS. The experiments presented here were all performed on the X07DB NanoXAS beamline at Swiss Light Source. All data recorded on this instrument used a photon energy of 900 eV.

An initial survey of this sample can be seen in Fig. 5.6. This shows the main issue with

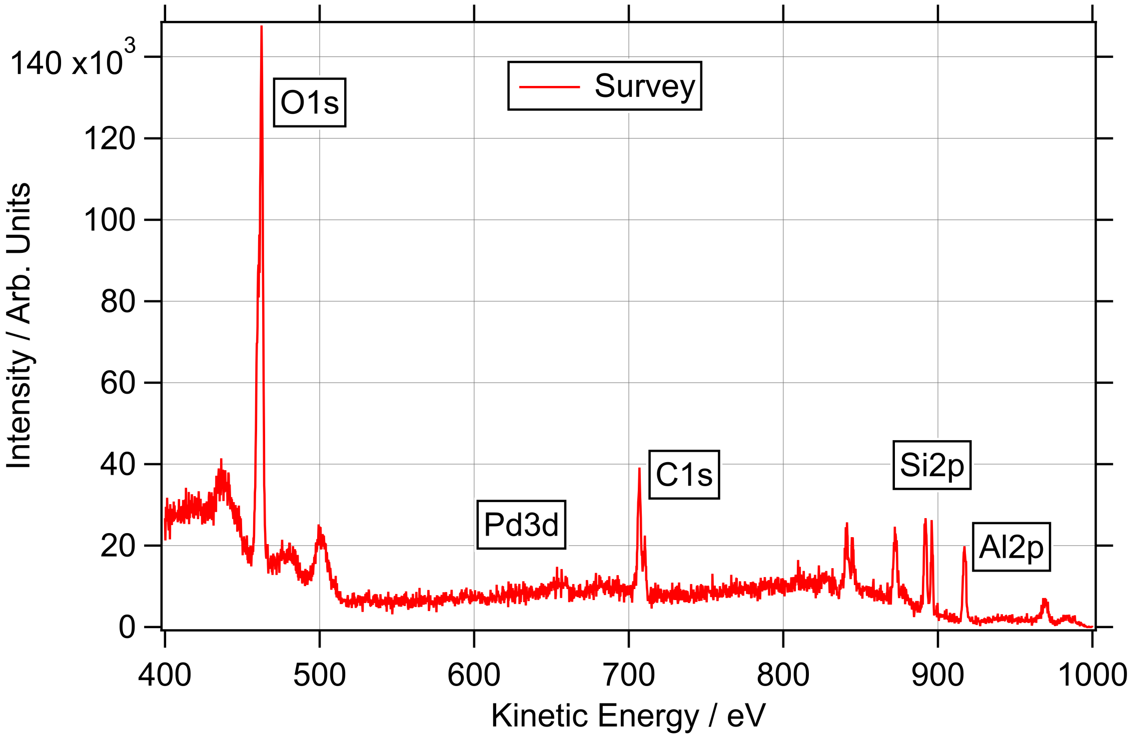

Figure 5.6: Survey XPS spectrum for a sample based on a silicon wafer, with spin coated alumina and palladium nanoparticles deposited using the cluster source. Recorded with a photon energy of 900 eV.

this sample - the alumina does not properly cover the silicon wafer, so silicon is still present in any spectra. However, unlike with the powder samples where silicon is observed, in this case it means that palladium nanoparticles had been deposited onto the silicon wafer in addition to the alumina. An example high resolution palladium spectrum is shown in Fig. 5.7. This shows the presence of twice as many palladium peaks as normal, due to the palladium on the silicon charging by approximately 3 eV less than those on the alumina support.

Despite the issues, and due to not having any other remaining model samples to study on the beamtime, this sample was further studied under reaction conditions. Principally this was done as the palladium signal observed was still strong enough to measure within a reasonable timescale, and the charging was not excessive, nor was it changing significantly over time. In Fig. 5.8 Pd 3d XPS spectra are shown for this sample. Over time, there is more and more charging of the alumina species, which moves the Pd $3d_{5/2}$ peak of the alumina-supported palladium under the Pd $3d_{3/2}$ peak of the silicon-supported palladium. This could make the fitting somewhat less reliable, although it makes the Pd $3d_{5/2}$ peak of the silicon-supported palladium more clear, giving a more reliable fit for this species. Overall,

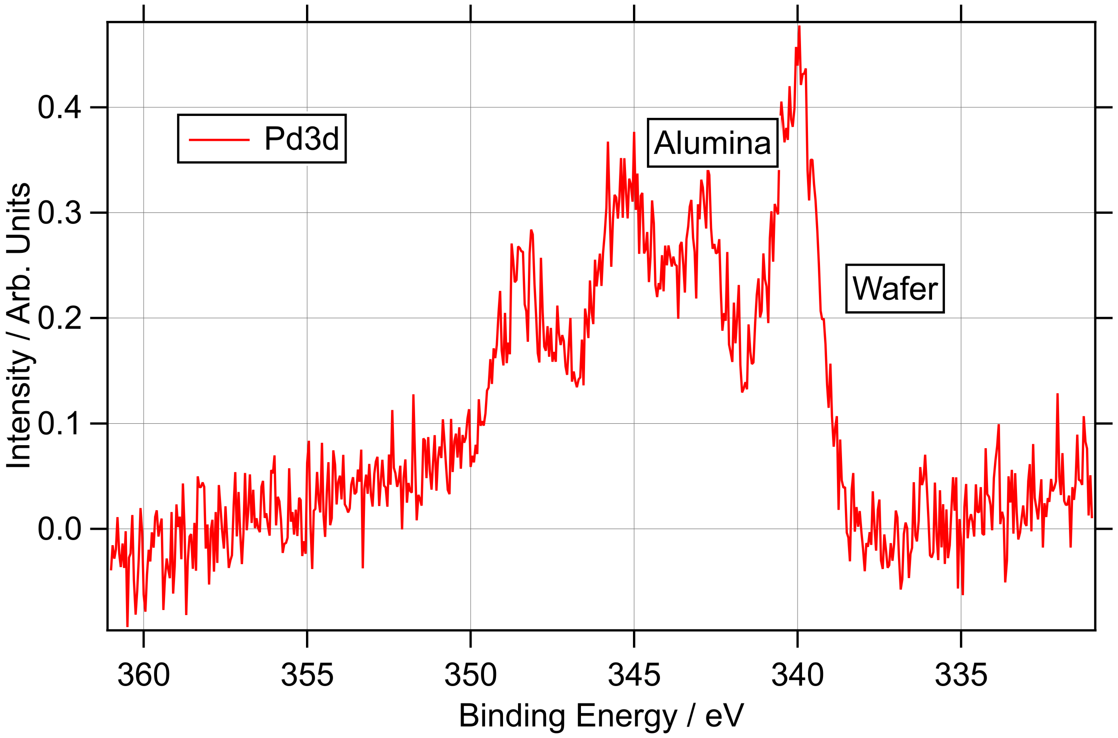

Figure 5.7: Pd 3d region XPS spectrum for a sample based on a silicon wafer, with spin coated alumina and palladium nanoparticles deposited using the cluster source.

the charging seen for the Pd on the alumina is generally 12 eV or less, which is better than for the majority of the normal powder catalyst samples, confirming this method would produce a viable support if the coverage issue could be rectified.

Though these spectra are not as clear as those for the powder samples, they still show similar variations to the powder catalysts under reaction conditions. Pre-reaction, it can be seen that the Pd is largely reduced, with only a small presence of Pd(II). With increasing temperature under reaction conditions, there is a notable presence of Pd(II). This initially increases, but there is still a large presence of Pd(0) under dry and wet conditions, even at the highest temperatures used in the experiment. The palladium on the alumina appears to more readily oxidise than the palladium supported directly on the silicon substrate, with large amounts of Pd(0) observed for the silicon-supported Pd at all temperatures.

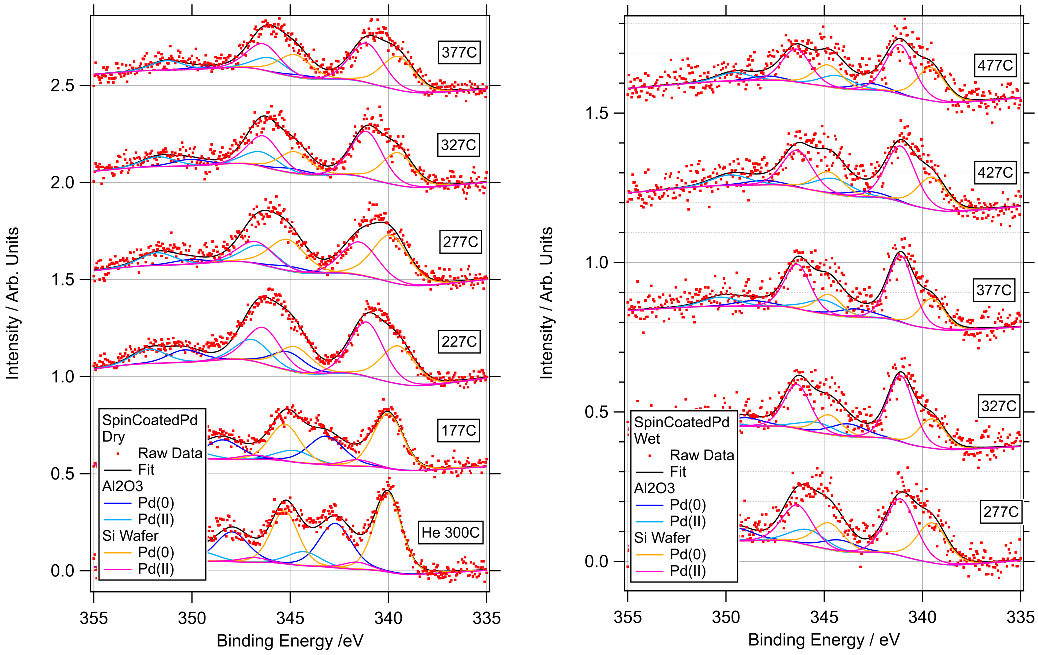

(a) Dry

(b) Wet

Figure 5.8: Pd 3d region XPS spectra for a sample based on a silicon wafer, with spin coated alumina and palladium nanoparticles deposited using the cluster source, recorded under dry and wet reaction conditions. Due to the nature of the sample, the binding energy scale has not been corrected.

5.5.1 Rejected Model Ideas

Naturally, much more was considered for this section of the project than was actually completed. Some of the more interesting ideas for potential models are outlined below.

Initial trials were conducted using $Al(OH)_3$, as this can be converted to γ-Al_2O_3 using specific heat treatments. Thin layers of this were spread, initially on microscope slides, and latterly on silicon wafers, but ultimately the large particle size was leading to an excessively thick layer formation, so this idea was deemed impractical for the intended purpose.

Using the supports prepared via anodization/spin coating, the suggestion was raised to coat these with nanoparticles by dipping them into the metal precursor solutions (or spreading this onto the support) and calcining, as this would be consistent with our impregnation preparation method for powder catalysts. This was rejected as the control over exact PGM loading would be too difficult, and it is important to have a model with at least a similar surface loading to our real catalysts.

Variations of the cluster source preparation method whereby control of particle size is achieved were considered, however this method has a number of drawbacks. The major issue is that typical cluster formation yields a maximum of 1-2 nm clusters, smaller than the nanoparticles we wished to model, which are typically 10-15 nm. Additionally, if a mass filter is used, any clusters outside of the size range are rejected, and consequently the deposition takes much longer for a given total loading - with this time increasing with increased specificity of cluster size.

An additional consideration for an application of the cluster source was the direct deposition of clusters onto a powder, such as the 3 μm-Al_2O_3 used for spin coating. Unfortunately, coating of a useful amount of powder would take much longer than coating the flat supports, due to the massively increased surface area. In addition, this powder would still have required supporting for synchrotron studies, ie by drop casting/spin coating, or by forming into a pellet, meaning it is not a complete solution to the issue. These would, however, have been useful in one aspect, which is that they would have been easy to subject to catalytic testing in the way described in the analysis section below.

5.6 Additional Experiments

As with the previous chapter, there were plans to continue this work that were ultimately prevented by the effects of the lockdown during 2020.

The best "realistic model" sample that was produced, with Pd clusters on an anodized alumina substrate, was unfortunately damaged beyond use during a beamtime. Due to the limited time during initial production, it was the only sample of its nature that we had. A lack of access to a cluster source made it impossible to get new equivalent samples produced.

There had been an intention to use the newly installed cluster source at Diamond Light Source, in place of the one used previously (based at Swansea University). Unfortunately, this was not delivered, installed and tested until much later than initially planned, so it would not have been practical to produce new samples using this during the required time.

The intention, beyond this, was to eventually produce model systems with different variations of "bimetallic" nanoparticles. One version of this would utilise a Pd-Pt alloy "target", which should generally produce bimetallic clusters. Another way would have been to use two separate targets, and sequentially deposit the palladium and platinum, to ensure the presence of monometallic nanoparticles of each.

Given the small particle size of deposited clusters, as noted previously, consideration had been given to trying to increase this. Calcination of powder catalysts is used to increase particle size, so it seemed that this could be a reasonable approach here also. Due to the lack of sample availability, for reasons outlined above, this was not attempted.

5.7 Discussion & Conclusions

This part of the project sought to produce model catalyst samples which were structurally similar to the powder catalysts, but which were easier to study spectroscopically in regards of charging and coverage.

The anodization/cluster source approach produced a sample with effective palladium loading equivalent to the powder catalysts, based on the XPS peak areas observed. In this regard, this section of the project can be considered successful. The charging for these samples was low, and the higher coverage made it faster to get good quality spectra than for the powder catalysts.

The spin-coating/cluster source approach produced a similarly reasonable model, but in this case the issue of poor coverage was not fixed. In fact, the presence of Pd clusters on silicon made the spectra less clear than for typical powder catalysts. Despite this, dynamic oxidation and reduction of palladium was observed for this sample during NAP-XPS measurements, which indicated that the preparation method could provide reasonable samples if the coverage issue was resolved.

Overall, this means some success has been had with production of ”realistic model” catalysts, but more study of the anodization/cluster source samples would be needed to see whether they behave similarly to powder catalysts under reaction conditions. In particular, a refined version of the anodization technique could be widely used to produce flat, repeatable substrates for a wide variety of metal oxide support systems, and across a range of catalytic applications.

6 Thin film & foil systems

6.1 Introduction

The previous chapter discussed the production of "model" catalyst samples that still retained the supported nanoparticulate nature of the real, functional catalysts. Whilst this is useful for studying more relevant effects, it is also interesting to study the intermetallic interactions that underpin their function by using more "unrealistic" model systems. A simple model system for these materials could simply be metallic foils. Complete oxidation of methane can still be observed over palladium foil, and many groups have used palladium foils as models for palladium catalysts in their studies. [33, 64, 188, 189] Prior ambient pressure studies have shown surface oxidation can be studied on palladium foils. [190] The catalytic activity is different, nevertheless, using metallic foils can still be very instructive for our understanding of the behaviour of bimetallic systems compared to the individual metals.

Another approach towards models is the deposition of thin films of metals onto a single crystal, a very "traditional surface science" type of system. Initial film experiments focused on the deposition of layers of palladium and platinum onto a rhenium single crystal. The hexagonal Re{0001} surface which was used here has a nearest neighbour distance of 2.74 $\mathring{A}$, which is within 1.1% of the values for Pd and Pt (2.75 $\mathring{A}$ and 2.77 $\mathring{A}$ respectively). Multiple photon energies were used for depth profiling, in order to understand how the bimetallic phase was changing at its surface, in its bulk, and at the metal-rhenium interface. The growth of palladium films on the Re{0001} has been studied previously and is well understood. [148,191] All experiments with this set up were performed in UHV conditions with the intent to study alloying behaviour of palladium and platinum. An article from Ruban, Skriver and Norskov provides the prediction that palladium and platinum will segregate differently when combined, depending on which is the "host" and which is the "solute". [87] Where Pd is the host to Pt, there is a moderate degree of anti-segregation, which is to say that platinum would preferentially move into the bulk of the palladium. Where platinum is the host to palladium, there is no preferential segregation nor anti-segregation, so no migration of palladium is expected at all. Sequential deposition of thin layers of each metal will allow us to study whether these behaviours are observed.

Our later experiments featured the study of thin foils of palladium and platinum individually, along with bimetallic foils with atomic ratios matching some of the bimetallic powder catalysts. For this, we performed temperature programmed near-ambient pressure XPS (TP-NAP-XPS) experiments under conditions very similar to the NAP-XPS experiments reported for the powder catalysts. This allowed us to study how the metals behaved under reaction conditions, without variables such as particle size and surface loading having an effect. The nature of the systems also allowed for much faster high resolution spectra to be recorded, making temperature programmed experiments feasible. The higher relative amounts of Pd and Pt mean that a given spectrum can be recorded much faster, meaning we can record more spectra within a beamtime, allowing for more gas conditions, more photon energies (giving more depth information) and more different sample compositions. All of this means we can build a much better overall picture of the inter-metallic interactions occurring under reaction conditions in a shorter amount of beamtime.

6.2 Bimetallic Films

The first attempt to study palladium-platinum interactions directly in this project was done using thin layers of platinum and palladium, deposited onto a Re{0001} single crystal.

The results presented below were all produced during an experimental session at the Materials Science beamline at Elettra Sincrotrone. With this being a UHV endstation, no ambient pressure experiments are presented. Where there is dosing of gases, these are O_2 or CO, generally of 10^{-7} mbar or less.

For these single crystal studies, a Re{0001} single crystal was used as a substrate for deposition. This is used because the lattice parameters of the crystal and deposited palladium and platinum are very similar [148]. The nearest neighbour distances are 2.75, 2.77 and 2.74 $\mathring{A}$ for Pd, Pt (both face-centred cubic(fcc)) and Re (hexagonal close-packed (hcp)) respectively. [149] Thin layers of palladium and platinum were deposited using an Oxford Instruments EGN4 evaporator. Palladium was evaporated at approximately 27 W and 11 nA, whilst platinum required 40 W and 11 nA. Over distances around 10 cm these conditions gave 1 ML of PGM after approximately 5 minutes. The crystal was typically heated to approximately 150 °C during deposition, whilst cleaning was typically performed by a high temperature (1500 °C+) flash. Where the sample is referred to as "annealed", this means it had been subjected to 10 minutes in oxygen (1x10^{-7} mbar) at 700 °C followed by 10 minutes in UHV at 500 °C. For removal of platinum, currently the crystal needs to be flashed to approximately 2000 °C, so it was not possible to remove this from the Re{0001} crystal during the beamtime at Materials Science, Elettra.

Throughout this section, the relative amounts of Pd and Pt on the crystal are referred to in monolayers (ML), where one monolayer is one atom per substrate surface atom. These amounts are based on initial calibration experiments performed using the metal evaporator.

As part of this, various systems were produced and studied. With the maximum operating temperatures of the system (1300 K), we were unable to effectively remove Pt by evaporation during the experiments. Initially palladium was deposited and studied individually, in two deposition cycles - first with 1ML Pd, then with a total of 3ML Pd. There were then two cycles of platinum addition and annealing, first giving 3ML Pd + 1ML Pt and 3ML Pd + 3ML Pt.

After this, the sample was flashed to high temperature, which removed all palladium, leaving behind most of the previously deposited platinum, approx. 2ML Pt. Additional depositions were then subsequently performed with 2ML Pd, 2ML Pt and then 2ML Pd, giving effective compositions of 2ML Pt + 2ML Pd, 4ML Pt + 2ML Pd, and 4ML Pt + 4ML Pd.

In total, this gave us a good range of compositions, from platinum rich to palladium rich, to allow us to study interactions in a variety of systems. It also allowed us to study the differences in behaviour resulting from the order of addition (ie Pt added to Pd, rather than Pd added to Pt).

In most cases, measurements were made at multiple photon energies, so that different sample depths could be probed. Given that only small amounts were being added to the surface in each step, significant differences can be seen when looking at core levels using different photon energies. The selected photon energies were 405, 650 and 900 eV, with additional energies used for studying the valence band. These correspond to kinetic energies of approximately 70, 315 and 565 eV for Pd $3d_{5/2}$, and 335, 580 and 830 eV for Pt $4f_{7/2}$. This means that the Pd spectra recorded at 650 eV and the Pt spectra recorded at 405 eV are sampling similar depths of the films. This is also true for the Pd 900 eV and Pt 650 eV spectra. It is important to note that the beamline resolution also varies with the varied photon energy. With a 100 μm exit slit the resolution at 405 eV is approximately 250 meV, as compared to 500 meV and 800 meV for photon energies of 650 and 900 eV respectively. [192]

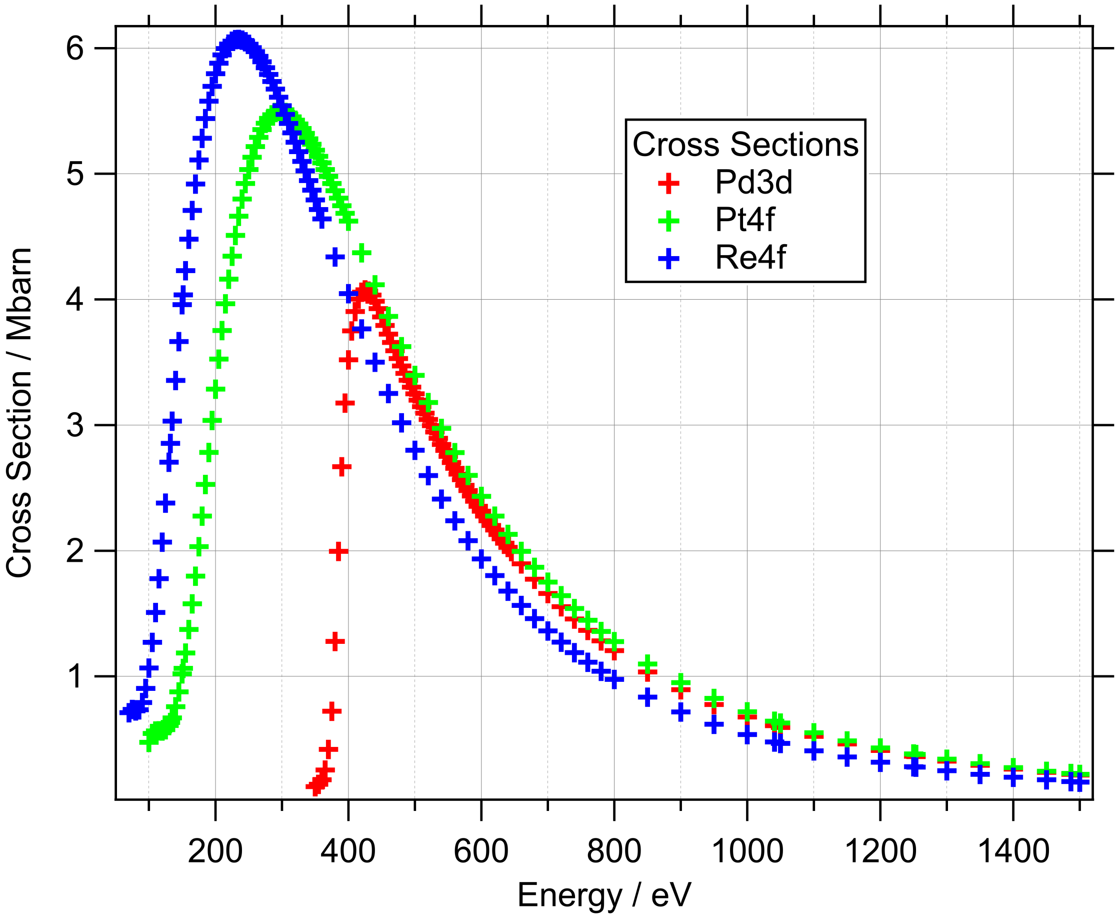

Figure 6.1: Photoionization cross section data for Re 4f, Pd 3d and Pt 4f.

In Fig. 6.1, the differences in cross sections for the three main metal peaks studied can be seen. The cross sections of palladium 3d and platinum 4f are very close for the 650 eV and 900 eV photon energies, with Pt 4f being slightly higher. At 405 eV, the cross section of Pt 4f is more notably higher than that of Pd 3d. The cross section of Re 4f is slightly lower than that of the other two levels at all used photon energies.

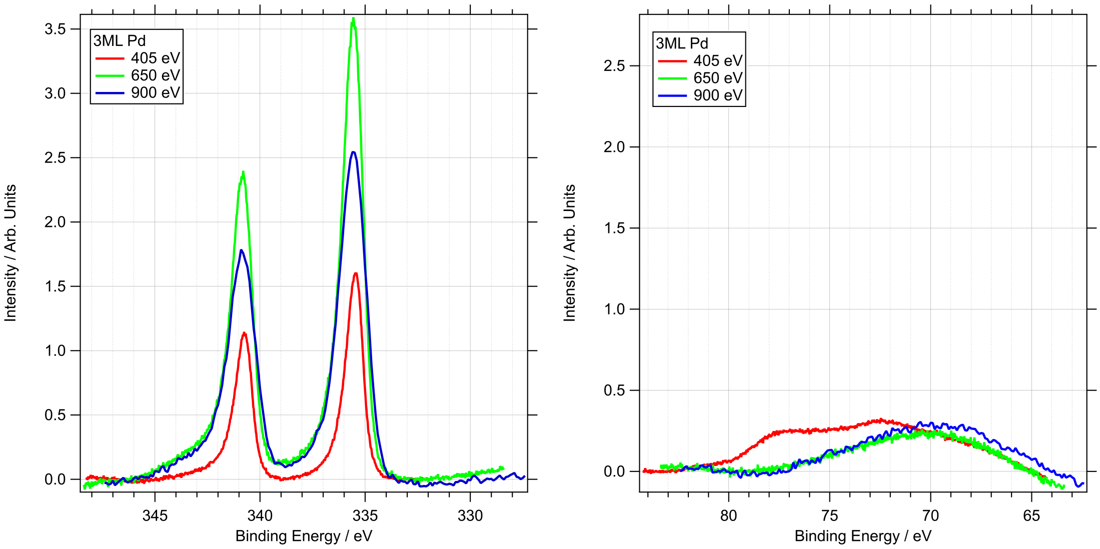

(a) Pd 3d

(b) Pt 4f

Figure 6.2: Pd 3d and Pt 4f XPS spectra for "3ML Pd" thin film on Re single crystal, recorded at 405, 650 and 900 eV photon energies. The binding energy of all spectra has been corrected using the measured Fermi energy level. The Pt 4f graphic has been rescaled to show the intensity of the background relative to the later platinum figures.

6.2.1 Palladium and Platinum core level XPS

The bulk of this work focused on the study of palladium and platinum core levels (Pd 3d and Pt 4f). In each of the figures here, the Pd 3d and Pt 4f region spectra will be shown together, as recorded at multiple photon energies, for given film compositions. For clarity, only 2-3 films compositions will be shown per figure. For cases where significant changes are observed, low kinetic energy spectra will be presented with fitted data, showing surface, bulk and interface peaks for Pd and Pt, and Pt-Re alloy peaks where relevant (once the sample had been flashed to 1000 °C or higher). For peak fitting, the following energies (all eV) are used, typically with ±0.1 eV: Pd $3d_{5/2}$ 334.6 (surface), 335.0 (bulk), 335.5 (Pd-Re interface); Pt $4f_{7/2}$ 70.7 (surface), 71.0 (bulk), 71.5 (Pt-Re interface) and 72.0 (Pt-Re alloy). [193–195] Surface Pd $3d_{5/2}$ and Pt $4f_{7/2}$ peak positions are verified experimentally by CO titrations on various film compositions, shown later in Fig. 6.8. For figures where peaks are fitted, a diagram showing the approximate levels of the relative species is also shown. These are not to scale, but show the way the distribution of the metals may change on the Re{0001} with annealing of different compositions.

The spectra for the first film is shown in Fig. 6.2, which is after deposition of only palladium, to approximately 3 ML total. The Pt 4f region shows the background in this region for each photon energy, as no platinum has yet been added to the rhenium. The palladium peaks are sharp and for all three used photon energies, with Pd 3d$_{5/2}$ consistently appearing with a binding energy of 335.5 eV. There is a relative difference of approx. 0.1-0.2 eV between the peak position at 405 eV photon energy and the other two higher photon energies. This is likely to be due to a surface core level shift of the first palladium layer, which is typically around 0.3 eV. [193]

After 3ML Pd had been studied, approximately 1 monolayer of platinum was deposited onto the crystal. This is shown as ”3ML Pd + 1ML Pt”. XPS spectra for this are shown in Fig. 6.3. The Pd 3d spectra appear unchanged from their appearance in ”3ML Pd”. The Pt 4f$_{7/2}$ peak appears initially at 71.0-71.1 eV, with a slightly higher binding energy for lower photon energy spectra. This combination of metals is then annealed at 500 °C in oxygen (5x10^{-8} mbar) for 10 minutes, to give ”3ML Pd + 1ML Pt Annealed”. Whilst the Pd 3d spectra taken at 405 eV and 900 eV are unchanged, there is a positive shift for the 650 eV spectrum, to around 335.8 eV (an increase of approx. 0.3 eV compared to pre-annealing). The platinum peaks show more significant shifts. For 405 eV and 650 eV this is 0.5 eV, whilst there is a smaller shift of 0.3 eV for the 900 eV measurement. In all cases this is a shift to higher binding energy with annealing. For this combination, it is expected that Pt would prefer to move to the bulk of a Pd-Pt alloy. This shift could be representative of a migration, with only the medium energy/depth Pd 3d signal affected.

An additional 2ML of platinum was added, to produce ”3ML Pd + 3ML Pt”, as shown in Fig. 6.4. There were 2 annealing steps after this addition. Pd 3d spectra show minimal changes throughout the addition of more Pt, and the following annealing stages. The addition of 2 additional monolayers of platinum creates initially 2 distinct Pt 4f$_{7/2}$ peaks, at 70.9 and 71.6 eV respectively in the case of the 650 eV spectrum (2 species are present in all, with slightly different positions). This lower binding energy species is the newly deposited Pt, as it resembles the platinum observed for ”3ML Pd + 1ML Pt”, whilst the higher binding energy peak is largely consistent with that composition post-annealing. The initial annealing converts the majority of the platinum to the higher binding energy species, indicating a similar process to that which happened for the 1ML Pt previously added, which is to say it migrates to the bulk of the Pd. There is broadness to the peak after the first annealing that is

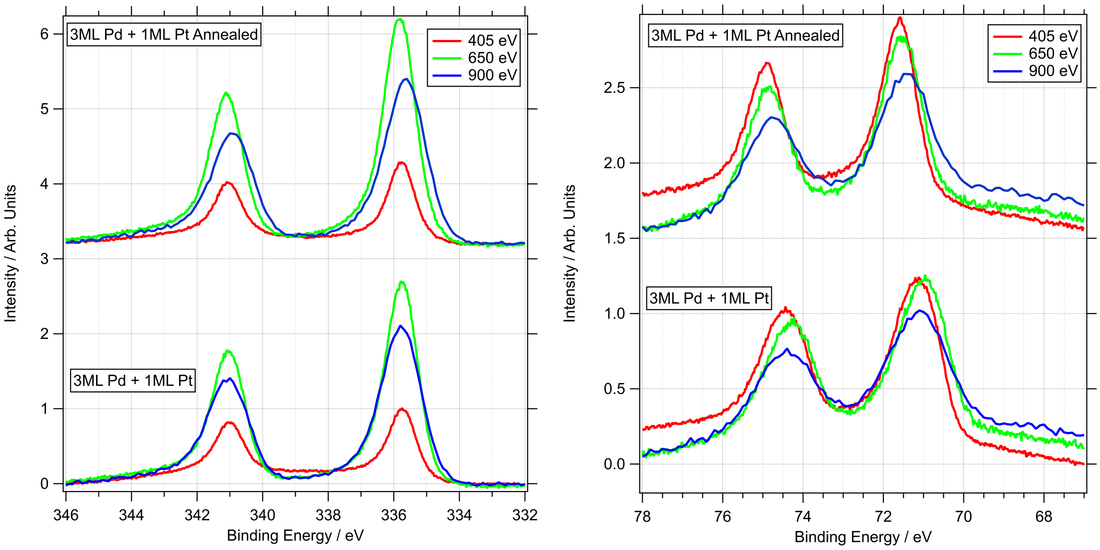

(a) Pd 3d

(b) Pt 4f

Figure 6.3: Pd 3d and Pt 4f XPS spectra for "3ML Pd + 1ML Pt" thin film on Re single crystal, before and after annealing, recorded at 405, 650 and 900 eV photon energies. The binding energy of all spectra has been corrected using the measured Fermi energy level.

largely removed after the second, indicating there is additional migration of some remaining surface platinum during this second annealing step. Fitted low kinetic energy spectra are shown in Figs. 6.4c and 6.4d for Pd 3d and Pt 4f respectively. The initial Pd spectrum - the result of 2ML Pt addition to a previously annealed 3ML Pd + 1ML Pt mixture - shows Pd to be primarily (75%) in Pd-Re interface sites, with smaller amounts assigned to bulk-like Pd (20%) and surface-like Pd (5%). Platinum is also primarily in a Pt-Re interface (74%) type state after addition, with small amounts of bulk-like (15%) and surface-like Pt (11%) also present. That Pt is immediately present at the interface after addition indicates significant amounts of the Re{0001} were not covered with Pd before the addition of 2Pt. It is therefore likely that the Pd and Pt previously deposited and annealed (at least partly) take the form of islands on the crystal surface. This can also explain the high amount of interface-like sites, as the first few layers can have an appearance characteristic of the crystal interface. Upon annealing, there is an increase in intensity for the bulk-type Pd (40%), with a corresponding decrease in the Pd-Re interface (48%). For platinum, the interface species now accounts of 97% of the intensity, whilst the remaining 3% is present in a surface-like state. This shows that, upon annealing to 700 °C, the platinum is preferentially migrating to the Re{0001}, whilst the palladium in part sits on top of this, hence the increase in bulk Pd observed.

Despite this, a significant amount of Pd is still present in interface-like form. From this data, it is unclear whether the interface is covered with a series of islands/crystallites of Pd and Pt individually, with bimetallic islands, or a mixture of the two.

After the completion of measurements on "3ML Pd + 3ML Pt", the crystal was flash heated to 1200 °C, to remove the palladium, and a small amount of the platinum. This gave a platinum only base to work from, which was approximated to "2ML Pt". This is shown in Fig. 6.5. To this, 2ML of Pd was added, then annealed. The palladium which is added to the platinum initially appears at a lower binding energy (335.1-335.3 eV, depending on photon energy), as compared to the palladium which was deposited onto rhenium (335.5 eV). After annealing, the Pd 3d peaks are largely unchanged, with only a small shift observed in the 900 eV measurement, of approx. -0.2 eV.

The platinum spectra once again appear as two peaks. The "2ML Pt" refers to the sample where a small amount of Pt was present post-flashing, and to which some additional platinum has been deposited, giving an approximate total of 2 monolayers. Despite there being no palladium present initially, this split platinum peak highly resembles the one seen for Pt addition in Fig. 6.4b, showing a segregation between the existing and newly deposited platinum. It is possible that this is the result of alloying between the platinum and rhenium as a result of the high temperature flash. For fitted data, a peak corresponding to the Pt $4f_{7/2}$ in the Pt-Re alloy is fitted at 701.8-702 eV binding energy. The platinum spectra are largely consistent before and after Pd addition. Once this has been annealed, there is again a shift towards the higher binding energy peak (as measured at 405 and 650 eV), though the lower binding energy peak still has a significant presence. This may be indicative that the palladium and platinum were not well alloyed during the annealing process, leaving more discrete areas of Pt than in the other mixed films. With this similarity in the raw spectra, the low energy spectra were fitted to see if subtle changes could be observed. These fitted spectra are shown in Fig. 6.5c and 6.5d for Pd and Pt respectively. The Pd 3d spectra pre- and post-annealing show differences of <5% for each peak position, with a slight shift towards more bulk-like Pd and a small loss in Pd-Re interface type sites. The Pt 4f also show only small changes of <8%, with a decrease in bulk-Pt and corresponding increases to Pt-Re interface and alloy type sites. This indicates that upon addition of Pd and subsequent annealing, there is only small amounts of restructuring. When platinum was added and

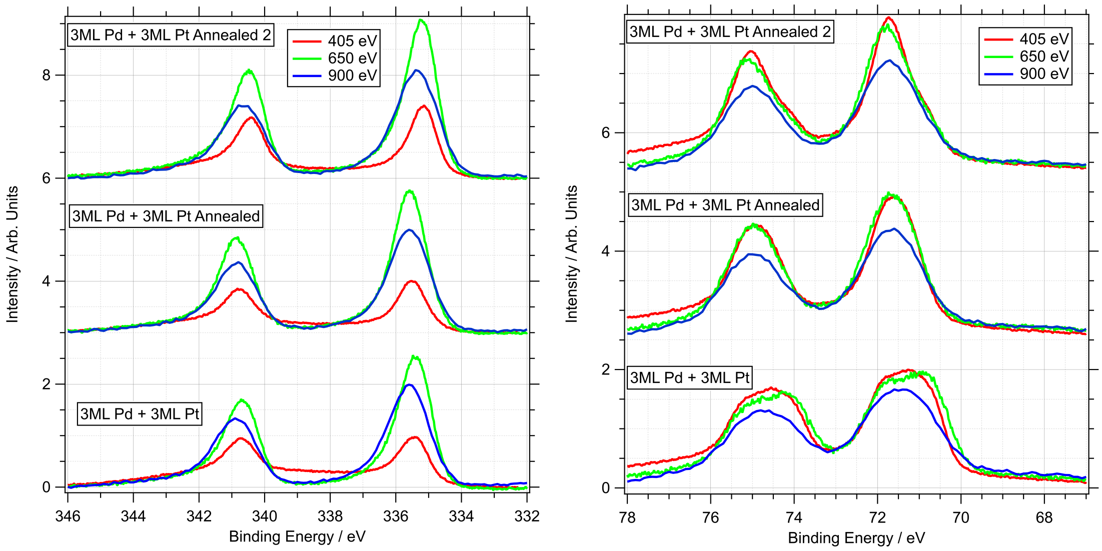

(a) Pd 3d (b) Pt 4f

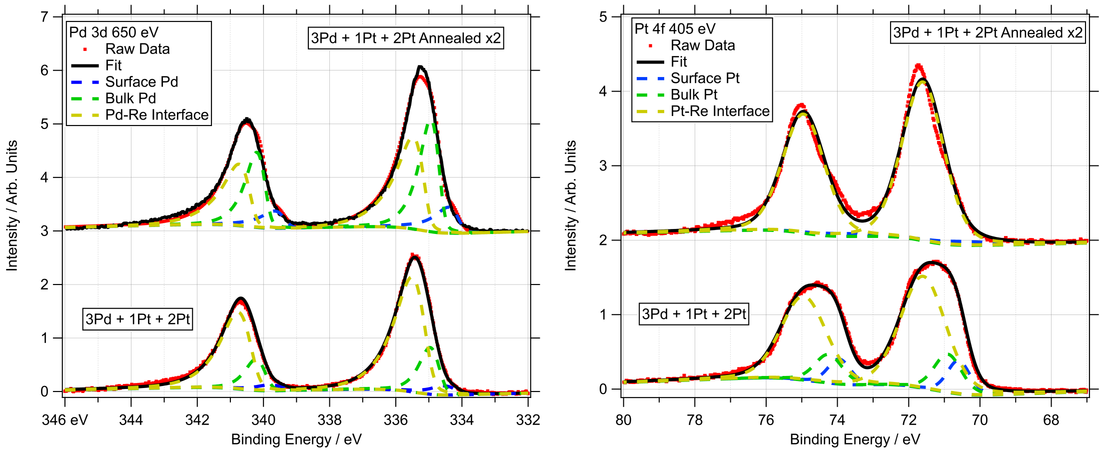

(c) Pd 3d 650 eV Fitted (d) Pt 4f 405 eV Fitted

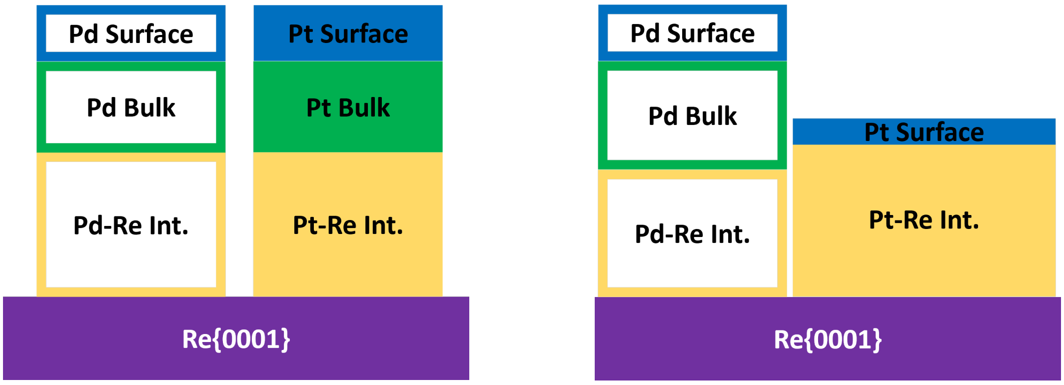

(e) 3ML Pd + 3ML Pt (f) 3ML Pd + 3ML Pt Annealed

Figure 6.4: Pd 3d and Pt 4f XPS spectra for "3ML Pd + 3ML Pt" thin film on Re single crystal, before and after annealing, recorded at 405, 650 and 900 eV photon energies. The binding energy of all spectra has been corrected using the measured Fermi energy level. Graphics are representative and not to scale.

annealed a greater change was observed, with platinum tending towards the interface with rhenium, with palladium moving away from this interface simultaneously. This shows that a similar structure should eventually be obtained irrelevant of deposition order, with platinum always tending towards the interface at the expense of palladium.

A further 2ML of Pt was then added to this annealed combination of Pd and Pt, which is shown in Fig. 6.6. The further Pt addition leads to a broad Pt peak, which may still be the combination of ”new” and ”old” platinum peaks. The annealing unusually seems to further segregate this combination, as the peaks split slightly further, which could indicate poor mixing of the metals during the annealing process. Fitted data for the low energy XPS for the 2ML Pd + 4ML Pt composition is shown are shown in Figs. 6.6c and 6.6d for Pd 3d and Pt 4f respectively. Upon deposition, significant amounts of platinum are already present in the Pt-Re interface sites (56%). Much of the remainder is present as bulk-like Pt (36%). Palladium is also present as a similar mix of interface (60%) and bulk (35%) type species. Upon annealing, palladium moves partially further towards the bulk (49%). Platinum has a decrease in interface sites (to 28%), but an increase in the higher binding energy alloy type sites (up to 25%) to compensate this. The bulk-type Pt is still significant, as 42%. This shows a case of platinum not significantly migrating to the surface upon annealing, but of the type of Pt-Re interactions changing, with more Pt appearing to alloy to the Re. The interface remaining mixed despite a much higher amount of platinum (4ML vs 2ML Pd) is consistent with our previous experiments, which consistently show 40-50% of the palladium signal post-annealing to be in interface-like sites. Platinum shows a higher tendency to have the bulk-type Pt form when the Pt-Re alloy is also present. This may indicate a preference for Pt to form thicker layers on top of this alloy interface, as opposed to on the bare Re{0001}.

The final batch of experiments for the thin films is shown in Fig. 6.7. This consisted of flashing the sample to 1200 °C again, leaving only platinum deposits, then depositing palladium for 30 minutes. Based on the calibrations, this was expected to be 5-6ML of palladium, in addition to the 4ML of platinum still present. Due to time limitations some spectra were not recorded at all energies for the flashed and freshly Pd deposited sample. All spectra were recorded for the final, annealed, condition. After the flash, it is clear no palladium is present on the sample, whilst the platinum is now more clearly split into 2 distinct peaks. As there is no palladium for it to alloy with, this could be assigned as bulk

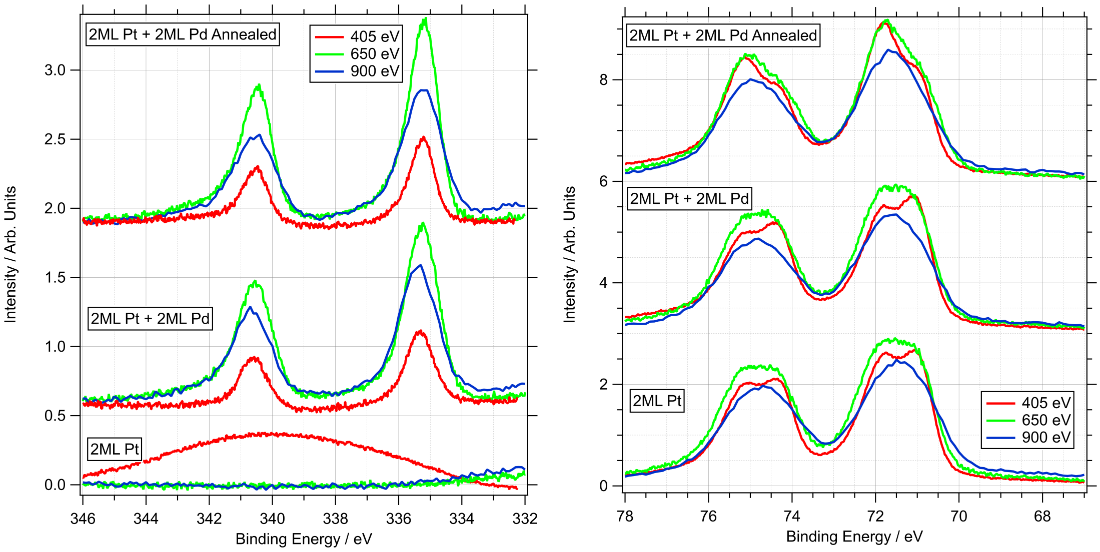

(a) Pd 3d

(b) Pt 4f

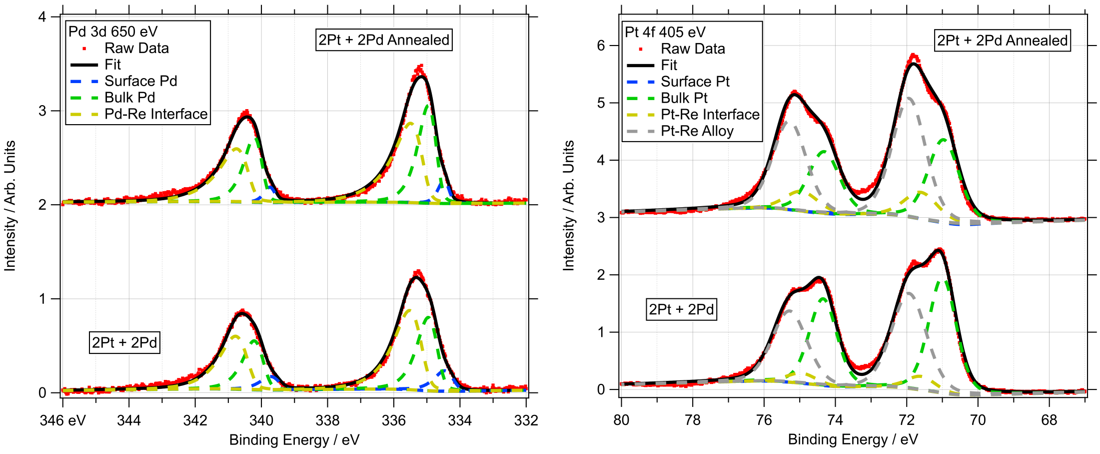

(c) Pd 3d 650 eV Fitted

(d) Pt 4f 405 eV Fitted

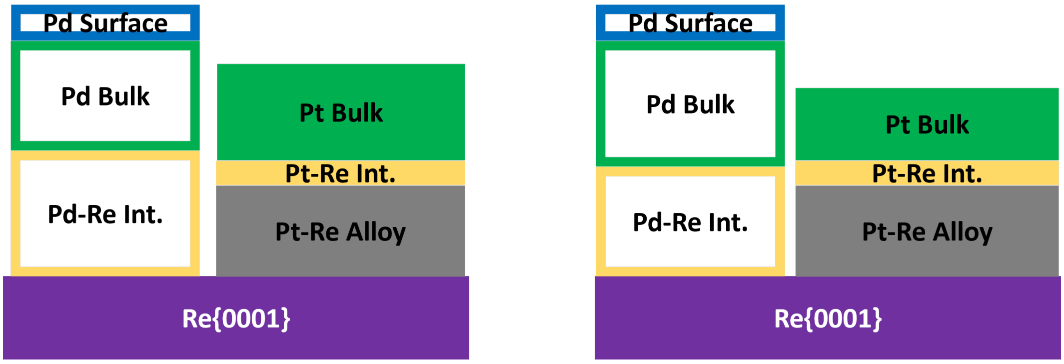

(e) 2ML Pd + 2ML Pt

(f) 2ML Pd + 2ML Pt Annealed

Figure 6.5: Pd 3d and Pt 4f XPS spectra for ”2ML Pt” thin film on Re single crystal, before and after addition of ”2ML Pd”, recorded at 405, 650 and 900 eV photon energies. The binding energy of all spectra has been corrected using the measured Fermi energy level. The Pd 3d spectra recorded at 405 eV for ”2ML Pt + 2ML Pd” and ”2ML Pt + 2ML Pd Annealed” have both had the background recorded in the ”2ML Pt” scan removed for clarity.

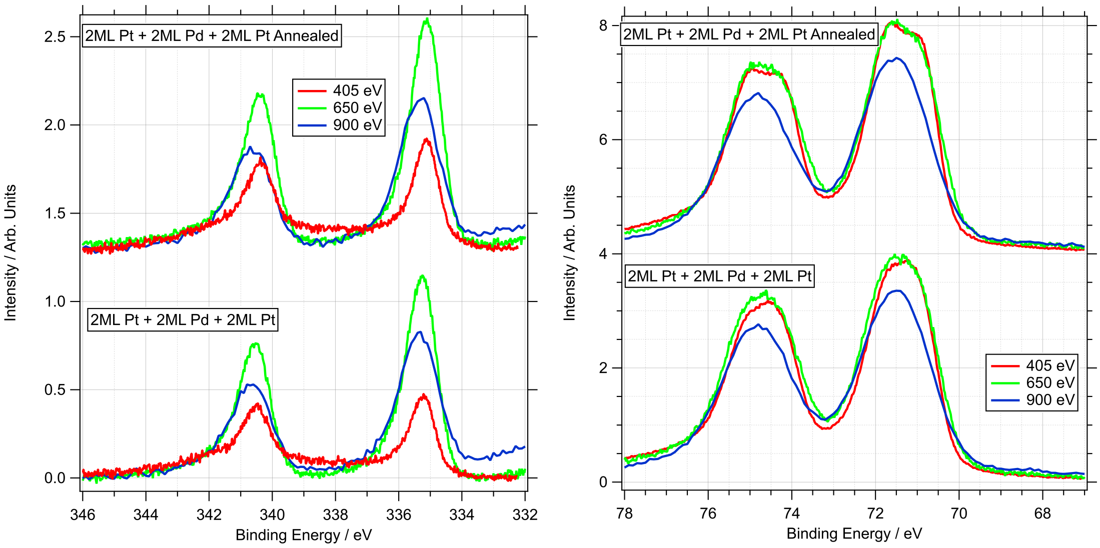

(a) Pd 3d

(b) Pt 4f

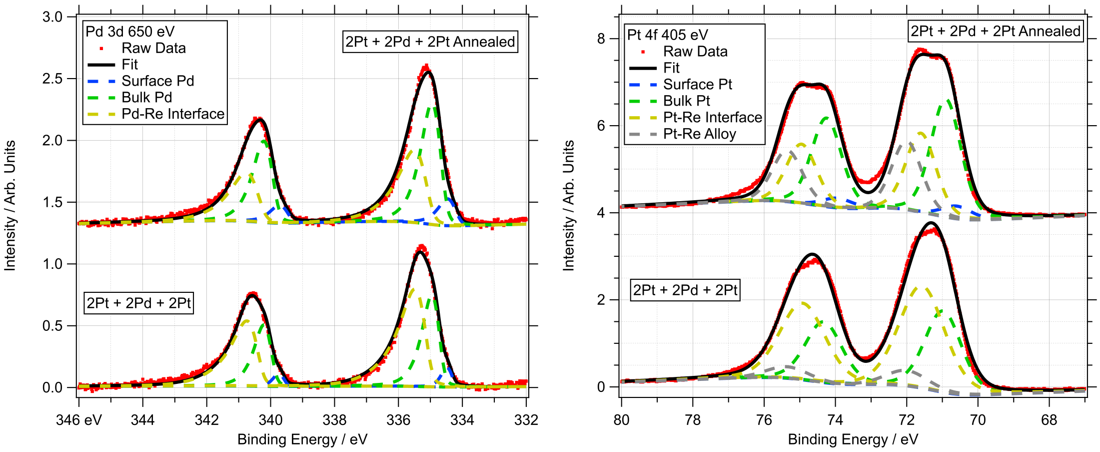

(c) Pd 3d 650 eV Fitted

(d) Pt 4f 405 eV Fitted

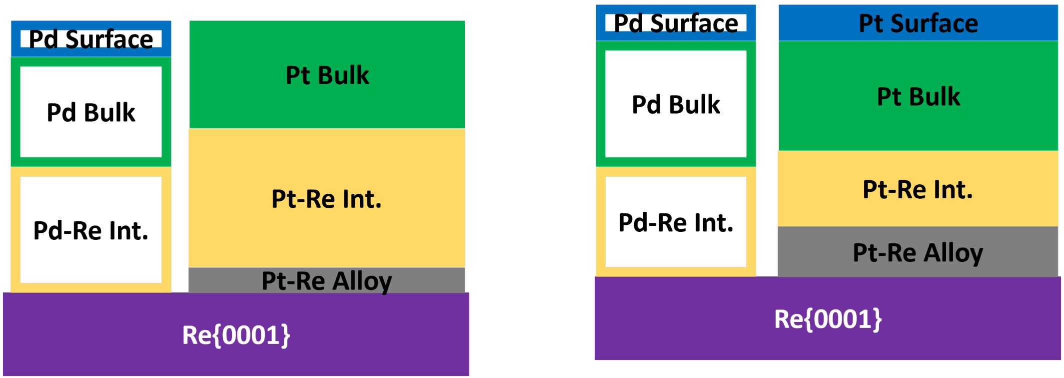

(e) 2ML Pt + 2ML Pd + 2ML Pt

(f) 2ML Pt + 2ML Pd + 2ML Pt Annealed

Figure 6.6: Pd 3d and Pt 4f XPS spectra for "2ML Pt + 2ML Pd + 2ML Pt" thin film on Re single crystal, before and after annealing, recorded at 405, 650 and 900 eV photon energies. The binding energy of all spectra has been corrected using the measured Fermi energy level. The Pd 3d spectra recorded at 405 eV for "2ML Pt + 2ML Pd + 2ML Pt" and "2ML Pt + 2ML Pd + 2ML Pt Annealed" have both had the background recorded in the "2ML Pt" scan removed for clarity.

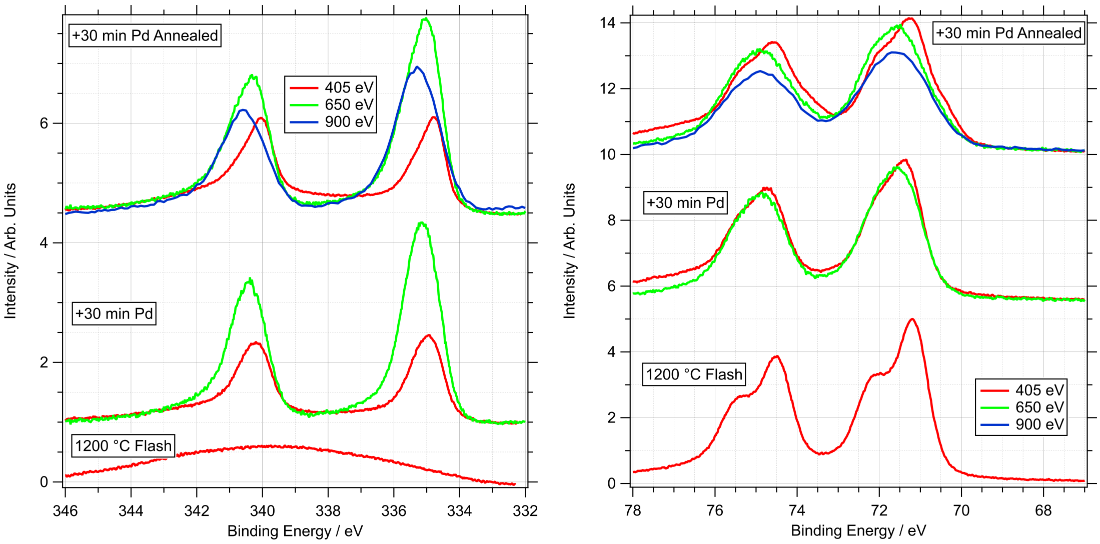

(a) Pd 3d

(b) Pt 4f

Figure 6.7: Pd 3d and Pt 4f XPS spectra for Re single crystal, after high temperature flash, Pd deposition and annealing, recorded at 405, 650 and 900 eV photon energies. The binding energy of all spectra has been corrected using the measured Fermi energy level.

and surface species.

Once palladium is deposited, this platinum splitting is less clear, though there are still clearly 2 distinct peaks. Palladium is present as a single species, with the Pd $3d_{5/2}$ peak appearing around 335.1 eV. After this has been annealed, the platinum spectra become less clear. As measured at 405 eV photon energy, it looks like there may be a third, lower binding energy species, which is not clearly present at other energies, indicating this may be a surface platinum. Whilst annealing would be expected to migrate platinum to the bulk, it is possible that some has migrated to the surface. At 650 eV, the more typical split peak structure is visible. Palladium as measured at 405 and 650 eV is consistent with itself pre- and post-annealing. The 900 eV measurement shows a relative shift, with the main peak around 335.4 eV.

With multiple film compositions, carbon monoxide was dosed to study the surface sites. The results of this are shown in Fig. 6.8. For both metals in both film compositions, notable changes are seen, as shown most clearly in the difference spectra on each plot. Figs. 6.8a and 6.8c show the Pd 3d spectra for 3Pd + 3Pt and 2 Pt + 2 Pd + 2Pt respectively. In both cases, the difference spectra show a peak at around 334.6-334.8 eV. As this is lost when CO is does, this is deemed to be the surface palladium peak. Figs. 6.8b and 6.8d show this data for Pt 4f. As with palladium, the difference spectra show the presence of surface platinum, with a peak position of 70.7-71.0 eV. As these values are consistent with previously reported Pd 3d and Pt 4f surface peak positions, we are confident this does represent surface sites for each metal. [193] All of these measurements were performed with low kinetic energy (315-335 eV), ensuring surface sensitivity with an inelastic mean free path of approximately 6 $\AA$. The CO dosing experiments show that for 2 different bimetallic films, both palladium and platinum are present at the surface. Whilst Pt is expected to prefer to segregate into the bulk of Pd, the high Pt : Pd ratio and low level heating (700 °C) are reasons for Pt to still be present at the surface. [87] With the small amounts of metal deposited, it is possible that even the annealed forms may largely feature islands of individual metals. In this case, platinum would remain at the surface due to an inability to move into the palladium bulk.

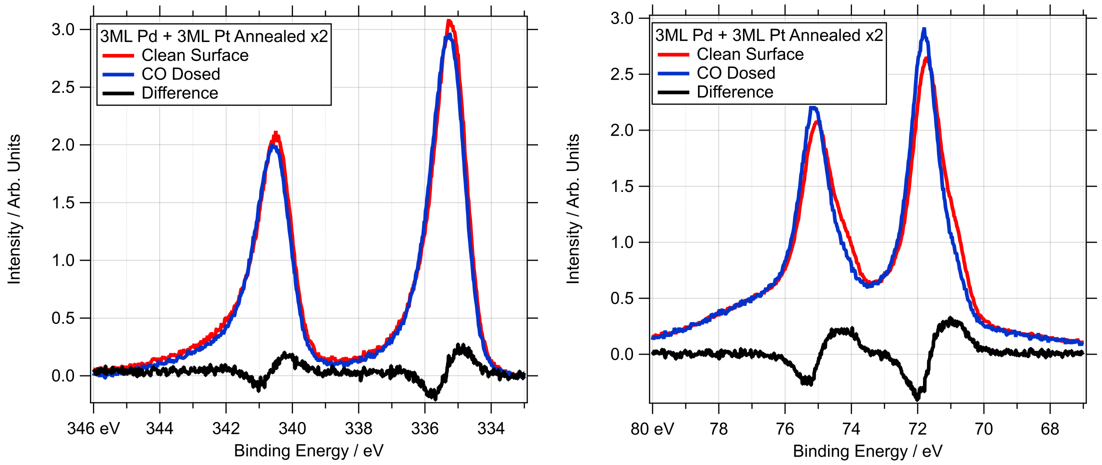

(a) 3Pd + 3Pt Annealed, Pd 3d

(b) 3Pd + 3Pt Annealed, Pt 4f

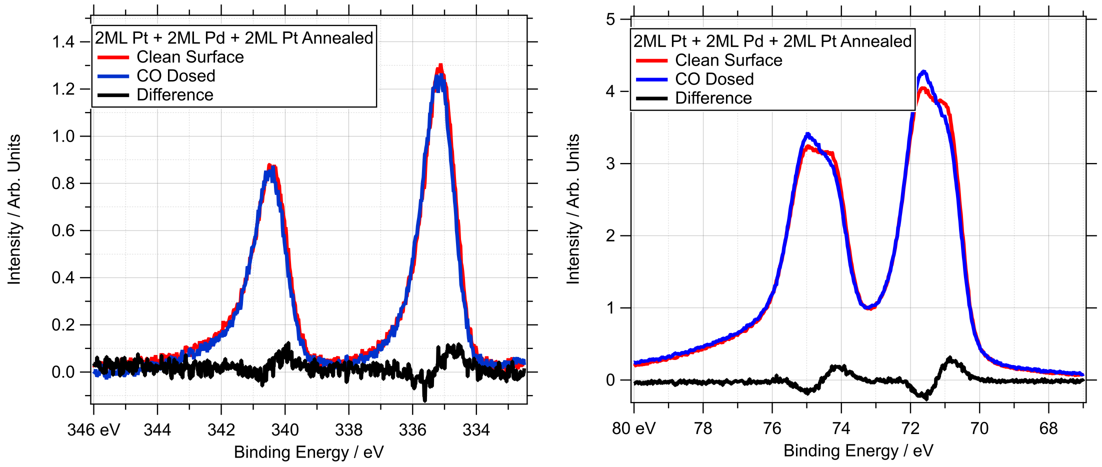

(c) 2Pd + 4Pt Annealed, Pd 3d

(d) 2Pd + 4Pt Annealed, Pt 4f

Figure 6.8: Pd 3d and Pt 4f XPS spectra for bimetallic films on a Re{0001} single crystal, after various stages of Pt addition and annealing, recorded at 405 eV and 650 eV photon energies for platinum and palladium respectively. This gives photon energies of approx. 334 eV for Pt $4f_{7/2}$ and 315 eV for Pd $3d_{5/2}$, ensuring the sample is being studied at a consistent depth for both metals. For each sub-figure, a difference spectrum is shown, which is produced from subtracting the "CO Dosed" spectrum from the "Clean Surface" spectrum. The binding energy of all spectra has been corrected using the measured Fermi energy level.

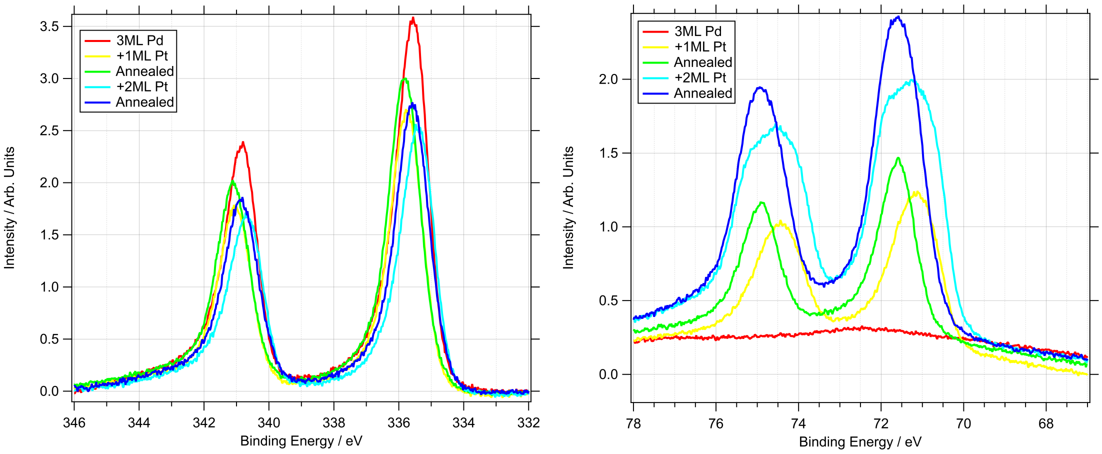

(a) Pd 3d (b) Pt 4f

Figure 6.9: Pd 3d and Pt 4f XPS spectra for Re single crystal, after various stages of Pt addition and annealing, recorded at 405 eV and 650 eV photon energies for platinum and palladium respectively, giving similar kinetic energies for both main peaks. The binding energy of all spectra has been corrected using the measured Fermi energy level.

6.2.2 Bimetallic Films Summary

Whilst the thin films are a far reach from the nature of the nanoparticle powder catalysts, they have still provided an interesting insight. This has shown that the addition order and annealing process can significantly affect the level of mixing and, as a result, the nature of the palladium and platinum. Platinum was shown to be more sensitive, with more clear shifts, and a greater segregation between ”surface” and ”bulk” states. With the nature of the nanoparticles generally being mixed but disordered, this suggests that the states of palladium and platinum observed will be highly dependant on the photon energy used, and so the depth probed. However, the low loading of the nanoparticles, and resulting long experiment time, means that using multiple photon energies is impractical for powder catalysts.

Some comparisons of Pd 3d and Pt 4f spectra after different parts of the preparation are shown in Fig. 6.9. Each annealing stage after Pt addition results in a minor positive shift for palladium. Platinum has a larger positive shift between addition and annealing. The second deposition shows a combination of both the ”surface” and ”combined” species. In both cases, the Pt peak post-annealing is the same, just varied in intensity due to total platinum presence.

An additional set of comparisons are shown in Fig. 6.10. No change is seen in Pd 3d with annealing post-Pd addition and annealing, other than a small increase in intensity with

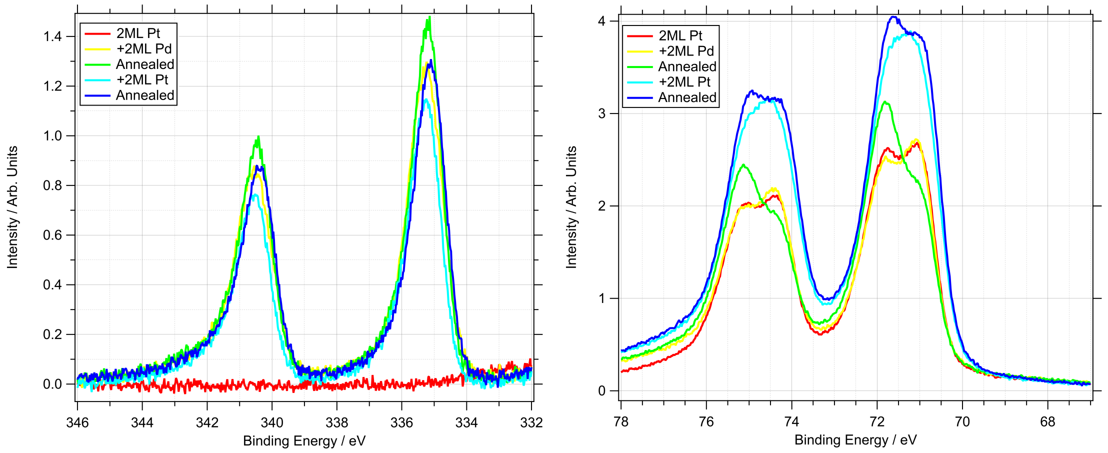

(a) Pd 3d (b) Pt 4f

Figure 6.10: Pd 3d and Pt 4f XPS spectra for Re single crystal, after various stages of Pt and Pd addition and annealing, recorded at 405 eV and 650 eV photon energies for platinum and palladium respectively, giving similar kinetic energies for both main peaks. The binding energy of all spectra has been corrected using the measured Fermi energy level.

annealing. There is a minimal change in platinum with this Pd addition, but a significant change after the annealing, with a shift in relative peak ratio towards the higher binding energy peak. There is also minimal change after Pt addition, with the exception of intensity decreasing due to the increased attenuation of the platinum added. When this mixture is annealed, there is a slight shift to lower binding energy for palladium, and an increase in intensity. The platinum peak splits significantly after this annealing, though the overall width is unchanged, indicating the same species are still present.

Overall, the addition of platinum to palladium looks to cause minimal change to the palladium, with the exception of the predicted intensity changes. More of an effect is seen in platinum, which seems to exist as different species when segregated and when combined with palladium.

6.3 Palladium Foil TP-AP-XPS

Palladium foils were studied under a range of methane oxidation conditions, mirroring those used for the powder catalysts. The foil was studied in oxygen (2.40 mbar), methane and oxygen (”stoichiometric” 1:2, 0.33 mbar and ”oxygen rich” 1:120, 2.39 mbar), and methane, oxygen and water (”stoic wet low” 1:2:2, 0.55 mbar, ”stoic wet” 1:2:100, 5.18 mbar, and ”oxygen rich wet” 1:120:100, 4.41 mbar). Moving the sample during the measurements allowed for the compensation of thermal expansion due to heating, which ensured a roughly consistent peak intensity across the full temperature range. The heating rate was set to 3.5 °C/minute such that a set of spectra (Pd 3d + O 1s) were recorded approximately every 5 °C. This kept the individual spectrum quality high enough, provided enough data points to monitor changes in the palladium and oxygen spectra, whilst also keeping a high enough ramp rate to be relevant. In each TP-XPS figure there are 3 components. In the top left is the 2-d TP-XPS image plot, showing the peak intensities across the relevant window for the full temperature range of the experiment. In the top right is a line scan plot, focusing on the Pd(0) or Pt(0) and Pd(II) or Pt(II). These take a line plot of 0.3 eV width at the relevant positions (approx. 335.0 eV for Pd(0), 336.7 eV for Pd(II), 71.0 eV for Pt(0) and 72.5 eV for Pt(II). This is used to show the changing intensity over heating more clearly, with the temperature axis matching that of the image plot. Below the image plot is a graph featuring a number of XPS spectra taken from specific temperatures, as shown by the grey dashed lines on the image plots. These are a sum of the spectra within 10 °C of this point (approx. 3 spectra), to increase the signal to noise ratio of the data. This is presented to clarify the nature of the spectrum at specific points of interest, mainly the beginning and end of the ramp, along with any points of oxidation state change.

The data presented in Figs. 6.11, 6.12 and 6.13 feature 2-d image plots of TP-XPS data for the Pd 3d region (top left), along with line scans of the peak intensities for Pd $3d_{5/2}$ for Pd(0) and Pd(II) peak positions (top right), and XPS spectra taken at a range of temperatures to highlight key points within the temperature ramp (bottom).

Measurements taken in stoichiometric conditions are shown in Fig. 6.11. In the dry condition, shown in Fig. 6.11a, the main transition from Pd(0) to Pd(II) occurs between 320-370 °C. The XPS spectra show that by 415 °C the Pd is nearly completely oxidised to Pd(II). When a small amount of water is added, there is an increase in the temperature of this transition. Fig. 6.11b shows the stoichiometric low water condition, where the palladium oxidation primarily occurs between 350 and 400 °C. By 490 °C there is minimal signal for Pd(0). When further water is added, giving the stoichiometric very wet condition, this transition moves to a higher temperature still. This is shown in Fig. 6.11c. Pd(0) is still the primary state up to 420 °C, with significant amounts of Pd(II) present from 450 °C. The XPS spectrum of the sample at 490 °C is shown, and shows that there is still a significant presence of Pd(0) at this highest temperature. The experiment was not pushed to higher temperatures to keep the range relevant to the methane oxidation catalysts, which even in wet conditions will reach 100% conversion below 450 °C. Overall the stoichiometric conditions show that the presence of water inhibits the oxidation of palladium, with an increased water presence causing greater inhibition.

TP-XPS data recorded under oxygen rich conditions are shown in Fig. 6.12. For the dry oxygen rich condition, shown in Fig. 6.12a, the Pd is fully oxidised by 410 °C. The transition occurs at a lower temperature than for the dry stoichiometric condition, with a crossover in intensity of the peaks around 325 °C, as compared to 350 °C. This is an expected result, given the significantly higher oxygen partial pressure (2.4 mbar compared to 0.2 mbar). When water is present, the transition again is inhibited, as was observed for stoichiometric conditions. This is shown in Fig. 6.12b. The intensity crossover here occurs at around 370 °C, 45 °C higher than in dry conditions. This transition is again at a lower temperature than the equivalent stoichiometric condition, by approximately 60 °C. This shows that the increased oxygen presence leads to lower temperature oxidation of palladium in both dry and wet conditions, with a greater difference observed in the presence of water.

In addition to the methane oxidation conditions, the foil was also studied in the presence of oxygen without methane, at the same pressure as used for the oxygen rich experiments (2.4 mbar). This is shown in Fig. 6.12c. The intensity crossover here occurs around 330 °C, very close to the transition for the oxygen rich dry condition (325 °C). However, when measured at a much higher temperature, 415 °C, there is still significant presence of reduced Pd, which is not observed when methane is present (see 410 °C spectra in Fig. 6.12a). This would indicate that palladium is more likely to oxidise at lower temperatures in a methane-oxygen mixture, as compared to an oxygen only condition.

The behaviour of the palladium under heating and cooling is shown in Fig. 6.13. Following

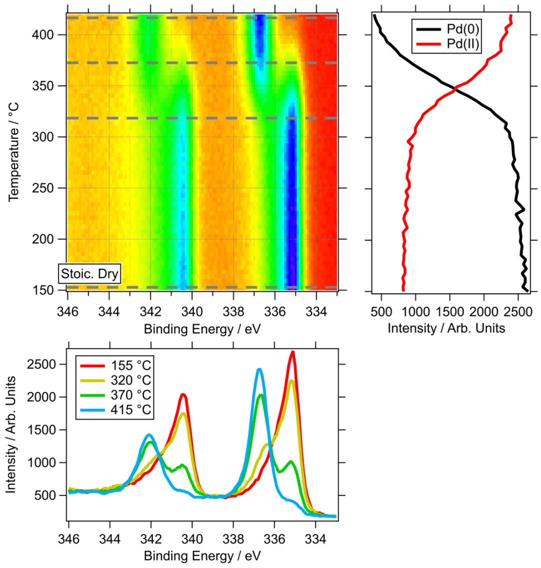

(a) Stoichiometric Dry Conditions

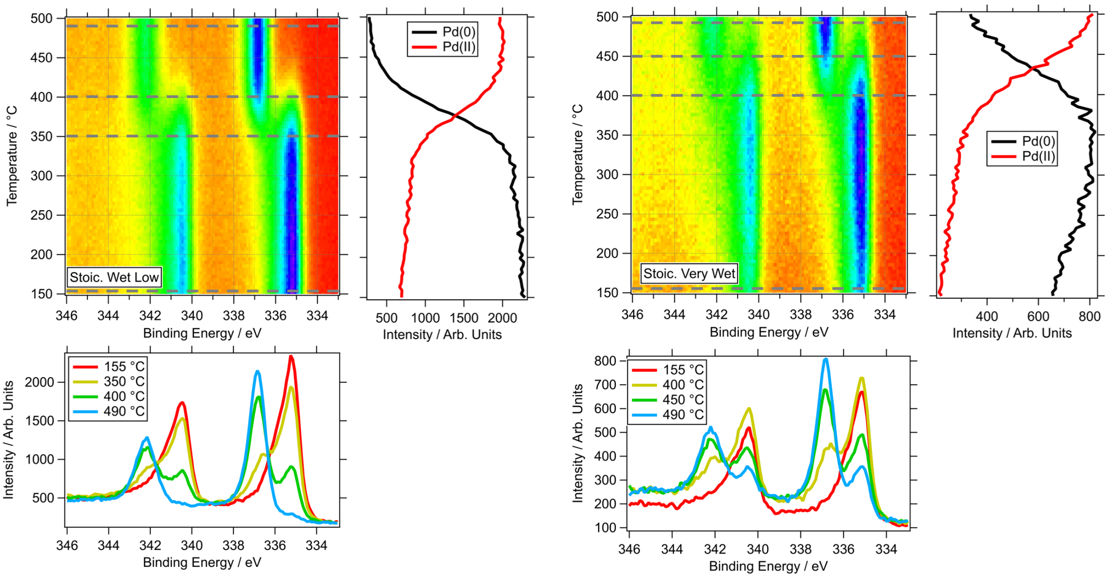

(b) Stoichiometric Low Wet Conditions

(c) Stoichiometric Very Wet Conditions

Figure 6.11: Pd 3d region TP-XPS data for Pd foil under stoichiometric dry and wet conditions. For each condition, 2d TP-XPS plots (top left), line scans on the metallic and oxide peak position (top right) and spectra from relevant temperatures (bottom) are shown. Each of the spectra shown in the bottom section are the combination of data over 10 °C, from the temperatures marked with grey dashed lines in the TP-XPS plots. Heating rate was 3.5 °C/min. Photon energy for all XPS was 750 eV.

the stoichiometric dry experiment, the sample was cooled in this mixture, shown in Fig. 6.13a. The palladium remains fully oxidised throughout this cooling, down to 160 °C. The intensity decreases during cooling, as the sample was not moved to compensate for thermal expansion in this experiment. To reduce the palladium again, it was necessary to heat in vacuum. The result of this heating is shown in Fig. 6.13b, where a sharp transition from Pd(II) to Pd(0) can be seen between 480 °C and 520 °C. By 540 °C no Pd(II) remains. The sample is then cooled to 150 °C in vacuum before the next experiment.

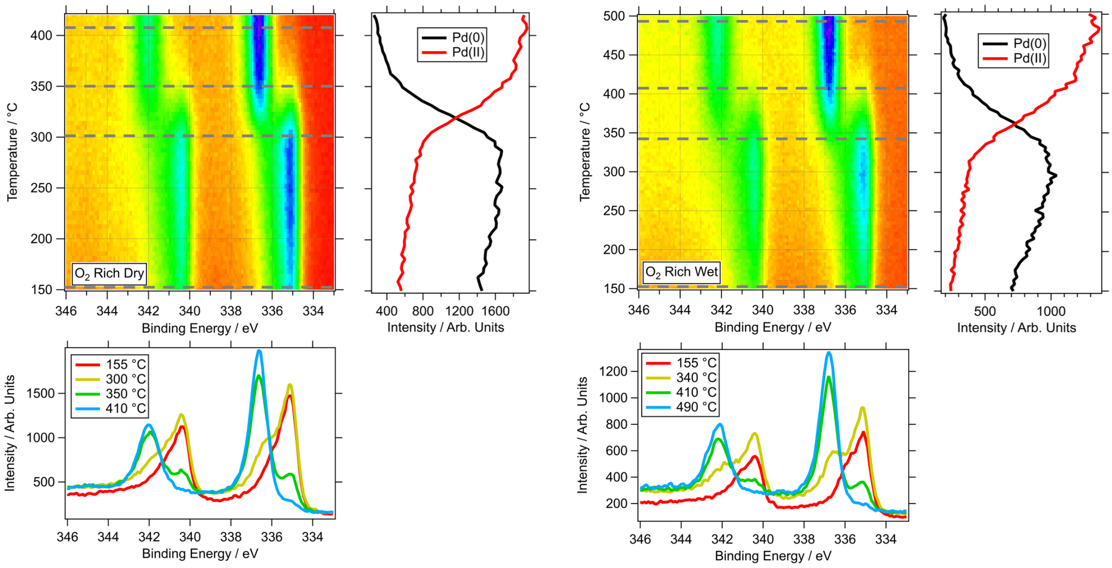

(a) Oxygen Rich Dry Conditions

(b) Oxygen Rich Wet Conditions

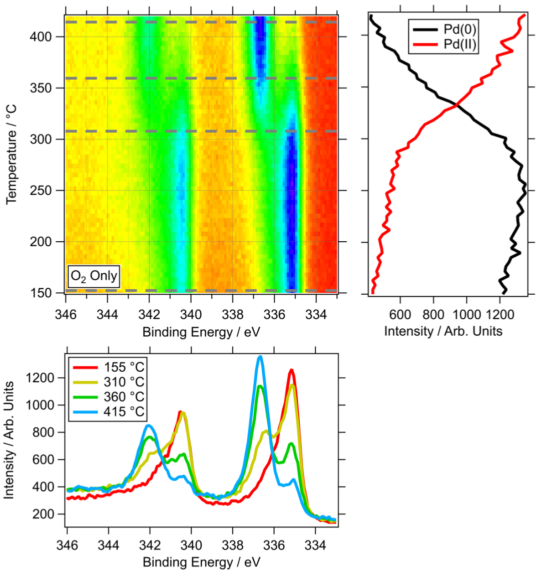

(c) Oxygen Only Conditions

Figure 6.12: Pd 3d region TP-XPS data for Pd foil under oxygen rich dry and wet conditions, and under oxygen only. For each condition, 2d TP-XPS plots (top left), line scans on the metallic and oxide peak position (top right) and spectra from relevant temperatures (bottom) are shown. Each of the spectra shown in the bottom section are the combination of data over 10 °C, from the temperatures marked with grey dashed lines in the TP-XPS plots. Heating rate was 3.5 °C/min. Photon energy for all XPS was 750 eV.

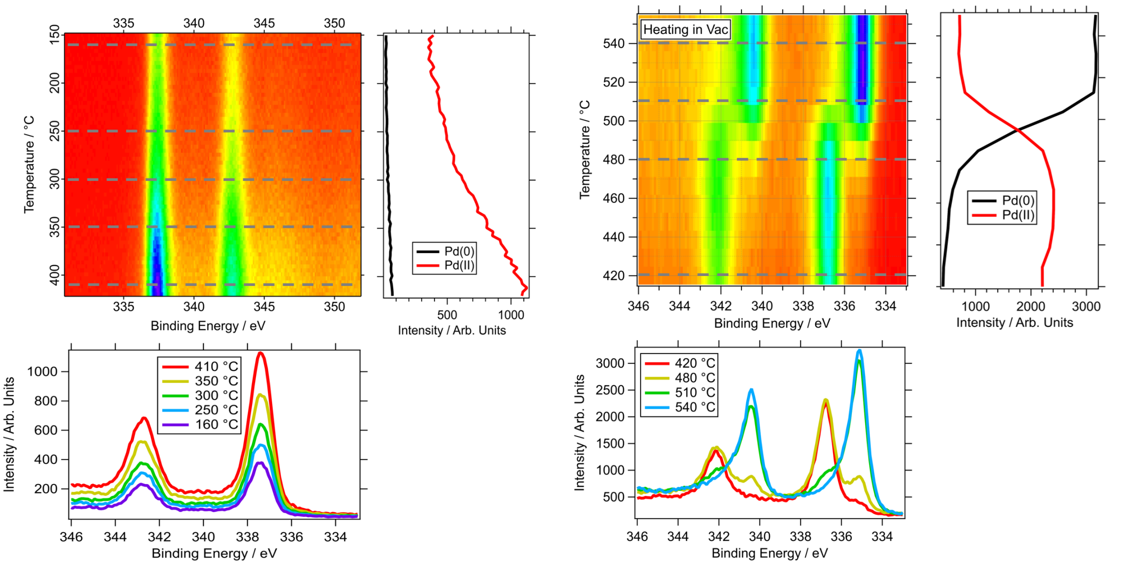

(a) Sample Cooling in stoichiometric dry

(b) Sample Heating in vaccum

Figure 6.13: Pd 3d region TP-XPS data for Pd foil during cooling and heating in stoichiometric dry conditions and vacuum respectively. For each condition, 2d TP-XPS plots (top left), line scans on the metallic and oxide peak position (top right) and spectra from relevant temperatures (bottom) are shown. Each of the spectra shown in the bottom section are the combination of data over 10 °C, from the temperatures marked with grey dashed lines in the TP-XPS plots. For heating in vacuum, heating rate was 3.5 °C/min. Photon energy for all XPS was 750 eV.

6.4 Platinum Foil TP-AP-XPS

Platinum foil was also studied in a similar way to that described previously for palladium. Heating in dry stoichiometric conditions showed no change in oxidation state up to 520 °C (the maximum temperature used). This is shown in Fig. 6.14. The line scans and individual XPS spectra both shown minimal change in peak position, but do highlight the decreasing intensity as a result of incomplete thermal expansion compensation. This is a result of using the same compensation as was used for palladium. From high resolution XPS data extracted from this, with a main Pt $4f_{7/2}$ peak position around 71.4 eV, it is evident that the platinum is reduced throughout. As a result of this dry condition showing no change, and the higher interest in bimetallic compositions, no further experiments were done on platinum foils.

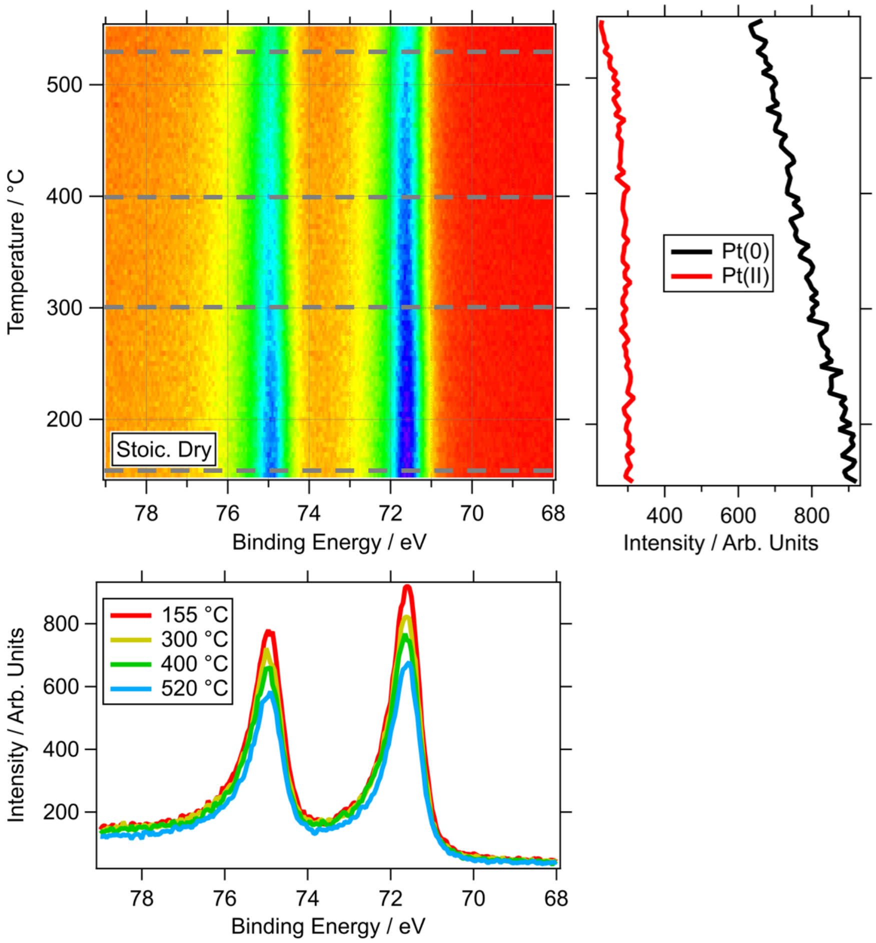

Figure 6.14: Pt 4f region TP-XPS data for Pt foil under stoichiometric dry conditions. For each region, 2d TP-XPS plots (top left), line scans on the metallic and oxide peak position (top right) and spectra from relevant temperatures (bottom) are shown. Each of the spectra shown in the bottom section are the combination of data over 10 °C, from the temperatures marked with grey dashed lines in the TP-XPS plots. Heating rate was 3.5 °C/min. Photon energy for all XPS was 750 eV.

6.5 Palladium-Platinum Foil TP-AP-XPS

Having observed significant variations in the oxidation behaviour of palladium under varied reaction conditions, we studied bimetallic foils, to understand the effects platinum could have on palladium oxidation. The work on powder bimetallic catalysts has shown significant palladium oxidation state changes under reaction conditions, and this work aimed to show whether these would be coupled to platinum changes in a bimetallic system.

For this work, we arranged for Pd88-Pt12 and Pd65-Pt35 alloy foils to be produced by Goodfellow. Each foil was 15x15 mm (each ±1 mm), with a thickness of 0.3 mm (±10%). These ratios are equivalent to the Pd:Pt atomic ratios in the 4.0Pd-1.0Pt and 2.5Pd-2.5Pt catalysts (these refer to weight percentage loading). For analysis, a piece of each sample measuring approx. 3x3 mm was used.

The hypothesis for this work was that, under a select condition, changing the Pd : Pt ratio should also change the onset of the palladium oxidation. With the results of the powder sample NAP-XPS, it was anticipated that a higher platinum loading may help to preserve Pd(0) to higher temperatures than for monometallic palladium. We also hoped to observe changes in Pt oxidation state, as this has been very difficult to study in the powder catalysts, and to relate these to the changes in palladium.

TP-XPS experiments performed on a Pd88-Pt12 foil are shown in Figs. 6.15 to 6.18. Fig. 6.15 shows the Pd88-Pt12 sample under stoichiometric dry conditions. The transition from Pd(0) to Pd(II), shown in Fig. 6.15a, occurs between 350-410 °C. The XPS spectrum recorded at 520 °C, however, shows a presence of Pd(0) still. When comparing this Pd88-Pt12 to the Pd only foil, the transition happens at a higher temperature, with a higher remaining presence of Pd(0) after further heating. The Pt 4f spectra, shown in Fig. 6.15b, show a transition at the same temperatures as seen for Pd. Unlike the palladium, the platinum does not oxidise as significantly. By the final spectrum taken at 520 °C, the Pt(0) and Pt(II) peaks are of similar intensity. This is shown in the line scans plot, where the Pt(0) decreases with minimal increase in the Pt(II). Considering the overall intensity, it looks likely that the platinum is migrating into the bulk of the foil at this stage, as previously suggested. [87]

Data for the Pd88-Pt12 foil under the two stoichiometric wet conditions are shown in Fig. 6.16. The stoichiometric low water condition is shown in Fig. 6.16a and 6.16b for Pd 3d and Pt 4f spectra respectively. The palladium is present primarily as Pd(0) throughout the

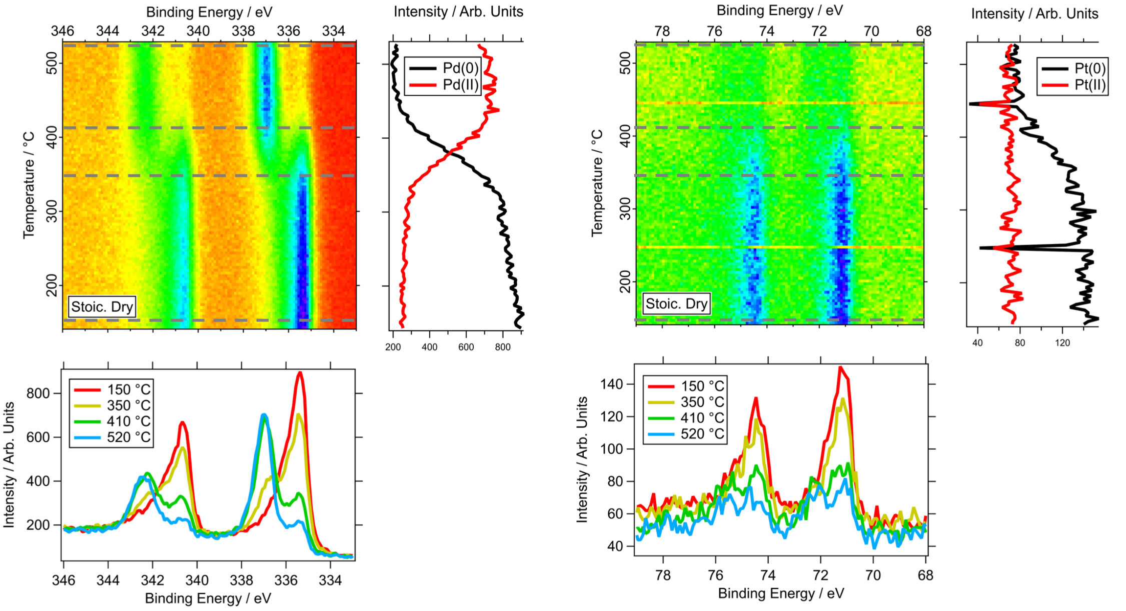

(a) Pd 3d, Stoichiometric dry

(b) Pt 4f, Stoichiometric dry

Figure 6.15: Pd 3d (left) and Pt 4d (right) region TP-XPS data for Pd88-Pt12 foil under stoichiometric dry conditions. For each region, 2d TP-XPS plots (top left), line scans on the metallic and oxide peak position (top right) and spectra from relevant temperatures (bottom) are shown. Each of the spectra shown in the bottom section are the combination of data over 10 °C, from the temperatures marked with grey dashed lines in the TP-XPS plots. Heating rate was 3.5 °C/min. Photon energy for all XPS was 750 eV.

heating ramp, up to 590 °C. In the measurement at 540 °C, shown in the XPS plot, there is a notable presence of Pt(II), but this is not present in the 590 °C spectrum. Minimal change is observed to the relative intensities of the Pt(0) or Pt(II) peaks, with only Pt(0) present based on the plotted spectra. When the water presence is higher, as shown in Fig. 6.16c and 6.16d, even the small Pd(II) presence seen in the low water condition is not observed. Both Pd and Pt appear to be reduced throughout the heating ramp from 150-590 °C.

As with the Pd-only foil, this indicates that the water presence inhibits the oxidation of palladium. The presence of platinum seems to further inhibit the oxidation of palladium under wet conditions, with minimal Pd(II) observed in either stoichiometric wet gas condition.

Data for the Pd88-Pt12 foil in oxygen rich conditions are shown in Fig. 6.17. The dry data, shown in Fig. 6.17a and 6.17b for Pd 3d and Pt 4f respectively, show both metals being primarily present in metallic forms throughout the experiment. The line scans show minimal relative changes in intensity for the metallic and oxidised peaks, and there is no significant variation in the individual XPS spectra shown. The oxygen rich wet condition data is shown in Fig. 6.17c and 6.17d. Unlike in the dry condition, there is formation of Pd(II) in this wet condition. Above 400 °C a peak starts to appear, which is clear by the last individual spectrum shown, recorded at 580 °C. There is still a higher amount of reduced Pd than oxidised Pd, but this is the only wet condition where significant amounts of Pd oxidation has been observed on this Pd88-Pt12 foil. The platinum, comparatively, does not appear to change over this temperature window, with the peak position (around 71 eV) indicating that Pt is metallic throughout.

TP-XPS data for the Pd88-Pt12 sample in oxygen is shown in Figs. 6.18a and 6.18b for Pd 3d and Pt 4f respectively. This is one of only 2 conditions where Pd is more oxidised than reduced by the final measurement, with the other being the stoichiometric dry condition (Fig. 6.15a). Here the intensity crossover happens around 350 °C, 30 °C lower than in the stoichiometric dry condition. By the measurement at 440 °C there is only a very minor presence of Pd(0) remaining. The Pt 4f spectra (Fig. 6.18b) show platinum splitting into two species at a similar temperature to the start of Pd(II) formation, 330 °C. By the 440 °C measurement, there is a higher amount of Pt(II) than Pt(0), something which has not been observed previously. For the stoichiometric dry condition (Fig. 6.15b) the final spectrum showed roughly equal amounts of Pt(II) and Pt(0).

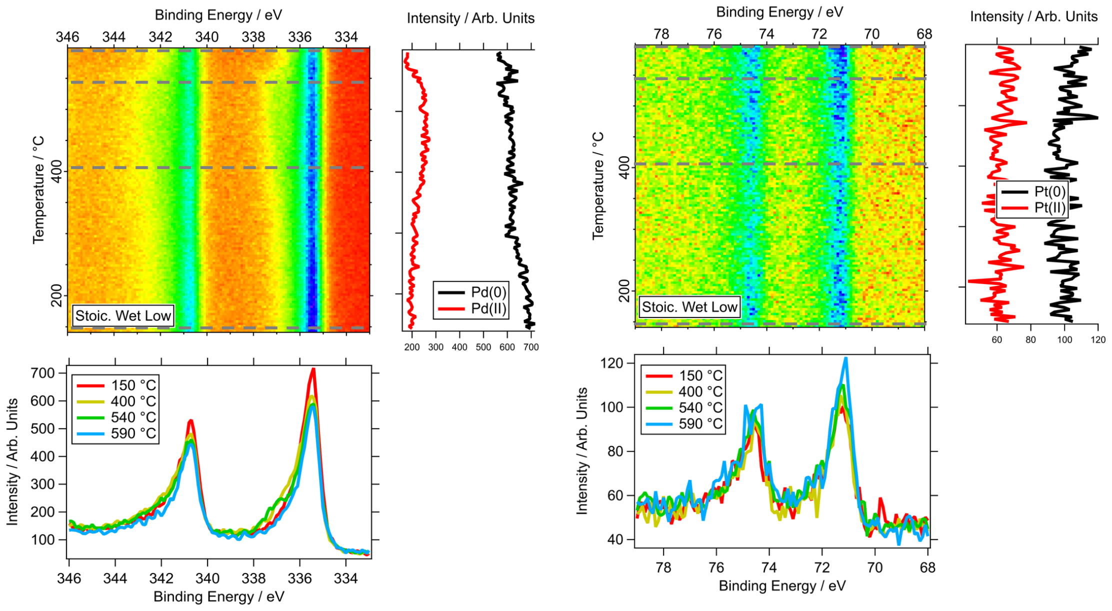

(a) Pd 3d, Stoichiometric low wet

(b) Pt 4f, Stoichiometric low wet

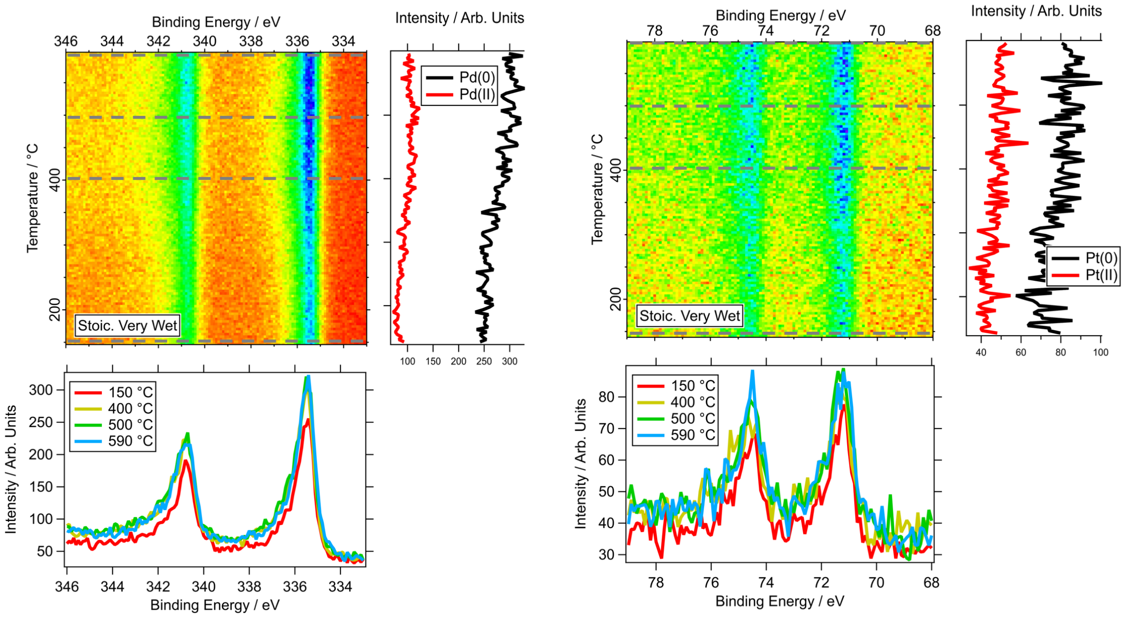

(c) Pd 3d, Stoichiometric very wet

(d) Pt 4f, Stoichiometric very wet

Figure 6.16: Pd 3d (left) and Pt 4d (right) region TP-XPS data for Pd88-Pt12 foil under various stoichiometric wet conditions. For each region, 2d TP-XPS plots (top left), line scans on the metallic and oxide peak position (top right) and spectra from relevant temperatures (bottom) are shown. Each of the spectra shown in the bottom section are the combination of data over 10 °C, from the temperatures marked with grey dashed lines in the TP-XPS plots. Heating rate was 3.5 °C/min. Photon energy for all XPS was 750 eV.

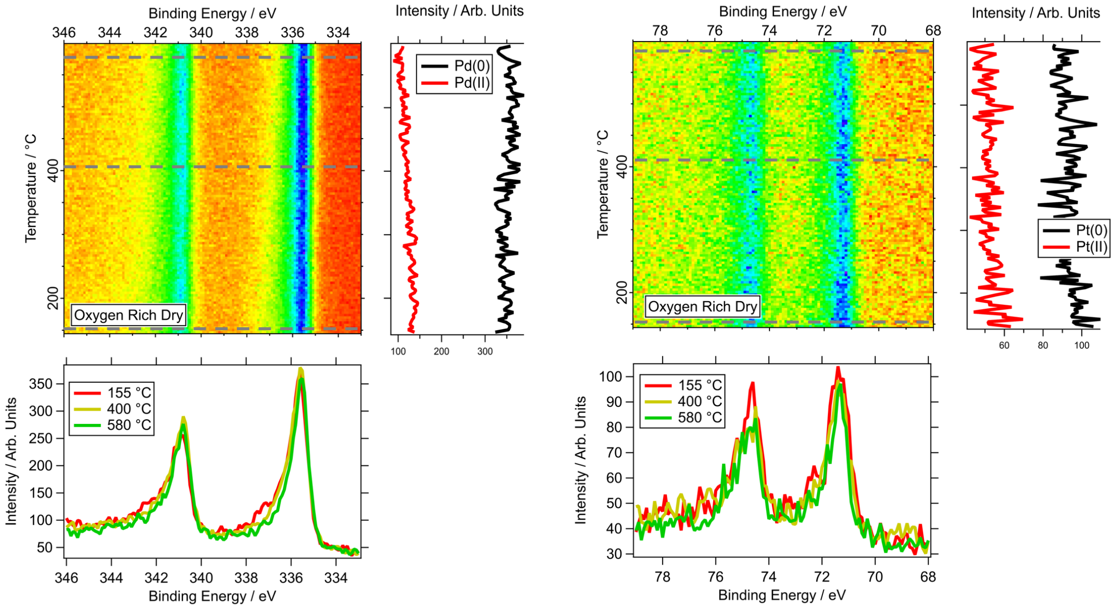

(a) Pd 3d, Oxygen rich dry

(b) Pt 4f, Oxygen rich dry

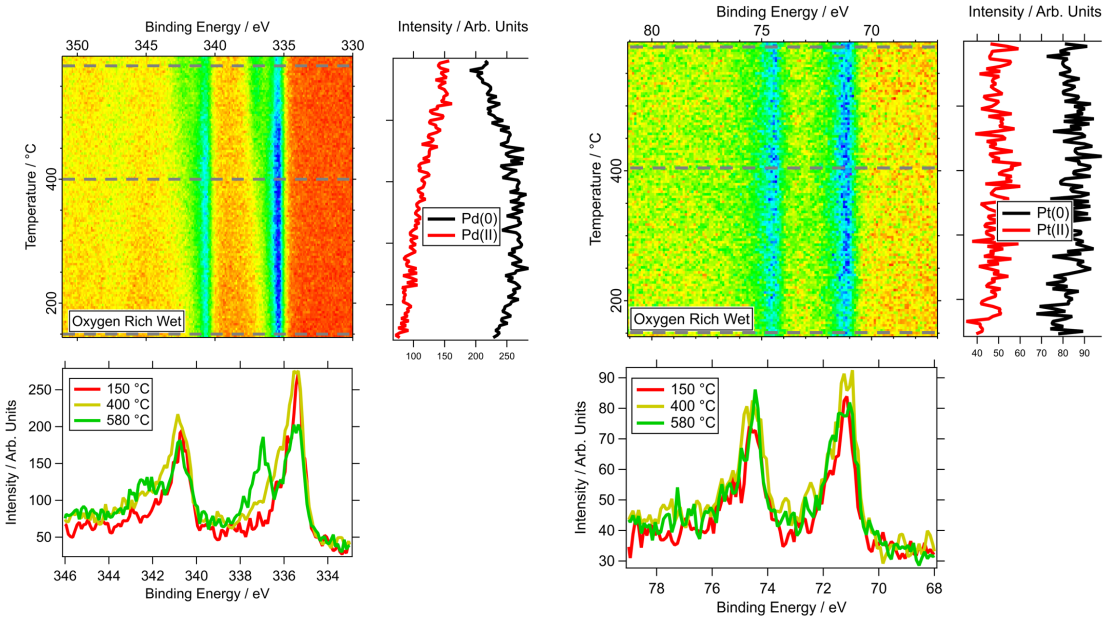

(c) Pd 3d, Oxygen rich wet

(d) Pt 4f, Oxygen rich wet

Figure 6.17: Pd 3d (left) and Pt 4d (right) region TP-XPS data for Pd88-Pt12 foil under oxygen rich dry and wet conditions. For each region, 2d TP-XPS plots (top left), line scans on the metallic and oxide peak position (top right) and spectra from relevant temperatures (bottom) are shown. Each of the spectra shown in the bottom section are the combination of data over 10 °C, from the temperatures marked with grey dashed lines in the TP-XPS plots. Heating rate was 3.5 °C/min. Photon energy for all XPS was 750 eV.

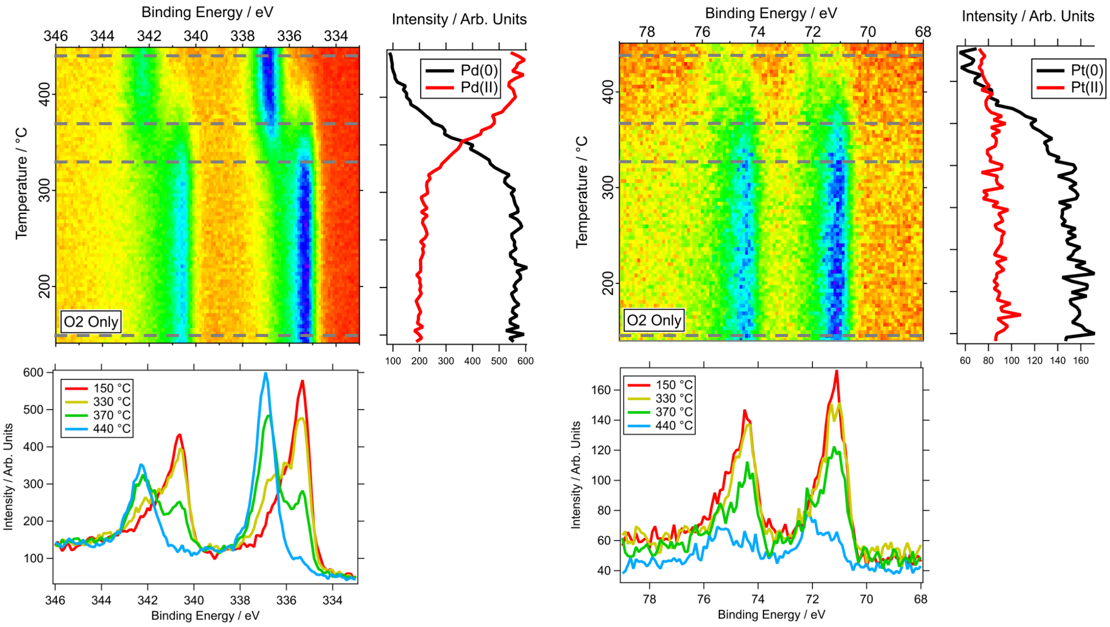

(a) Pd 3d, Oxygen only

(b) Pt 4f, Oxygen only

Figure 6.18: Pd 3d (left) and Pt 4d (right) region TP-XPS data for Pd88-Pt12 foil under oxygen only conditions. For each region, 2d TP-XPS plots (top left), line scans on the metallic and oxide peak position (top right) and spectra from relevant temperatures (bottom) are shown. Each of the spectra shown in the bottom section are the combination of data over 10 °C, from the temperatures marked with grey dashed lines in the TP-XPS plots. Heating rate was 3.5 °C/min. Photon energy for all XPS was 750 eV.

The Pd88-Pt12 foil was more resistant to oxidation of palladium than the Pd foil. Significant Pd(II) was only seen in one methane oxidation condition - stoichiometric dry - with the palladium largely remaining reduced in other conditions. Where major Pd oxidation was observed, the platinum appeared to be split into both metal and oxide, with a significant loss in intensity indicating migration from the surface to the bulk. The transformation of Pt happened from the same temperatures as the onset of Pd oxidation.

The data from the TP-XPS experiments conducted on a Pd65-Pt35 foil are shown in Figs. 6.19 to 6.21. Data recorded under stoichiometric methane oxidation conditions are presented in Fig. 6.19. The Pd 3d data (Fig. 6.19a) for this condition show an unusual behaviour. From 300 °C upwards, the Pd(0) intensity decreases. Above 420 °C, the Pd(II) peak intensity increases, to the point where - at 500 °C - it is of similar intensity to the Pd(0) peak (see XPS spectra and line scans). Above 550 °C, however, the palladium reduces again, such that by the 580 °C spectrum there is no evidence of oxidised Pd. The Pt 4f data is shown in Fig. 6.19b. The Pt $4f_{7/2}$ peak intensity for Pt(0) decreases similarly to that shown for Pd, as seen in the line scans. This may indicate that, for this temperature range (250-500 °C), there was an error with the movement that compensates for the thermal expansion of the sample. There is no significant change in the oxidation state of platinum, with no peak forming in the expected Pt(II) position (approx. 72.5 eV).

When compared to the other bimetallic foil, Pd88-Pt12, the Pd65-Pt35 shows much less Pd oxidation under stoichiometric dry conditions. Platinum remains reduced, whereas it split to be a mixture of Pt(0) and Pt(II) in the more Pd rich foil. This may indicate that the increased Pt presence is beneficial to preserving the reduced state of palladium under reaction conditions.

The wet stoichiometric methane oxidation TP-XPS data for Pd65-Pt35 are shown in Fig. 6.20. Figs. 6.20a and 6.20b show the Pd 3d and Pt 4f data respectively for the low water stoichiometric condition. In this case, no oxidation of Pd or Pt is observed, with a general decrease in intensity for both Pd and Pt over the course of the heating ramp. This is expected to be the result of the thermal compensation movement not being fully calibrated. Similarly, no oxidation of Pd or Pt is seen in the very wet stoichiometric condition, as shown in Figs. 6.20c and 6.20d. There is again an unusual intensity change, but as this is consistent between Pd and Pt (see line scans), it is again assumed to be the result of the thermal compensation

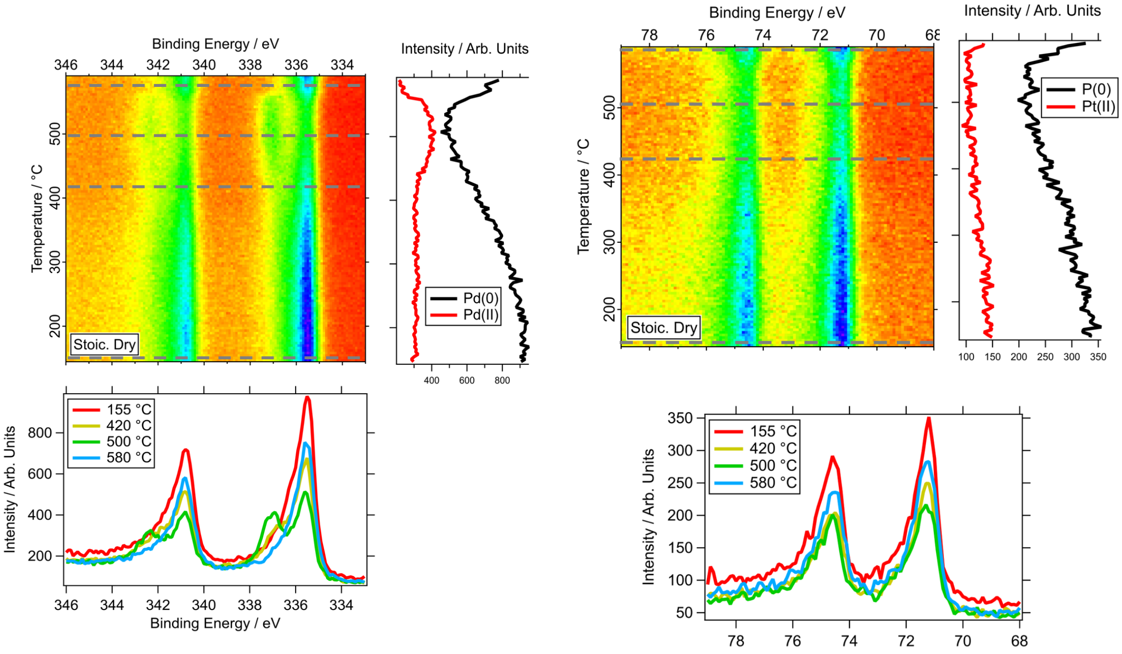

(a) Pd 3d, Stoichiometric dry

(b) Pt 4f, Stoichiometric dry

Figure 6.19: Pd 3d (left) and Pt 4d (right) region TP-XPS data for Pd65-Pt35 foil under stoichiometric dry conditions. For each region, 2d TP-XPS plots (top left), line scans on the metallic and oxide peak position (top right) and spectra from relevant temperatures (bottom) are shown. Each of the spectra shown in the bottom section are the combination of data over 10 °C, from the temperatures marked with grey dashed lines in the TP-XPS plots. Heating rate was 3.5 °C/min. Photon energy for all XPS was 750 eV.

movement, rather than a genuine sample change. Given the limited Pd oxidation seen in stoichiometric dry conditions for this sample, and the general inhibiting effect of water, the lack of Pd oxidation in these two conditions is an expected result.

The Pd65-Pt35 TP-XPS data under oxygen rich conditions are shown in Fig. 6.21. The dry oxygen rich methane oxidation condition data are shown in Figs. 6.21a and 6.21b for Pd and Pt respectively. Palladium shows significant oxidation under this condition, with an intensity crossover around 470 °C. There is still a notable amount of Pd(0) present at the maximum temperature of 590 °C. At the same time, there is a decrease in the Pt(0) intensity, resulting in an increase in Pt(II) : Pt(0) ratio. For the oxygen rich wet condition, shown in Figs. 6.21c and 6.21d, the behaviour of Pd and Pt is very similar to the dry condition. The transition from Pd(0) to Pd(II) happens at a similar temperature range, with the crossover in intensity again happening around 470 °C. As with the dry test, the final 590 °C measurement still shows a Pd(0) presence. The Pt 4f data is also very similar in dry and wet conditions, with a decrease seen for Pt(0) leading to an increased Pt(II) : Pt(0) ratio. The similarities between dry and wet conditions here are very unusual. Typically we observe an inhibition to Pd oxidation with increased water presence, as shown for Pd and Pd88-Pt12 foils previously. For Pd65-Pt35 however, the water presence seems to have minimal effect on Pd or Pt. Given that the Pd65-Pt35 does show differences in dry or wet when the oxygen is only present in stoichiometric amounts, it can be concluded here that for this composition of foil the effect of oxygen concentration in the feed has more of an impact than the presence of water.

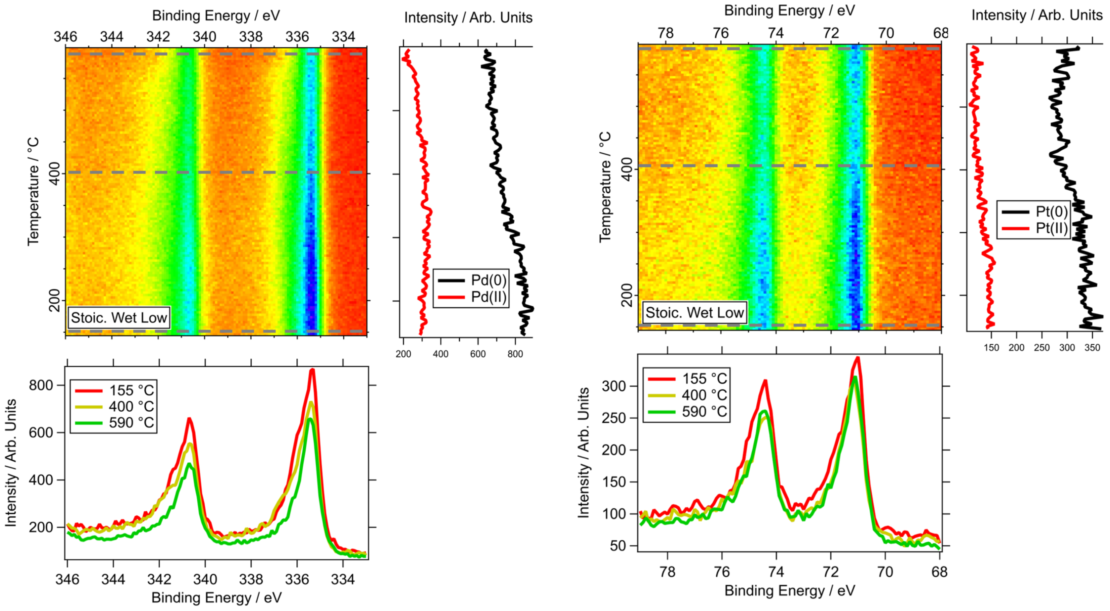

(a) Pd 3d, Stoichiometric low wet (b) Pt 4f, Stoichiometric low wet

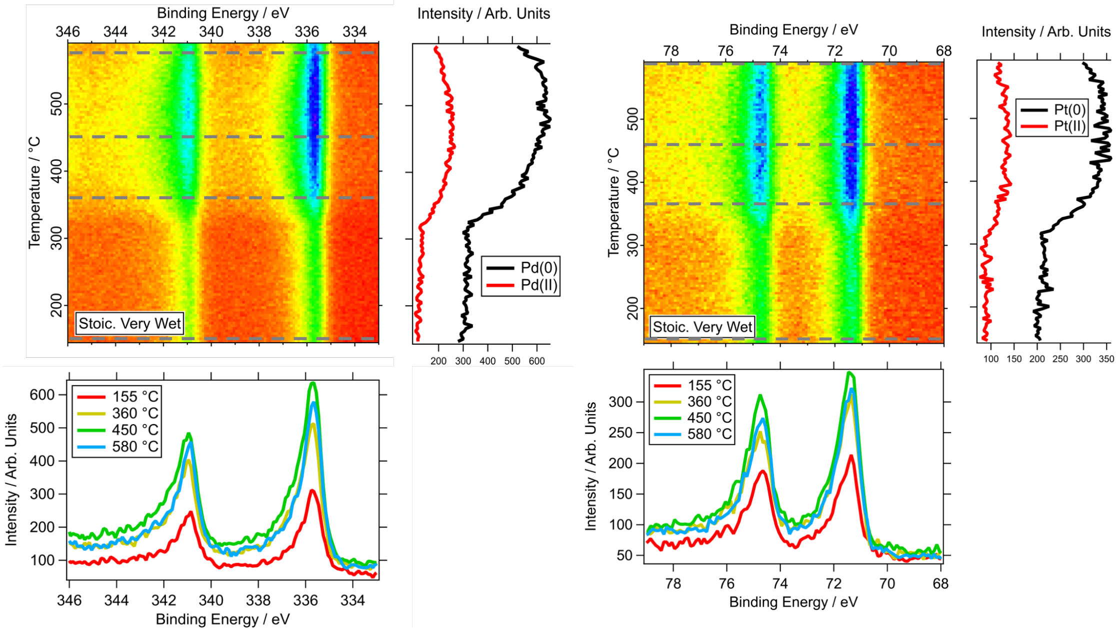

(c) Pd 3d, Stoichiometric very wet (d) Pt 4f, Stoichiometric very wet

Figure 6.20: Pd 3d (left) and Pt 4d (right) region TP-XPS data for Pd65-Pt35 foil under various stoichiometric wet conditions. For each region, 2d TP-XPS plots (top left), line scans on the metallic and oxide peak position (top right) and spectra from relevant temperatures (bottom) are shown. Each of the spectra shown in the bottom section are the combination of data over 10 °C, from the temperatures marked with grey dashed lines in the TP-XPS plots. Heating rate was 3.5 °C/min. Photon energy for all XPS was 750 eV.

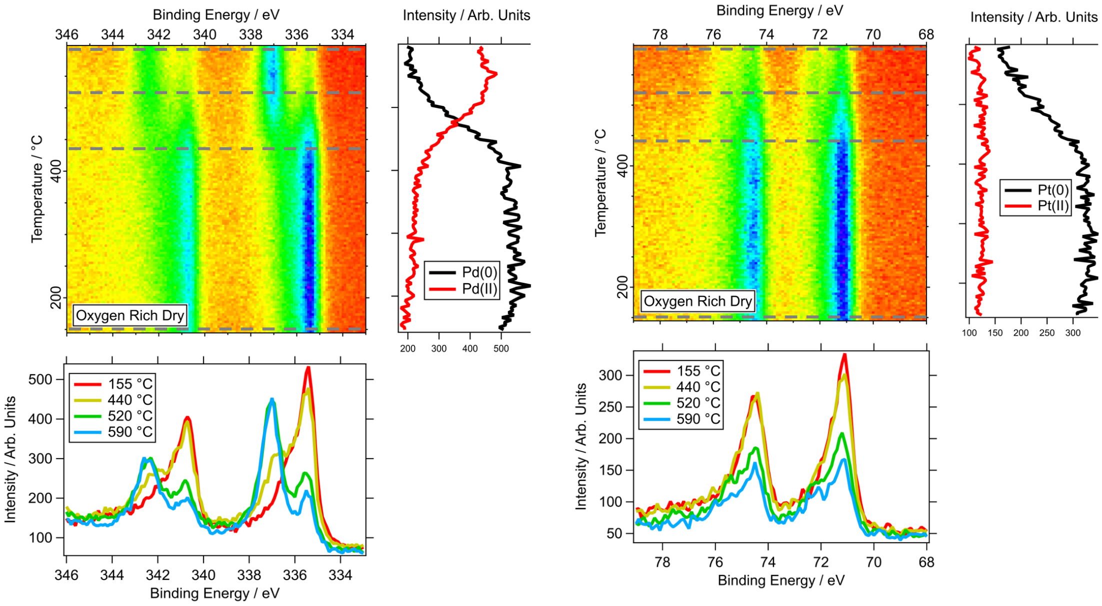

(a) Pd 3d, Oxygen rich dry

(b) Pt 4f, Oxygen rich dry

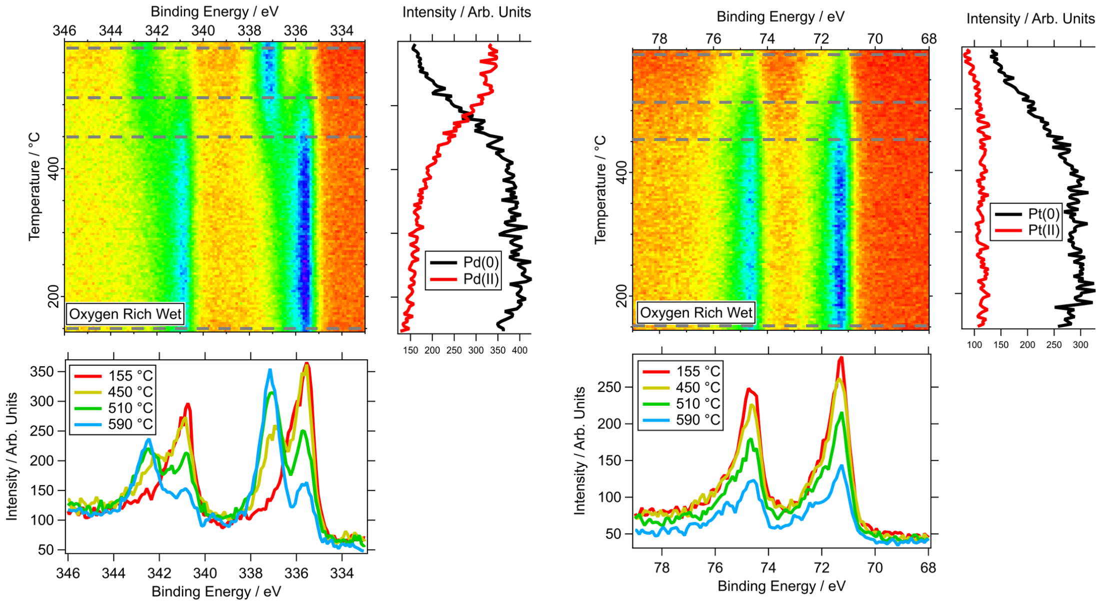

(c) Pd 3d, Oxygen rich wet

(d) Pt 4f, Oxygen rich wet

Figure 6.21: Pd 3d (left) and Pt 4d (right) region TP-XPS data for Pd65-Pt35 foil under oxygen rich dry and wet conditions. For each region, 2d TP-XPS plots (top left), line scans on the metallic and oxide peak position (top right) and spectra from relevant temperatures (bottom) are shown. Each of the spectra shown in the bottom section are the combination of data over 10 °C, from the temperatures marked with grey dashed lines in the TP-XPS plots. Heating rate was 3.5 °C/min. Photon energy for all XPS was 750 eV.

6.6 Conclusions

Whilst work on model systems is not always directly applicable to our real catalysts, it can help with understanding fundamental behaviours of metals in relevant environments, in a way that is simply not possible when only studying powder samples. Primarily, the grain size is significantly different, but there are also the support effects typically seen for nanoparticle catalysts to consider.

The thin films on single crystals showed that the alloying of Pd and Pt had significant effects, with shifts for both Pd and Pt for certain combinations compared to the pre-annealed versions. Overall palladium seemed to be less affected in regards to surface state than platinum, suggesting the effects on palladium are not significant, although this does not align with our other results. The platinum showed a strong tendency to move to the interface with the Re{0001}, as compared to palladium.

Work on metallic foils gave a good insight into how palladium, and palladium-platinum alloys behaved under reaction conditions. Palladium oxidation is seen to occur at higher temperatures in stoichiometric conditions as compared to oxygen rich, and in wet conditions as compared to dry. Increased water presence only served to further inhibit this oxidation. Most interestingly for Pd, we saw an earlier onset of oxidation under dry methane oxidation conditions than under oxygen alone.

For either bimetallic composition, significant inhibition of palladium oxidation was observed. For the Pd88-Pt12 foil, Pd oxidation to Pd(II) was seen under stoichiometric dry and oxygen only conditions, but not under any of the other 4 tested conditions. For Pd65-Pt35, full oxidation of Pd was only seen under oxygen rich conditions, and not under any stoichiometric condition. Initially we suggested that the bimetallic foils would show oxidation at higher temperatures due to an inhibition effect from the platinum. However, it was not expected that the different ratios led to this inhibition happening in very different ways. Overall, this is indicative of the platinum presence helping to retain the reduced state of palladium under reaction conditions. Studying the platinum spectra throughout, it appears that platinum migrates to the bulk at the point at which palladium oxidation occurs. It is clear that the presence of platinum has a significant effect on palladium under methane oxidation conditions, with the surface presence of Pt seemingly aiding the resistance to Pd oxidation. Bimetallic catalysts being more resistant to oxidation is broadly in agreement with the findings from the powder catalyst work presented earlier, which showed that the bimetallic catalysts were more likely to retain significant amounts of Pd(0) under reaction conditions.

7 Summary & Conclusions

A wide range of palladium, platinum, and palladium-platinum systems - both real powder catalysts and models - were studied for complete methane oxidation.

Powder catalyst studies showed that palladium was significantly better than platinum in all relevant tested conditions. Exchanging palladium for platinum showed some benefits, most importantly decreasing the deactivation suffered in wet conditions - a key negative of palladium catalysts. Small exchanges of Pd for Pt maintained most of the dry and wet activity of Pd, and reduced the effective catalyst cost due to the lower comparative cost of platinum.

NAP-XPS measurements allowed measurements of surface chemical states of catalysts under representative gas conditions at relevant temperatures. NAP-XPS was utilised to investigate whether studying the surface states could aid the understanding and development of catalysts for methane oxidation. It showed correlations between activity and palladium oxidation state for alumina-supported samples, with benefits seen to having a presence of both Pd(0) and Pd(II) on the surface. Pd-Pt catalysts often had a higher amount of Pd(0) compared to palladium monometallic catalysts, which were more often fully oxidised to Pd(II).

Support variations compared silica, alumina and silica-alumina supported catalysts of equivalent loading. A mixed silica-alumina support - $90Al_2O_3$-$10SiO_2$ - typically gave the best activity, though the margins between this, silica and alumina were often very small for a given condition and catalyst composition. NAP-XPS of these catalysts showed variations that were not always consistent with the activity variations, indicating that the surface state is less important than other effects from the support.

When combining considerations for activity in multiple conditions with the cost, 4.0Pd or 4.0Pd-1.0Pt supported on either $90Al_2O_3$-$10SiO_2$ or Al_2O_3 would be the most logical choices for complete methane oxidation catalysts arising from this work.

Issues with charging and signal in NAP-XPS experiments prompted the development of flat, uniform model catalysts, utilising thin layers of alumina with nanoparticles of palladium deposited onto the surface using a cluster source. This method allowed for the production of samples with similar surface loadings to the powder catalysts, which were superior in regards to sample charging for XPS. Additionally, they were shown to behave in similar ways under methane oxidation conditions by NAP-XPS, with dynamic reduction and oxidation of palladium, although catalytic activity was not observed in this case. This production method could prove useful in the surface studies for many metal oxide supported catalysts across a wide range of applications.

Thin layer studies of platinum and palladium attempted to further understanding of the effects of combining the two metals on the chemical properties of both. Both metals appeared to form significant interface layers with the Re{0001} crystal, with bulk-like Pd and Pt above. Only very minor amounts (typically less than 10%) of surface-like sites were observed, based on the core level shifts. Annealing on mixed samples tended to see platinum preferentially migrate to the interface with rhenium. Based on the observed shifts, it is likely Pd and Pt were often in discrete islands on the surface of the rhenium crystal.

Studies of palladium and palladium-platinum foils showed that the reaction condition significantly affects the onset of palladium oxidation. Lower oxygen and higher water presence were both inhibiting with regards to Pd oxidation. Where bimetallic films were studied, a higher Pt loading generally further inhibited the palladium oxidation, with platinum often moving to the bulk whilst palladium eventually oxidised at the surface. This gives an insight into possible reasons for the more reduced nature of the Pd-Pt nanoparticle catalysts and the resulting strong catalytic activity.

8 Outlook & Future Work

Various options for additional research within the scope of this project are outlined below.

Studies on the acidity of all supports (and samples) should be considered, as this is understood to be a key issue for catalysts which are inhibited by operation in wet conditions. It is an important property to understand, to better understand the activity changes which are observed with different supports, as this is not always fully understood from the research completed during this project. In addition to this, activity tests focusing on solely the support materials would provide additional information, which could better explain the variations observed.

With the "realistic model" catalysts systems proving successful within their scope here, this could be expanded to cover other systems. It provided a flat, uniform support with minimal contaminants and very low charging under an XPS beam, solving issues which make analysis of insulating supports difficult and unreliable. Whilst this was tested using only alumina as support, it could be viable on various metals where the oxide is the desirable support phase, and where this can be produced from the metal via anodization. The cluster source deposition method can be used for many metals - whilst only palladium was deposited for this work, others such as platinum or gold could also theoretically be prepared this way, both of which can be catalysts for a range of processes.

The continued development of NAP-XPS to allow for more realistic reaction conditions will also be useful for this reaction and many others. Experiments in this project typically used a maximum of 10% of the real reactor pressures of relevant reactant gases, and whilst this is enough to often see reaction progress, it is still not an ideal situation. In addition to the pressure, the flow rate is also a very important consideration, as the flow rate in a catalytic reactor is often higher than that used in a NAP-XPS chamber.

Bibliography

[1] Chris Morgan. 40 years of cleaner air: The evolution of the autocatalyst. *Johnson Matthey Technology Review*, 58(4):217–220, 2014.

[2] AECC. AECC - Legislation for Sustainable Mobility - Euro 7 and Euro VII - Accessed 06/05/2021.

[3] European Commission. Emissions in the automotive sector — Internal Market, Industry, Entrepreneurship and SMEs - Accessed 06/05/2021, 2019.

[4] Paul J. Millington and Andrew P.E. York. Opportunities for platinum group metals in future emissions control technology. *Platinum Metals Review*, 56(1):58–60, 2012.

[5] Web of Science. Web of Science Search - Catalysis - Accessed 06/05/2021.

[6] Web of Science. Web of Science Search - Chemistry - Accessed 06/05/2021.

[7] Web of Science. Web of Science Search - Ambient Pressure XPS - Accessed 06/05/2021.

[8] Web of Science. Web of Science Search - Palladium Platinum Bimetallic - Accessed 06/05/2021.

[9] Web of Science. Web of Science Search - Complete Methane Oxidation - Accessed 06/05/2021.

[10] Jan Willem Erisman, Mark A. Sutton, James Galloway, Zbigniew Klimont, and Wilfried Winiwarter. How a century of ammonia synthesis changed the world. *Nature Geoscience*, 1(10):636–639, 2008.

[11] Huazhang Liu. *Ammonia Synthesis Catalysts: Innovation and Practice.* World Scientific.

[12] USGS. Nitrogen Statistics and Information - Accessed 06/05/2021, 2021.

[13] Grazia Leonzio. Methanol synthesis: Optimal solution for a better efficiency of the process. *Processes*, 6(3), 2018.

[14] Benjamín Cañete, Carlos E. Gigola, and Nélida B. Brignole. Synthesis gas processes for methanol production via CH4 reforming with CO2, H2O, and O2. *Industrial and Engineering Chemistry Research*, 53(17):7103–7112, 2014.

[15] Alvin B Stiles, Frank Chen, Jeffrey B Harrison, Xiaodong Hu, David A Storm, and H X Yang. Catalytic Conversion of Synthesis Gas to Methanol and Other Oxygenated Products. *Industrial and Engineering Chemistry Research*, 30:811–821, 1991.

[16] Raquel De María, Ismael Díaz, Manuel Rodríguez, and Adrián Sáiz. Industrial methanol from syngas: Kinetic study and process simulation. *International Journal of Chemical Reactor Engineering*, 11(1):469–477, 2013.

[17] Xiao Zhao, Min Yin, Liang Ma, Liang Liang, Changpeng Liu, Jianhui Liao, Tianhong Lu, and Wei Xing. Recent advances in catalysts for direct methanol fuel cells. *Energy and Environmental Science*, 4(8):2736–2753, 2011.

[18] Jing Liu, Chun Tao Liu, Lei Zhao, and Zhen Bo Wang. Highly Durable Direct Methanol Fuel Cell with Double-Layered Catalyst Cathode. *Journal of Nanomaterials*, 2015, 2015.

[19] Kingshuk Dutta. *Direct Methanol Fuel Cell Technology*. Elsevier, 2020.

[20] Nofal Khamis Soliman. Factors affecting CO oxidation reaction over nanosized materials: A review. *Journal of Materials Research and Technology*, 8(2):2395–2407, 2019.

[21] You Zhou, Zongyuan Wang, and Changjun Liu. Perspective on CO oxidation over Pd-based catalysts. *Catalysis Science and Technology*, 5(1):69–81, 2015.

[22] Ndepana A. Gaya, Victor Charles, Innocent Joseph, and Hitler Louis. A review on CO oxidation, methanol synthesis, and propylene epoxidation over supported gold catalysts. *Catalysis for Sustainable Energy*, 6(1):13–37, 2019.

[23] Lichen Liu and Avelino Corma. Metal Catalysts for Heterogeneous Catalysis: From Single Atoms to Nanoclusters and Nanoparticles. *Chemical Reviews*, 118(10):4981–5079, 2018.

[24] Huabin Zhang, Guigao Liu, Li Shi, and Jinhua Ye. Single-Atom Catalysts: Emerging Multifunctional Materials in Heterogeneous Catalysis. *Advanced Energy Materials*, 8(1):1–24, 2018.

[25] Robert Schlögl. Heterogeneous catalysis. *Angewandte Chemie - International Edition*, 54(11):3465–3520, 2015.

[26] Zhen Guo, Bin Liu, Qinghong Zhang, Weiping Deng, Ye Wang, and Yanhui Yang. Recent advances in heterogeneous selective oxidation catalysis for sustainable chemistry. *Chemical Society Reviews*, 43(10):3480–3524, 2014.

[27] John Meurig Thomas and W. John Thomas. *Principles and Practice of Heterogeneous Catalysis*. John Wiley & Sons, Incorporated, 2015.

[28] Julian R. H. Ross. *Contemporary Catalysis Fundamentals and Current Applications*. Elsevier, 2018.

[29] Rutger A. van Santen. *Modern Heterogeneous Catalysis: An Introduction*. John Wiley & Sons, Incorporated, 2017.

[30] David Knight. *Humphry Davy: Science & Power*. Blackwell, 1992.

[31] William Parks Yant and Charles Hawk. the Activity of Various Metals and Metal Oxide Catalysts in Promoting the Oxidation of Methane By Air. *Journal of the American Chemical Society*, 49(6):1454–1460, 1927.

[32] Tony Maillet, C. Solleau, Jacques Barbier, and Daniel Duprez. Oxidation of carbon monoxide, propene, propane and methane over a Pd/Al2O3 catalyst. Effect of the chemical state of Pd. *Applied Catalysis B: Environmental*, 14(1-2):85–95, 1997.

[33] Mansour Aryafar and F Zaera. Kinetic study of the catalytic oxidation of alkanes over nickel, palladium, and platinum foils. *Catalysis Letters*, 48:173–183, 1997.

[34] Hassan Windawi. Controlling the Exhaust Emissions from Alternative Fuel Vehicles. *Platinum Metals Review*, 36(4):185–195, 1992.

[35] Shyi-min Lu and Shyi-min Lu. A global survey of gas hydrate development and reserves: Specifically in the marine field. *Renewable and Sustainable Energy Reviews*, 41(January 2015):884–900, 2017.

[36] Nils Olof Nylund, Kimmo Erkkilä, Maija Lappi, and Markku Ikonen. Transit bus emission study: comparison of emissions from diesel and natural gas buses. Technical report, 2004.

[37] José Ma López, Álvaro Gómez, Francisco Aparicio, and Fco Javier Sánchez. Comparison of GHG emissions from diesel, biodiesel and natural gas refuse trucks of the City of Madrid. *Applied Energy*, 86(5):610–615, 2009.

[38] Marc E.J. Stettler, William J.B. Midgley, Jacob J. Swanson, David Cebon, and Adam M. Boies. Greenhouse Gas and Noxious Emissions from Dual Fuel Diesel and Natural Gas Heavy Goods Vehicles. *Environmental Science and Technology*, 50(4):2018–2026, 2016.

[39] Martijn Gilbert. A Fleet of Biomethane Buses in Reading. Technical report, Clean Fleets, 2014.

[40] Donnie J. Worth, Marc E. J. Stettler, Paul Dickinson, Kieran Hegarty, and Adam M. Boies. Characterization and Evaluation of Methane Oxidation Catalysts for Dual-Fuel Diesel and Natural Gas Engines. *Emission Control Science and Technology*, 2(4):204–214, 2016.

[41] Zhenhua Li and Gar B Hoflund. A Review on Complete Oxidation of Methane at Low Temperatures. *Journal of Natural Gas Chemistry*, 12:153–160, 2003.

[42] Martin Schmal, Mariana M. V. M. Souza, Violeta Virginia Alegre, Mônica Antunes Pereira da Silva, Deborah Vargas César, and Carlos A. C. Perez. Methane oxidation - effect of support, precursor and pretreatment conditions - in situ reaction XPS and DRIFT. *Catalysis Today*, 118(3-4):392–401, 2006.

[43] Matteo Monai, Tiziano Montini, Michele Melchionna, Tomáš Duchoň, Peter Kúš, Chen Chen, Nataliya Tsud, Lucia Nasi, Kevin C. Prince, Kateřina Veltruská, Vladimír Matolín, Mahmoud M. Khader, Raymond J. Gorte, and Paolo Fornasiero. The effect of

sulfur dioxide on the activity of hierarchical Pd-based catalysts in methane combustion. *Applied Catalysis B: Environmental*, 202:72–83, 2017.

[44] Henry Liander. The Ultilisation of Natural Gases For The Ammonia Process. *Transactions of the Faraday Society*, 0(25):462–472, 1929.

[45] Bjørn Christian Enger, Rune Lødeng, and Anders Holmen. A review of catalytic partial oxidation of methane to synthesis gas with emphasis on reaction mechanisms over transition metal catalysts. *Applied Catalysis A: General*, 346(1-2):1–27, 2008.

[46] Velu Subramani and Santosh K. Gangwal. A Review of Recent Literature to Search for an Efficient Catalytic Process for the Conversion of Syngas to Ethanol. *Energy & Fuels*, 22(2):814–839, 2008.

[47] Johnson Matthey. The environmental profile of Platinum Group Metals (PGMs). Technical Report 2, 2017.

[48] Marjolein L. Toebes, Jos A. Van Dillen, and Krijn P. De Jong. Synthesis of supported palladium catalysts. *Journal of Molecular Catalysis A: Chemical*, 173(1-2):75–98, 2001.

[49] Manhong Liu, Weiyong Yu, Hanfan Liu, and Jingming Zheng. Preparation and Characterization of Polymer-Stabilized Ruthenium-Platinum and Ruthenium-Palladium Bimetallic Colloids and Their Catalytic Properties for Hydrogenation of o-Chloronitrobenzene. *Journal of Colloid and Interface Science*, 214(2):231–237, 1999.

[50] R. B. Anderson, K. C. Stein, J. J. Feenan, and L. J. E. Hofer. Catalytic Oxidation of Methane. *Industrial and Engineering Chemistry*, 53(10):809–812, 1961.

[51] J. G. Firth and H. B. Holland. Catalytic oxidation of methane over noble metals. *Transactions of the Faraday Society*, 65:1121–1127, 1969.

[52] James J. Chen and Ell Ruckenstein. Role of interfacial phenomena in the behavior of alumina-supported palladium crystallites in oxygen. *Journal of Physical Chemistry*, 85(11):1606–1612, 1981.

[53] Jon G. McCarty. Kinetics of PdO combustion catalysis. *Catalysis Today*, 26(3-4):283–293, 1995.

[54] Edouard Garbowski, Christiane Feumi-Jantou, Najat Mouaddib, and Michel Primet. Catalytic combustion of methane over palladium supported on alumina catalysts: Evidence for reconstruction of particles. *Applied Catalysis A: General*, 109(2):277–291, mar 1994.

[55] Robert R. Burch and Francisco J. Urbano. Investigation of the active state of supported palladium catalysts in the combustion of methane. *Applied Catalysis A: General*, 124(1):121–138, 1995.

[56] Yun Xiang Pan, Chang Jun Liu, and Peng Shi. The cleavage of the methane C-H bond over PdO/H-BEA: A density functional theory study. *Applied Surface Science*, 254(17):5587–5593, 2008.

[57] Santhosh Kumar Matam, M H Aguirre, A Weidenkaff, and D Ferri. Revisiting the Problem of Active Sites for Methane Combustion on Pd / Al 2 O 3 by Operando XANES in a Lab-Scale Fixed-Bed Reactor. *Journal of Physical Chemistry C*, 114:9439–9443, 2010.

[58] Anders Hellman, Andrea Resta, Natalia M. Martin, Johan Gustafson, Adriana Trinchero, Per-Anders Carlsson, Olivier Balmes, Roberto Felici, R. Van Rijn, Joost W.M. Frenken, J. N. Andersen, Edvin Lundgren, and Henrik Grönbeck. The active phase of palladium during methane oxidation. *Journal of Physical Chemistry Letters*, 3(6):678–682, 2012.

[59] Victor Yu Bychkov, Yu P. Tulenin, Marina M. Slinko, Alexander K. Khudorozhkov, V. I. Bukhtiyarov, Sergey Sokolov, and Vladimir N. Korchak. Self-oscillations during methane oxidation over Pd/Al2O3: Variations of Pd oxidation state and their effect on Pd catalytic activity. *Applied Catalysis A: General*, 522:40–44, 2016.

[60] William S. Epling and Gar B. Hoflund. Catalytic Oxidation of Methane over ZrO2-Supported Pd Catalysts. *Journal of Catalysis*, 182(1):5–12, 1999.

[61] H. Maeda, Y. Kinoshita, K. R. Reddy, Kohichi Muto, Shin'ichi Komai, Naonobu Katada, and Miki Niwa. Activity of palladium loaded on zeolites in the combustion of methane. *Applied Catalysis A: General*, 163(1-2):59–69, 1997.

[62] Andrey W. Petrov, Davide Ferri, Frank Krumeich, Maarten Nachtegaal, Jeroen A. Van Bokhoven, and Oliver Kröcher. Stable complete methane oxidation over palladium based zeolite catalysts. *Nature Communications*, 9(1), 2018.

[63] Lílian Maria Tosta Simplício, Soraia Teixeira Brandão, Emerson Andrade Sales, Luca Lietti, and François Bozon-Verduraz. Methane combustion over PdO-alumina catalysts: The effect of palladium precursors. *Applied Catalysis B: Environmental*, 63(1-2):9–14, 2006.

[64] E. H. Voogt, Ad J.M. Mens, Onno L.J. Gijzeman, and John Wilhelm Geus. XPS analysis of palladium oxide layers and particles. *Surface Science*, 350(1-3):21–31, 1996.

[65] Tsutomu Shimizu, Aamir D. Abid, Gregory A. Poskrebyshev, Hai Y. Wang, James A. Nabity, Jeffrey R. Engel, Jianhan Yu, David T. Wickham, Brian Van Devener, Scott L. Anderson, and Skip L. Williams. Methane ignition catalyzed by in situ generated palladium nanoparticles. *Combustion and Flame*, 157(3):421–435, 2010.

[66] Ya Huei Cathy Chin, Mónica García-Diéguez, and Enrique Iglesia. Dynamics and thermodynamics of Pd-PdO phase transitions: Effects of pd cluster size and kinetic implications for catalytic methane combustion. *Journal of Physical Chemistry C*, 120(3):1446–1460, 2016.

[67] Xiu-hui Gao, Sheng Wang, Dian-nan Gao, Wei-gang Liu, Zhi-ping Chen, Ming-zhe Wang, and Shu-dong Wang. Catalytic combustion of methane over Pd/MWCNTs under lean fuel conditions. *Journal of Fuel Chemistry and Technology*, 44(8):928–936, 2016.

[68] Robert Burch, Francisco J. Urbano, and P. K. Loader. Methane combustion over palladium catalysts: The effect of carbon dioxide and water on activity. *Applied Catalysis A: General*, 123(94):173–184, 1995.

[69] Atsushi Satsuma, Takumi Tojo, Kohei Okuda, Yuta Yamamoto, Shigeo Arai, and Junya Oyama. Effect of preparation method of Co-promoted Pd/alumina for methane combustion. *Catalysis Today*, 242(B):308–314, 2015.

[70] Baohua Yue, Renxian Zhou, Yuejuan Wang, Xiaoxiang Han, and Xiaoming Zheng. Study on the combustion behavior of methane over Ce-Zr-modified Pd/Al2O3 catalysts. *Applied Surface Science*, 246(1-3):36–43, 2005.

[71] Chao Xiao, Yong Yang, Dan Meng, Lan Dong, Lili Luo, and Zhaoyi Tan. Stable and active monolithic palladium catalyst for catalytic oxidation of methane using nanozeolite silicalite-1 coating on cordierite. *Applied Catalysis A: General*, 531:197–202, 2017.

[72] Qifu Huang, Wenzhi Li, Qizhao Lin, Xusheng Zheng, Haibin Pan, Dong Pi, Chunyu Shao, Chao Hu, and Haitao Zhang. Catalytic performance of Pd–NiCo2O4/SiO2 in lean methane combustion at low temperature. *Journal of the Energy Institute*, pages 1–10, 2017.

[73] Zhou Jun Wang, Yuan Liu, Peng Shi, Chang Jun Liu, and Yan Liu. Al-MCM-41 supported palladium catalyst for methane combustion: Effect of the preparation methodologies. *Applied Catalysis B: Environmental*, 90(3-4):570–577, 2009.

[74] Sterling E. Voltz, Charles R. Morgan, David Liederman, and Solomon M. Jacob. Kinetic Study of Carbon Monoxide and Propylene Oxidation on Platinum Catalysts. *Industrial & Engineering Chemistry Product Research and Development*, 12(4):294–301, 1973.

[75] Chang Hwan Kim, Gongshin Qi, Kevin Dahlberg, and Wei Li. Strontium-Doped Perovskites Rival. *Science*, 327(5973):1624–1627, 2010.

[76] Hans-Ulrich Blaser, Hans-Peter Jalett, Manfred Müller, and Martin Studer. Enantioselective hydrogenation of α-ketoesters using cinchona modified platinum catalysts and related systems: A review. *Catalysis Today*, 37(4):441–463, 1997.

[77] John W. Shabaker, Rupali R. Davda, George W. Huber, Randy D. Cortright, and James A. Dumesic. Aqueous-phase reforming of methanol and ethylene glycol over alumina-supported platinum catalysts. *Journal of Catalysis*, 215(2):344–352, 2003.

[78] Robert R. Burch and P. K. Loader. Investigation of methane oxidation on Pt/Al2O3 catalysts under transient reaction conditions. *Applied Catalysis A: General*, 122(2):169–190, 1995.

[79] Elin Becker, Per Anders Carlsson, Henrik Grönbeck, and Magnus Skoglundh. Methane oxidation over alumina supported platinum investigated by time-resolved in situ XANES spectroscopy. *Journal of Catalysis*, 252(1):11–17, 2007.

[80] Ashraf Amin, Ali Abedi, Robert Hayes, Martin Votsmeier, and William Epling. Methane oxidation hysteresis over Pt/Al2O3. *Applied Catalysis A: General*, 478:91–97, 2014.

[81] André Rosa Martins, Luciene Santos Carvalho, Patrício Reyes, Javier Mario Grau, and Maria do Carmo Rangel. Hydrogen production on alumina-supported platinum catalysts. *Molecular Catalysis*, 429:1–9, 2017.

[82] Mariana M V M Souza and Martin Schmal. Combination of carbon dioxide reforming and partial oxidation of methane over supported platinum catalysts. *Applied Catalysis A: General*, 255(1):83–92, 2003.

[83] A. Bitsch-Larsen, R. Horn, and L. D. Schmidt. Catalytic partial oxidation of methane on rhodium and platinum: Spatial profiles at elevated pressure. *Applied Catalysis A: General*, 348(2):165–172, 2008.

[84] Naoki Toshima, Tetsu Yonezawa, and Kakuta Kushihashi. Polymer-protected palladium–platinum bimetallic clusters: preparation, catalytic properties and structural considerations. *Journal of the Chemical Society, Faraday Transactions*, 89(14):2537–2543, 1993.

[85] Naoki Toshima, Masafumi Harada, Tetsu Yonezawa, Kakuta Kushihashi, and Kiyotaka Asakura. Structural Analysis of Polymer-Protected Pd / Pt Bimetallic Clusters as Dispersed Catalysts by Using Extended X-ray Absorption Fine Structure Spectroscopy A /. *Journal of Physical Chemistry*, 95(15):7448–7453, 1991.

[86] Levente Vitos, Andrei V. Ruban, Hans L. Skriver, and János Kollár. The surface energy of metals. *Surface Science*, 411(1-2):186–202, 1998.

[87] Andrei V. Ruban, H. L. Skriver, and Jens K. Nørskov. Surface segregation energies in transition-metal alloys. *Physical Review B*, 59(24):15990–16000, 1999.

[88] Leon C A Van Den Oetelaar, O W Nooij, S Oerlemans, Arnoud W Denier Van Der Gon, H H Brongersma, Leon Lefferts, A. G. Roosenbrand, and J. A. R. van Veen. Surface Segregation in Supported Pd - Pt Nanoclusters and Alloys. *Journal of Physical Chemistry B*, 5647(97):3445–3455, 1998.

[89] Patricio Alberto Reyes, Alejandra Figueroa, Gina Pecchi, and J. L.G. Fierro. Catalytic combustion of methane on Pd-Cu/SiO2 catalysts. *Catalysis Today*, 62(2-3):209–217, 2000.

[90] Seung Uk Son, Youngjin Jang, Jongnam Park, Hyon Bin Na, Hyun Min Park, Hyung Joong Yun, Jouhahn Lee, and Taeghwan Hyeon. Designed Synthesis of Atom-Economical Pd/Ni Bimetallic Nanoparticle-Based Catalysts for Sonogashira Coupling Reactions. *Journal of the American Chemical Society*, 126(16):5026–5027, 2004.

[91] Tatsumi Ishihara, Hiroyoshi Shigematsu, Yumi Abe, and Yusaku Takita. Effects of Additives on the Activity of Palladium Catalysts for Methane Combustion. *Chemistry Letters*, 22(3):407–410, 1993.

[92] Kohji Narui, Hirohide Yata, Keiichi Furuta, Akio Nishida, Yasuhiko Kohtoku, and Tokuo Matsuzaki. Effects of addition of Pt to PdO/Al2O3 catalyst on catalytic activity for methane combustion and TEM observations of supported particles. *Applied Catalysis A: General*, 179(1-2):165–173, 1999.

[93] Katarina Persson, Anders G. Ersson, Kjell Jansson, J. L.G. Fierro, and Sven G. Järås. Influence of molar ratio on Pd-Pt catalysts for methane combustion. *Journal of Catalysis*, 243(1):14–24, 2006.

[94] Katarina Persson. *Bimetallic Palladium Catalysts for Methane Combustion in Gas Turbines*. PhD thesis, KTH Royal Institute of Technology, 2006.

[95] Gregory Lapisardi, Laetitia Urfels, Patrick Gélin, Michel Primet, Akim Kaddouri, Edouard Garbowski, Stephanie Toppi, and Emmanuel Tena. Superior catalytic behaviour of Pt-doped Pd catalysts in the complete oxidation of methane at low temperature. *Catalysis Today*, 117(4):564–568, 2006.

[96] Emmett D Goodman, Sheng Dai, An-chih Yang, Cody J Wrasman, Alessandro Gallo, Simon R Bare, Adam S Ho, Thomas F Jaramillo, George W Graham, Xiaoqing Pan,

and Matteo Cargnello. Uniform Pt/Pd Bimetallic Nanocrystals Demonstrate Platinum Effect on Palladium Methane Combustion Activity and Stability. *ACS Catalysis*, 7:4372–4380, 2017.

[97] Reza Abbasi, Guangyu Huang, Georgeta M. Istratescu, Long Wu, and Robert E. Hayes. Methane oxidation over Pt, Pt: Pd, and Pd based catalysts: Effects of pre-treatment. *Canadian Journal of Chemical Engineering*, 93(8):1474–1482, 2015.

[98] Ahmed I. Osman, Jehad K. Abu-Dahrieh, Fathima Laffir, Teresa Curtin, Jillian M. Thompson, and David W. Rooney. A bimetallic catalyst on a dual component support for low temperature total methane oxidation. *Applied Catalysis B: Environmental*, 187:408–418, 2016.

[99] Natalia M. Martin, Johan Nilsson, Magnus Skoglundh, Emma C. Adams, Xueting Wang, Gudmund Smedler, Agnes Raj, David Thompsett, Giovanni Agostini, Stefan Carlson, Katarina Norén, and Per-Anders Carlsson. Study of methane oxidation over alumina supported Pd–Pt catalysts using operando DRIFTS/MS and in situ XAS techniques. *Catalysis, Structure & Reactivity*, 3(1-2):24–32, 2017.

[100] Svetlana A. Yashnik, Yu A. Chesalov, A. V. Ishchenko, V. V. Kaichev, and Zinfer Rishatovich Ismagilov. Effect of Pt addition on sulfur dioxide and water vapor tolerance of Pd-Mn-hexaaluminate catalysts for high-temperature oxidation of methane. *Applied Catalysis B: Environmental*, 204:89–106, 2017.

[101] Byungkwon Lim, Jinguo Wang, Pedro H.C. Camargo, Claire M. Cobley, Moon J. Kim, and Younan Xia. Twin-induced growth of palladium-platinum alloy nanocrystals. *Angewandte Chemie - International Edition*, 48(34):6304–6308, 2009.

[102] Xiaoqing Huang, Huihui Zhang, Changyou Guo, Zhiyou Zhou, and Nanfeng Zheng. Simplifying the creation of hollow metallic nanostructures: One-pot synthesis of hollow palladium/platinum single-crystalline nanocubes. *Angewandte Chemie - International Edition*, 48(26):4808–4812, 2009.

[103] Liang Wang, Yoshihiro Nemoto, and Yusuke Yamauchi. Direct synthesis of spatially-controlled Pt-on-Pd bimetallic nanodendrites with superior electrocatalytic Activity. *Journal of the American Chemical Society*, 133(25):9674–9677, 2011.

[104] Monica Trueba and Stefano P. Trasatti. γ-alumina as a support for catalysts: A review of fundamental aspects. *European Journal of Inorganic Chemistry*, (17):3393–3403, 2005.

[105] Herman Pines and Werner O. Haag. Alumina: Catalyst and Support. I. Alumina, its Intrinsic Acidity and Catalytic Activity. *Journal of the American Chemical Society*, 82(10):2471–2483, 1960.

[106] Peter Munnik, Petra E. De Jongh, and Krijn P. De Jong. Recent Developments in the Synthesis of Supported Catalysts. *Chemical Reviews*, 115(14):6687–6718, 2015.

[107] Preeti S Shinde, Pradnya S Suryawanshi, Kanchan K Patil, Vedika M Belekar, Sandeep A Sankpal, Sagar D Delekar, and Sushilkumar A Jadhav. A Brief Overview of Recent Progress in Porous Silica as Catalyst Supports. pages 1–17, 2021.

[108] Byoung-koun Min, Ashok Kumar Santra, and David Wayne Goodman. Understanding silica-supported metal catalysts: Pd/silica as a case study. *Catalysis Today*, 85(2-4):113–124, 2003.

[109] Subhashish Dey and Ganesh Chandra Dhal. Cerium catalysts applications in carbon monoxide oxidations. *Materials Science for Energy Technologies*, 3:6–24, 2020.

[110] Marta Boaro, Sara Colussi, and Alessandro Trovarelli. Ceria-based materials in hydrogenation and reforming reactions for CO 2 valorization, feb 2019.

[111] Tiziano Montini, Michele Melchionna, Matteo Monai, and Paolo Fornasiero. Fundamentals and Catalytic Applications of CeO2-Based Materials. *Chemical Reviews*, 116(10):5987–6041, 2016.

[112] Kuan Chang, Haochen Zhang, Mu Jeng Cheng, and Qi Lu. Application of Ceria in CO2 Conversion Catalysis. *ACS Catalysis*, 10(1):613–631, 2020.

[113] Maia Montaña, María S.Leguizamón Aparicio, Marco A. Ocsachoque, Marisa B. Navas, Ivoneide De C.L. Barros, Enrique Rodriguez-Castellón, Mónica L. Casella, and Ileana D. Lick. Zirconia-supported silver nanoparticles for the catalytic combustion of pollutants originating from mobile sources. *Catalysts*, 9(3), 2019.

[114] Nicola Scotti, Filippo Bossola, Federica Zaccheria, and Nicoletta Ravasio. Copper–zirconia catalysts: Powerful multifunctional catalytic tools to approach sustainable processes. *Catalysts*, 10(2), 2020.

[115] Yiqing Zhao, Hyuntae Sohn, Bo Hu, Jens Niklas, Oleg G. Poluektov, Jun Tian, Massimiliano Delferro, and Adam S. Hock. Zirconium Modification Promotes Catalytic Activity of a Single-Site Cobalt Heterogeneous Catalyst for Propane Dehydrogenation. *ACS Omega*, 3(9):11117–11127, 2018.

[116] Christine Bozo, Nolven Guilhaume, and Jean-Marie Herrmann. Role of the Ceria–Zirconia Support in the Reactivity of Platinum and Palladium Catalysts for Methane Total Oxidation under Lean Conditions. *Journal of Catalysis*, 203(2):393–406, 2001.

[117] Koh-ichi Muto, Naonobu Katada, and Miki Niwa. Complete oxidation of methane on supported palladium catalyst: Support effect. *Applied Catalysis A: General*, 134(2):203–215, 1996.

[118] Shuwu Yang, Angel Maroto-Valiente, M. Benito-Gonzalez, Inmaculada Rodriguez-Ramos, and Antonio Ricardo Guerrero-Ruiz. Methane combustion over supported palladium catalysts I: Reactivity and active phase. *Applied Catalysis B: Environmental*, 28(3-4):223–233, 2000.

[119] Phillipe O. Thevenin, Eugenia Pocoroba, Lars J. Pettersson, Hannu Karhu, I. J. Väyrynen, and Sven G. Järås. Characterization and Activity of Supported Palladium Combustion Catalysts. *Journal of Catalysis*, 207(1):139–149, 2002.

[120] Philippe O. Thevenin, Ana Alcalde, Lars J. Pettersson, Sven G. Järås, and José Luis G. Fierro. Catalytic combustion of methane over cerium-doped palladium catalysts. *Journal of Catalysis*, 215(1):78–86, 2003.

[121] Katarina Persson, Anders G. Ersson, Sara Colussi, Alessandro Trovarelli, and Sven G. Järås. Catalytic combustion of methane over bimetallic Pd-Pt catalysts: The influence of support materials. *Applied Catalysis B: Environmental*, 66(3-4):175–185, 2006.

[122] Hisao Yoshida, Tomoyuki Nakajima, Yoshiteru Yazawa, and Tadashi Hattori. Support effect on methane combustion over palladium catalysts. *Applied Catalysis B: Environmental*, 71(1-2):70–79, 2007.

[123] Emiel J.M. Hensen, Dilip G. Poduval, Volkan Degirmenci, D. A.J.Michel Ligthart, Wenbin Chen, Françoise Maugé, Marcello S. Rigutto, and J. A.Rob Van Veen. Acidity characterization of amorphous silica-alumina. *Journal of Physical Chemistry C*, 116(40):21416–21429, 2012.

[124] H. Terryn, P. C. Snijders, J. van den Brand, J. H. W. de Wit, and W. G. Sloof. Acid Base Characterization of Aluminum Oxide Surfaces with XPS. *The Journal of Physical Chemistry B*, 108(19):6017–6024, 2004.

[125] Joshua J Willis, Alessandro Gallo, Dimosthenis Sokaras, Hassan Aljama, Stanislaw H Nowak, Emmett D Goodman, Liheng Wu, Christopher J Tassone, Thomas F Jaramillo, Frank Abild-pedersen, and Matteo Cargnello. Systematic Structure Property Relationship Studies in Palladium Catalyzed Methane Complete Combustion. *ACS Catalysis*, pages 7810–7821, 2017.

[126] Rachel Price, Tuğçe Eralp-Erden, Ethan Crumlin, Sana Rani, Sonia Garcia, Richard Smith, Liam Deacon, Chanan Euaruksakul, and Georg Held. The Partial Oxidation of Methane Over Pd/Al2O3 Catalyst Nanoparticles Studied In-Situ by Near Ambient-Pressure X-ray Photoelectron Spectroscopy. *Topics in Catalysis*, 59(5-7):516–525, 2016.

[127] C. F. Cullis, T. G. Nevell, and D. L. Trimm. Role of the catalyst support in the oxidation of methane over palladium. *Journal of the Chemical Society, Faraday Transactions 1*, 68:1406, 1972.

[128] Joep C. van Giezen, F. R. van den Berg, J. L. Kleinen, A. Jos van Dillen, and John W. Geus. The Effect of Water on the Activity of Supported Palladium Catalysts in the Catalytic Combustion of Methane. *Catalysis Today*, 47(1-4):287–293, 1999.

[129] Dragos Ciuparu and Lisa Pfefferle. Support and water effects on palladium based methane combustion catalysts. *Applied Catalysis A: General*, 209(1-2):415–428, 2001.

[130] Ryuji Kikuchi, Shingo Maeda, Kazunari Sasaki, Stefan Wennerström, and Koichi Eguchi. Low-temperature methane oxidation over oxide-supported Pd catalysts: Inhibitory effect of water vapor. *Applied Catalysis A: General*, 232(1-2):23–28, 2002.

[131] Feng Zhang, Can Hakanoglu, Jose A. Hinojosa, and Jason F. Weaver. Inhibition of methane adsorption on PdO(101) by water and molecular oxygen. *Surface Science*, 617:249–255, 2013.

[132] Mina Alyani and Kevin J Smith. Kinetic Analysis of the Inhibition of CH4 Oxidation by H2O on PdO/Al2O3 and CeO2/PdO/Al2O3 Catalysts. *Industrial and Engineering Chemistry Research*, 55:8309–8318, 2016.

[133] Peter Velin, Martin Ek, Magnus Skoglundh, Andreas Schaefer, Agnes Raj, David Thompsett, Gudmund Smedler, and Per Anders Carlsson. Water Inhibition in Methane Oxidation over Alumina Supported Palladium Catalysts. *Journal of Physical Chemistry C*, 123(42):25724–25737, 2019.

[134] Dragos Ciuparu, Emily Perkins, and Lisa Pfefferle. In situ DR-FTIR investigation of surface hydroxyls on gamma-Al2O3 supported PdO catalysts during methane combustion. *Applied Catalysis A: General*, 263:145–153, 2004.

[135] Mathieu Digne, Philippe Sautet, Pascal Raybaud, Patrick Euzen, and Herve Toulhoat. Hydroxyl Groups on γ-Alumina Surfaces: A DFT Study. *Journal of Catalysis*, 211(1):1–5, 2002.

[136] Mathieu Digne, Philippe Sautet, Pascal Raybaud, Patrick Euzen, and Herve Toulhoat. Use of DFT to achieve a rational understanding of acid-basic properties of γ-alumina surfaces. *Journal of Catalysis*, 226(1):54–68, 2004.

[137] Pit Losch, Weixin Huang, Olena Vozniuk, Emmett D Goodman, Wolfgang Schmidt, and Matteo Cargnello. Modular Pd / Zeolite Composites Demonstrating the Key Role of Support Hydrophobic / Hydrophilic Character in Methane Catalytic Combustion. *ACS Catalysis*, 9:4742–4753, 2019.

[138] Rahman Gholami, Mina Alyani, and Kevin Smith. *Deactivation of Pd Catalysts by Water during Low Temperature Methane Oxidation Relevant to Natural Gas Vehicle Converters*, volume 5. 2015.

[139] Ida Friberg, Nadezda Sadokhina, and Louise Olsson. Complete methane oxidation over Ba modified Pd/Al2O3: The effect of water vapor. *Applied Catalysis B: Environmental*, 231(March):242–250, 2018.

[140] Marcus Olofsson, Nadezda Sadokhina, Ulf Nylén, Louise Olsson, and Gudmund Smedler. The influence of gas composition on Pd-based catalyst activity in methane oxidation inhibition and promotion by NO. *Applied Catalysis B: Environmental*, 200:351–360, 2016.

[141] Tai Chiang Yu and Henry Shaw. The effect of sulfur poisoning on methane oxidation over palladium supported on γ-alumina catalysts. *Applied Catalysis B: Environmental*, 18(1-2):105–114, 1998.

[142] Deborah L. Mowery and Robert L. McCormick. Deactivation of alumina supported and unsupported Pdo methane oxidation catalyst: The effect of water on sulfate poisoning. *Applied Catalysis B: Environmental*, 34(4):287–297, 2001.

[143] Jenny M. Jones, Valerie A. Dupont, R. Brydson, D. J. Fullerton, Noor Shawal Nasri, Andrew Barry Ross, and Aidan V.K. Westwood. Sulphur poisoning and regeneration of precious metal catalysed methane combustion. *Catalysis Today*, 81(4):589–601, 2003.

[144] Hom N. Sharma, Vinit Sharma, Ashish B. Mhadeshwar, and Rampi Ramprasad. Why Pt survives but Pd suffers from SOx poisoning? *Journal of Physical Chemistry Letters*, 6(7):1140–1148, 2015.

[145] Djamela Bounechada, Sheedeh Fouladvand, Lisa Kylhammar, Torben Pingel, Eva Olsson, Magnus Skoglundh, Johan Gustafson, Marco Di Michiel, Mark A. Newton, and Per Anders Carlsson. Mechanisms behind sulfur promoted oxidation of methane. *Physical Chemistry Chemical Physics*, 15(22):8648–8661, 2013.

[146] Lisa Kylhammar, Per Anders Carlsson, and Magnus Skoglundh. Sulfur promoted low-temperature oxidation of methane over ceria supported platinum catalysts. *Journal of Catalysis*, 284(1):50–59, 2011.

[147] Francisco Zaera. Nanostructured materials for applications in heterogeneous catalysis. *Chemical Society Reviews*, 42(7):2746–2762, 2013.

[148] Jorge Ontaneda, Roger A. Bennett, and Ricardo Grau-Crespo. Electronic Structure of Pd Multilayers on Re(0001): The Role of Charge Transfer. *Journal of Physical Chemistry C*, 119(41):23436–23444, 2015.

[149] Charles Kittel. *Introduction to Solid State Physics*. John Wiley & Sons, Incorporated, 2004.

[150] Richard E. Palmer, Rongsheng Cai, and Jerome Vernieres. Synthesis without Solvents: The Cluster (Nanoparticle) Beam Route to Catalysts and Sensors. *Accounts of Chemical Research*, 51(9):2296–2304, 2018.

[151] Junyuan Xu, Shane Murphy, Dehua Xiong, Rongsheng Cai, Xian Kui Wei, Marc Heggen, Emanuele Barborini, Simone Vinati, Rafal E. Dunin-Borkowski, Richard E. Palmer, and Lifeng Liu. Cluster Beam Deposition of Ultrafine Cobalt and Ruthenium Clusters for Efficient and Stable Oxygen Evolution Reaction. *ACS Applied Energy Materials*, 1(7):3013–3018, 2018.

[152] John F Watts and John Wolstenholme. *An Introduction to Surface Analysis by XPS and AES*. John Wiley & Sons, Incorporated, 2003.

[153] Heinrich Hertz. Ueber einen Einfluss des ultravioletten Lichtes auf die electrische Entladung. *Annalen Der Physik*, 267(8):983–1000, 1887.

[154] Philipp Lenard. Ueber die lichtelektrische Wirkung. *Annalen Der Physik*, 313(5):149–198, 1902.

[155] Albert Einstein. Über einen die Erzeugung und Verwandlung des Lichtes betreffenden heuristischen Gesichtspunkt. *Annalen Der Physik*, 322(6):132–148, 1905.

[156] David E. Starr, Z. Liu, Michael Hävecker, Axel Knop-Gericke, and Hendrik Bluhm. Investigation of solid/vapor interfaces using ambient pressure X-ray photoelectron spectroscopy. *Chemical Society Reviews*, 42(13):5833–5857, 2013.

[157] D Briggs and M P Seah. *Practical Surface Analysis, Auger and X-ray Photoelectron Spectroscopy*. Practical Surface Analysis. Wiley, 1996.

[158] D. Frank Ogletree, Hendrik Bluhm, Gennadi Lebedev, Charles S. Fadley, Zahid Hussain, and Miquel Salmeron. A differentially pumped electrostatic lens system for pho-

toemission studies in the millibar range. *Review of Scientific Instruments*, 73(11):3872, 2002.

[159] Georg Held, Federica Venturini, David C. Grinter, Pilar Ferrer, Rosa Arrigo, Liam Deacon, Wilson Quevedo Garzon, Kanak Roy, Alex Large, Christopher Stephens, Andrew Watts, Paul Larkin, Matthew Hand, Hongchang Wang, Linda Pratt, James J. Mudd, Thomas Richardson, Suren Patel, Michael Hillman, and Stewart Scott. Ambient-pressure endstation of the Versatile Soft X-ray (VerSoX) beamline at Diamond Light Source. *Journal of Synchrotron Radiation*, 27(5):1153–1166, 2020.

[160] Joachim Schnadt, Jan Knudsen, Jesper N. Andersen, Hans Siegbahn, Annette Pietzsch, Franz Hennies, Niclas Johansson, Nils Mårtensson, Gunnar Öhrwall, Stephan Bahr, Sven Mähl, and Oliver Schaff. The new ambient-pressure X-ray photoelectron spectroscopy instrument at MAX-lab. *Journal of Synchrotron Radiation*, 19(5):701–704, 2012.

[161] Zbynek Novotny, Dino Aegerter, Nicolò Comini, Benjamin Tobler, Luca Artiglia, Urs Maier, Thomas Moehl, Emiliana Fabbri, Thomas Huthwelker, Thomas J. Schmidt, Markus Ammann, Jeroen A. Van Bokhoven, Jörg Raabe, and Jürg Osterwalder. Probing the solid-liquid interface with tender x rays: A new ambient-pressure X-ray photoelectron spectroscopy endstation at the Swiss Light Source. *Review of Scientific Instruments*, 91(2), 2020.

[162] Paul S. Bagus, Eugene S. Ilton, and Connie J. Nelin. The interpretation of XPS spectra: Insights into materials properties. *Surface Science Reports*, 68(2):273–304, 2013.

[163] K. S. Kim, A. F. Gossmann, and Nicholas Winograd. X-ray photoelectron spectroscopic studies of palladium oxides and the palladium-oxygen electrode. *Analytical Chemistry*, 46(2):197–200, 1974.

[164] Dragos Ciuparu, Maxim R. Lyubovsky, Eric Altman, Lisa D. Pfefferle, and Abhaya Datye. Catalytic Combustion of Methane Over Palladium-Based Catalysts. *Catalysis Reviews*, 44(4):593–649, 2002.

[165] Johan Nilsson, Per Anders Carlsson, Natalia M. Martin, Emma C. Adams, Giovanni Agostini, Henrik Grönbeck, and Magnus Skoglundh. Methane oxidation over

Pd/Al2O3under rich/lean cycling followed by operando XAFS and modulation excitation spectroscopy. *Journal of Catalysis*, 356:237–245, 2017.

[166] Xavier Auvray and Anthony Thuault. Effect of Microwave Drying, Calcination and Aging of Pt/Al2O3 on Platinum Dispersion. *Catalysts*, 8(9):348, 2018.

[167] James B. Miller and Manaswita Malatpure. Pd catalysts for total oxidation of methane: Support effects. *Applied Catalysis A: General*, 495:54–62, 2015.

[168] Chen Chen, Yu Hao Yeh, Matteo Cargnello, Christopher B. Murray, Paolo Fornasiero, and Raymond J. Gorte. Methane oxidation on Pd@ZrO2/Si-Al2O3 is enhanced by surface reduction of ZrO2. *ACS Catalysis*, 4(11):3902–3909, 2014.

[169] Matteo Monai, Tiziano Montini, Chen Chen, Emiliano Fonda, Raymond J Gorte, and Paolo Fornasiero. Methane Catalytic Combustion over Hierarchical Pd @ CeO2/Si-Al2O3: Effect of the Presence of Water. *ChemCatChem*, 7(14):2038–2046, 2015.

[170] Sichem Guerrero, Paulo Araya, and Eduardo E. Wolf. Methane oxidation on Pd supported on high area zirconia catalysts. *Applied Catalysis A: General*, 298(1-2):243–253, 2006.

[171] Akimi Ayame and Teruhilo Kitagawa. X-Ray photoelectron spectroscopic measurement and chemical characteristics of silica, alumina and silica-alumina. *Bunseki Kagaku*, 40(11):673–678, 1991.

[172] Sandeeran Govender and Holger B. Friedrich. Monoliths: A review of the basics, preparation methods and their relevance to oxidation. *Catalysts*, 7(2), 2017.

[173] Lyubov A. Isupova, Galina M. Alikina, Olga I. Snegurenko, Vladislav A. Sadykov, and Sergei V. Tsybulya. Monolith honeycomb mixed oxide catalysts for methane oxidation. *Studies in Surface Science and Catalysis*, 130 D:3783–3788, 2000.

[174] Renate Schwiedernoch, Steffen Tischer, Chrys Correa, and Olaf Deutschmann. Experimental and numerical study on the transient behavior of partial oxidation of methane in a catalytic monolith. *Chemical Engineering Science*, 58(3-6):633–642, 2003.

[175] Arezoo Hosseini, Kerem Cagatay Içli, Macit Özenbaş, and CIgdem Erçelebi. Fabrication and characterization of spin-coated TiO2 films. *Energy Procedia*, 60(C):191–198, 2014.

[176] Kyu Seog Hwang and Byung Hoon Kim. Preparation of highly oriented LaNiO3 thin films by spin-coating technique. *Journal of Sol-Gel Science and Technology*, 14(2):203–207, 1999.

[177] Wan Young Chung, Go Sakai, Kengo Shimanoe, Norio Miura, Duk Dong Lee, and Noboru Yamazoe. Gas sensing properties of indium oxide thin film on silicon substrate prepared by spin-coating method. *Japanese Journal of Applied Physics, Part 1: Regular Papers and Short Notes and Review Papers*, 37(9 A):4994–4998, 1998.

[178] Christine Hummelgård, John Gustavsson, Ann Cornell, Håkan Olin, and Joakim Bäckström. Spin coated titanium-ruthenium oxide thin films. *Thin Solid Films*, 536:74–80, 2013.

[179] Adriane D.V. Souza, Cezar C. Arruda, Leandro Fernandes, Maria L.P. Antunes, Pedro K. Kiyohara, and Rafael Salomão. Characterization of aluminum hydroxide (Al(OH)3) for use as a porogenic agent in castable ceramics. *Journal of the European Ceramic Society*, 35(2):803–812, 2015.

[180] Grzegorz D. Sulka, Sigrid Stroobants, Victor V. Moshchalkov, Gustaaf Borghs, and J. P. Celis. Synthesis of Well-Ordered Nanopores by Anodizing Aluminum Foils in Sulfuric Acid. (July):1–8, 2002.

[181] Long Ba and Wei Sang Li. Influence of anodizing conditions on the ordered pore formation in anodic alumina. *Journal of Physics D: Applied Physics*, 33(20):2527–2531, 2000.

[182] Grzegorz D. Sulka and Krzysztof G. Parkoła. Temperature influence on well-ordered nanopore structures grown by anodization of aluminium in sulphuric acid. 52:1880–1888, 2007.

[183] Grzegorz D Sulka and Krzysztof G Parko. Anodising potential influence on well-ordered nanostructures formed by anodisation of aluminium in sulphuric acid. 515:338–345, 2006.

[184] A. O. Araoyinbo, A. F.M. Noor, Srimala Sreekantan, and A. Aziz. Voltage effect on electrochemical anodization of aluminum at ambient temperature. *International Journal of Mechanical and Materials Engineering*, 5(1):53–58, 2010.

[185] Wernick S. Pinner and P. G. Sheasby. *The Surface Treatment and Finishing of Aluminium and Its Alloys (Volumes 1 & 2)*. Finishing Publications Ltd.

[186] Dong Hwang Chen, Cheng Chuan Wang, and Ting Chia Huang. Preparation of palladium ultrafine particles in reverse micelles. *Journal of Colloid and Interface Science*, 210(1):123–129, 1999.

[187] Ming Li Wu, Dong Hwang Chen, and Ting Chia Huang. Synthesis of Au/Pd bimetallic nanoparticles in reverse micelles. *Langmuir*, 17(13):3877–3883, 2001.

[188] Detre Teschner, Alexey Pestryakov, Evgueni Yu Kleimenov, Michael Hävecker, Hendrik Bluhm, Hermann Sauer, Axel Knop-Gericke, and Robert Schlögl. High-pressure X-ray photoelectron spectroscopy of palladium model hydrogenation catalysts. Part 2: Hydrogenation of trans-2-pentene on palladium. *Journal of Catalysis*, 230(1):195–203, 2005.

[189] Guanghui Zhu, Ken Ichiro Fujimoto, Dmitri Yu Zemlyanov, Abhaya K. Datye, and Fabio H. Ribeiro. Coverage of palladium by silicon oxide during reduction in H2 and complete oxidation of methane. *Journal of Catalysis*, 225(1):170–178, 2004.

[190] Dmitry Zemlyanov, Bernhard Klötzer, Harald Gabasch, Andrew Smeltz, Fabio H. Ribeiro, Spiros Zafeiratos, Detre Teschner, Peter Schnörch, Elaine Vass, Michael Hävecker, Axel Knop-Gericke, and Robert Schlögl. Kinetics of palladium oxidation in the mbar pressure range: Ambient pressure XPS study. *Topics in Catalysis*, 56(11):885–895, 2013.

[191] Haitham A. Etman, Zhasmina V. Zheleva, Georg Held, and Roger A. Bennett. Epitaxial growth of ultrathin palladium films on Re{0001}. *Journal of Physical Chemistry C*, 115(10):4191–4199, 2011.

[192] Elettra Sincrotrone Trieste. Materials Science Beamline - Accessed 31/05/2021.

[193] Reinhard Denecke and Nils Martensson. *Adsorbed Layers on Surfaces*. SpringerMaterials, 2005.

[194] Jorge Ontaneda, Roger A Bennett, and Ricardo Grau-crespo. Electronic Structure of Pd Multilayers on Re (0001): The Role of Charge Transfer. (0001), 2015.

[195] Friedrich P. Leisenberger, Georg Koller, Michael Sock, Svetlozar Surnev, Michael G. Ramsey, Falko P. Netzer, Bernhard Klötzer, and Konrad Hayek. Surface and subsurface oxygen on Pd(111). *Surface Science*, 445(2-3):380–393, 2000.